

**IMPROVED RAILWAY VEHICLE
INSPECTION AND MONITORING
THROUGH THE INTEGRATION OF
MULTIPLE MONITORING TECHNOLOGIES**

by

Zhenhe Zhang

A thesis submitted to
The University of Birmingham
for the degree of
DOCTOR OF PHILOSOPHY

School of Engineering
College of Engineering and Physical Sciences
University of Birmingham
December 2016

UNIVERSITY OF
BIRMINGHAM

University of Birmingham Research Archive

e-theses repository

This unpublished thesis/dissertation is copyright of the author and/or third parties. The intellectual property rights of the author or third parties in respect of this work are as defined by The Copyright Designs and Patents Act 1988 or as modified by any successor legislation.

Any use made of information contained in this thesis/dissertation must be in accordance with that legislation and must be properly acknowledged. Further distribution or reproduction in any format is prohibited without the permission of the copyright holder.

Abstract

The effectiveness and efficiency of railway vehicle condition monitoring is increasingly critical to railway operations as it directly affects safety, reliability, maintenance efficiency, and overall system performance. Although there are a vast number of railway vehicle condition monitoring technologies, wayside systems are becoming increasingly popular because of the reduced cost of a single monitoring point, and because they do not interfere with the existing railway line. Acoustic sensing and visual imaging are two wayside monitoring technologies that can be applied to monitor the condition of vehicle components such as roller bearing, gearboxes, couplers, and pantographs, etc. The central hypothesis of this thesis is that it is possible to integrate acoustic sensing and visual imaging technologies to achieve enhancement in condition monitoring of railway vehicles. So this thesis presents improvements in railway vehicle condition monitoring through the integration of acoustic sensing and visual imaging technologies.

The work presented in this thesis considers not only improvements achieved through integration, but also individual enhancements of the different technologies. A novel signal processing algorithm has been developed for bearing vibration signal analysis. Named Empirical Mode Envelope with Minimum Entropy (EMEME), it combines the Envelope from Empirical Mode Decomposition (EMD) and Minimum Entropy Deconvolution (MED) approaches with an Energy Moment technique to improve the feature selection stage of the EMD algorithm.

A second novel signal processing algorithm has also been developed for bearing audio signals. The proposed algorithm is divided into SNR enhancement and non-stationary feature extraction. In the first stage, Linear Predictive Coding (LPC) and Empirical Mode Decomposition (EMD) are used to reduce the level of noise, in order to achieve SNR

enhancement. In the second stage, Spectral Kurtosis (SK) is used to extract the non-stationary features of the signal, and from this it is possible to infer details about faults in tapered-roller-bearings. Additionally, the potential for using vision imaging technology to achieve coupler and pantograph condition monitoring has been demonstrated through the development of custom processing chains to process recorded images and identify suitable metrics.

The work has involved the development of a number of instrumentation systems. An axle bearing test rig has been developed to carry out experiments using vibration and acoustic sensors in the laboratory.

In field tests, single microphone has been expanded to microphone array in order to widen the signal acquisition coverage area. The microphone array is built in horizontal linear shape because a good performance in one-dimensional direction could enhance the bearing audio signal acquisition in field tests. The designed acoustic system has been verified at a research testing site; a fully integrated system has been produced to carry out the final field tests on the Network Rail High Speed 1 Line. This thesis considers not only one integration solution, but two solutions operating at different levels of integration. Both integration solutions have the potential to rival the existing commercialised condition monitoring systems in terms of practicality and operating line speed. The achievements of the integration described in this thesis were demonstrated at the only high speed line in the UK, Network Rail's High Speed 1 Line. The thesis defines integration solutions on two levels: a basic combination of systems and a more closely integrated combination of signals within those systems. System level integration can achieve more comprehensive information on the vehicle condition than each single solution, and its installation does not interfere with the existing railway infrastructure. In particular, the high-speed vision imaging CM system is capable of inspecting and monitoring pantographs, as well as train door & window statuses; while the acoustic CM system is capable of inspecting bearings and wheelflats from the trackside. Signal level

integration is achieved using the imaging speed measurement system (ISMS) developed as part of this study. A speed measurement system is needed by the acoustic system, because the microphone array needs train location to target the sound sources, as well as forming acoustic beam of each single microphone. Furthermore, acoustic beam needs accurate and high resolution train speed to eliminate the frequency shift brought from the Doppler Effect. The ISMS uses high speed vision imaging technology to identify and track key components of the vehicle. This provides the support to acoustic sensing technology of speed measurement information with high accuracy and does not interfere with the existing railway infrastructure.

Keywords: Railway; Condition monitoring; railway vehicle condition monitoring; integration; acoustic sensing technology; vision imaging technology; roller bearing; pantograph; coupler; bearing inspection; high frequency responding filtering; HFRT; Spectral Kurtosis; empirical mode decomposition; EMD; minimum entropy deconvolution; MED; Linear Prediction Coefficients; LPC; data-adaptive techniques; Imaging Speed Monitoring System; ISMS; computer vision; high speed imaging;

Acknowledgement

Thanks to the Birmingham Centre for Railway Research and Education (BCRRE) and School of Engineering in University of Birmingham for providing my sponsorship to accomplish this research work. Also, I would like to thank the following fellows for their contribution to this PhD work:

Firstly and most importantly, thanks Dr. Edward Stewart for being an excellent supervisor, companion and more like a relative both in the UK and China. I also would like to thank him for being patient in reading and correcting my frustratingly casual writing.

Thanks Prof. Clive Roberts for supporting me through this PhD, continuously trusting on me working with Edd since the 2nd year of my PhD and every “well done” for my achievement.

Thanks Dr. Mani Entezami for his contribution in most of the hardware system construction, and selflessly sharing data with me for the exchange of Chinese rice cakes.

Also thanks the colleagues in N112 for tolerating me being crazy and annoying while generating this paper work.

I also would like to thank Sung Hee Cho for organising Beer nights; Dr. Tosaphol Ratniyomchai for always rejecting my badminton playing invitations that leaves me more time on writing; Katherine Slater for anglicising part of this thesis; and Miss. Lu Chen for keeping urging me hurry up and finish my thesis.

Finally, I would like to thank my parents for giving birth on me and providing me love and support.

Table of Contents

Abstract.....	3
Acknowledgement	6
Table of Contents.....	7
List of Figures	10
List of Tables	18
1 Introduction.....	19
1.1 Overview	19
1.2 The need for condition monitoring and non-destructive testing in the railway ..	20
1.3 The need for railway vehicle condition monitoring	21
1.4 Key vehicle components suitable for monitoring.....	23
1.5 Way-side condition monitoring of railway vehicles	24
1.6 The need for integration	26
1.7 Approaches to integration	27
1.8 Hypothesis and objectives	28
1.9 Thesis structure.....	30
2 Review of railway vehicle inspection and monitoring technologies	33
2.1 Vehicle health monitoring	34
2.2 Roller bearing inspection and monitoring technologies	44
2.3 Vision imaging inspection and monitoring technologies	49
2.4 Conclusion.....	55
3 Review of railway condition-based digital signal processing technologies	58
3.1 Overview	58
3.2 Roller bearing acoustic signal processing technologies	58
3.3 Image processing – Computer vision technologies.....	79

3.4	Conclusion.....	81
4	Methodology.....	82
4.1	Methodology decomposition.....	82
4.2	Summary	94
5	Acoustic sensing technology application.....	96
5.1	Overview	96
5.2	Vibration sensor application – Lab based	99
5.3	Acoustic microphone application – Lab based.....	119
5.4	Acoustic microphone application on the Class 117 train – field tests based	133
5.5	Summary	150
6	Vision imaging technology application	152
6.1	Overview	152
6.2	Hardware system overview	152
6.3	Computer vision techniques overview	163
6.4	Case study – Coupler condition monitoring application.....	171
6.5	Case study – Pantograph condition monitoring application.....	177
6.6	Summary	182
7	Integration of the condition monitoring sensing technologies.....	184
7.1	Integration of monitoring systems.....	185
7.2	Field tests on the Network Rail High Speed 1 Line	187
7.3	System and signal level integrated system on the High Speed 1 Line	191
7.4	System level integration	192
7.5	Signal level integration.....	206
7.6	Conclusions	226
8	Conclusion and future work.....	228
8.1	Contribution to knowledge	228
8.2	Conclusion.....	233
8.3	Future work	234

APPENDIX A.....	235
References.....	236

List of Figures

Figure 1.1- Railway accidents considered in the D-RAIL FP7 project by cause [1].....	22
Figure 2.1- Track IQ company hot box detector [41].....	40
Figure 1.2- An example of a buffer-and-chain coupler [7].....	41
Figure 1.3- An example of a Z-shaped pantograph [9].....	42
Figure 2.2- Tapered-roller-bearing [43].....	44
Figure 2.3- roller damage of tapered-roller-bearing [45].....	45
Figure 2.4- outer race defect of tapered-roller-bearing [46]	45
Figure 2.5- cage & roller damage of tapered-roller-bearing.....	45
Figure 2.6- System concept of vision-based monitoring system [74]	51
Figure 2.7- Image with blue clip in [81].....	52
Figure 2.8- Pantograph detection [85]	53
Figure 2.9- The image from a brake pad inspection device [87].....	54
Figure 2.10- Field-of-view of the visible image [90]	55
Figure 3.1- Waveform of a simple periodic signal's EMD procedure	76
Figure 3.2- The waveform of a simple periodic signal's MED procedure	79
Figure 4.1- The diagram of methodology for the integrated system development.....	83
Figure 4.2- Bearing dimensions diagrams adapted from [183]	86
Figure 4.3- Bearing test rig and vibration sensor.....	89

Figure 4.4- Anechoic Chamber room	90
Figure 4.5- Bearing test rig and acoustic sensor (microphone)	91
Figure 4.6- The test location at research testing site.....	92
Figure 4.7- Test train.....	93
Figure 4.8- Location of the site.....	94
Figure 5.1- Overview diagram of chapter 5.....	97
Figure 5.2- Typical faults of tapered-roller-bearing	100
Figure 5.3- The flowchart of the proposed method process	104
Figure 5.4 - IMFs frequency ranges.....	105
Figure 5.5- EMD procedure of the healthy bearing	106
Figure 5.6- Effect of MED iterations when applied to F1 faulty vibration signal.....	107
Figure 5.7- Effect of MED iterations when applied to F2 faulty vibration signal.....	108
Figure 5.8- FFT envelope of healthy and faulty bearing spinning at250 RPM (Top) healthy bearing (Middle) outer race damaged bearing (Bottom) roller damaged bearing 's EMEME algorithm processed data.....	110
Figure 5.9- FFT envelope of healthy and faulty bearing spinning at1000 RPM (Top) healthy bearing (Middle) outer race damaged bearing (Bottom) roller damaged bearing 's EMEME algorithm processed data.....	111
Figure 5.10 - Conventional envelope method (left) vs EMEME (right) at 500 RPM no added noise	112

Figure 5.11 - Conventional envelope method (left) vs EMEME (right) at 500 RPM with noise SNR of 5	113
Figure 5.12 - Conventional envelope method (left) vs EMEME (right) at 500 RPM with noise SNR of 1.5	114
Figure 5.13 – Distribution of amplitude values of IMF components generated using the energy moment and traditional energy techniques	115
Figure 5.14 – FFT envelopes generated using the energy moment feature extraction method and IMF(1).....	116
Figure 5.15 - Signals from faulty bearing, (left) simple system (right) Complex system including gearbox.....	117
Figure 5.16 – Distribution of amplitude values of IMF components generated using the energy moment and traditional energy techniques for the complex system including gearbox noise	118
Figure 5.17 – FFT envelopes for a signal including gearbox noise, (left) IMF selected using the energy moment technique (EM) and for IMF(1) (right) IMFs selected using the energy moment technique (EM) and the traditional energy (TE) method.....	118
Figure 5.18 – Flowchart of the novel processing algorithm on the acoustic signal.....	122
Figure 5.19 – Signal of the outer race damaged bearing spinning at 400 RPM (Top) original signal (Bottom) acoustic noise filtered signal.....	123
Figure 5.20 – (top) PSD and (bottom) SK computed in different frequency resolution ($N_w = 8, 16, 32, 64, 128, 256, 512, 1024$). The analysed signal is from an outer race damaged bearing @ 400RPM	125

Figure 5.21 – Kurtogram of the signal from an outer race damaged bearing @ 400RPM....	127
Figure 5.22 – (a) Input acoustic signal and (b) magnitude of the envelope 0 Hz, 24 which maximises the kurtogram, together with its 0.1% signification threshold.....	128
Figure 5.23- FFT envelope of healthy and faulty bearing spinning at400 RPM (Top) healthy bearing (Middle) outer race damaged bearing (Bottom) roller damaged bearing 's processed acoustic data.....	130
Figure 5.24- FFT envelope of healthy and faulty bearing spinning at1000 RPM (Top) healthy bearing (Middle) outer race damaged bearing (Bottom) roller damaged bearing 's processed acoustic data.....	131
Figure 5.25- Test train.....	133
Figure 5.26 – Horizontal linear array.....	134
Figure 5.27 – Acoustic funnel.....	135
Figure 5.28- Lightgate speed measurement system.....	136
Figure 5.29- Lightgate signals for a single axle.....	137
Figure 5.30- Beamforming arrangement.....	138
Figure 5.31- Flow chart of the time-domain beamforming algorithm working flow	140
Figure 5.32 – Field test arrangement plan overview.....	141
Figure 5.33 – Final set up at the test site.....	142
Figure 5.34 – 2-D spectrogram of the 8 kHz tone	143
Figure 5.35 – 2-D spectrogram of the beamforming processed 8 kHz tone	144

Figure 5.36 – Original signal of the roller damage fault tone.....	145
Figure 5.37 – Beamforming algorithm processed signal of the roller damage fault tone	145
Figure 5.38 – The processed signal of roller damage fault tone (Top) beamforming processed and high-pass filtered signal (Bottom) beamforming processed, high-pass filtered and acoustic noise filtered signal.....	146
Figure 5.39 – Kurtogram of the processed signal of roller damage fault tone	148
Figure 5.40- FFT envelope of roller damaged bearing's processed acoustic data	149
Figure 6.1- Image capture device (FASTCAM Mini UX100)	158
Figure 6.2- Example axle bearing lid.....	163
Figure 6.3- Map of the applied computer vision techniques	164
Figure 6.4- A 3*3 block in the source image.....	165
Figure 6.5- Two 3*3 kernels of Sobel operator (left) G_x – Horizontal kernel (right) G_y – Vertical kernel.....	166
Figure 6.6- Two 3*3 kernels of Prewitt operator (left) G_x – Horizontal kernel (right) G_y – Vertical kernel.....	166
Figure 6.7- Test train.....	171
Figure 6.8- Flow chart of the coupler extraction and tracking procedure	172
Figure 6.9- The eight self-created masks for the 1 st erode operation.....	173
Figure 6.10- Original picture	174
Figure 6.11- The image represented in gradient magnitude	174

Figure 6.12- Edge detection, erode and thinning processed Image	175
Figure 6.13- Closed holes filled and erode processed Image	175
Figure 6.14- Coupler extraction result	176
Figure 6.15- British Rail Class 395 used in the ISMS tests at the High Speed 1 Line [207]	177
Figure 6.16- Original picture of pantograph	178
Figure 6.17- Flow chart of the pantograph extraction and tracking procedure	179
Figure 6.18- The pantograph image represented in gradient magnitude	180
Figure 6.19- Edge detection processed Image	180
Figure 6.20- Erode and thinning processed Image	181
Figure 6.21- Hough line transform processed image	181
Figure 6.22- Pantograph extraction result.....	182
Figure 7.1- Site measurements.....	188
Figure 7.2- Lightgate stand.....	189
Figure 7.3- Field test plan for the integrated system	190
Figure 7.4- Integrated system frame	191
Figure 7.5- System level integration system.....	193
Figure 7.6- Original image with the stitching strip from the high-speed vision system.....	196
Figure 7.7- Stitched image.....	197
Figure 7.8- Flow chart of the and vehicle side view extraction and tracking procedure	197

Figure 7.9- The image represented in gradient magnitude: (Top) Overhead line area, (Bottom) vehicle main body side view	198
Figure 7.10- Edge detection processed image: (Top) Overhead line area, (Bottom) vehicle main body side view	198
Figure 7.11- Erode (Top) and thinning (Bottom) processing applied to the overhead line area of the image.....	199
Figure 7.12- Hough Line transform processed image: (Top) Overhead line area, (Bottom) vehicle main body side view.....	199
Figure 7.13- Pantograph and vehicle side view inspection result.....	200
Figure 7.14- GOTCHA system on High-speed 1 line [42].....	201
Figure 7.15- Acoustic signal of a high speed train: (Blue) the original signal, (Red) the pre-processed signal	202
Figure 7.16- Acoustic signal from an axlebox: (Blue) the signal before ANF processing, (Red) the signal after ANF processing.....	203
Figure 7.17- RMS values of ten sets of data (ten trains)	204
Figure 7.18- RMS values of data set with wheelflat versus ten sets of data (ten trains) in healthy condition.....	205
Figure 7.19- Field test plan overview	209
Figure 7.20- Example image captured by the high speed camera	210
Figure 7.21- Lightgate signals for a single axle.....	211
Figure 7.22- Speed/time curves from the ISMS and the lightgate systems	212

Figure 7.23- Flow chart of the wheel tracking procedure.....	213
Figure 7.24- Stage 1, (a): the original RGB image; (b): the rail detection; (c): removal of the ballast section from the image	214
Figure 7.25- Stage 2, (a): edge detection; (b): mathematical morphology operations	214
Figure 7.26- Stage 3, (a): circle detection; (b): wheel profile retrieval	215
Figure 7.27- The lightgate based speed measurement system at the High Speed 1Line	217
Figure 7.28- The waveform of lightgate and high speed camera signals	218
Figure 7.29- Example image of extracted wheel profile.....	219
Figure 7.30- The light gate No.1 signal of a British Rail Class 395 train	221
Figure 7.31- The light gate No.3 signal of a British Rail Class 395 train	222
Figure 7.32- Speed/time curves from the ISMS and the lightgate speed measurement systems	224

List of Tables

Table 2.1- List of major types of fault of vehicle components [7]	35
Table 4.1- Examples of scaling factor	87
Table 4.2 – Dimension of the Type 801023AB tapered roller bearing	87
Table 5.1- Bearing test fault conditions	100
Table 5.2 - Example of characteristic frequencies of the bearings	101
Table 6.1- Table of frame rate and corresponding maximum resolution	159
Table 6.2- Table of key features	160
Table 7.1- High-speed camera settings in system level integration.....	194

1 Introduction

1.1 Overview

This thesis is about developing intelligent solutions to integrate existing technologies in order to achieve improvements in railway vehicle condition monitoring.

Condition monitoring (CM) is the process of monitoring a parameter of condition in machinery (vibration, temperature etc.), in order to identify a significant change which can reveal the development of a fault. Condition monitoring has a unique benefit in that conditions that would shorten normal lifespan can be addressed before they develop into a major failure [1]. Presently, research into condition monitoring (CM) is a global academic topic. Its development originally focused on improving system safety but has since led to a wider range of benefits. Railway vehicle condition monitoring prevents accidents, happening to save lives, but it also provides economic benefits to railway service providers and infrastructure maintainers. Condition monitoring technologies cover a wide range of disciplines including civil, mechanical and electronic engineering. Correspondingly, there are a large number of technologies available for monitoring the condition of various components.

Research into CM technologies focuses mainly on achieving improvements in each individual technology in isolation. While this is important and work to this effect is demonstrated in this thesis, there is currently comparably little work focused on the improvement of monitoring performance through the integration of distinct systems. This is considered in this thesis on two levels: a basic combination of systems and a more closely integrated combination of signals.

In this thesis, an instrumentation framework, capable of obtaining and integrating data from multiple CM systems, is demonstrated and applications are discussed. Data processing

solutions are demonstrated and evaluated for each monitoring type and application. The systems developed are demonstrated at the laboratory stage, with the use of field tests, and then further extended to be installed on the Network Rail High Speed 1 Line. Through this development, limitations of the individual CM systems are identified. This thesis identifies the need for integration of CM systems, as well as demonstrating the integration process in terms of both the hardware system and data streams.

1.2 The need for condition monitoring and non-destructive testing in the railway

Progress in Civil, Mechanical and Electronic engineering is continuously driving enhancements within specific condition monitoring (CM) techniques. Condition monitoring is widely applied in various manufactory machineries, as well as transportation systems which are often complex and can involve such machinery systems. The increasing popularity of condition monitoring techniques is because of the range of benefits that they bring, the most significant are listed below:

- 1) Increase the system availability;
- 2) Improve the operating efficiency;
- 3) Provide improved safety;
- 4) Allow the system to operate for longer periods;
- 5) Reduce the energy consumption using optimised operation strategy;
- 6) Reduce the instantaneous train electrical tractive and braking power by optimization;
- 7) Eliminate chronic failures;
- 8) Allow maintenance planning;
- 9) Prevent catastrophic damage to systems;

- 10) Only perform maintenance when necessary, especially meaningful in the case of component replacement in complicated mechanical systems;
- 11) Reduced need for spare parts stock;
- 12) Shorter maintenance time, etc.

From an economic point of view, a condition monitoring procedure should not interrupt the normal operation of the system, especially large-scale mechanical systems such as the railway. Consequently, there is a division of condition monitoring focused on evaluating the properties of materials, components, or systems without causing damage. This is known as Non-destructive testing (NDT). In the current railway industry, NDT technologies are widely applied in infrastructure and rail vehicles condition monitoring.

1.3 The need for railway vehicle condition monitoring

The current situation in the area of railway vehicle safety is quite concerning. Figure 1.1 is taken from a recent study published by Det Norske Veritas Ltd. (DNV) as part of the D-RAIL FP7 project. It considers the causes of the railway accidents that have been reported in 23 countries in recent years [2]. The report reveals that out of 700 accidents considered, 38% of them were due to rolling stock faults. Consequently, in the current railway industry, various efforts being are made to minimize consequences of high-speed rail vehicle derailments. This work is being carried out through a combination of empirical observations and cross collaboration with the research institutes.

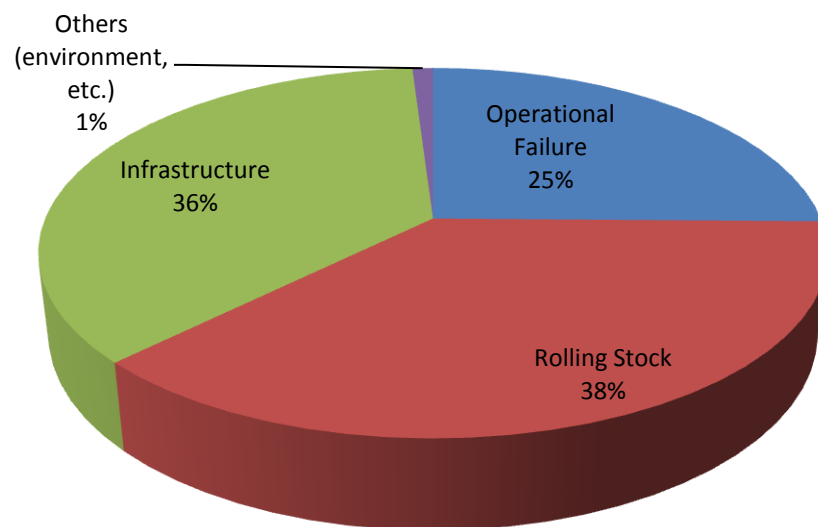


Figure 1.1- Railway accidents considered in the D-RAIL FP7 project by cause [2]

In recent years, advancements in safety practices have considerably reduced the risk of accidents, making rail travel to one of the safest modes of transportation. The introduction of active safety measures to reduce the probability of unwanted events has reduced derailments caused by over-speeding or high-speed train collisions [3]. However, derailments due to mechanical failures affecting wheelset guidance on rails continue to occur despite refined inspection techniques and more reliable vehicles [4]. The current most common maintenance strategy in the railway industry is scheduled maintenance. There is a desire to transform this time-based maintenance strategy to a condition-based strategy as it could save on unnecessary maintenance time and cost. To accomplish this transformation, potential failures should be foreseen so that maintenance can be carried out at the right time. In addition to capability, condition monitoring systems also need to demonstrate reliability in order for companies to trust them.

1.4 Key vehicle components suitable for monitoring

A number of equipment related accidents in the railway industry are due to failed railway vehicle components. Moreover, the continuing increase in train operating speeds means that catastrophic failure of some components, such as a wheel or axle, or other mechanical component, may result in a very serious derailment. In 1996 there was a collision between two trains at Rickerscote, Stafford. A freight train travelling south towards Wolverhampton became derailed. The derailed wagons blocked the adjacent line and were run into by a travelling post office train causing a Royal Mail employee to be killed. The direct cause of the accident was reported as the fracture in mid-span of an axle fitted to one of the 2 axle wagons in the freight train [5]. In 1998 a serious high-speed-rail derailment happened at Eschede in Germany. In the Eschede train disaster, a high-speed train derailed and crashed into a road bridge causing deaths and serious injuries. This accident remained one of the worst rail disasters in the history of the Federal Republic of Germany and the worst high-speed-rail disaster worldwide. The cause was identified and reported as a single fatigue crack in one wheel. The defective wheel caused the train to derail when it finally failed at a set of points [6]. In 2011 an in-service train operating on the Belfast to Dublin line suffered a bearing failure which was confirmed when an axlebox was found to be smoking at Connolly Station [7]. Fortunately, there were no casualties in this accident as the way-side hot axlebox detection equipment had identified the failure causing the train to be stopped.

Wheel section faults are mainly caused by the wheel-rail interface [8], which is impossible to manually monitor when the vehicle is in service; increased axle load is a significant contributor to likely failure [8], the condition of which is difficult to manually monitor in the depot, regardless of being in service. These obstacles make it difficult to progress maintenance practices beyond the level of scheduled maintenance. To overcome these difficulties, condition monitoring makes its contribution in the realisation of transformation

from scheduled maintenance to condition-based maintenance. It can monitor the health condition of components and therefore drive maintenance schedules and practices, while also providing diagnostic information to manufacturers in order for them to improve the design of the components in the first place.

A railway vehicle consists of hundreds of components, but not all need to be monitored. For example seats in the carriages, interior lighting within the vehicle, air-conditioning systems, etc. are not key components that guarantee the safety of the vehicle. Some components, however, are critical to vehicle safety. The wear or failure of rotating components such as wheel sets, axles, gearboxes, roller bearings or the fatigue of cyclical components such as dampers found on bogies could lead to derailment. The failure of detection systems such as those used in train doors could trap the passengers and lead to them being dragged along the platform, while the failure of actuation systems for a pantograph could result in power loss for the train or a coupler could lead to vehicle detachment and possibly to a collision. Failure of any of these could result in serious accidents. Ultrasonic sensors, accelerometers, thermal sensors, acoustic sensors and other sensing techniques have been applied to provide condition monitoring of these components. These techniques are discussed in detail in the literature review chapter (chapter 0).

1.5 Way-side condition monitoring of railway vehicles

Considering the mechanically moving key components of the vehicle, most involve a regular movement either rotationally or cyclically. A good way to identify faults in these components is to “feel” for vibrations in the component which increase as the component becomes more damaged. Sensors such as accelerometers can be used to measure these vibrations, essentially acting as a “touch” sensor. Touch sensors are key components in onboard measurement systems. However, these sensors have to be installed on the vehicle, and on every component that is to be monitored.

If a vibration in a component is big enough it starts to move the air around it. At certain frequencies, this air movement can be heard as a sound. “Listening” for a fault is another condition monitoring approach which doesn’t require physical contact with the component being monitored. The main disadvantage of listening based condition monitoring systems is that it is hard to listen to just the component and so the systems are usually less sensitive than touch versions. If the component is moving, e.g. on a railway vehicle, you have to listen to a moving object and this is even harder. The advantage, however, is that one monitoring system can be used for all of the trains in a fleet.

Condition monitoring systems can therefore be divided into two types, onboard and wayside. Onboard systems use direct measurements to obtain the clearest indicators of condition, but it is a costly approach as the system has to be installed on each carriage to be inspected. Considering this economic factor, condition monitoring systems have started to move to the trackside where they are also known as wayside condition monitoring systems. These wayside systems are popular and widely used in both research work and industry. In addition, wayside monitoring has advantages when physical access to the object being inspected is limited. Wayside condition monitoring systems can provide effective vehicle condition monitoring without the need for any physical contact, and thus without interfering with the existing railway system.

Consequently, the rail industry has invested heavily in wayside monitoring to minimise the likelihood of a catastrophic derailment [9]. Various wayside monitoring systems, such as the GOTCHA monitoring architecture and the RailBam bearing acoustic monitoring system are used in the railway industry for condition monitoring of railway vehicles to reduce delays, improve operating efficiency, and minimise the possibility of serious accidents and unnecessary costs. Systems such as these are still being developed with incremental

improvements to the hardware and processing algorithms such as those demonstrated in chapter 5.

1.6 The need for integration

Being non-contact is one of the most outstanding advantages of wayside condition monitoring systems. Although they are more complex in both data collection and processing, the potential economic benefit still drives research in this area. Each railway vehicle component has a range of corresponding CM technologies, this is explored in the literature review in chapter 0. However, even the most appropriate condition monitoring techniques for each type of fault still have shortcomings. For example, hot axle box detectors are only able to detect faults at late stages of development immediately before catastrophic failure is likely to happen [10]; Acoustic Emission sensing systems, used for crack detection in wheels and rails, need access to the track area to install the sensors. A review of the advantages and disadvantages of vehicle condition monitoring techniques is presented in chapter 0.

The usual approach to overcoming shortcomings in the independent CM techniques is to make improvements to their hardware or processing algorithms. This is generally done in isolation. However, some limitations cannot be overcome by a technology itself. For example, wheel flats can be heard when the train moves on the track. The repeating contact between the wheel's irregular surface and rail head generates the noise which acoustic monitoring systems listen to. However, listening to a vehicle can hardly tell if the train door is properly closed or if the carriages are securely coupled. These components can be more easily monitored by looking at them, i.e. by sight. Therefore, the integration of eyes and ears, which are similar to acoustic sensing and vision imaging in the railway condition monitoring context, could help overcome each other's limitations by obtaining and combining extra information. Furthermore, with a sufficient understanding of each independent technology, a closer integration of multiple monitoring technologies could be another way to enhance the

performance of each component of more closely integrated inspection and monitoring systems. The approaches to integration considered in this study, are discussed in section 1.7.

1.7 Approaches to integration

This thesis will consider two potential approaches to the integration of multiple condition monitoring technologies. These are described as “system level” and “signal level”.

Considering the integration between these technologies from the perspective of a system level, the outputs of the two (or more) monitoring systems can be combined such that a carriage should to be paid particular attention on if it is identified as being at risk by both systems. Such integration can lead to better business decisions being made than those based on information from each individual monitoring system. Such combined decisions can increase the efficiency of maintenance arrangements to save costs [11]. Beyond this, it may also be possible to integrate the independent techniques using a more intelligent approach. This would require a more detailed understanding of each technology in order to identify the limitations of each and therefore how one technique can support the other.

Section 1.6 considered two senses, listening and seeing. An acoustic based condition monitoring system listens to the target components as the railway vehicle passes. The precise location of where the audio signal comes from is therefore important as the system needs to listen to the correct place at the right time. In addition to being able to assess the condition of specific components, vision imaging systems can “see” the precise position of a passing train. Systems like high-speed cameras can therefore be used to provide real-time speed measurements of fast moving train and information about the position of important components. Therefore, the integration between visual and audio systems at the signal level can support improved acoustic measurements by providing better targeting solutions.

1.8 Hypothesis and objectives

The central hypothesis addressed in this thesis is, is it possible to integrate independent condition monitoring technologies to achieve enhancements in condition monitoring of railway vehicles. The following four questions are used to direct the study:

- (1) What components of a railway vehicle could be reliably inspected?
- (2) What are the most appropriate technologies or methods for detecting different vehicle component faults?
- (3) Can these technologies be improved in isolation?
- (4) Is there benefit in integrating multiple technologies or methods to improve fault detection and diagnosis?
 - a. What are the benefits from integration?
 - b. How to achieve the benefit?

Several of these questions can be answered from the literature. As the integration of two technologies involves both hardware system development and data analysis, the literature will be considered in two parts. The components to be monitored will be reviewed in chapter 0. This will include corresponding existing monitoring technologies for railway vehicle components as well as considering the strengths and weaknesses of each individual technique. Signal processing techniques appropriate for railway applications are reviewed in chapter 3.

With the first two questions being addressed through the literature, the remaining two questions present clear objectives for the study. The objectives of the study are to process the data streams from the independent condition monitoring technologies to improve the

monitoring performance in isolation, and then to develop integration solutions at both the system and signal level to achieve further benefits. The review of the literature carried out in Chapter 0 will identify two condition monitoring technologies to be further considered throughout the thesis.

The third question above relates to the individual improvement of monitoring technologies. To obtain a good understanding of each technology, and to support later integration, laboratory-based experiments and proof-of-concept field tests were carried out using the two selected CM technologies. The methodology used is discussed in chapter 4. Laboratory-based experiments provide a platform to understand the properties of the recorded signals, and proof-of-concept field tests can validate the development efforts in a real world scenario. The field tests are further divided into those carried out at a research centre site and those on the Network Rail High Speed 1 Line. The hardware development process is verified in the laboratory-based experiments in controlled conditions first, and then expanded to the proof-of-concept field tests. This evaluation work allows the hardware systems and signal processing algorithms to be investigated in depth. Isolated improvements are demonstrated, and areas suitable for integration are identified in chapters 5 and 6.

The fourth question in the hypothesis relates to integration and is the core of this thesis. The relevant development work includes obtaining a good understanding of two technologies to be integrated during the investigation required to answer to the question about individual improvement. Integration plans and the development of the integrated system are demonstrated in chapter 7. The hardware system development mainly focuses on the integrated system frame which physically integrates two independent CM technologies together. The system level integration plan and signal level integration plan are the approaches used to achieve the benefits from integration and are discussed in chapter 7. The

achievements from integration are demonstrated through the results from the field tests on the Network Rail High Speed 1 Line in shown in chapter 7.

1.9 Thesis structure

The detailed structure of the thesis is given below:

- i. Chapter 1 is the introduction chapter. In this chapter, the background of the work is presented along with an introduction to condition monitoring and non-destructive testing in all aspects of railway vehicle condition monitoring. In the second part of the chapter, the importance of the integration of multiple technologies is addressed. The last part of the chapter describes the hypothesis and objectives of the study, and presents the thesis structure.
- ii. Chapter 2 presents a review of the railway vehicle components that need to be monitored, and the corresponding monitoring technologies. The technologies are considered by the category of vehicle related faults that they can be used to address. As one of the key components to be considered in this thesis is axle bearings, roller bearing inspection and monitoring technologies, especially the acoustic sensing technologies, are reviewed in detail. The chapter also includes a review of machine vision monitoring technologies.
- iii. Chapter 3 presents a review of signal processing techniques that can be used in the railway. As the technologies to be integrated are acoustic sensing and vision imaging, the review of signal processing techniques is divided into roller bearing acoustic signal processing and image processing techniques.
- iv. Chapter 4 is the methodology chapter. The work is decomposed into sub-tasks: laboratory experiments, field tests at a research testing site, and field tests at the High Speed 1 Line. The methodologies of the hardware system design and test set-up for

each task are discussed. The monitoring system and test program then drives the development of the processing algorithms.

- v. Chapter 5 is about the development and demonstration of acoustic sensing technology. It is considered in several applications: vibration sensor based inspection and monitoring experiments in the laboratory, acoustic sensor (microphone) inspection and monitoring experiments in the laboratory, and acoustic sensor (microphone) inspection and monitoring field tests. The vibration sensor based inspection and monitoring application has been generated a journal paper which is demonstrated in section 5.2. The microphone based inspection and monitoring application is going to generate another journal paper currently in development. The three applications require three different signal processing solutions. In this chapter, the development procedure and results for each application are individually demonstrated.
- vi. Chapter 6 presents a demonstration of vision imaging technology for a range of applications. It starts with a hardware system overview and a discussion of the key parameters involved in high-speed camera selection. There is then a discussion of computer vision techniques appropriate for the required image processing. The chapter describes how the vision imaging technology has been applied in two cases: coupler and pantograph inspection and monitoring. The results of each case are demonstrated individually.
- vii. Chapter 7 describes the integration of the acoustic sensing and vision imaging technologies. The chapter starts with a discussion of the integration plans. The integration is considered at the system level and the signal level, and a plan is made for each type of integration. The field tests for system level integration were carried out at the High Speed 1 Line. The test set-up is described and the inspection and monitoring results from system level integration are demonstrated. The development

and demonstration of signal level integration has used three scenarios: a test train at a research site, a passenger train on the Birmingham Cross-city line, and a passenger train on the High Speed 1 Line. The results and analysis of the signal level integration system are demonstrated for each scenario. A paper describing the ISMS and demonstrating this signal level integration with the acoustic system has been published by the author.

- viii. Chapter 8 presents the conclusions drawn from this thesis. The chapter states the hypothesis of this thesis has been validated and presents the achievement in this work. This chapter also suggests further areas of related research.
- ix. Appendix.

2 Review of railway vehicle inspection and monitoring technologies

Railway services play an important role in transport networks in the UK and Europe. With the existing rail network, passengers can easily travel cross-border and intercity between the UK and Europe. In 2014, the total number of rail passenger kilometres travelled in the UK was 62 billion, an increase of 3.4 percent on 2013, and a 17 percent increase compared to 2010 [12]. These increasing figures in national railway usage indicate that rail services are becoming more popular as a choice of transportation. To provide a good and reliable service, railway companies check and maintain the railway infrastructure and vehicles on a regular basis. Railway safety is a core issue in need of attention. In order to ensure safe railway operations, as well as meet the growing demands for cost efficiency, reliability and safety for railway vehicles and services [13], condition monitoring routines are often implemented [14].

Condition monitoring routines are usually employed using non-destructive testing (NDT) methodologies. NDT is a broad name for a variety of methods and procedures concerned with examining all aspects of uniformity, quality and serviceability of materials and structures, without causing damage to the material that is being inspected [14].

Research on the application of NDT methods has been ongoing since 1877 [15]. Visual inspection is the basic approach for many railway components, which is usually conducted by skilled personnel. Other NDT technologies are used as a complement circumstantially. The first rail inspection vehicle using magnetic inducing sensors was developed in the 1920s [16]. Magnetic induction was the only technology available for the high speed inspection of rails until 1953, when ultrasonic transducers were added to test vehicles for the first time [16]. Since then, the NDT concept for the high speed inspection of rails has remained largely

unaltered [17]. The NDT of railway vehicles is equally as important as the NDT of the railway infrastructure.

2.1 Vehicle health monitoring

Vehicles with poorly performing components, such as axle bearings, gearbox, wheels, brake, bogie, flange or axle, are likely to need maintenance. In the railway industry, the maintenance strategy has been cycle-based and depot-based maintenance for years. The cycle-based strategy carries out the maintenance when the life cycle of the vehicle components is estimated to be approaching the end; while the depot-based strategy is to bring the vehicle to the depot to carry out the inspection and repair work within a certain maintenance cycle. Both of these two strategies are based on an estimation of the component's condition to form the maintenance plan. Wayside monitoring systems have been widely discussed and considered for improving the railway maintenance scheme. Wayside monitoring systems, which are installed along the sides of tracks, are becoming commonly used in railways to monitor the vehicle condition. One reason for the use of wayside monitoring systems for vehicles is that the cost of monitoring can be extremely high if devices need to be installed on each vehicle. Another reason is that an increased amount of monitoring devices on the vehicle also increases the complexity of the alarm system, which can result in a higher risk of creating false alarms [18]. Many wayside monitoring systems are connected to the railway network, and can transmit extensive information about vehicle condition to the terminal in order to assist the maintenance decision making.

A variety of fault types occur in vehicle components. Researchers have been working on the development of applicable inspection methods for decades. The major fault types and corresponding monitoring technologies are set out in Table 2.1 below:

Table 2.1- List of major types of fault of vehicle components [8]

Fault Name	Fault description
Wheel relative faults	Wheel section faults are mainly caused by the wheel-rail interface, including wheel impact relative faults, wheel profile wear faults, cracked wheel faults and wheel slide faults.
Bearing faults	Bearing faults are normally caused by defects in the geometric structure components, such as taper/roller, inner race, outer race and cage.
Gearbox faults	Similar to bearing, gearbox faults also occur in the geometric structure. Tooth breakage and misalignments of the shafts are the most two common faults.
Bogie faults	Bogies operate in a crabwise motion, moving diagonal to the direction of travel, or try to turn around a corner all the time cause increased wear. Bogie wear fault is the key issue of its maintenance. Inspection of bogie is by the measurement of the components it contact with in order to infer its behaviour.
Axle faults	Increasing axle load results in failure being more likely to occur. In order to monitor the condition of axle, the axle load can be determined by measuring bending of the rail web or foot; and it is possible to use a load cell to determine the axle load.
Coupler faults	The most common coupler fault is decoupling caused by worn parts of the mechanical components. Manual visual inspection in the depot is used to detect this fault.
Pantograph	Anomalous dynamic behaviour of the pantograph reveals an unhealthy condition. The worst situation is detachment from the overhead line, in which case the air cylinder releases air pressure dropping pantograph without control.

There are different ways to categorise the monitoring technologies, either by using sensing technology, such as mechanical sensors, acoustic sensors, thermal cameras or range finding lasers, or by the type of fault. In this thesis, the author reviews the monitoring technologies by the category of fault. The key faults and their corresponding technologies are described in the following sections.

2.1.1 Wheel impact relative faults inspection and monitoring

The strain-based wheel impact monitor (WIM) is a widely used non-contact method of quantifying the extent of damage on the wheel. Strain in the rail foot or web may be used as a direct measure of the load at the rail head, which bends the rail [8].

The advantage of this system is that the relationship between the wheel and the rail could previously only be calibrated by mechanical means. However, using the strain-based method, the force between the wheel and the rail can only be monitored for 90 percent of the wheel revolution, at best [19]. Accelerometer-based WIM, which measures the motion of the rail by installing accelerometers, can overcome the shortcomings of the strain-based method. One of the advantages of this method over strain-based WIM is its ability to detect impact across the section of rail, providing condition monitoring for the entire circumference of the wheel. However, there is little information available about the processing of accelerometer output [8]. Kalay et al. [20] reported the peak acceleration as a measure of damage, although this is considered to be only one way of reporting the response of an accelerometer. Lechowicz and Hunt [21] reported wheel impact loads in kiloNewtons, although they provided no indication of their method.

2.1.2 Wheel profile wear faults inspection and monitoring

Wheel profile is an important factor in the wheel-rail system inspection; it is critical to both the stability of a vehicle and the rate of wear and rolling resistance of the wheel and rail. Condition monitoring of the wheel profile can allow scheduled maintenance of each vehicle.

Wheel profile detectors work by using digital image acquisition and manipulation to determine the exact wheel profile. The collected information is compared against the standard profile and then a report is generated to reflect the difference between the actual and template profile. This allows the maintenance to be planned in advance and removes the need for

manual profile inspection. In some cases of commercially available wheel profiling devices, such as the wheel parameters measuring system in Mermec [22], the image acquisition equipment is installed in a box which is dug into the ballast. Lasers are often used as a source of illumination while a digital camera captures the images of the wheel profile. Some wheel profile measuring devices can also be lit by ambient lighting. The performance of a wheel profile detector is dependent upon the alignment of the lighting and the camera, relative to the track and to each other [23] [24].

2.1.3 Cracked wheel faults inspection and monitoring

A cracked wheel can spall, causing wheel-rail impact. In the worst case scenario, a wheel with a very large crack can fracture, resulting in a derailment [25]. There are a number of methods of non-destructive inspection of vehicle components, amongst which ultrasonic evaluation has found favour as a means of automatic inspection of wheels [25] [26] [27] [28] [29]. However, this inspection necessarily occurs at very low speeds at the present stage of system development. Researchers are focusing on improving the data processing speed of the system in order to allow it to work at high speeds. Using electromagnetic acoustic transducers, cracks can be detected when they are small, then the wheel can be turned using a lathe until the crack is machined out. The advantage of this method is that an acoustic couplant between the transducer and test specimen is not required [29]. However, details of this method are scarce. Other researchers have used water as a couplant to pass ultrasonic waves into the wheel [25] [28]. By exciting shear waves in the wheel, it was possible to detect 1.2 mm and 7.1 mm wide cuts of major and minor dimensions, respectively [30].

2.1.4 Wheel slide faults inspection and monitoring

Many factors can cause sliding or skidding wheels to occur; the two most likely factors are mechanical failure and human error. When wheels are sliding or skidding, they are not rolling

as fast as they should, compared to the velocity of the vehicle. Sliding wheel detectors are systems designed to detect sliding or skidding wheels by measuring the velocity difference. There are also mechanical sliding wheel detectors. They use the velocity difference between the sliding wheels and the vehicle by placing a roller in contact with the flange of the passing wheel. The roller rotates backwards when the wheel is rotating forward normally, but changes direction when the wheel is sliding [31].

A hot/cold wheel detector can detect the heat signature of the wheel, and detect anomalies when skidding or sliding occurs. At the same time, an infrared camera is also used to detect sliding wheels, by detecting the heat built up at the sliding contact point [8].

2.1.5 Bogie wear and hunting faults inspection and monitoring

Cyclic motion of a rail vehicle (transient lateral motion ('hunting') instability) leads to increased wear of vehicle components, physical damage of tracks, and in extreme cases, can also result in derailment [8]. Similarly, bogies operating in a crabwise motion, moving diagonal to the direction of travel, or continuously trying to turn a corner, cause increased wear and could result in a derailment. There are two methods of measuring the condition of bogies and vehicle 'hunting'. One is to measure the loads applied to the rail as a result of the condition of the bogie and vehicle 'hunting' by using a strain gauge bonded to the rail. The other is using non-contact devices (optical) to observe the effects of poor bogie performance, such as the angle of the wheel relative to the rail (angle of attack) or vehicle 'hunting' [8].

2.1.6 Axle load faults inspection and monitoring

The axle load can be determined using strain gauges, which can measure the bend of the rail web or foot. It is also possible to use a load cell to determine the axle load. Weigh in motion technology is used to detect the axle load. The monitoring devices can also be used to detect an overladen vehicle. One manufacturer offers three load cell-based weigh-in-motion

devices [32]. Many wheel impact monitoring systems are capable of determining both the static axle load and the dynamic wheel load. Theoretically, the mean load on the rail over one revolution of a wheel approximately equals the static axle load, although there are some speed effects which need to be accounted for [8].

2.1.7 Bearing wear and gearbox faults inspection and monitoring

Roller element bearings have widespread domestic and industrial applications. They are extensively applied in the transportation and manufacturing industries, where they perform an important role. In the vast majority of rotating machines, roller bearings are one of the most critical mechanical components. They can normally work well in non-ideal conditions, but sometimes minor problems can cause bearings to fail rapidly and unpredictably. For instance, the small vibrating load on the train could gradually press out the lubricant between the races and rollers or balls of bearings. The bearing fails without lubricant, even though it is not rotating and thus apparently cannot be used. Therefore, without proper early inspection, a seized bearing could shear the axle, resulting in a train derailment.

Hot axle box detectors are intended as a device to prevent the seizure of bearings, especially when the train is in service. They have been in use since the 1960s. As is well known, an axle bearing will become very hot when it is close to failing [33]. The working principle of a hot box detector is to detect the heat emitted by the bearing and report the imminent failure. Bearings can heat up and seize extremely rapidly; just prior to seizing, they will heat up to the point where they would trigger a hot box alarm. The commercially available detectors are normally installed in a box alongside the track (shown in Figure 2.1). However, the record time for passing a hot box detector (normal condition, no alarm triggered) and failing before the next hot box detector, is 96 s [8]; this is one of the major shortcomings of standalone hot box detectors. Another shortcoming is their low sensitivity to incipient damage [34].

The limitations of the hot box detector as a predictive device have led to the development of acoustic bearing defect monitoring. Bearing defects produce vibrations at frequencies related to the geometry of the defect [33]. Acoustic bearing monitors determine the response of the bearing as the vehicle rolls by, thus enabling bearing inspection without disassembling the bogie. It is intended that the method should differentiate between a healthy bearing and spalling of the cup or cone, or spalled, etched, or seamed rollers [35]. It is also possible to determine the extent of damage in the bearing using the cross spectral density, the energy, and the frequency spectrum [36]. More details of bearing faults and bearing monitoring technologies will be discussed in Section 2.2.



Figure 2.1- Track IQ company hot box detector [37]

2.1.8 Coupler inspection and monitoring

A coupler is a mechanical component used to connect rolling stock in a train. There are a number of standard designs for couplers, and their reliable operation is key to the safe operation of the railway.

The standard type of coupling in the railway in the UK has evolved from a traditional British coupling mechanism called a buffer and chain coupling shown in **Error! Reference source**

ot found.. The coupling mechanism has been developed and now uses various, more advanced, types of coupler such as the Albert coupler, Dellner coupler, Wedgelock, etc.



Figure 2.2- An example of a buffer-and-chain coupler [38]

There was an accident in Canada in 2014 [39] in which a locomotive was decoupled from the following wagons when making a left hand turn resulting in a collision with a security building at the track side. Unlike the current situation in axle bearing monitoring, coupler condition is generally inspected manually, and little literature is available on research into coupler inspection.

2.1.9 Pantograph inspection and monitoring

A pantograph is a mechanism mounted on the roof of a railway vehicle to collect power through contact with overhead line. Most common types of pantograph in use today are Z-shaped pantographs [40] which have evolved to provide a more compact and responsive single-arm design at high speeds. A single-arm Z-shaped pantograph is shown in **Error! eference source not found..**



Figure 2.3- An example of a Z-shaped pantograph [40]

The contact between a pantograph and the overhead line must require a sufficient lifting force to apply a consistent force to the contact wire when the train moves [41]. Anomalies in either the pantograph or the overhead line can result in contact loss, which can lead to an accident. There was an accident in 2012 in which a pantograph assembly fell from the roof of a passenger train, breaking two windows. Fortunately there were no casualties. The accident report identified that the pantograph head had lost contact with the overhead line resulting in the pantograph arm hitting the overhead line support structure and falling down from the roof due to an electrical insulator being broken [42].

Pantograph monitoring is therefore important both for safety and reliability because it is through the pantograph that power is supplied from the overhead line. Research on pantograph monitoring generally focuses on the contact between the pantograph and the overhead line system, such as the contact between pantograph and catenary [43], the contact strip [41], etc.

2.1.10 Conclusion

The vehicle components listed above are mostly the steering and shaft relevant components because these components are critical to the safety of the railway vehicles. Train wheelsets consist of three key component types, the wheels, the axle and the bearings. Between them, these components make up a large proportion of the rolling stock equipment related accidents in the rail industry [2]. To avoid catastrophic failure, wheelsets are inspected at regular intervals in order to detect the presence of defects or faults. Effective wheelset inspection requires its removal from the train bogie at appropriate maintenance intervals. However, wheel and axle bearing defects and other causes of railway vehicle failure can develop in service and evolve very rapidly. The performance of current in-service bearing inspection and monitoring technologies, which has been reviewed above, can be further improved. Roller bearings are therefore one of the key vehicle components to be considered in this thesis.

At the same time, pantograph and coupler, these two key components of railway vehicle needs the contribution in developing their automatic condition monitoring technologies. In the railway industry, there are several monitoring platforms to measure the quality of various aspects of vehicles. For example, the Gotcha system [44] has been applied to railway lines. Within the system, the most common modules used are Wheel Defect Detection to monitor the quality of the wheels and the Weighing in Motion to determine the load of a passing vehicle. Vision imaging technology is becoming increasingly popular as a non-destructive condition monitoring technique. It can inspect various mechanical components of a vehicle. These techniques are discussed in the literature review chapter (chapter 2.3). So it has been chosen as another technology in this thesis to monitor the condition of pantograph and coupler, and to integrate with acoustic sensing technology. In the following chapters, the review of roller bearing inspection and monitoring technologies and vision imaging inspection and monitoring technology are going to present in order.

2.2 Roller bearing inspection and monitoring technologies

Roller element bearings have been extensively applied in the transportation and manufacturing industries, where they are playing an important role. In the vast majority of rotating machines, roller bearings are one of the most critical mechanical components.

A bearing carries a load by placing round elements between two bearing rings. As shown in Figure 2.4, which depicts a bearing also known as a rolling bearing (ISO 15), the three main parts are: outer race, roller, and inner race.

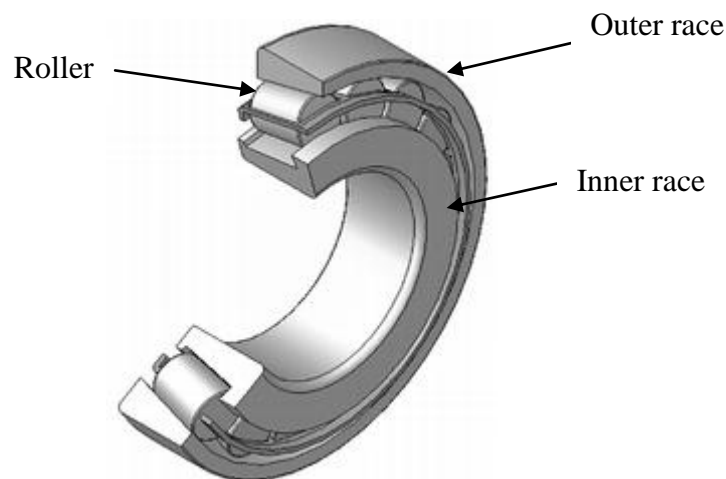


Figure 2.4- Tapered-roller-bearing [45]

2.2.1 Bearing failure

Rolling element bearing faults are generally categorised into four groups: roller damage, inner race defect, outer race defect and cage damage [46].

Figure 2.5, Figure 2.6 and Figure 2.7 are the three different types of bearing faults. The roller damage condition is shown in Figure 2.5. In general, damage to the roller is caused by scratches and spalling. As seen from the photo, both of these two types of damage have occurred on the rollers. The outer race defect condition is shown in Figure 2.6. Defect of the outer race is mainly caused by rolling scratches, and is exactly the same as inner race defect.

In the photo, series rolling scratches can be seen on both the upper and lower part of the outer race. The cage damage condition is shown in Figure 2.7. It can be seen from the photo that one section of the cage is cracked and the roller in that section is scratched as well.



Figure 2.5- roller damage of tapered-roller-bearing [47]



Figure 2.6- outer race defect of tapered-roller-bearing [48]

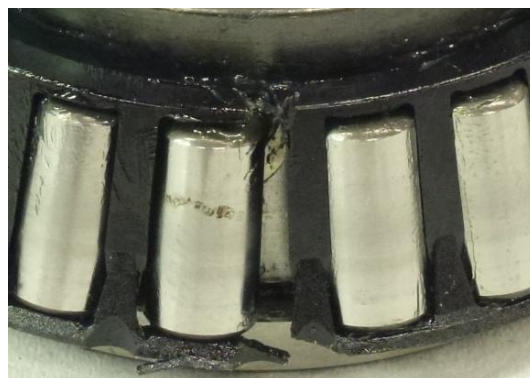


Figure 2.7- cage & roller damage of tapered-roller-bearing

A proper inspection and monitoring method for bearings should be able to detect any of these defects. The advanced detection requirement is to not only simply detect the defect, but also to distinguish the type of defect.

2.2.2 Inspection and monitoring of roller bearing

To meet the requirements for inspection and monitoring, a proper technology should be capable of informing the train service providers of the rate of degradation. When the condition of the bearings approaches the triggering threshold of the maintenance scheme, maintenance planning can immediately be carried out. In this way, passenger and freight travel will not be affected by short notice maintenance. A large number of publications have been written about roller bearing diagnosis methods, in which the technologies can be broadly classified as vibration and acoustic measurements, temperature measurements and wear debris analysis [49]. Of these, vibration and acoustic measurements are the two most widely used methods. Several technologies have been applied to measure the vibration and acoustic responses from a defective bearing: vibration measurements in time and frequency domains, the shock pulse method, sound pressure and sound intensity technologies, and the acoustic emission method. In this thesis, vibration and acoustic measurements technologies are used and applied. These two technologies are introduced in detail in the following sections.

2.2.3 Vibration measurements

As an element of machinery in a rotating system, the bearing itself is a source of vibration and noise due to its manufacturing design and the interactions between the rolling elements and races [50]. However, there are other sources of bearing vibration which are not generated by the bearing itself. Lynagh et al. presented an analytic model of bearing vibration to describe the inside of a bearing and its supporting mechanical system [51]. The factors

causing the vibration are numerous. The main sources are the rolling element characteristic frequencies, so called bearing inherent frequencies, which are generated by bearings in any supporting structure of rolling elements. These characteristic frequencies of each bearing have four different values from different sources: fundamental train frequency, ball pass frequency outer race, ball pass frequency inner race and ball passing frequency. The fundamentals will be explained in section 5.1.1. Researchers working in the field of bearing diagnosis always emphasise these characteristic frequencies to diagnose bearing faults [52, 53]. Another main source of vibration is out-of-balance rotation caused by the variance between the centre of the shaft axis and the geometric centre of the bearings [51]. There are many other sources of bearing vibration which are regarded as secondary effects, such as waviness of rolling elements and the existence of abnormal ball elements and races [51]. These anomalies also contribute to the vibration spectrum of the bearing, but are significant at high frequencies. The secondary effects are important in understanding the behaviour of the machinery system. With the respect to the diagnosis of the bearing, the anomalies caused by secondary effects are outside the range in which bearing inherent frequencies fall. When defects occur in the bearing, the vibration energy at the responding characteristic frequencies significantly increases [54].

The non-stationarity of the bearing signal is a result of the random fluctuations of the bearing signals during the experiment [55]. Each bearing element has specific characteristic frequencies, which are the geometric properties of the bearing; these properties are widely used as direct information about the fault in the bearing diagnosis, and are called characteristic defect frequencies [56]. Due to the non-stationarity of the bearing signal, it is difficult to identify significant peaks at the characteristic frequencies in the spectrum unless the defect is predominant [57]. Hence, preparation (pre-processing) of the vibration data for standard envelope analysis technologies [58] is very important and can be complex. A brief review of vibration monitoring technologies in the time and frequency domain and the results

on rolling element bearings, including recent works, is presented by Tandon and Choudhury [49]. Analysis of frequency domains, combined with statistical features, has been one of the most effective methods of processing.

Recently, researchers found that the vibration measurement can detect defects only when they appear on the surface, but acoustic emission monitoring can detect the growth of subsurface cracks [49]. This is the advantage of acoustic emission monitoring over vibration monitoring.

2.2.4 Acoustic measurements

2.2.4.1 Acoustic emission sensor

Acoustic emission (AE) is the phenomenon of transient elastic wave generation due to a rapid release of strain energy caused by a structural alteration in a solid material under mechanical or thermal stresses. Generation and propagation of cracks, and growth of twins associated with plastic deformation are among the primary sources of AE [49].

AE instruments consist of a transducer, a preamplifier and a signal-processing unit. The transducer type is mostly piezoelectric. It has a very high natural frequency, and its response is resonant-type. In the preamplifier, a suitable filter can be used to control the bandwidth of the AE signal. The advantage of AE monitoring over vibration monitoring is that it can detect the growth of subsurface cracks, while the vibration measurement is only capable of detecting the crack on the surface [8]. Another advantage is that the AE signal can be controlled in a very high bandwidth, which can simplify the noise separation.

Several studies have been conducted to investigate the AE measurement of defective bearings [59, 60, 61, 62, 63, 64]. Tandon et al. demonstrated the usefulness of some acoustic emission parameters, such as peak amplitude and count, for the detection of defects in radially loaded ball bearings at low and normal speeds [65]. Tandon also applied the adaptive filtering technology to demodulate the useful AE signal from the background AE noise [66]. The

usefulness of the demodulated AE signal has been demonstrated by other researchers in rolling element bearings diagnosis [67, 68, 69].

2.2.4.2 *Air-coupled acoustic sensor (microphone/ microphone array)*

A traditional acoustic sensor, such as a microphone, can also be used for roller bearing inspection and monitoring. The most outstanding advantage of an acoustic sensor over vibration and acoustic emission monitoring systems is that the installation of the sensor is air coupled, whereas the sensors in the other two systems need to be surface coupled on the bearing cage or rail. In certain circumstances where physical access to the bearing is limited or difficult, it is more practical to use the traditional acoustic sensor monitoring system [70].

In this monitoring system, the microphone array is used to record sounds from passing vehicles. The sensors focus on the axle bearings. It is well known that bearing defects produce vibrations at frequencies that can be connected to the characteristics of the defect [71, 72]. Until the 1990s, there was little literature available on sound measurements as an inspection technology [49]. However, in the last decade, this technology has grown in use. There are two commercial products which are examples of this technology: TADSTM and RailBAMTM. These systems have been used in North America and Australia, where they have been evaluated with satisfactory results [73, 74]. Recently, TADSTM has been used in the railway industry in China, where it has also had satisfactory results. Although these systems cannot currently detect all bearing defects, the predictive performance is where the hot box detector cannot compare.

2.3 Vision imaging inspection and monitoring technologies

The inspection and monitoring technologies were reviewed by the categories of fault set out above. The vision imaging inspection and monitoring technology can be used for monitoring a large amount of applications, such as bogie wear, lateral displacement, hunting and angle

attack of wheelsets, brake pad, springs, missing end cap bolts and coupler faults. The potential application possibilities of vision technology are laid out in [8]. The detailed review of vision inspection and monitoring is discussed in this section. The vision imaging inspection referred to here is not the manual process conducted by inspection personnel, but the application of computer vision to railway condition monitoring. There is not a standard definition of computer vision is beyond the scope of this thesis, but in general terms it is an inverse process of how human beings understand the world using their visual system [75]. It is an automated process supported by various complex algorithms. Although the realisation of automation is not easy to achieve, the benefits are significant.

The application of computer vision to railway condition monitoring is new, and it has only become popular in the last two decades. The installation methods of the image recording instruments are categorised as: the camera installed on the vehicle (such as on top of the locomotive, or on the bogie), the camera installed wayside, and the camera installed underground.

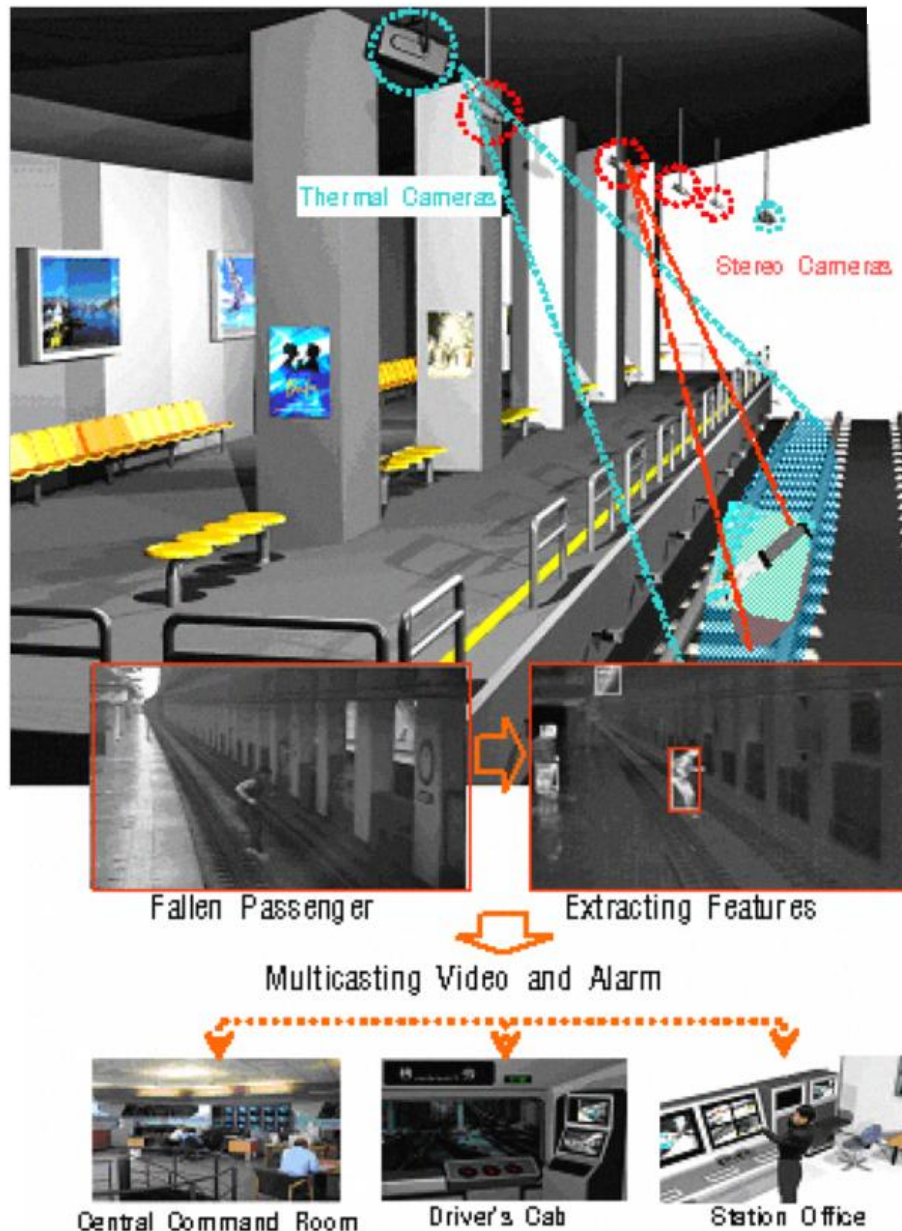


Figure 2.8- System concept of vision-based monitoring system [76]

In 2001, Chow et al. implemented a neural vision system to monitor the passenger flow on underground railway station platforms [77]. The camera is installed on the platform to record the passengers. The aim of the system is management of crowds on the platform in order to prevent accidents from happening, such as passengers falling off the platform edge. In the following year, Prassler et al. [78] proposed a method for detecting and tracking motion in a crowded environment, aiming to enhance the image processing algorithms. The recording

instrument is a laser rangefinder, installed in the station. This vision monitoring system can be applied to airports, shopping malls and convention centres as well as railways.

Other researchers have also followed the trend to apply vision systems to railway station platform condition monitoring, such as [79, 76, 80, 81, 82]. Oh et al. integrated a stereo camera and a thermal camera to monitor the passenger flow at the platform. The concept of this system is to detect accidents in the track area, such as fallen passengers on the track, passengers beyond the safety line or stuck between the train doors, and so on. Once the possible danger is detected, the result with a video and alarm message is transmitted to the central command room (CCR), the train driver's cab and the station office [76].



Figure 2.9- Image with blue clip in [83]

Vision monitoring systems have also been applied to railway infrastructure and vehicle condition monitoring.

In 2006, Singh et al. developed a vision based system to report missing clips, find and count the newly replaced clips (coloured blue) in order to realize the autonomous rail track components visual inspection [83]. Four years later, Resendiz et al. carried out similar

research to Singh, enhancing the performance of the visual inspection system, which is capable of inspecting clips as well as spikes and anchors [84]. Researchers are still working on track vision monitoring systems [85, 86]. They enhance the system performance by expanding the inspection cover range as well as improving the development of algorithms.

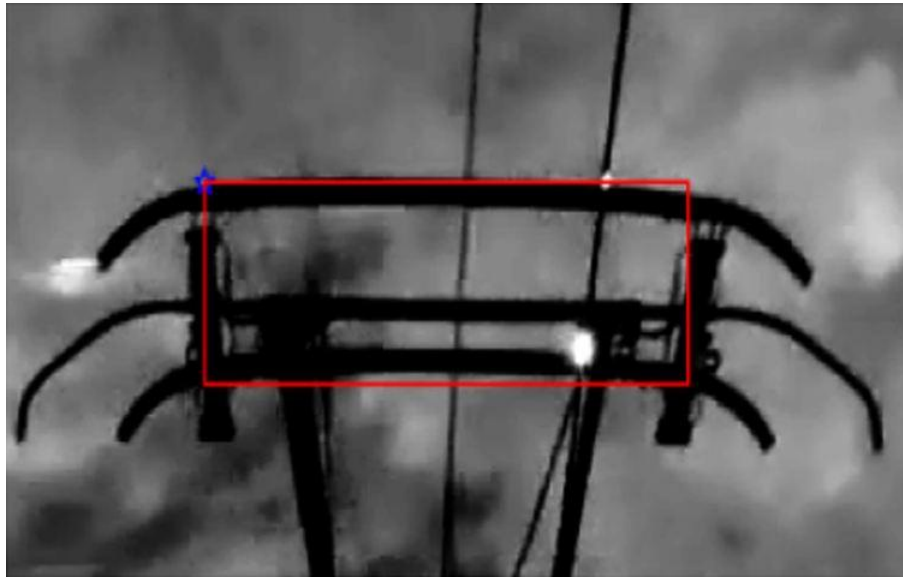


Figure 2.10- Pantograph detection [87]

Recently, the application of vision monitoring systems has become more popular. Aydin applied a vision system to the monitoring of the pantograph-catenary system [87]. Marmo et al. applied vision technology to support train drivers in reading the railway signalling code at the wayside [88]. In these cases the cameras are installed on top of the locomotive.

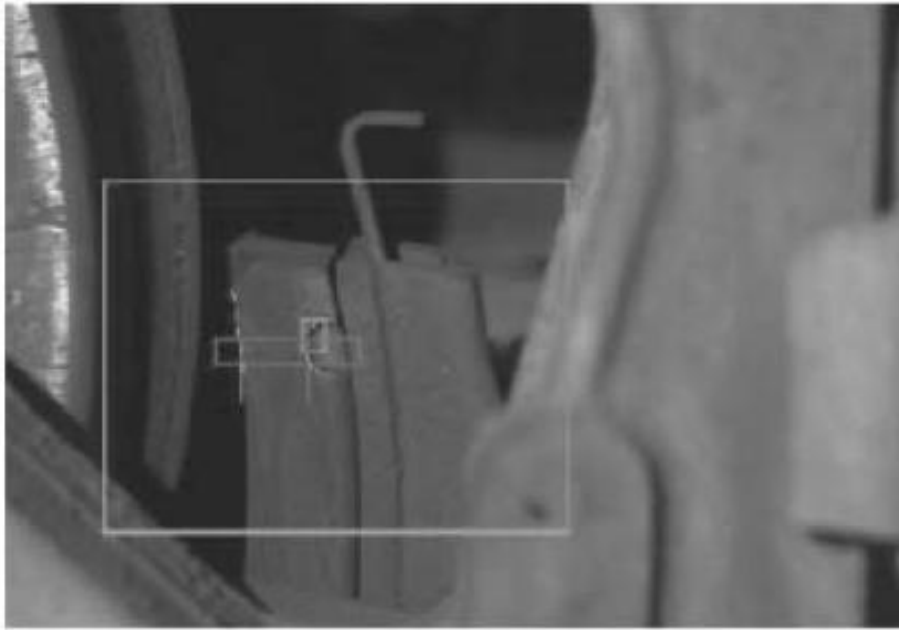


Figure 2.11- The image from a brake pad inspection device [89]

A further use of the vision system is in detecting the extent of brake pad wear. Commercial devices are capable of detecting pad wear to within ± 0.1 to 1.0 mm [36] [90] [91]. The same technology can determine the spring nest deflection to within ± 1 mm and identify broken springs. Vision imaging has also been used to determine whether handbrakes are on, monitor the condition of bearing adapters, and count the number of end cap bolts on a passing bearing. The same equipment could detect coupler faults, such as broken pins, knuckles, and missing bolts, and detect open doors. Images of the door latch are used to determine whether the handle is in the correct (closed) position on the car. Recently, Ahuja et al. developed a vision monitoring system underneath the train in order to detect anomalies including disc brake conditions and incipient failure of electrical systems [92].



Figure 2.12- Field-of-view of the visible image [92]

At this time, there is no system available that completely satisfies the security requirements imposed by the railway system [93]. The current situation motivates further investigative development in this field, with the aim of developing strategies to integrate diverse sensor types, such as cameras, thermal sensors, lasers, etc.

Having reviewed the application of the vision monitoring systems which are currently available, the processing of video data sets is also important. The processing technologies are called computer vision; an explanation of computer vision technologies is included in section 3.3.

2.4 Conclusion

In this chapter, the current situation of railway vehicle inspection and monitoring technologies has been reviewed. The roller bearing and its corresponding inspection and monitoring technologies have been selected to begin the research work due to the critical role it plays in the safety of the vehicle wheeling system. Vision imaging inspection and

monitoring technology could be applied to various components in the railway vehicle, as well as the infrastructure system. These applications have been reviewed in this chapter.

As the corresponding inspection and monitoring technologies of roller bearing, acoustic sensing technology includes directly coupled vibration sensors (accelerometers) and more traditional acoustic sensors (microphones). The vibration sensors (accelerometers) was driven by the need of improvement of hot box detector which is reviewed in chapter 2.2.2. However, its installation requires directly contact with bearing lid. The direct “touch” brings signal in good quality from vibration sensors which are well isolated from the surrounding noise found in the vicinity of a bearing lid. Vibration sensors is useful in laboratory tests to prove that an axle bearing monitoring system works correctly, while its disadvantages are the requirement for touching as well as the requirement for high volume sensors installation. However, the wayside acoustic sensor (microphone) monitoring system is a non-contact system which monitors axle bearings by “hearing” the sound generated by bearing rotation when the train moves. Its installation is not limited by access to the object being inspected.

Considering the advantages and drawback of both approaches, the research work started with the vibration sensor experiments in the laboratory. Carrying out experiments in the laboratory first can reduce the number of variables allowing effort to be concentrated on inspecting and characterising the bearings. The acoustic sensor (microphone) technique has been applied in both the laboratory and field tests. The details of experiments programme are discussed in chapter 4.

The other wayside condition monitoring technique is vision imaging which monitors the condition of vehicle by “seeing”. Among the reviewed vehicle components, the current status of pantograph and coupler inspection and monitoring needs the contribution into transferring the manual inspection to automatic. Therefore, vision imaging technology is selected to validate the potential for pantograph and coupler wayside CM systems.

Having reviewed railway vehicle inspection and monitoring technologies in this chapter, chapter 3 will provide a review of signal processing technologies.

3 Review of railway condition-based digital signal processing technologies

3.1 Overview

Railway condition-based digital signal processing technologies are reviewed in this chapter. More specifically, the digital signal processing technologies of roller bearing acoustic signal and high-speed camera imaging processing are demonstrated.

In terms of digital signal processing techniques, the approaches applied to railway condition-based digital signals are the same as the applications in other areas. Hundreds of thousands of papers appear in this area every year, including theoretical and practical applications. Some published reviews place emphasis on specific systems or diagnostic components [94, 95, 96, 97, 98, 99], and some reviews focus on the processing algorithms and models [100, 101]. The measurement technologies used in this work are acoustic sensing technology and vision imaging technology, and the diagnostic objects are components of the railway vehicle, which more specifically are roller bearings, coupler, pantograph and door/window opening status. Therefore, this thesis reviews the research on signal processing techniques for roller bearing inspection and monitoring, as well as the technologies for vision imaging inspection and monitoring applications.

3.2 Roller bearing acoustic signal processing technologies

3.2.1 Overview

Randall and Antoni divided the processing procedure of the roller bearing signal into two stages: separation of bearing signals from discrete frequency noise and enhancement of the bearing signals [100]. The purpose of the first stage is to mitigate the noise masking of

relatively weak bearing signals. Gears are one of the major sources of the noise, and such signals are strong, even without any faults [100]. A number of techniques are capable of achieving the goal of the first stage, with different pros and cons, such as: linear prediction coding (LPC), adaptive noise cancellation (ANC), self-adaptive noise cancellation (SANC), discrete/random separation (DRS) and time synchronous averaging (TSA). ANC is capable of separating two uncorrelated components using a reference signal containing one of them [100]. When it was first proposed [102, 103], it was applied to the extraction of a faulty bearing signal. However, the reference signal, on which ANC strongly relies, is not easily obtained. SANC is capable of separating the two signal components when one of them is deterministic and the other is random using adaptive filter. Since it uses an adaptive filter, it is capable of adjusting to small speed variations. However, the computational cost would be high, especially for filters of high orders. For this reason, DRS was proposed and has been applied to the separation of a gearbox vibration signal into its deterministic components and random components [104]. TSA is effective on the occasions when there is a need to remove discrete frequency components with minimum disruption of the residual signal. In practice, TSA works by averaging together a series of signal segments which correspond to one period of a synchronising signal [105]. Because of the effectiveness of LPC on audio signal filtering, LPC is one of the most frequently used techniques in audio signal applications (i.e. vocal speech signal) [106]. The fundamental is explained in section 3.2.2.

The signal to noise ratio increases after the first stage. In the second stage, the goal is to enhance and extract the bearing signal from the output of the first stage. In order to achieve this goal, research on the bearing signal properties should be carried out. In Jardine et al.'s review paper, the features are categorised into time domain and frequency domain, and the corresponding analysis approaches are reviewed in the paper [101]. However, a heated debate on the effectiveness of time domain features and frequency domain features is still running. There are various time domain features and extraction techniques [107, 108, 109, 110, 111,

112]. Among these techniques, the features most commonly used for the roller bearing acoustic signal are amplitude, rms, kurtosis, crest factor, count and events [113]. These are time domain features which are effective in inferring the faulty information about the roller bearing.

The advantage of frequency domain analysis over time domain analysis is its ability to easily identify and isolate a certain frequency component of interest [101]. The most widely used technique is spectrum analysis by means of Fast Fourier Transform (FFT). There are other useful spectra for signal processing, which have advantages over FFT spectrum in certain cases, such as cepstrum, bispectrum, trispectrum and holospectrum. Cepstrum is capable of detecting harmonics and sideband patterns in a power spectrum [114]. There are several different definitions of cepstrum, but in practice, cepstrum is most commonly defined as the inverse Fourier transform of the logarithmic power spectrum [101]. Bispectrum and trispectrum are high-order spectrum, which are also called high-order statistics [115]. Application of both bispectrum and trispectrum to bearing fault diagnostics was discussed in [116]. A review of holospectrum and its application was given in [117].

One limitation of the frequency domain techniques above is their inability to handle non-stationary waveform signals, which is one of the common properties of the rotating machinery system, especially when faults occur [118, 119]. The reason for this is that these FFT based techniques do not have a sense of time, but only see the signal as a whole. It is crucial that the technique is able to take both time and frequency into account in order to decompose the signal into a certain period of time windows where the section of signal could be approximately viewed as a stationary. Short-time Fourier transform (STFT) or spectrogram (the power of STFT) works by dividing the whole signal into short-time windows and applying Fourier transform on each element. However, it can only be applied to non-stationary signals with slow dynamic change due to its limitations in time-frequency

resolution [101]. Wigner-Ville distribution can overcome the limitations of spectrogram because it does not work based on signal segmentation. However, the interference terms formed by the transformation itself make interpretation of the estimated distribution difficult [120]. In order to compensate for the shortcomings of Wigner-Viller distribution, Choi-Williams distribution has been developed. It can not only minimise the interference terms, but it can also avoid the interference terms between the forward and backward harmonic components by transforming complex signals into the forward and backward pass analytic signals [121].

Wavelet transform differs from the distributions discussed above. It is a time-scale representation of a signal. The fundamentals of wavelet theory have been discussed in previous researches. A detailed explanation of wavelet transform and its application can be found in [122].

Wavelet transform is made up of a family of wavelets. Let $\psi(t)$ be the mother wavelet; the corresponding family of wavelets consists of a series of son wavelets. The relation between the mother wavelet and son wavelets is shown as follows:

$$\psi_{a,b}(t) = |a|^{-\frac{1}{2}} \psi\left(\frac{t-b}{a}\right) \quad (3-1)$$

where a is scale factor and b is time location, $|a|^{-\frac{1}{2}}$ is a factor to ensure energy preservation. A continuous wavelet transform of signal $x(t)$ is defined as:

$$W(a, b) = |a|^{-\frac{1}{2}} \int x(t) \psi^*\left(\frac{t-b}{a}\right) dt \quad (3-2)$$

where “*” denotes complex conjugate.

The wavelet transform $W(a, b)$ can be considered as functions of translation b each with fixed scale a . As shown in equation (3-2), wavelet transform gives the information of $x(t)$ at different levels of resolution; $W(a, b)$ is the convolution between $x(t)$ and the wavelet function;

the wavelet function measures the similarity between the signal and each son wavelet. In recent years, the wavelet has been suggested by some researchers [123] for extraction of signals in low signal to noise ratio [124].

In the same way as Fourier transform, wavelet transform also has discrete form. The discrete wavelet transform is obtained by discretising a and b . Among the discretisation methods, Dyadic discretisation is the most popular [125]. Although the discrete wavelet transform saves a lot of computation time, its shortcomings make it unsuitable for feature extraction. For example, it demands that the wavelet must be orthogonal, which makes it difficult to find a proper wavelet for the feature extraction. In addition, the sampling intervals in the time-scale plane are sparse, because of which the interesting feature components cannot be extracted and separated from the irrelevant components. Discrete wavelet transform cannot meet an important requirement of feature extraction, which is time invariant [126] . Thus, continuous wavelet transform is used for feature extraction. Morlet wavelet is commonly used because it is very similar to the impulse-like feature of the defective bearing [125, 127].

There is one common feature of the frequency domain techniques mentioned above, such as FFT, spectrogram and wavelet transform, which is that they need to specify the central frequency and bandwidth of their components. However, in some scenarios, particularly when there is significant noise in the signal, it is difficult to define parameters such as the central frequency and bandwidth of the band-pass filter [128]. Elsha et al. suggest improved effectiveness when using an adaptive filter in identifying a naturally degraded bearing under conditions of “relatively large background noise” [129].

In 1996, Huang et al. proposed a new technique called Empirical Mode Decomposition (EMD). The advantage of EMD is that it does not need historical data of the system or pre-knowledge of the signal when it is working on the signal decomposition [130]. It is a time domain filtering technique, but possesses a band pass filter nature which can be well suited to

recover the filtered non linear and non stationary signals. EMD can also optimise the signal distortion, which makes up for the limitation of the conventional band pass filter [131]. The fundamental of EMD is explained in section 3.2.7.1.

More recently, as an extension to kurtosis (introduced in section 3.2.7.1) in the frequency domain, spectral kurtosis (SK) (introduced in section 3.2.6) has been widely used in roller bearing acoustic signal processing and analysis. It is commonly used in the rotating element inspection and monitoring. SK can overcome the shortcomings of the traditional frequency domain analysis techniques by automatically setting the parameters such as the central frequency and bandwidth by itself. SK also has the advantage of not requiring historical data of the system or pre-knowledge of the signal [118]. Especially when SK is applied to the roller bearing diagnosis, kurtosis can tell in which frequency components the faults are located. It was first introduced by Dwyer in [132]. He defined SK as “the normalised fourth-order moment of the real part of the short-time Fourier transform”. Since then, SK was rarely brought into use [133] until Antoni gave a correct formalisation of SK by means of the Wold-Cramér decomposition of “conditionally non-stationary processes” in [118]. More importantly, he proposed a short-time Fourier transform (STFT) based estimator of SK which helps to link theoretical concepts with practical applications.

At a time when frequency domain processing and analysis techniques are contributing to most publications about roller bearing acoustic signal processing, in the opinion of Pandya et al. and other researchers, the time domain features are effective in making an accurate diagnosis of various bearing faults and have high precision and low computational burden compared to the frequency domain features [131, 134].

Researchers who support computational intelligence methods have the opinion that the major defect frequencies are affected by the shaft speed of the machinery system. This effect results in there being difficulty in determining the actual features because of side bands

neighbouring these frequencies [135]. Time domain features also manifest robustness in the presence of load and speed variations [136]. In addition, optimised feature selection results in enhanced fault detection performance [137].

Samanta and Al-Balushi firstly proposed an approach for rolling element bearing diagnosis using artificial neural networks (ANN) in 2003. The time domain characteristic features of vibration signals had been used as the input to the ANN; years later the researchers were still working on the best way to carry out experiments [138, 139].

Rotating machinery fault diagnosis based on multi-class support vector machines (SVMs) was proposed by Yang et al. in 2005. They carried out experiments to compare multiple-class SVMs with SVMs and other Neural Networks; the results illustrated that the proposed approach can diagnose any condition, and the average fault diagnosis accuracy is over 90% [140]. A new method based on particle swarm optimization (PSO), which is capable of picking out the most appropriate fault features in a shorter time, designed to improve the performance of the SVM classifier, was presented in the application of fault diagnosis of the turbo pump rotor by Yuan et al. in 2007 [141, 142]. They also stated the new method exhibits fewer errors and has better real-time capacity than the method based on Principle Component Analysis (PCA) and SVM, or the method based on Genetic Algorithm (GA) and SVM. In [143], Samanta et al. applied PSO combined with other Computational Intelligence (CI) techniques to bearing fault detection in machines. The results were compared with other techniques such as GA and PCA, which illustrated the effectiveness of the selected features and the classifier in the detection of the machine condition [143]. The enthusiasm for machine learning methods remains high among researchers. Sugumaran et al. noted that attempts to design various machine learning methods, combined with different feature selection criteria, are still ongoing [144]. In 2012, Jiang et al. performed bearing fault diagnosis experiments to evaluate the fuzzy lattice classifier (FLC). They compared the

performance of FLC with the fuzzy lattice reasoning (FLR) model as well as the other widely used classification methods, and drew the conclusion that the FLC exhibits a satisfactory classification performance with higher computation efficiency [145]. Many researchers have found that the K nearest neighbour (KNN) algorithm achieves good performance in experimental data sets [131]. Pandya et al. presented their work using supervised machine learning methods for solving data mining problems for fault classification of bearing acoustic emission signals [131]. KNN was selected as the most appropriate classifier in their work. The results showed the proposed classification model and optimised feature selection have potential for improving bearing fault diagnosis.

Computational intelligence methods help to understand bearing anomalous behaviours by matching the faulty bearing scenarios with the healthy scenarios. They need a large volume of bearing data sets. However, it is the author's view that the bearing condition cannot be repeated as time passes. The developed model cannot reveal the bearing condition accurately, only the process of the bearing degrading.

As one of the objectives of the work in this thesis is to improve the performance of condition monitoring technology, the research in this thesis focuses on emphasising the investigation of bearing faulty feature extraction.

In this research work, the author has reviewed both time domain features and frequency domain features, and has applied them to different scenarios. The results indicate that the effectiveness of features depends on the experiment environment, which can strongly affect the signal quality. The details are explained and demonstrated with the experimental results in chapter 5.

In the following sections, the useful processing techniques in this work are explained, based on mathematical complexity, from the most basic to the more advanced.

3.2.2 Linear prediction coding

Linear prediction coding (LPC) is viewed as a subset of filter theory in that it is a filter designed of a series of linear prediction coefficients. The fundamental of LPC is that a given sample at time n , $x(n)$, can be approximated as a linear combination of the past k samples [146, 147]. It can be described by the following equation:

$$x(n) \approx -a_1x(n-1) - a_2x(n-2) - \dots - a_px(n-p) \quad (3-3)$$

where a_1, a_2, \dots, a_p are LPC, and the estimated current value $x(n)$ is obtained as a weighted sum of the p previous values.

In the case of a roller bearing acoustic signal, the actual current value is the combination of the predicated value and a noise term:

$$y(n) = x(n) + e(n) \quad (3-4)$$

So equation (3-3) is transformed into:

$$x(n) = -\sum_{k=1}^p a(k)y(n-k) \quad (3-5)$$

The $a(k)$ can be obtained using the Levinson-Durbin recursive (LDR) algorithm. The detailed fundamental of the LPC can be referred to [148, 149].

Combining equations (3-4) and (3-5), the equation is transformed into:

$$y(n) + \sum_{k=1}^p a(k)y(n-k) = e(n) \quad (3-6)$$

The Fourier-transformed representation is:

$$Y(f)A(f) = E(f) \quad (3-7)$$

So:

$$Y(f) = \frac{E(f)}{A(f)} \quad (3-8)$$

Equation (3-8) can be viewed as a system with the transfer function $A^{-1}(f)$. Because the transfer function is an all-pole filter, the system is an autoregressive (AR) system. $Y(f)$ is the output of the system excited by the forcing function $E(f)$. The forcing function $E(f)$ is white, containing stationary white noise and impulses [100]. Therefore, having removed the deterministic components from the signal, the “prewhitened” residual signal is left, which contains the non-linear bearing signal.

3.2.3 Frequency domain analysis techniques

Fast Fourier Transform (FFT) is a powerful technique for fault detection and diagnosis, assessing the frequency content of a signal, i.e. its spectrum. Fast Fourier Transform (FFT) transforms a real signal sampled in the time domain into a representation in the frequency domain [150]. Assuming the original signal is in the form of N real samples of the signal sampled regularly at the sampling frequency f_s Hz, the samples are spaced ΔT seconds apart.

$$f_s = \frac{1}{\Delta T} \quad (3-9)$$

The signal represented in the frequency domain consists of the same number of values, but they are complex numbers in contrast to the real values in the original signal. According to the Nyquist frequency theory, there is one complex number for each frequency from 0 to $f_s/2$. Normally the original sampled signal is assumed not to include any information above the Nyquist frequency, because the information in the bandwidth of 0 to $f_s/2$ and $f_s/2$ to f_s is axial symmetric. The amplitude of these complex numbers gives the energy at each frequency. Usually the original signal is real and the FFT computed in Matlab includes half

the energy in a symmetric part (even symmetry for amplitude, odd symmetry for phase) that does not concern the developer.

FFT assumes that the original signal repeats indefinitely [151]. If the original signal consists of a single co-sinusoidal signal, the FFT will contain a single spike at its one side spectrum.

Examining the magnitude of the spectrum as a function of frequency is referred to as Envelope Analysis [152]. A further, related technique is called Spectrogram Analysis [153]. This is where the signal is split into overlapping sections, and an Envelope Analysis is undertaken for each section of the signal. This is often used to study changes in the harmonic content of waveforms over time.

Detection using the spectral envelope typically depends on comparing the spectrum of a vibration, measured using accelerometers attached to the equipment being monitored, to a reference spectrum known to be from a healthy specimen. Changes in the spectrum from the reference spectrum, generally in terms of the amplitude at certain frequencies exceeding some threshold, are used to indicate the abnormal behaviours. For example, in many rotating machines an increase in vibration indicates a reduction in rotational symmetry that indicates a problem. Or, unexpected vibrations coming from a rotating machine may indicate that something has come loose. The frequency at which the change occurs may give a clue as to the underlying cause, or it may simply trigger a closer inspection.

3.2.4 High Frequency Resonance Technique (HFRT)

HFRT was developed in a US army research laboratory in 1974 [154]. It is used to demodulate the high frequency components related to the fault to their carrier frequencies. The resolution of signal spectral envelope varies depending on the length of sensor data. At higher rotational speeds a shorter period can be adequate and at lower speeds a longer length of data is required to achieve an adequate level of accuracy for the final frequency analysis.

Generally this method consists of three stages: apply a high-pass/band-pass filter to the raw signal; remove the lower frequencies that are of less interest; undertake an envelope analysis to identify individual impact events within that signal. To perform this, Hilbert transform is used in order to find the envelope of the signal [155]; for further smoothening and finding the low frequency components of the envelope a low pass filter is applied.

The rotating machinery signal is thought of as containing some periodic components, for example, at the cage rotation frequency, but it can also contain spikes caused by momentary contact with damaged areas of a roller. These spikes can represent the excitation of mechanical resonances in the parts of the bearing and in the supporting superstructure. Hence, the FFT of the bearing acoustic signal contains not only the fundamental frequencies expected to be observed from a bearing (low frequencies) but also high frequencies that are structural resonances in response to spikes caused by damage in the bearing momentarily being loaded.

In the application of this scenario, the spectrum based analysis methods above are not powerful, because FFT is limited as it does not have any sense of time, but only of the signal as a whole, so the information can be extracted when the feature of interest does not generate a long-term excitation.

3.2.5 Kurtosis and Skewness

Other than the frequency domain analysis methods explained above, there are also existing statistical analysis methods. Kurtosis is a non-dimensional quantity that measures the “peakiness” of a signal relative to the Gaussian (i.e. Normal) Distribution. It is defined as the fourth central moment divided by the square of the variance [156]. Skewness is defined as the third central moment.

Moments are used to analyse data; typically for statistical data the mean and variance are commonly used. The mean is typically defined by:

$$\bar{x} = \frac{1}{N} \sum_{i=1}^N x_i \quad (3-10)$$

where x_i is the recorded data.

In fact, given a set of data taken from measurement devices, the mean defined above is an estimate of the mean of some theoretical underlying process, but the difference does not affect the analysis results.

The n^{th} central moment (moment of the mean) is defined as:

$$\mu_n = \frac{1}{N} \sum_{i=1}^N (x_i - \bar{x})^n \quad (3-11)$$

where N is the number of samples within the measured/analysed data set.

The ‘central’ part of ‘central moment’ means that the moment is computed about the mean, or centre of the signal. The first central moment is zero by definition.

The second central moment is the ‘variance’. Technically, the variance is assumed to be a property of some underlying distribution [157] and the equation above gives an estimate of the variance. However, given a set of data, one can equally define the variance of the data as above. The square root of variance is the standard deviation, σ , the second defining parameter of a normal distribution after the mean.

One measure considered for data analysis is “skewness”, defined from the third central moment by [158]

$$S = \frac{\mu_3}{\sigma^3} = \frac{\mu_3}{\mu_2^{3/2}} \quad (3-12)$$

Skewness is a measure of the degree of asymmetry of a distribution. A symmetric distributed data set has zero skewness. As the mean is removed, skewness does not indicate that there is more positive data than negative data, but it means that the positive going peaks are in some sense more significant than the negative going peaks, or *vice versa*. In principle, the skewness should not be an important factor in the analysis of bearing or gearbox fault signatures.

Kurtosis is a non-dimensional quantity that measures the relative “peakiness” of a signal relative to the Gaussian (i.e. Normal) Distribution. It is defined as the fourth central moment (μ_4) divided by the square of the variance (Standard Deviation to the power of 4 (σ^4) or μ_2^2): [156]

$$K = \frac{\mu_4}{\mu_2^2} \quad (3-13)$$

As it is the fourth power, it gives particularly high weighting to samples with large deviations from the mean and largely ignores the smaller values. Dividing by the square of the variance normalises the value to avoid the spread of the signal changing the kurtosis value. Therefore, kurtosis is independent of the mean and the variance. For a normal distributed data (e.g. a healthy component), the kurtosis value is 3. For a sinusoidal signal, the kurtosis is around 1.5 and for signals with repetitive impulsive type responses, the kurtosis can become very high. In a simplistic version, kurtosis gives a good indication that the data contains many spikes.

As an extension to kurtosis, Spectral Kurtosis (SK) [159] is a statistical parameter that indicates how this characteristic of a signal varies with frequency. More details are explained in Section 3.2.6.

3.2.6 Spectral kurtosis

The SK can be viewed as a combination of the frequency domain analysis and the statistical analysis. There are two important rules of the proposed STFT-based SK: one is that the overlap of the time window should be at least 75% of the window length; the other rule is to use the appropriate duration of the analysis window [118]. As there are no rules for setting the duration of the analysis window, the strategy is to compute the STFT-based SK for different durations and then select the maximum value overall level of the SK in the frequency band of interest, which leads to the concept of the “kurtogram” [160].

Faults associated with rolling element bearings give rise to modulated impulses, so the SK value is abnormally large for frequency windows where the fault signal is dominant and small where the spectrum is dominated by healthy or stationary signals. The spectral kurtosis can be computed by dividing the signal into frequency bands and computing the time-domain kurtosis for each band. The results are somewhat sensitive to the choice of bandwidths used. The bandwidths for each frequency need to encompass the whole spectral range of the original data, or certain interesting features can be lost. If the bandwidths are too narrow, the kurtosis can collapse.

This method can indicate the frequency band which is mostly related to the fault. Then the designed band-pass filter can be applied without any prior information on the system, which can extract the fault signal from its noisy environment, and therefore provide information on the nature of the fault [160].

3.2.7 Self-adaptive techniques

Self-adaptive techniques are another method of roller bearing signal analysis. In [129], Elsha et al. suggest the effectiveness of self-adaptive techniques when using an adaptive filter in

identifying a naturally degraded bearing under conditions of “relatively large background noise”.

Adaptive techniques, also called data driven techniques, are applied as a pre-processing step because of their ability to overcome the problem of periodic noise being injected into the signal from one rotating element by another. Empirical Mode Decomposition (EMD) is one such adaptive technique. It is based on the decomposition of the signal in order to generate less complex data sets [128]. Minimum Entropy Deconvolution (MED) is another adaptive signal processing technique [161, 162]. It is effective at de-convolving impulsive sources from a mixture of signals [161, 163, 164, 165, 166].

The EMD method is a time-domain processing technique which can be applied to reduce the level of noise within a signal [167]. Conversely, MED can be used to emphasise an impulsive element within a signal [166]. These two techniques can therefore be combined to both reduce the noise within a signal and to emphasise the components of the signal that are of interest. Such processing has been applied in the area of roller bearing diagnostics [168, 169]. In these cases, the result of the first EMD iteration is used in the processing chain. In other EMD applications, it is common to consider multiple iterations of the process and select the result demonstrating the greatest level of energy [119]. The method used to select the most appropriate EMD iteration result is particularly important when combining multiple processing techniques. In addition to methods such as traditional energy and energy entropy, the energy moment technique is particularly suited to signals with non-stationary characteristics [119]. In [170], Zhang et al. proposed a combination of EMD and MED methods to filter noise and to extract key signal features. The energy moment technique is used to identify the most appropriate EMD iteration. These techniques together are referred to as Empirical Mode Envelope with Minimum Entropy (EMEME).

3.2.7.1 Fundamentals of EMD

EMD is an adaptive technique, also known as a data driven technique. It was originally proposed by Huang et al. in [130]; encouraging results of the application of EMD to signals obtained from rotational mechanical systems are reported in [167, 171, 172]. The EMD method decomposes the signal into different sub-signals, which are the intrinsic mode functions (IMFs). A detailed introduction to the EMD method can be found in [130].

EMD focuses on extracting the stationary points of the signal [168]. Assuming a generic signal $x(t)$, the maxima and the minima of which are interpolated by means of a spline to obtain $Max(t)$ and $Min(t)$ respectively.

These two curves are able to represent the envelope of $x(t)$. The average signal from these two splines is called $mean(t)$. $x_1(t)$, shown in equation (1), can be calculated by subtracting the $mean(t)$ from the original signal $x(t)$:

$$x_1(t) = x(t) - mean(t) \quad (3-14)$$

If the resulting signal $x_1(t)$ is an intrinsic mode function (IMF), the algorithm ends. Otherwise, the previous steps are repeated as per equation (2). This iterative procedure is known as the “sifting process”.

$$x_n(t) = x_{n-1}(t) - mean_{n-1}(t) \quad (3-15)$$

To be an IMF, the signal must meet the following requirements:

- 1) The number of extrema in $x_n(t)$ equals the number of zero crossings.
- 2) The mean between the local maxima and local minima splines in $x_n(t)$ is equal to zero at any point.

In the sifting process $Max(t)$, $Min(t)$ and $mean(t)$ are recomputed so that $mean(t)$ can be subtracted from the previous signal $x_{n-1}(t)$. When the first IMF, $C_1(t)$, is extracted the sifting process stops.

Then, $C_1(t)$ is subtracted from the original signal $x(t)$:

$$r_1(t) = x(t) - C_1(t) \quad (3-16)$$

The signal $r_1(t)$ is treated as the original signal for the second IMF calculation by means of the sifting process:

$$r_2(t) = r_1(t) - C_2(t) \quad (3-17)$$

The EMD algorithm generates the final IMF, $C_N(t)$, when the residual signal $r_N(t)$ is a constant or monotonic function. The threshold to stop the procedure is described as:

$$\delta(r_N(t)) < \delta_{stop} \quad (3-18)$$

where $\delta(r_N(t))$ is the residual signal of $r_N(t)$ and δ_{stop} is the threshold to stop.

The IMFs extracted by the EMD algorithm can be considered to be sub-signals of the original signal. These sub-signals expose components that can be used for latter signal processing.

In order to demonstrate the EMD algorithm in practice, a simple periodic signal is used as an input passing through the EMD module. It is defined as:

$$x(t) = \sin(8\pi t) + 2 \sin(20\pi t) + 0.6 \sin(63\pi t) \quad (3-19)$$

The output of $x(t)$ can be seen in Figure 3.1.

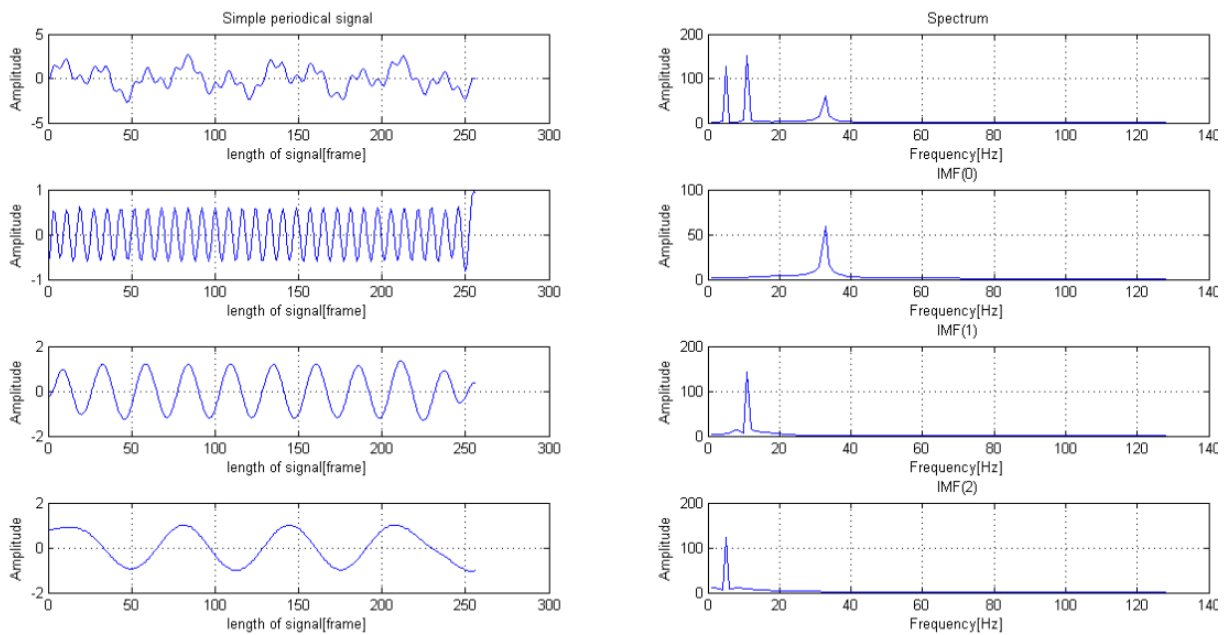


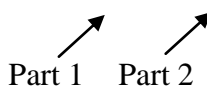
Figure 3.1- Waveform of a simple periodic signal's EMD procedure

As discussed above, the IMFs (intrinsic mode functions) are the outcome of the EMD algorithm. IMF(0) contains the highest frequency sub-signal, then IMF(1) contains the second highest, and so on in a similar fashion. Take this simple periodic signal in Figure 3.1 as an example. There are three frequencies contained in the signal: 8 Hz, 20 Hz, and 63 Hz, which can be seen in the spectrum of the signal. After IMF(0) has been extracted, the 63 Hz sub-signal is separated from the original signal; then IMF(1) is extracted and the 20 Hz sub-signal is also separated. By this analogy, IMF(2) is then extracted and the 8 Hz sub-signal is separated. To sum up, all three of the IMFs which contain the sub-signals can be viewed in the graph.

3.2.7.2 Fundamentals of MED

The Minimum Entropy Deconvolution (MED) algorithm enhances the peakedness of the signal by emphasising the transient components. It aims to reduce the randomness of a signal by minimising its entropy.

A generic signal $g(t)$ can be considered as two component parts as per equation 9:

$$g(t) = h(t) * w(t) + \eta(t) \quad (3-20)$$


Part 1 is the convolution between the component related to the system behaviour $h(t)$ and its excitation $w(t)$. Part 2 represents randomly distributed noise.

When the signal $g(t)$ passes through a filter $f(t)$, it is represented as $u(t)$:

$$u(t) = g(t) * f(t) = h(t) * w(t) * f(t) + \eta(t) * f(t) \quad (3-21)$$

This can also be presented in the discrete domain:

$$u(n) = g(n) * f(n) = \sum_{i=1}^{M-1} f(i)v(n - 1) \quad (3-22)$$

with $n = 0,1,2, \dots, T + M - 2$; where T is the length of the convolution between the signals, and M is the length of the filter.

Key to this stage of the MED process, as discussed in [162], is choosing the value of the filter length (M). In the paper by Pennacchi et al. [173], the filter length is selected based on the characteristic period of the system (i.e. for rotating components the filter length is chosen to be the same as the period of rotation).

The objective of this filtering is to retain (or maximise) the contribution from the first part of the signal, while minimising that from the components associated with the noise. The result of this action is that the signal entropy is reduced. By iteratively repeating the process the algorithm identifies the output $u(n)$ that has an optimal match to $h(t)$, and thereby minimises

the signal entropy. The signal entropy is evaluated using the Varimax norm [161]:

$$V(u(t)) = \frac{\sum_{j=0}^N u^4(j)}{(\sum_{j=0}^N u^2(j))^2} \quad (3-23)$$

with $N = T+M-2$.

In practice, MED is particularly effective at separating frequent impulses resulting from shocks generated by localised defects [166]. In theory, MED is particularly effective in the separation of subsequent bursts present in the experimental signals. To demonstrate the working principle of MED, a simple periodic signal is introduced as an input passing through the MED module. Assume the input signal is $x_1(t)$, the noise is $n(t)$, then the system input is:

$$x(t) = x_1(t) + n(t) \quad (3-24)$$

where:

$$x_1(t) = \sin\left(2\pi \times \frac{1}{10} \times t\right) \quad (3-25)$$

$$n(t) = \sin\left(2\pi \times \frac{1}{5} \times t\right) \quad (3-26)$$

The period of the input signal $T_1 = 10$ and the noise period $T_n = 5$. As discussed in the methodology section, for the MED “filter”, the filter length is set as the same order of the characteristic period of the system which is the period of input signal T_1 . The waveforms of the system input and the MED filtered signal are shown in

Figure 3.2.

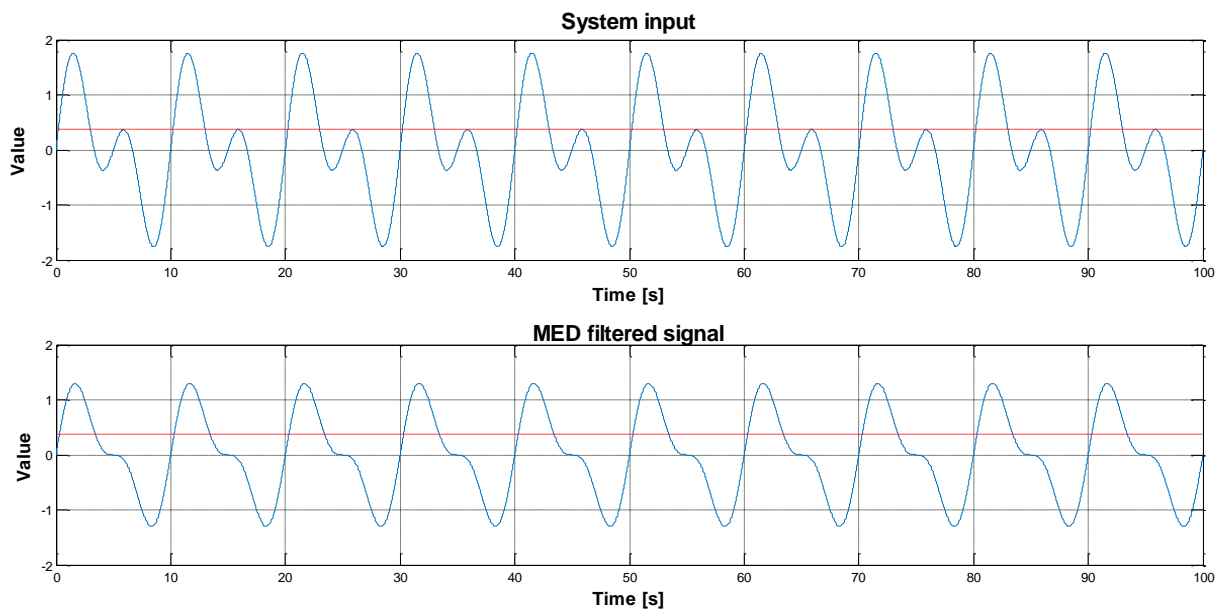


Figure 3.2- The waveform of a simple periodic signal’s MED procedure

The waveform of system input $x(t)$ is on the top, which is the overlay of $\sin\left(2\pi \times \frac{1}{10} \times t\right)$ and $\sin\left(2\pi \times \frac{1}{5} \times t\right)$. The waveform at the bottom is the output of the MED “filter”. It can be seen that the volume of noise is minimized, whereas the target input signal is highlighted.

3.3 Image processing – Computer vision technologies

As mentioned in section 2.3, computer vision techniques are the algorithms used in the image processing and analysis. There is not a standard definition of computer vision, but it is an inverse process of how human beings understand the world using their visual system [75]. Humans and animals can reconstruct the properties of image easily, such as illumination and colour distributions, whereas computer vision algorithms are often error prone [75]. The concept of computer vision is well explained in Szeliski’s book [75]. The status of computer vision development stated in the book is severe; the dream of having a computer interpret an image at the same level as a two-year old (such as counting all of the animals in a picture) remains an unachievable task [75].

The key requirements for computer vision techniques for the railway are feature extraction and motion detection. These requirements are based on basic computer vision, not comparable to applications such as person movement tracking or face recognition. With regard to feature extraction, edges are often used to extract the features of objects in the image, because the object boundaries can generate sharp changes in brightness [174]. The image is downgraded into binary image after the feature extraction using the edge detectors. An overview of the edge detectors is discussed in detail in section 6.3.1. Morphological image processing is normally followed by the edge detection processed image because it is suitable for the processing of binary images. Morphological processing could dilate and erode the target area, as well as thinning the edge of the area within the image, depending on the features the researcher is interested in. An overview of Morphological image processing is discussed in detail in section 6.3.2. In a railway application, Chow et al. used the edge detection technique in the feature extraction of people in a crowd [77]; Marmo et al. used the edge detection and morphological technique in the detection of railway luminous electric signals at the trackside [88]; Singh et al. [83], Resendiz et al. [84] and Zheng et al. [85] used the edge detection and morphological technique in the feature extraction of the track and track components (clips, bolts, etc.). Edges are suitable for describing the contours of natural objects [175].

In the railway application, the components to be inspected are man-made products that have many straight lines, circles and other standard shapes. For this kind of application, there are techniques which can precisely extract the features of standard shapes. These techniques are well explained in Szeliski's book [175]. Hough transform is one of the most frequently used techniques. In [88], the authors used Hough transform to find the straight lines of poles at the trackside. They also proposed an approach with a lower computational cost compared to circular Hough transform to find circular luminous electric signals.

With respect to motion detection, one of the simplest strategies is to compare the differences between successive images [176, 177], however, noise in the image has a great effect on the differences, resulting in incorrect judgements. This strategy is also inefficient, especially when the motion is slow. An alternative strategy is to compare images by regions [178, 179] rather than comparing between pixels. The region comparison is capable of reducing the influence of noise [93]. Edges can also be used in motion detection [180], which makes the strategy more capable of detecting the presence of illumination changes [93].

In this thesis, computer vision techniques are applied to provide train speed information and extract the features of key vehicle components from the trackside. The requirement for accuracy is the key element of the speed information extraction, while the robustness of the feature extraction strategy is the key requirement of the vehicle components inspection.

3.4 Conclusion

In this chapter, the current situation of railway condition-based digital signal processing technologies has been reviewed. Roller bearing acoustic signal processing technologies have been reviewed. Feature extraction processing techniques have been selected for emphasis in this research work in order to achieve an improvement in the performance of bearing inspection and monitoring. Computer vision technologies could be applied to the inspection and monitoring of various of components in a railway vehicle. These applications have been reviewed in this chapter.

Having reviewed both railway vehicle inspection and monitoring technologies and railway condition-based digital signal processing technologies, the methodology will be discussed in Chapter 4.

4 Methodology

This chapter is discussing the methodology for investigating the potential integration of the two way side condition monitoring technologies. Acoustic sensing and vision imaging, are the target technologies to construct the integrated system. The methodology for the integrated system development involves the hardware system construction and experiments set-up.

In order to carry out an intelligent approach to realize the integration between the two technologies, the research should start with the two technologies in isolation to gain the knowledge through their working fundamentals.

The acoustic sensing technology consists of vibration sensor which is installed on the surface of bearing lid; and the acoustic microphone which is air-coupled with the bearing, listening to and recording the sound generated by the spinning bearing with certain amount of noise. In terms of the intelligent integration plan, with a high-speed video recording device, the vision imaging technology can support the acoustic inspection and monitoring system in directing the sound beam of each single microphone to form an integrated acoustic signal.

4.1 Methodology decomposition

Based on the objective analysis, the task of the system development should be decomposed into:

1. Develop the hardware systems of acoustic inspection and monitoring application
 - a. Vibration sensor
 - b. Acoustic microphone
2. Develop a hardware system of vision imaging inspection and monitoring application
3. Develop a hardware system of integrated inspection and monitoring application

The development phase of each system is decomposed into two parts:

- i. Laboratory-based experiments in controlled conditions
- ii. Proof-of-concept field tests

Working in this way enables parameters and their effects to be fully understood, and provides consistent conditions under which to evaluate different analysis methods.

Based on the decomposed development phases, the methodology of the work in this thesis is formed and shown in Figure 4.1.

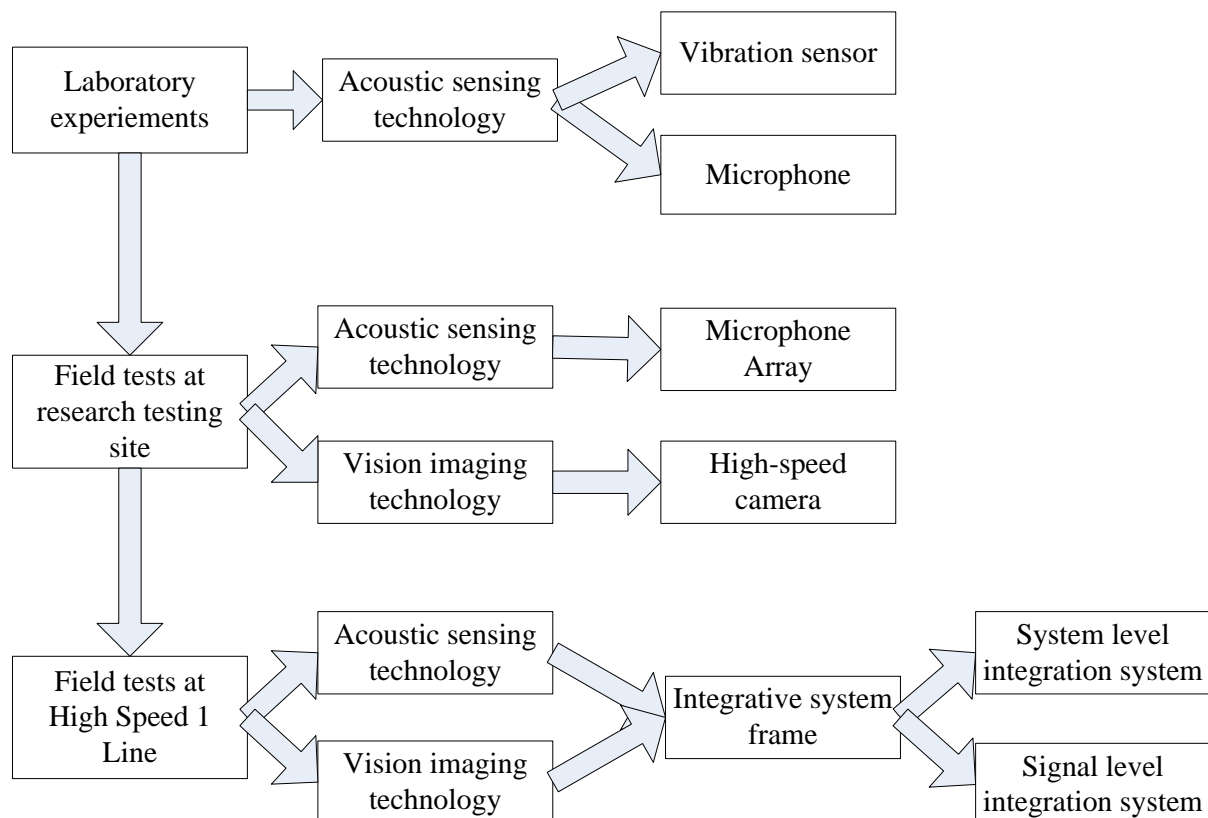


Figure 4.1- The diagram of methodology for the integrated system development

In the diagram of the methodologies, there are three different scenarios: the laboratory experiments and two field tests. The laboratory experiments only applied to the acoustic sensing technology research work in both the vibration sensor and acoustic microphone. The laboratory experiments for vision imaging technology are not so useful because the

development of image processing algorithm is case-oriented. Firstly, the real train is impossible to move to the laboratory. Also, the outdoor environment, such as brightness and image background are difficult to simulate. So in the phase of laboratory experiments, the system design and experiments is acoustic sensing technology only.

4.1.1 The laboratory-based experiments

The simple way to understand the machine behaviour of a particular component with a number of different conditions is to subject the machine to a certain working condition, introduce the different damage conditions, and take measurements of the behaviour in each case. The advantage of this approach is that little prior knowledge of the inter-relationship of variables is required as these can, theoretically, be measured. However, there are a number of difficulties with this approach, especially in the railway environment and where the conditions involve inflicting damage on the components. These difficulties include cost, safety, reproducibility and a large number of variables, some of which may be unknown.

4.1.1.1 Impact on the experiment programme design

A great deal of investigation can be carried out using mathematical modelling. This has the advantage of being able to create a great number of controlled scenarios at low cost and with no safety implications. However, this cannot be done successfully without comprehensive knowledge of the inter-relationship of the variables within the system.

In the situations above we have, at one extreme, a means of obtaining “facts” in a very expensive and time-consuming way. At the other extreme we have a quick and economical method of making “estimates”, but the quality of those estimates is very dependent on supporting facts.

In between these extremes are two compromise methods. The first is to test the component on a laboratory test rig that reproduces some of the required conditions. When dealing with large

railway vehicle components, the costs and risks associated with the necessarily large test rig and the purchase of a number of number of test components become prohibitive.

This leaves one method - that of testing a small-scale model, in this case using a smaller bearing of a similar design to that of interest on a test rig specially designed for that size of bearing. Advantages include improved safety, low costs of building the test rig and purchasing the bearings under test. The difficulties lie in identifying and quantifying the consequences of scaling in order to relate test parameters and results to those of the full-size component. So, a literature review was carried out to investigate the issues of scaling before the commencement of work. The following section discusses the issues considered.

4.1.1.2 Implications of Scaling

If a scale model is to behave in exactly the same way as the full-size equipment, then the model should have complete similitude with the full-size item. It is usual to take a particular linear dimension as the reference scaling factor. Whilst the determination of explicit scaling factors, such as length, width, and displacement scaling of linear dimensions is simple, derivation of the implicit scaling factors for springs, moments of inertia, forces and frequencies (excitation and forcing) is relatively more complicated. This scaling can be calculated using dimensional analysis using a number of different methods. These methods are described in the text book by Baker et al in reference [181]. A great deal of work has been carried out on the subject of scaling, mainly in the fields of materials, marine engineering and fluid dynamics. Most references to scale modelling of mechanical systems, while being useful documents, necessarily deal with simple or simplified systems, for example reference [182] gives a good account of the similitude concept. A number of researchers have studied vibration in rotating machines, but mainly using full-size tests. One paper, reference [183], is more relevant to the application in this thesis and illustrates the potential complexity of the scaling issues relating to the vibration of rotor bearings.

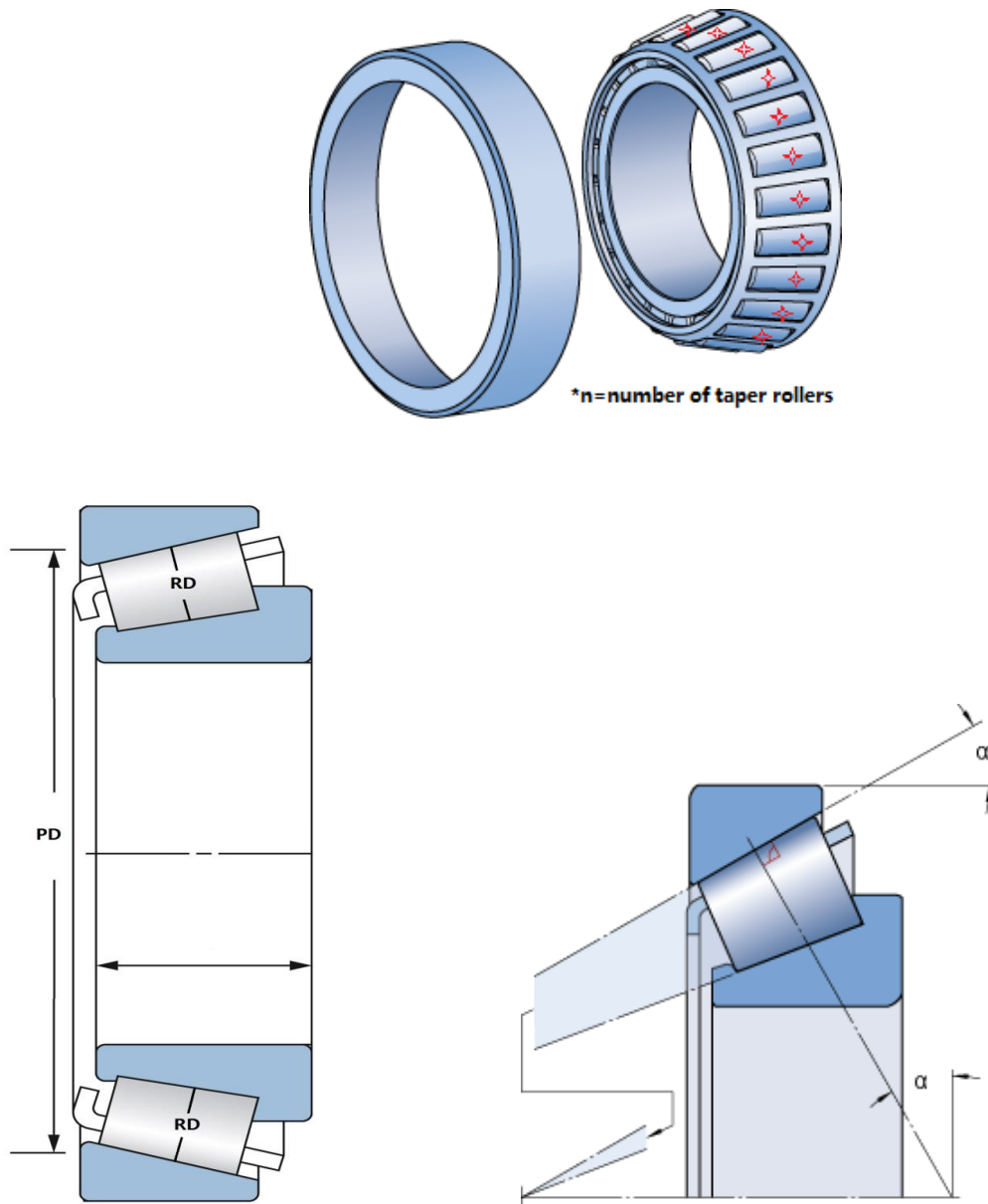


Figure 4.2- Bearing dimensions diagrams adapted from [184]

References [182] and [183] show derivations for scaling of relevant parameters, some of which are reproduced in Table 4.1. These parameters are relevant to the calculation of rolling-element characteristic frequencies, shown in Figure 4.2. These frequencies are important to the diagnosis of the bearing health condition and the verification of the signal processing algorithms.

Reference scaling factor for shaft diameter, d , is λ_d .

Table 4.1- Examples of scaling factor

Dimension	Scaling factor	Example dimensions	
		Full size system	Scale model
Roller diameter (RD)	λ_d^2	RD	$\lambda_d^2 * RD$
Pitch diameter (PD)	λ_d^3	PD	$\lambda_d^3 * PD$
Number of rollers (n)	1	n	n
Contact angle (α)	$1/\lambda_d$	α	$1/\lambda_d * \alpha$
Rotating speed (rpm)	$1/\lambda_d$	v	$1/\lambda_d * v$

Correct scaling of all parameters, while possible, is unlikely to be practicable. Here, the majority of the scaling factors of the model are correct. Therefore the results of a particular test on the scale model may not be the same as for the full size model, so the results, too, are subject to scaling.

The scaled automotive axle-bearing used in this work is the Type 801023AB tapered roller bearing. The dimension and scaling relations are listed in Table 4.2.

Table 4.2 – Dimension of the Type 801023AB tapered roller bearing

Dimension	Scaling factor	Example dimensions	
		Full size system	Scale model
Roller diameter (mm)	0.25	23	5.3
Pitch diameter (mm)	0.125	300	42.5
Number of rollers (n)	1	21	21
Contact angle ($^\circ$)	2	6.9	13.8
Rotating speed (rpm)	2	500	1000

In order to carry out the laboratory-based experiments in controlled conditions, test rigs need to be designed. In order to test the full-size and scaled bearings in the laboratory at the same time, the design of the test rig has the requirement of being capable to put both full-size and reduced-scale bearings tested on one test rig in the same acoustic environment – effective back-to-back tests. In order to design the test rig, it is first necessary to obtain suitable scaled test components. The bearings selected for the tests are as follows:

The work has been based on the full-size train axle bearing, Tarol 130/230-U-TVP, a tapered roller bearing supplied to Hitachi by FAG. Advice was sought from FAG on the selection of a scaled bearing of suitable size, proportions and loading and they recommend the Type 801023AB tapered roller bearing from their automotive range.

4.1.1.3 Bearing test rig

In order to carry out the laboratory tests on the roller bearings a test rig was built, this is shown in figure Figure 4.3. The key features of the test rig are as follows:

1. Single 2.2 kW electric motor to drive the shaft, via a belt for isolation, at varying speeds.
2. A hydraulic jack under each test bearing to apply a vertical load.
3. Pressure gauges (analogue and digital) to measure and monitor the applied load.
4. A tachometer to measure the rotational speed of the shaft.

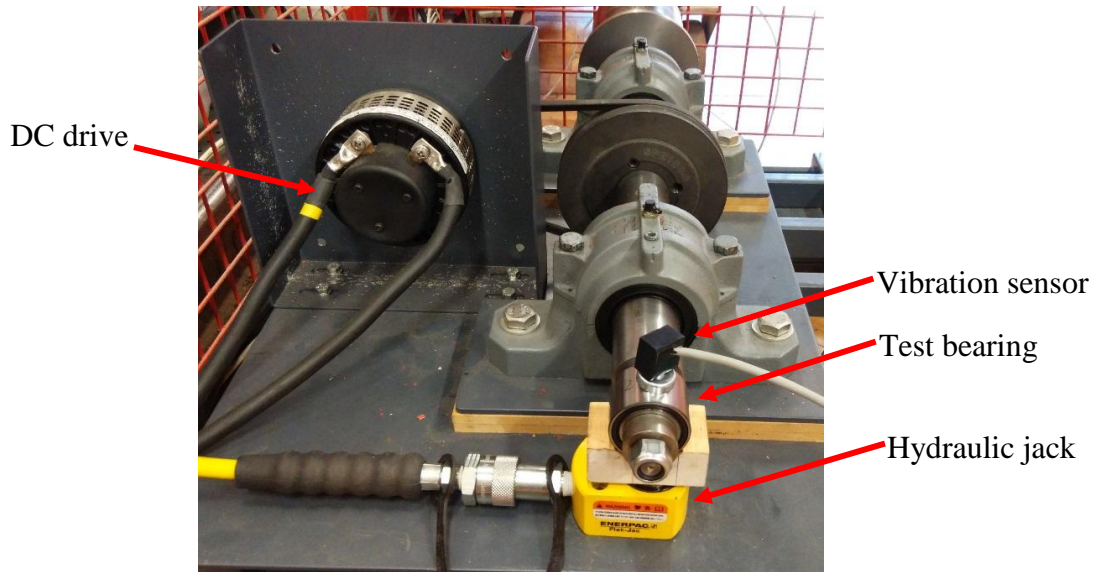


Figure 4.3- Bearing test rig and vibration sensor

External loads are applied using hydraulic jacks via wooden “saddles” matched to the bearing casing, and the rotational speed of the driving motor(s) can be varied as required.

4.1.1.4 *Anechoic chamber room*

Using anechoic chamber room (shown in Figure 4.4) in the laboratory experiments stage of the acoustic system development is a popular approach because it can reduce the number of variables (majorly the echo reflection in this case), allowing effort to be concentrated on detecting and characterizing the noise from bearings, initially in the absence of external noise. Background noise can then be introduced artificially, and the system re-evaluated and fine-tuned to cope accordingly.



Figure 4.4- Anechoic Chamber room

An additional and important benefit of the use of the anechoic chamber is safety. This is a completely isolated facility with controlled access. Only those personnel directly involved in the tests have access to the area and the chamber is equipped with a control room so that test personnel are isolated from the rig when it is running at high speeds.

The system of acoustic sensor application is shown in Figure 4.5. Two microphones are mounted in front of the bearing while the vibration sensor is mounted on top of the bearing cage. The DC drive drives the bearing spinning with the simulated load from the hydraulic jack at the bottom.

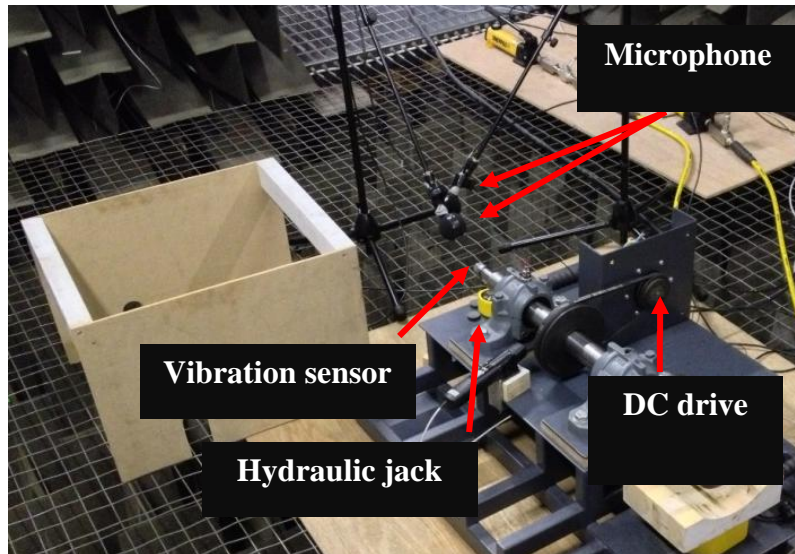


Figure 4.5- Bearing test rig and acoustic sensor (microphone)

4.1.2 The proof-of-concept field tests

The proof-of-concept field tests are to evaluate the ability of the system. In terms of acoustic system, it is to detect emerging problems with bearings in a real-world environment; the vision imaging technology is to extract and track the coupler, pantograph, train doors and windows etc. within the captured images in order to establish inspection and monitoring strategy with.

This includes the challenges of capturing the sound from a moving vehicle rather than a static test rig, and isolating the required signal from the other noise generated by the vehicle and the wheel/ rail interface in particular.

With respect to the vision imaging system, the high-speed camera is assembled at the trackside along with the acoustic system to support directing the sound beam. The author has another publication presenting the tests of the vision imaging system [185].

4.1.2.1 The field tests at research testing site

In this field tests stage, the acoustic and vision imaging systems were brought to the Motorail Long Marston storage site. The site connects to the national railway network at Honeybourne via a section of line operated by Network Rail. The selection of the test site is shown in Figure 4.6. It shows the loop of track used for the field test. The originally selected test section is shown on the diagram along with the actual test section.

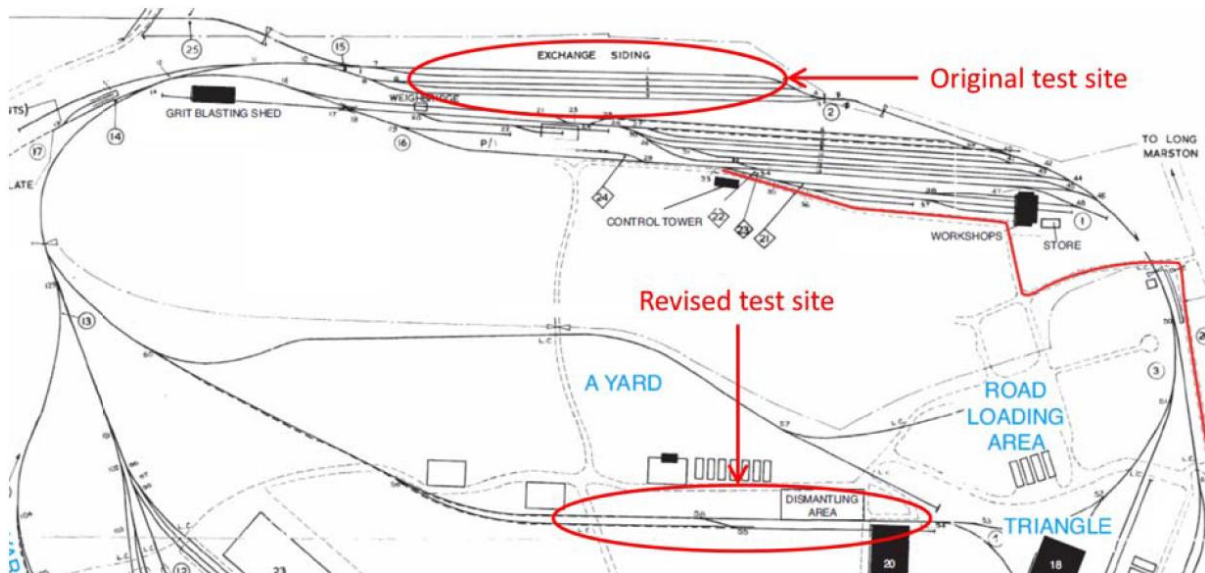


Figure 4.6- The test location at research testing site

The original test site was selected because of the concrete floor condition nearby which easy the installation of the system. But the curve section around it does not allow the vehicle staying at a constant speed. The revised test site can solve this problem. The vehicle can ride at a constant speed on the testing section as there is a long straight line before and after that area. The test train is a Class 117 train consisted of a single car DMU hauling two tea wagons as shown in Figure 4.7, and test speeds of approximately 50 km/h were achieved.



Figure 4.7- Test train

4.1.2.2 The field tests on the Network Rail High Speed 1 Line

The field tests at research testing site have extended the application of the acoustic system from the laboratory to the real track site. Also, the tests of vision imaging provide the imaging data to be worked on (chapter6). Thinking of the robustness of the systems when applied to the in-service trains, the speed of the inspecting train needs to be faster.

So in the third stage of the system development, the acoustic and vision imaging systems were brought to the Network Rail High Speed 1 Line. The field test was on the Network Rail High Speed 1 Line. The location is at Nashenden. The entrance for the site is located off the Maidstone Rd, Chatham, Kent ME5 9QG, shown in Figure 4.8.

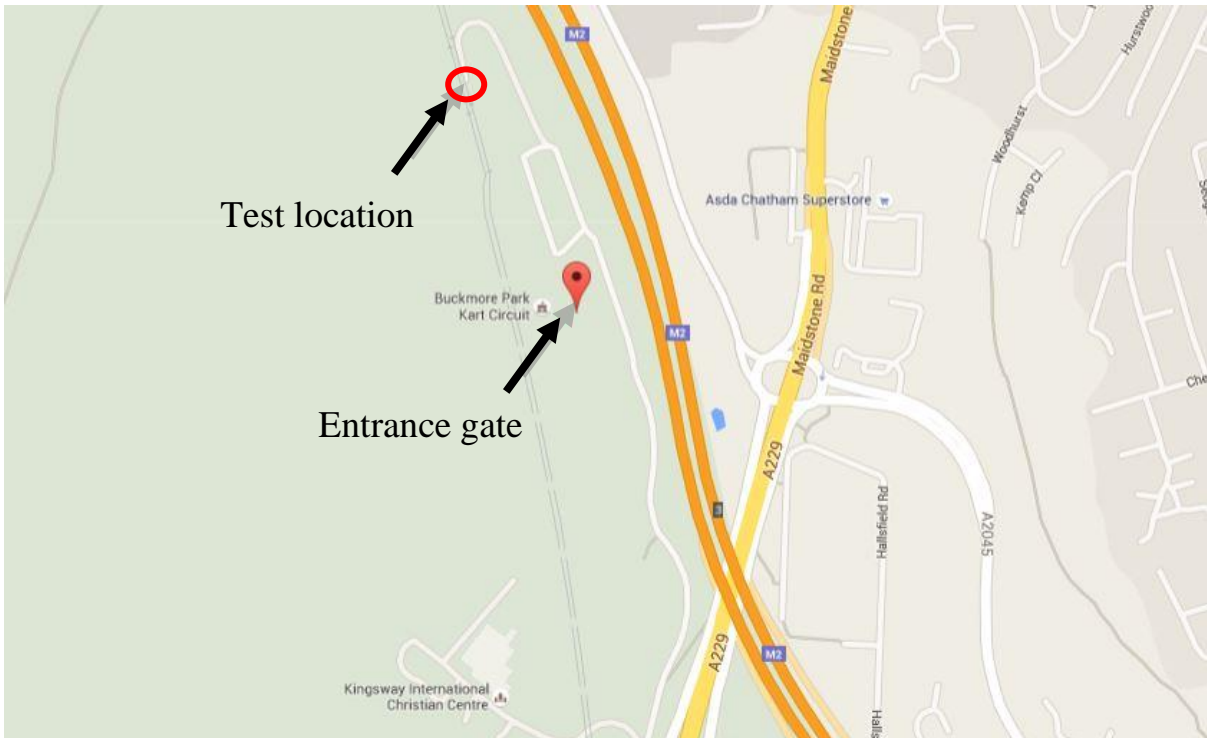


Figure 4.8- Location of the site

The requirements of the system structure are the railway industry standard which does not allow the unassembled hardware pieces being brought to the site. So there was a frame (shown in chapter 7) built for assembling the integrated system of acoustic and vision imaging technologies.

It was a blind test as the inspecting vehicles are in-service passenger trains. The aim of the tests was testing the robustness of acoustic and vision imaging system (chapter 7), and more importantly, testing and validating the integration plans (system level integration and signal level integration) of the integrated system (chapter 7).

4.2 Summary

The methodology of the integrated system development has been discussed in this chapter. A proper and intelligent integration plan is always based on the well understanding of each integrating elements. From this point of view, the work has been decomposed into the

investigation on acoustic sensing and vision imaging technology in isolation and end with the integration system development. Furthermore, during the investigation in each stage, the methodologies have been decomposed into the laboratory experiments and field test. It can help optimise the understanding of each technology, as well as design the proper systems for the future applications on the railway lines.

From the signal processing perspective, the methodologies discussed in this chapter is the signal enhancement through the optimisation of the mechanical system design. The system design was carried out as a team that the author was supported by several experienced research fellows. So the development of signal processing algorithms is going to be demonstrated next. In the next three chapters, the applications of acoustic sensing technology, vision imaging technology and the integration condition monitoring technology are going to be discussed with the corresponding signal processing algorithms.

5 Acoustic sensing technology application

5.1 Overview

This chapter is the demonstration of research work on acoustic sensing technology. Recall the hypothesis of this thesis is that it is possible to achieve improvement of the independent condition monitoring (CM) technologies in isolation. In this work, the acoustic sensing technologies consist of accelerometer (vibration sensor) and acoustic sensor (microphone). Two novel processing algorithms were developed. One has generated a published journal paper and another currently in development.

The accelerometer (vibration sensor) is installed on the bearing cage (shown in Figure 4.3), can detect the vibration generated from the axle bearing rotating. The vibration signal can indicate the anomalies inside the cage. The acoustic sensor (microphone) does not require the contact of bearing cage (shown in Figure 4.5). It can listen and record the sound generated by the axle bearing from wayside, but the signal of which is surrounded with high volume noise. From this point of view, the analysis of vibration signal is suitable to start with in order to obtain the understanding of the behaviour of bearing.

As per reviewed in the review chapter of railway condition-based digital signal processing technologies, the processing procedure of the roller bearing signal is divided into the separation of bearing signals from discrete frequency noise, and the enhancement of useful bearing faulty information inside the signal. The proposed processing chains were following this procedure to develop.

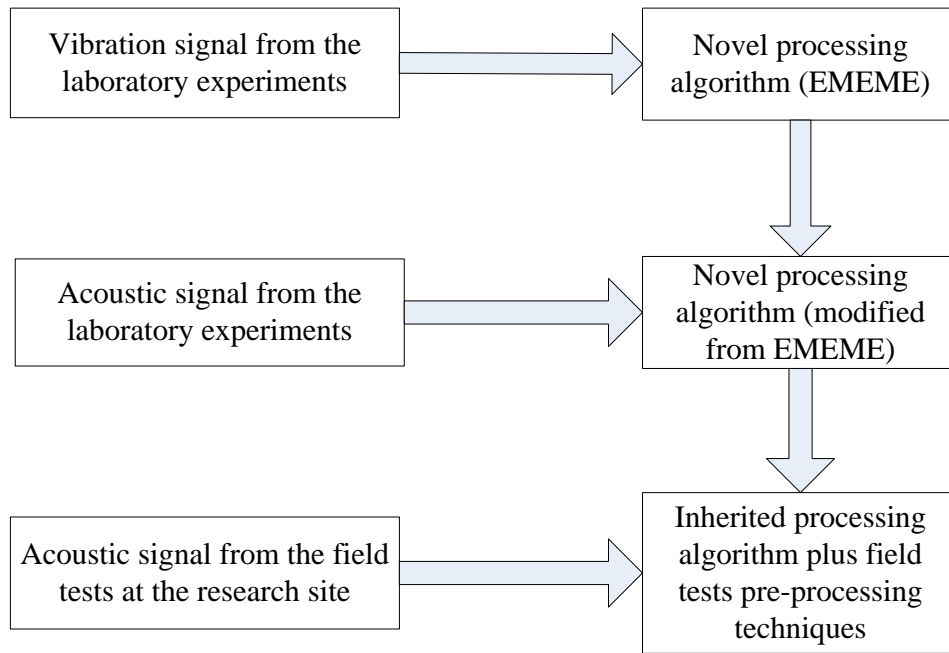


Figure 5.1- Overview diagram of chapter 5

Consequently, the objective in this chapter is to develop the proper signal processing chains to analysis the signal from the acoustic inspection and monitoring system. The development procedure is shown in the overview diagram in Figure. Three data scenarios require three processing chains which share the common of the signal features and their own applications oriented. A novel processing algorithm was developed on the vibration signal from the laboratory experiments, named Empirical Mode Envelope with Minimum Entropy (EMEME). Another novel processing algorithm was developed on the acoustic signal from the laboratory experiments which has used the spectral kurtosis and kurtogram technique. The processing algorithm was inherited from the one development from the acoustic signal in the laboratory. Additionally, the pre-processing techniques required from the field tests signal have been applied.

5.1.1 Rolling-element characteristic frequencies

The rolling-element characteristic frequencies are important to the roller bearing health condition monitoring because the amplitude of these frequencies would significantly increase when any faults occur on the bearing components, such as inner race, outer race and rollers.

An impact event appears within the signal when either a rolling element strikes a race fault, or a fault on a rolling element strikes a race. The geometric relationships between the roller and race components determine the timings of these impacts, and thus the characteristic fault frequencies of the bearing. Each different type of fault (as previously described) is illustrated by a different characteristic fault frequency. The presence of faults can also increase the vibration energy.

For a bearing with a stationary outer race, the following equations define the characteristic frequencies [49].

FTF, Fundamental Train Frequency, fault on the cage or mechanical looseness

$$f = \frac{\omega_r}{2} \left(1 - \frac{RD}{PD} \cos \alpha\right) \quad (5-1)$$

BPFO, Ball Passing Frequency Outer Race, local fault on outer race

$$f = \frac{n}{2} \omega_r \left(1 + \frac{RD}{PD} \cos \alpha\right) \quad (5-2)$$

BPFI, Ball Passing Frequency Inner Race, local fault on inner race

$$f = \frac{n}{2} \omega_r \left(1 - \frac{RD}{PD} \cos \alpha\right) \quad (5-3)$$

BFF, Ball Fault Frequency = 2 * BSF, Ball Spin Frequency, local fault on rolling element

$$f = \frac{PD}{2RD} \omega_r \left(1 - \left(\frac{RD}{PD} \cos \alpha\right)^2\right) \quad (5-4)$$

where f is the frequency of the item [Hz]; ω_r is the shaft rotation rate [revs⁻¹] or [Hz]; RD is the roller diameter [m]; PD is the mean roller race diameter [m]; α is the contact angle [rad]; and n is the number of rollers.

In the following results demonstration chapters, the rolling-element characteristic frequencies are important in the verification stage of the proposed algorithms.

5.2 Vibration sensor application – Lab based

In this section, the data are collected in the laboratory using a surface-coupled vibration sensor mounted on the top of the bearing cage (Figure 4.3). All the data were collected in the BCRRE laboratory at the University of Birmingham.

5.2.1 Introductory tests

Bearing defects can be caused by manufacturing errors, improper installation or abrasive wear, such as surface roughness, waviness, misalignments and off-size rolling elements [186, 187, 188, 50, 189]. Other types of bearing faults are localised, such as cracks, pits and spalls on the rolling surfaces. Defects are generally categorised into four types: roller defect, damaged cage, inner and outer race faults [46].

A number of faults were artificially induced into the automotive bearings used in this study. Examples of these induced faults are presented here:

- 1) Roller fault; scratch and spalling of the roller, shown in Figure 5.2(a).
- 2) Outer race fault; scratching over approximately 30% of the outer race circumference, shown in Figure 5.2(b).
- 3) Damaged cage and roller fault; a small scratch on the roller along with a broken section of the cage, shown in Figure 5.2(c).

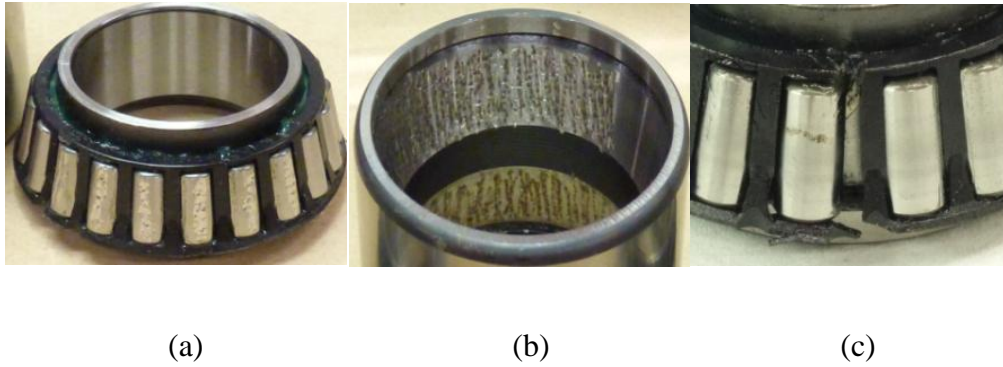


Figure 5.2- Typical faults of tapered-roller-bearing

The particular bearing faults used in this work are characterised as shown in Table 5.1.

Table 5.1- Bearing test fault conditions

Bearing Test ID	Description
F0	Good condition, no introduced defects.
F1	Minor damage (single small shallow fault) to one small area on each outer race, consisting of surface roughening by means of an electrical discharge engraver. Fault length 1.7% of circumference.
F2	Minor damage to one small area of one roller in each cage, again consisting of surface roughening by electrical discharge engraver. Fault length 10% of circumference.

A basic requirement of any bearing condition monitoring system is to identify faults, but not necessarily to categorise them. More advanced bearing monitoring systems, such as those presented in chapter 0, allow different bearing faults to be individually identified and categorised.

5.2.2 Test programme

Experiments were carried out at various speeds to support the evaluation of the processing techniques. The speed range is set based on the scaling theory in Table 4.1, the relationship between the spinning speeds of the scaled bearing and the train speed is:

$$v = 1/\lambda_d * V = 1/\lambda_d * V_T/D = 1/\lambda_d * V_T/(2 * \pi * d) \quad (5-5)$$

where v is the spinning speeds of the scaled bearing, λ_d is the scaling factor, V is the corresponding shaft speed of the train, D is the perimeter of the wheel, d is the diameter of the wheel, V_T is the train speed. Use the average wheel diameter of 1 metre, when the spinning speed of the scaled bearing is 500 RPM, the corresponding train speed is approximately 100 km/h. The train speed is approximately 200 km/h when the spinning speed of the scaled bearing is 1000 RPM. The test rig is shaking seriously when the spinning speed is over 1000 RPM. So at the development stage, preliminary 500 RPM and 1000 RPM tests were undertaken; for the main tests a wider range from 250 RPM to 1000 RPM was used. This speed range can cover the train speed from a normal speed to a high speed train standard. The characteristic frequencies for the test bearing are shown in Table 5.2 for each of the different test speeds.

Table 5.2 - Example of characteristic frequencies of the bearings

Scaled bearing (Hz)	Speed (RPM)					
	250	300	400	500	600	1000
FTF	1.8	2.2	2.9	3.6	4.4	7.3
BPFO	38.4	46.1	61.5	76.9	92.3	153.8
BPFI	49.05	58.8	78.5	98.1	117.7	196.2
BFF	32.9	39.5	52.7	65.85	79	131.7

Having known the test setup in the laboratory, the next step is to investigate the data processing methods to extract the information of the introductory bearing faults.

5.2.3 Novel processing algorithm on the experimental vibration signal

This section describes the processing method of the testing results, which is called the Empirical Mode Envelope with Minimum Entropy (EMEME) algorithm developed by the author [190]. The new technique combines elements from the Empirical Mode Decomposition (EMD) and Minimum Entropy Deconvolution (MED) approaches with an Energy Moment technique to improve the feature selection stage of the EMD algorithm.

The fundamental of EMD and MED has been introduced and described in chapter 3. So the following subsection is introducing the fundamental of Energy Moment technique which helps select the representative IMF.

5.2.3.1 *IMF selection by energy moment*

EMD can be used to identify a number of IMFs corresponding to the key sub-signals within an original signal. Some of these IMFs will be more appropriate for use in further processing than others. There are a number of methods to identify the most appropriate IMF such as the rotating frequency phenomena of rolling elements [168], energy of the IMFs [191], and energy entropy of the IMFs [192]. However, these methods disregard the distribution features of each IMF signal's energy [119]. Therefore, the extracted components of the signal may not accurately represent the nature of the fault.

In order to enhance the performance of feature extraction algorithms, IMF energy moment can be used as a method for the selection of a suitable IMF to represent the most important elements of the original signal. The energy moment technique calculates the energy distribution of each IMF in the time-domain. [119] illustrates the effectiveness of the energy moment technique by evaluating it using multiple sets of simulated signals.

Eq.(6) is the energy moment calculation (EM) for continuous signals and Eq.(7) is used for

discrete signals: A series of IMFs generated by EMD is $IMF_i(t)$, $i = 1, 2, 3, \dots$.

$$EM_i = \int t \cdot |IMF_i(t)|^2 dt \quad (5-6)$$

$$EM_i = \sum_{k=1}^n (k \cdot \Delta t) |IMF_i(k \cdot \Delta t)|^2 \quad (5-7)$$

where Δt is the sampling period; n is the total number of data samples.

Then, the normalised eigenvector of the signal based on the energy moment is:

$$E = [E_1, E_2, E_3, \dots, E_n] / \sum_{i=1}^n E_i \quad (5-8)$$

where each element of E corresponds to the percentage of the energy moment of the $IMF_i(t)$.

The IMF with the highest energy moment is then selected as the representative IMF.

5.2.3.2 Empirical Mode Envelope with Minimum Entropy (EMEME)

The EMEME method proposed in this paper results from the combination of the EMD and MED algorithms with the use of the energy moment technique for IMF selection. The first stage is to apply the EMD algorithm to the experimental signals, to generate a series of IMFs, and then to select the IMF with the greatest energy moment value as described in section 5.2.3.1. The second stage is then to apply the MED algorithm to minimise the signal's entropy, thereby emphasising key periodically occurring impulsive features.

In roller bearing diagnostics, the signals of interest are generally analytic signals, i.e. in the frequency domain representation any negative components can be disregarded. Such signals are affected by slippage occurring between the rolling elements and the races due to the presence of localised faults [168]. The analytic signal of the representative IMF, $r_k(t)$, is calculated and then used in the MED algorithm.

The Hilbert transform of the representative IMF $r_k(t)$ is:

$$H[r_k(t)] = \frac{1}{\pi} \int_{-\infty}^{\infty} r_k(t') / (t - t') dt' \quad (5-9)$$

The analytic signal of the representative IMF $r_k(t)$ [193] is:

$$z(t) = r_k(t) + jH[r_k(t)] = a(t)\exp(j\varphi(t)) \quad (5-10)$$

where

$$a(t) = \sqrt{r_k(t)^2 + H[r_k(t)]^2} \quad (5-11)$$

$$\varphi(t) = \arctan(H[r_k(t)]/r_k(t)) \quad (5-12)$$

In which $a(t)$ is the envelope, and $\varphi(t)$ is the angular characteristic of the analytical signal.

The behaviour of the envelope $a(t)$ is important as it preserves the energy of the measured signal. The MED process is applied to this envelope.

Figure 5.3 demonstrates the stages involved in applying the EMEME technique to a vibration signal.

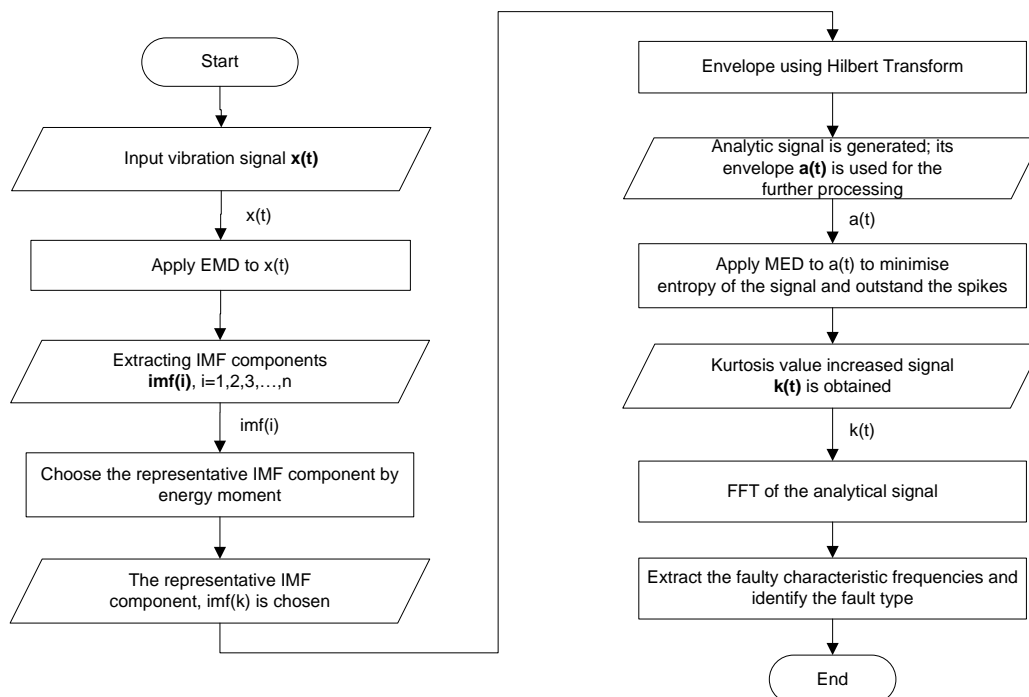


Figure 5.3- The flowchart of the proposed method process

5.2.3.3 EMD applied to experimental signal

In this section, EMD is applied to signals recorded from a healthy bearing at a speed of 500 RPM. By applying EMD, a series of 20 IMFs were extracted. IMF components extracted earlier in the process have a broader range of frequencies, and therefore cover a wider range of the frequency components from the original broadband signal. To demonstrate this fact, EMD was first applied to Gaussian noise and an FFT spectrum of the results was generated. The first 5 IMFs along with the original signal are shown in Figure 5.4.

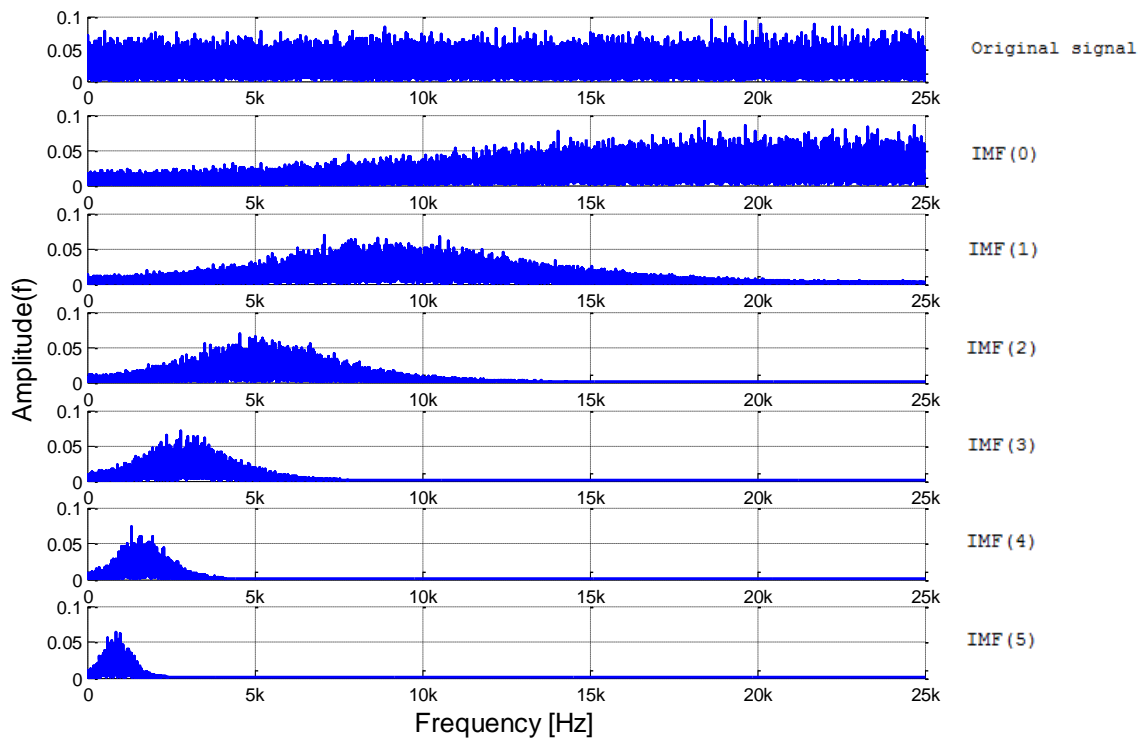


Figure 5.4 - IMFs frequency ranges

Figure 5.5 shows the original signal, and the IMFs and residuals arising from the application of EMD. The original signal and the residuals (obtained by removing the IMF from the original) are shown in the left hand column while the IMFs themselves are shown on the right.

The IMF component with the greatest apparent similarity is not always selected as the representative IMF because the relevant part of the signal can sometimes be masked by noise.

The EMD method decomposes the signal into different oscillation modes in the time domain, defined by the time between the local maxima or minima [194]. Hence the IMF components extracted earlier in the process are not always those with the greatest energy due to the alignment of the IMF with the periodicity of the fault.

The representative IMF should have the highest time-related energy, earlier introduced as the energy moment. The energy moment of each IMF signal is used to select the representative IMF. In this case, IMF(2) is chosen to be the representative IMF.

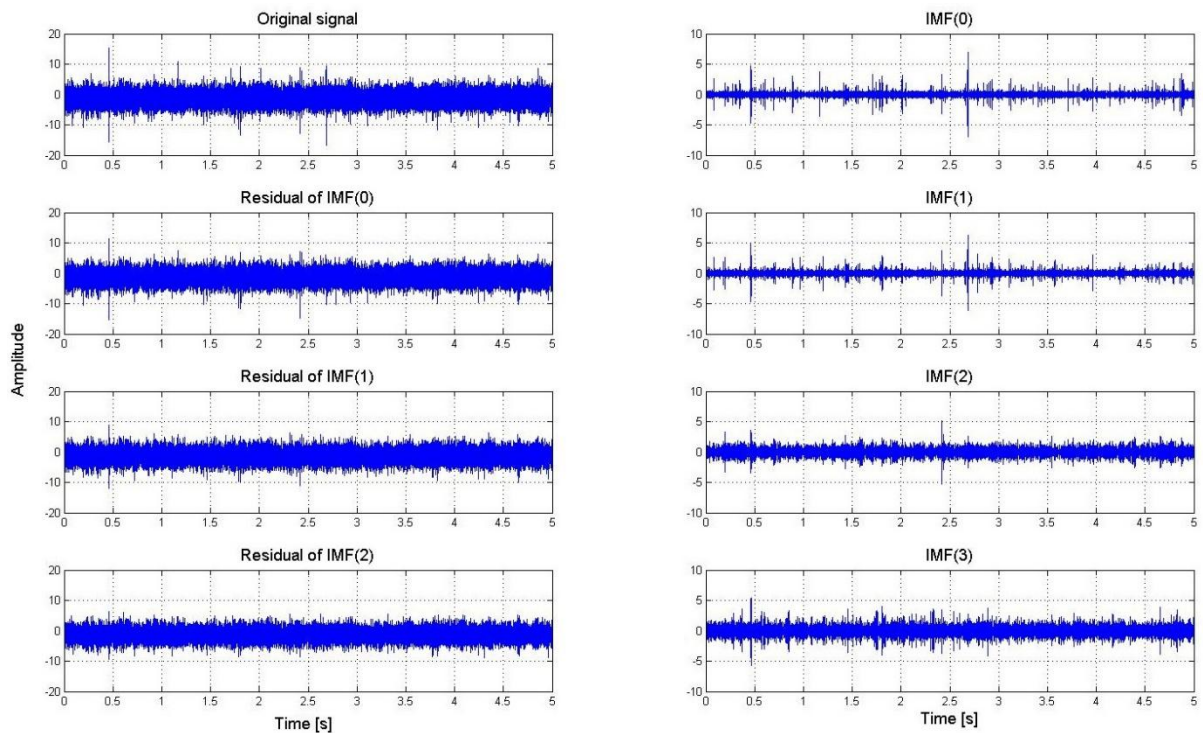


Figure 5.5- EMD procedure of the healthy bearing

5.2.3.4 MED applied to the representative IMF envelope

MED is applied to the representative IMF of F1 and F2 and the results are shown in Figure 5.6 and Figure 5.7.

A non-dimensional quantity that measures the relative “peakedness” of a signal relative to the Gaussian distribution (known as Kurtosis) is calculated and shown in the figures to

demonstrate the effectiveness of the MED. For normally distributed data, such as the distribution of the natural vibrations of a healthy bearing [195], the kurtosis value is 3. For signals with repetitive impulsive forces, the kurtosis can be much greater. Although kurtosis cannot identify a particular type of defect, it can be used to indicate if there is defect present in a bearing. In this case, the vibrations resulting from the motion arising from the irregularities in the bearing's internal components can lead to a significantly increased kurtosis value. In Figure 5.6 and Figure 5.7, the filter length of the MED is set to correspond to the bearing's rotational speed (in Hz). The figures show that the kurtosis values of the signals filtered by MED increase, this indicates that the spikes related to the bearing faults are enhanced.

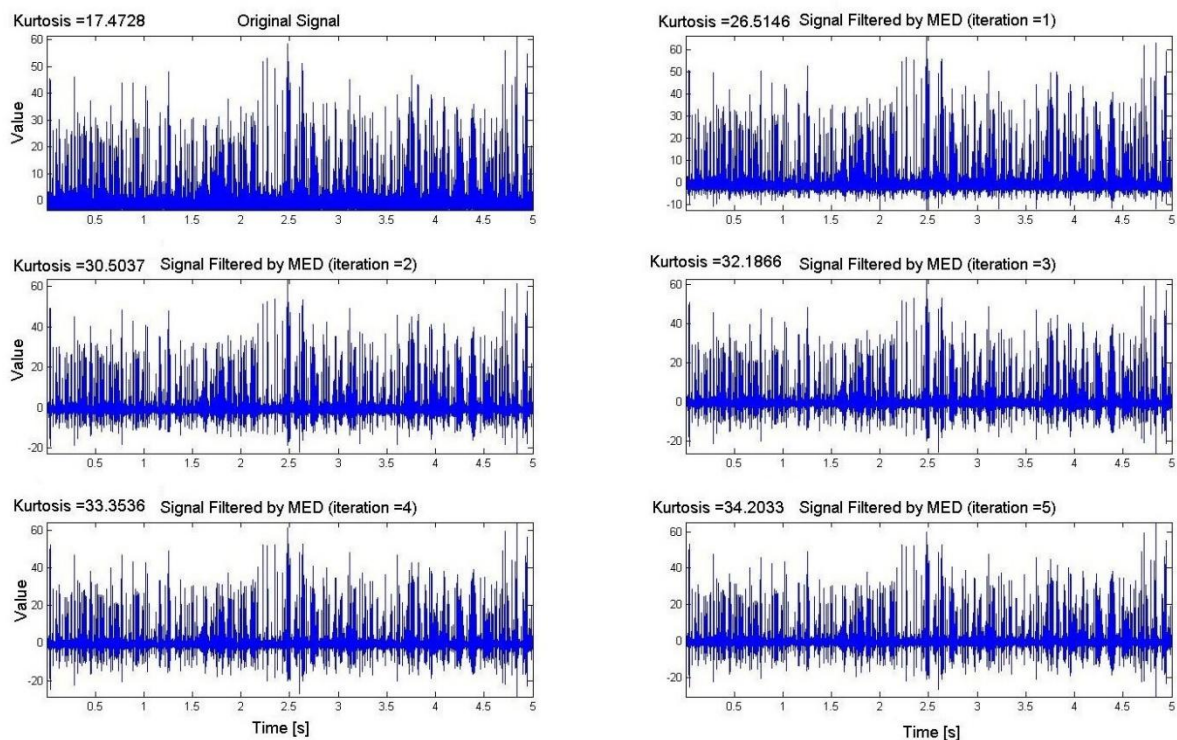


Figure 5.6- Effect of MED iterations when applied to F1 faulty vibration signal

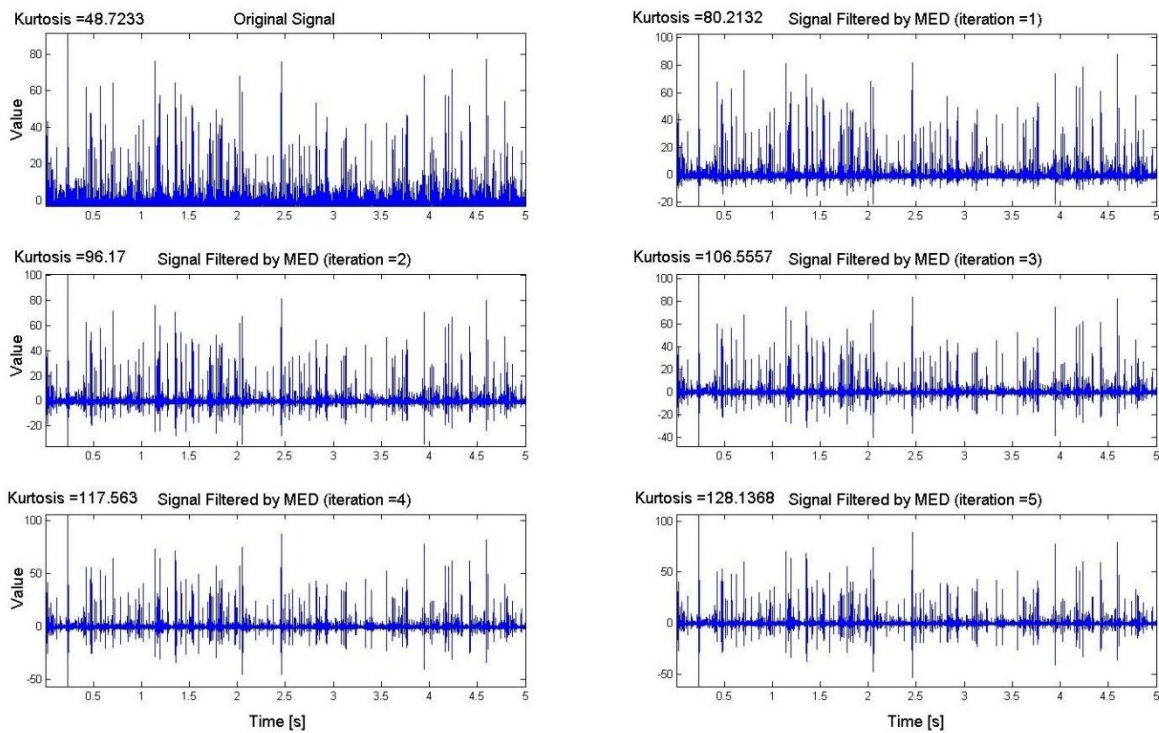


Figure 5.7- Effect of MED iterations when applied to F2 faulty vibration signal

5.2.3.5 Verification of EMEME results

Frequency domain analysis is used to verify the EMEME result. The results of the healthy and faulty bearings are shown in this section where the feasibility of the method is also evaluated under induced noisy conditions. Vibration data recorded from faulty bearings with minor damage on the outer race and on the roller (F1 and F2), spinning at speeds from 250 RPM to 1000 RPM, are used to evaluate the method.

The results of the lowest rotational speed of 250 RPM (i.e. 4.17 Hz) and the highest speed of 1000RPM (i.e. 16.7 Hz) are presented. The former case illustrates the bearing diagnosis results when the bearing vibration is weak and the latter shows the results when the vibration noise is high. A Fast Fourier Transform (FFT) has been applied to the signals obtained with EMEME. The spectrums are shown in Figure 5.8 and Figure 5.9. The equivalent results from F0 healthy bearing are also presented for comparison purposes, in order to clearly indicate the abnormal behaviour of the faults.

In the spectrums presented here, the arrows indicate the calculated principle bearing frequencies (see Table 5.2) for both cases. A certain amount of out-of-balance rotation can be clearly seen in the two graphs, which is the primary unbalance at the shaft speed (ω_r) [51]. The bearing inherent frequencies have also been calculated and are shown in the two graphs. These are the Fundamental Train Frequency (f_c), the Ball Frequency of the Outer Race (f_{bo}), the Ball Frequency of the Inner Race (f_{bi}), and the Ball Fault Frequency (f_{bf}).

Comparing the healthy results for the two cases; the difference between the average background noise level and the characteristic frequencies shown in the 250 RPM situation is of greater magnitude than in the 1000 RPM scenario. This implies a greater level of background noise in the measurement taken at higher speed.

Comparing the healthy (F0) and faulty bearings (F1 and F2); the out-of-balance level, indicated by the shaft speed, is always the highest component in the spectrum of F0, while the appropriate fault frequencies (Ball Frequency of the Outer Race for F1 and Ball Fault Frequency for F2) are highlighted in their respective spectrums. This demonstrates that the EMEME approach is capable of extracting and emphasising the faulty information from defective bearing signals without pre-knowledge of the fault type.

The peaks numbered 1, 2, and 4 in Figure 5.8 and Figure 5.9 correspond to the frequencies of the principle 1st harmonic of the shaft speeds. The peaks numbered 3 and 5 are at the frequencies of the principle 1st harmonic of the respective fault frequencies (f_{bo} for the bearing with the damaged outer race, and f_{bf} for the bearing with the damaged roller). This demonstrates that the EMEME approach can be used to identify not only the fundamental frequency, but also the first harmonic components of fault information in the frequency domain.

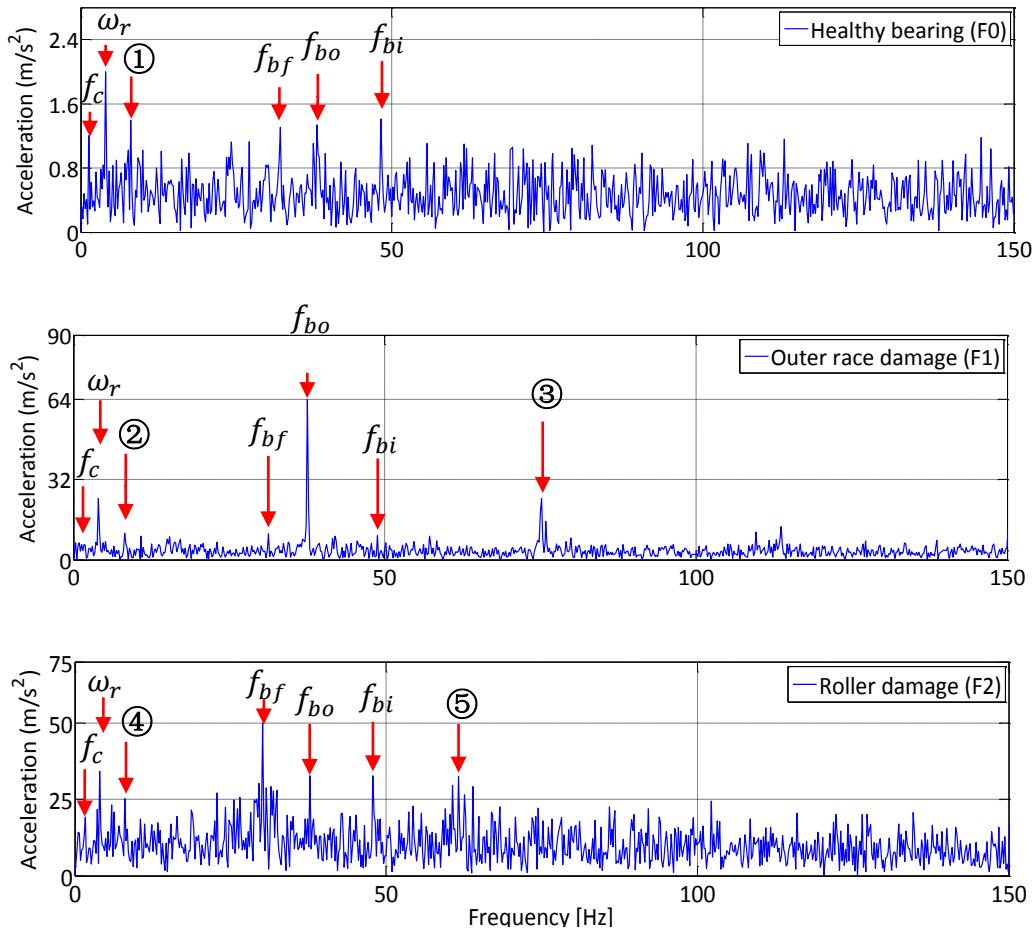


Figure 5.8- FFT envelope of healthy and faulty bearing spinning at 250 RPM (Top) healthy bearing (Middle) outer race damaged bearing (Bottom) roller damaged bearing 's EMEME algorithm processed data

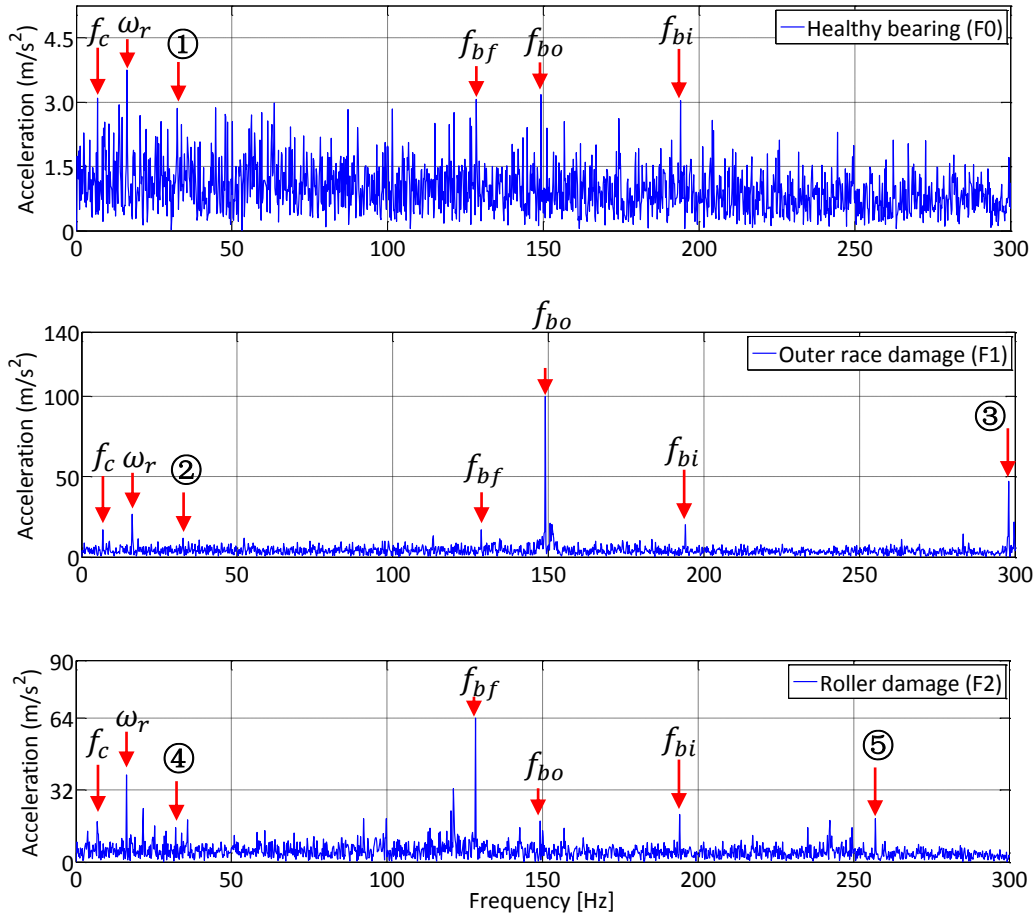


Figure 5.9- FFT envelope of healthy and faulty bearing spinning at 1000 RPM (Top) healthy bearing (Middle) outer race damaged bearing (Bottom) roller damaged bearing 's EMEME algorithm processed data

5.2.3.6 Comparison to conventional HFRT

The envelope analysis technique discussed in the introduction of this thesis is also known as the High Frequency Resonance Technique (HFRT). HFRT operates by applying specific filters to emphasise particular frequency bands of interest, usually above 4 kHz, within the signal [49, 58]. Low amplitude, high frequency, components are then shifted to a lower frequency range where the modulating signal can be extracted. An FFT is then applied to the resulting signals to give a final frequency characterisation.

In this section, traditional HFRT is compared to the new EMEME method presented in this thesis. Figure 5.10 shows the results of applying the HFRT (left) and EMEME (right) processing methods to data recorded from the test rig using a bearing with an induced outer race fault rotating at 500 RPM. Normalised acceleration is used to describe the amplitude of each frequency component, in order to simplify comparison of the waveforms. Both methods clearly identify the primary fault frequency and the Ball Frequency of the Outer Race (f_{bo}). The HFRT method also identifies the next 3 harmonics, while the EMEME technique highlights the 1st harmonic more clearly, but then does not indicate the higher harmonics as well.

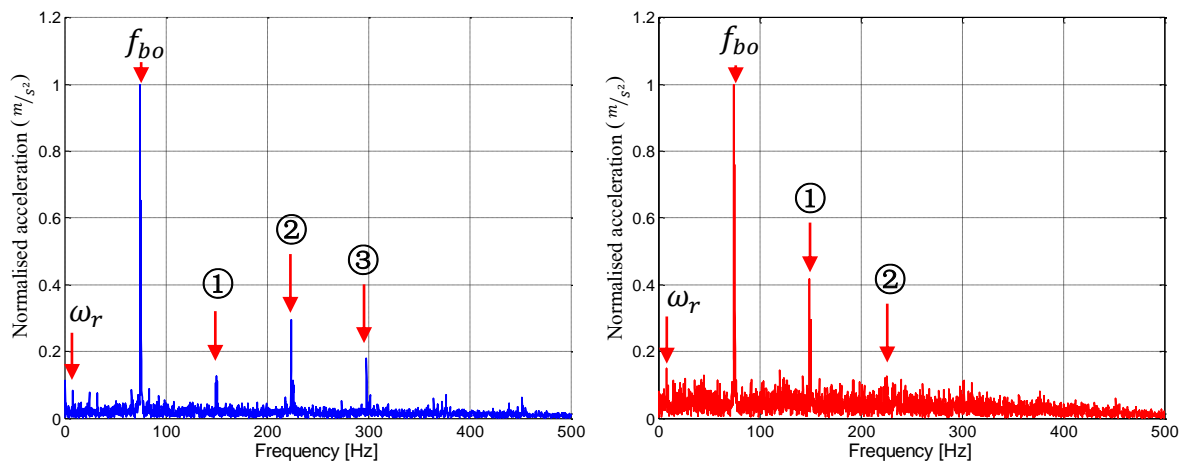


Figure 5.10 - Conventional envelope method (left) vs EMEME (right) at 500 RPM no added noise

The comparison presented in Figure 5.10 shows the use of both HFRT and EMEME in low noise (laboratory) conditions. In order to make the test more representative, and also to further challenge the algorithms, artificial Gaussian noise was introduced into the signals using MATLAB prior to processing [196]. The level of noise inserted into the signal generated a Signal to Noise Ratio (SNR) of 5. The results of the algorithms applied to the noisy signal are shown in Figure 5.11 with the HFRT on the left and the EMEME on the right.

With the addition of the noise the standard HFRT processing performs less well, particularly in relation to the 1st harmonic which is barely visible in the spectrum. The EMEME technique, however, still clearly shows the primary fault frequency with the 1st harmonic, as well as a further 4 harmonics to a lesser extent.

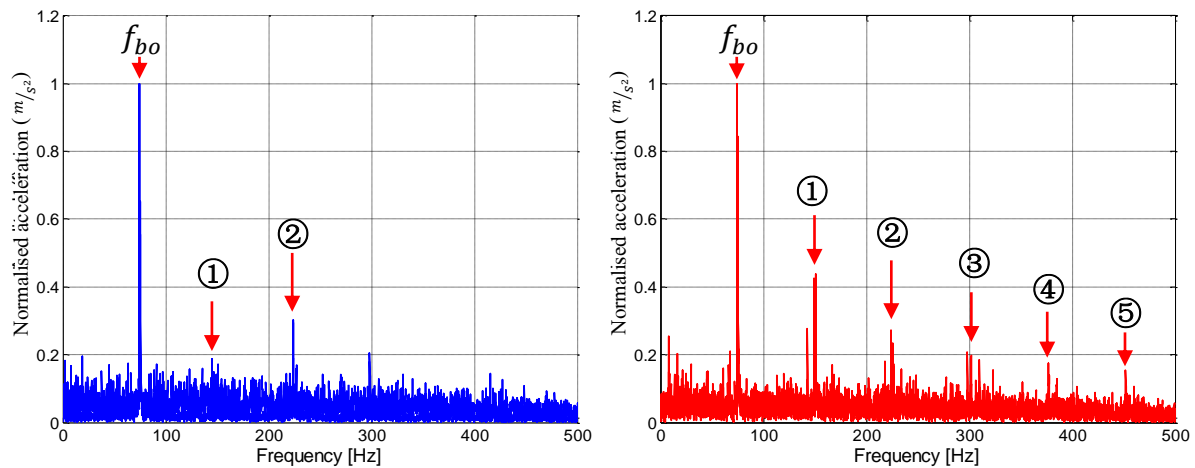


Figure 5.11 - Conventional envelope method (left) vs EMEME (right) at 500 RPM with noise
SNR of 5

Increasing the level of noise introduced into the signals from an SNR of 5 to an SNR of 1.5 further increases the challenge to the algorithms. The results, shown in Figure 5.12, indicate that the noise floor in the spectrum resulting from the HFRT processing is increased to a point where only the fundamental fault frequency is clearly identifiable. Conversely, even with this increased level of noise, the EMEME processing still provides clear indications of both the fundamental fault frequency and the 1st harmonic.

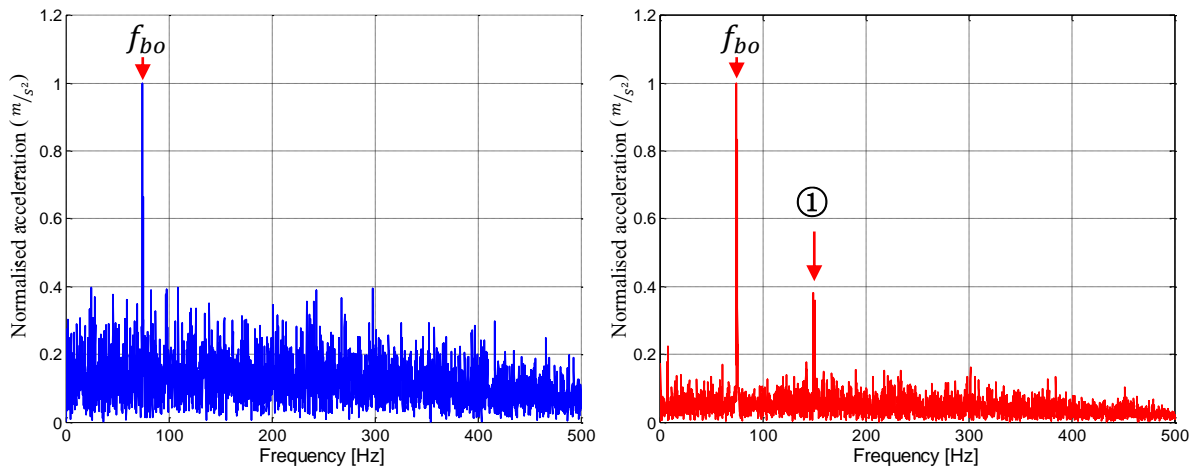


Figure 5.12 - Conventional envelope method (left) vs EMEME (right) at 500 RPM with noise
SNR of 1.5

5.2.3.7 The enhancement of energy moment feature extraction method

To illustrate the advantages of using the energy moment technique to select the representative IMF, a comparison has been made between it, traditional energy evaluation methods [193], and selecting just the first IMF as used in [168].

Taking the case of the F1 faulty bearing as an example; a chart showing the results of the traditional energy evaluation method and the energy moment technique for different IMFs is presented in Figure 5.13. The chart shows the distribution of the amplitude values for the top 10 IMFs, calculated as per equation (5-7) and (5-8) in the case of the energy moment and as per [193] for the traditional energy technique.

In both cases, the second (rather than the first) IMF is found to be that with the highest value. To further evaluate the selection of the second IMF (as selected by the energy moment feature extraction method) compared to the first IMF, Fast Fourier Transforms (FFTs) of the processed signals are shown in Figure 5.14. The noise level present in the spectrum corresponding to the chosen IMF, IMF(2), is reduced and hence the shaft speed and the 2nd harmonic of the fault frequency are more clearly visible.

For this example, and with minimal noise in the signal, Figure 5.13 shows only a very minor difference in amplitude between the 2nd IMF identified using the energy moment technique and the traditional energy approach. This difference is greater in scenarios with lower signal to noise ratios.

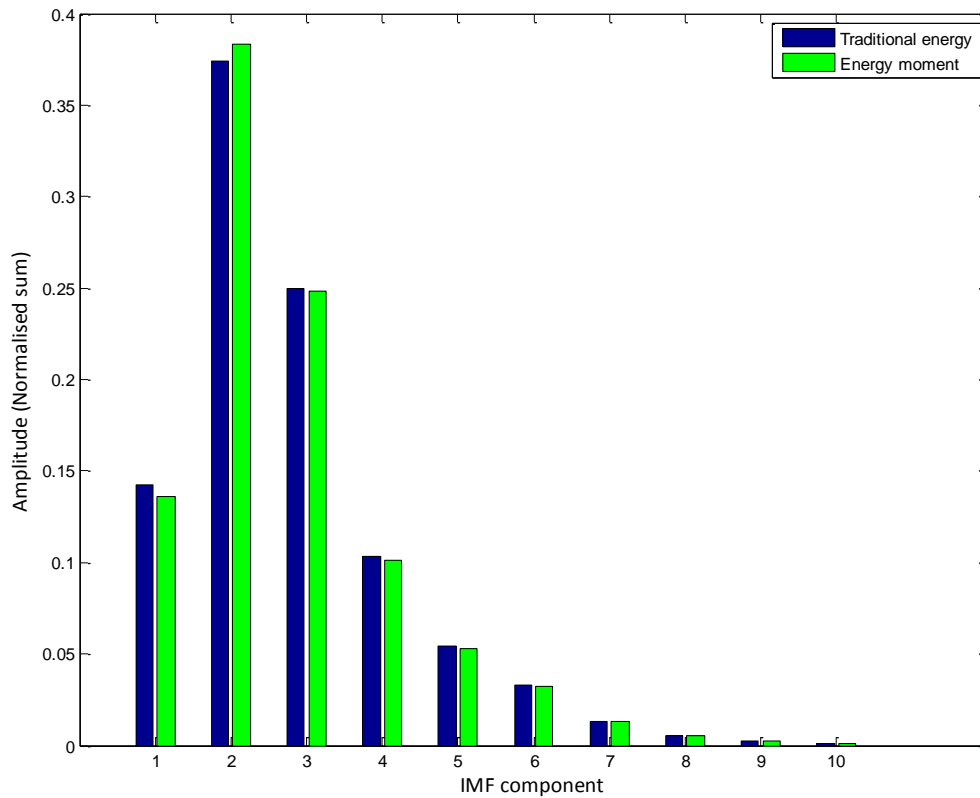


Figure 5.13 – Distribution of amplitude values of IMF components generated using the energy moment and traditional energy techniques

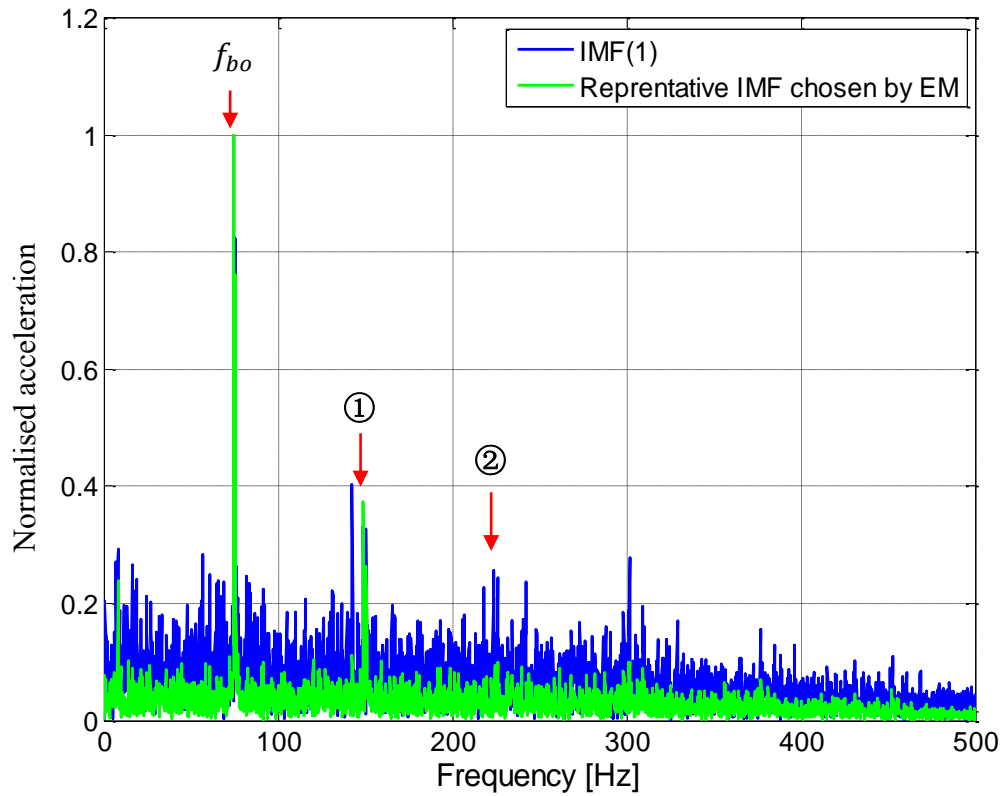


Figure 5.14 – FFT envelopes generated using the energy moment feature extraction method and IMF(1)

In order to evaluate the use of the energy moment IMF selection technique for noisy environments; data was collected from the same faulty bearing installed in a complex system including a Radicon Series J gearbox with a 4.94:1 ratio [197]. Figure 5.15 shows the signals recorded from both the roller defective bearing (left), and the faulty bearing coupled to the gearbox (right).

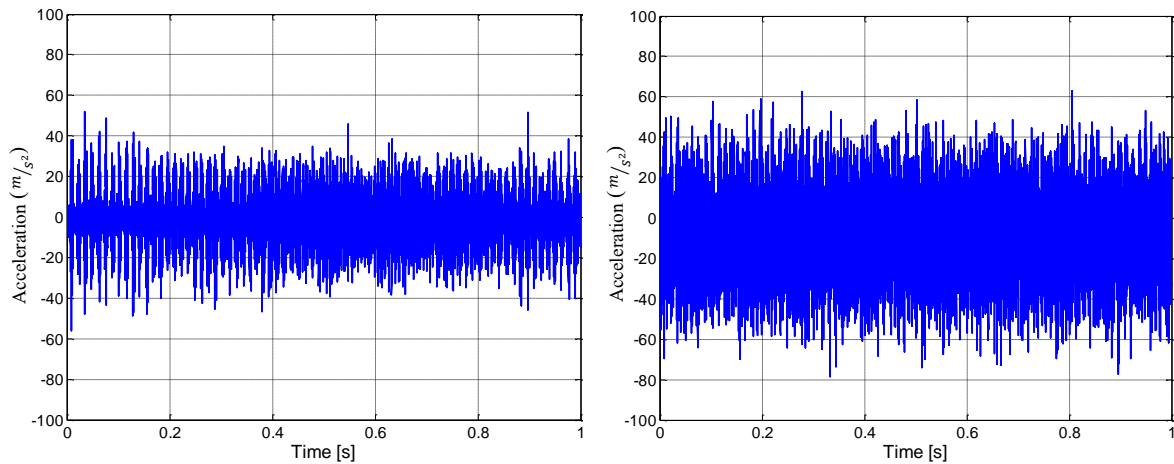


Figure 5.15 - Signals from faulty bearing, (left) simple system (right) Complex system including gearbox

Figure 5.16 shows the distribution of the amplitude values of the top 10 IMFs for the traditional energy and energy moment evaluation techniques in this case. In this case, with increased signal noise, the IMF selected by the two techniques is different. The energy moment technique selects the second IMF, while the traditional energy approach selects the fourth.

As with the original example, the Fast Fourier Transforms (FFTs) of the processed signals are shown in Figure 5.17. All of the three techniques considered identify a key vibration resulting from an outer race fault, the Ball Frequency of the Outer Race (f_{bo}). The graph on the left presents a comparison between the energy moment feature extraction method and selecting only IMF(1) (the technique used in [168]). The graph on the right shows a comparison between the energy moment and traditional energy methods for IMF selection.

In the figure, the greatest fault frequency amplitude is seen to be in the envelope generated from the IMF selected using the energy moment processing technique. The traditional energy approach generates greater peak values than those generated from IMF(1).

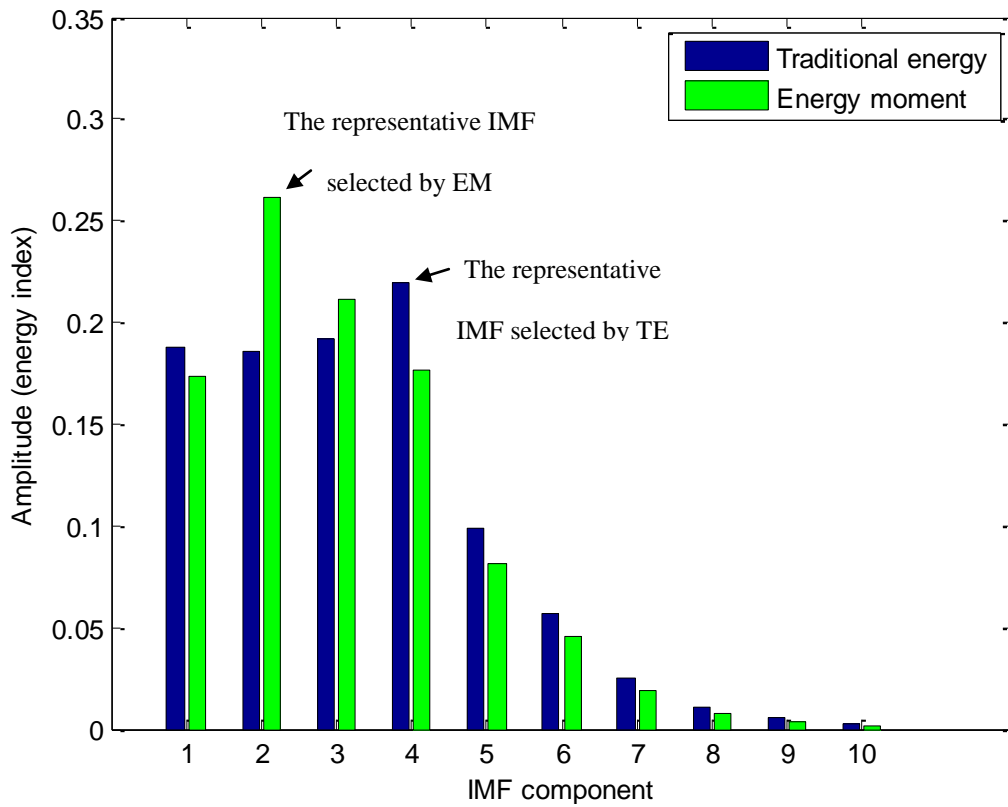


Figure 5.16 – Distribution of amplitude values of IMF components generated using the energy moment and traditional energy techniques for the complex system including gearbox noise

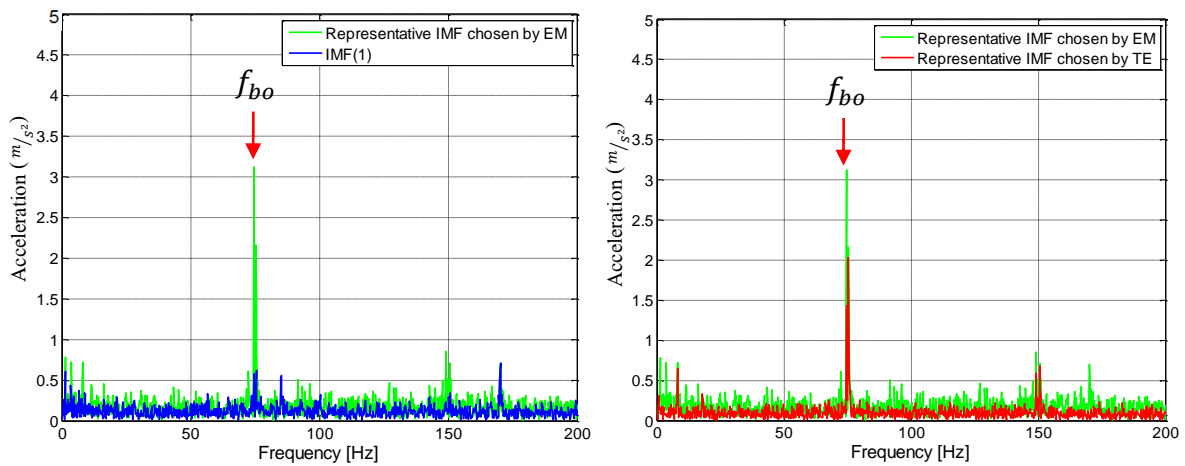


Figure 5.17 – FFT envelopes for a signal including gearbox noise, (left) IMF selected using the energy moment technique (EM) and for IMF(1) (right) IMFs selected using the energy moment technique (EM) and the traditional energy (TE) method

5.2.3.8 *Summary*

The EMEME technique has been applied to the vibration data of the roller bearing spinning on the test rig. It can extract the introductory faults information and to generate frequency spectra which demonstrate the key frequencies associated with each different fault type. The clarity of these elements of the spectra is indicative of the improved performance of the technique. Tests have been carried out with particularly minor levels of the selected faults in order to demonstrate the technique's ability to detect early stage (minor) symptoms. Additional comparisons with conventional envelope processing and EMD/MED techniques using a statically selected IMF have also been carried out. This has shown that the proposed technique is also suitable for use in complex systems and noisy environments, and provides a clearer identification of faults within the results spectra.

In addition to the suitability of the EMEME technique for identifying the fundamental fault frequency in a complex system; results presented in this thesis indicate improved capability for the identification of harmonics associated with this fundamental fault frequency. These harmonics can be used to improve the reliability of the classification of a fault associated with the bearing.

5.3 Acoustic microphone application – Lab based

In the last section, the application of the vibration sensor has been discussed. A novel processing algorithm is demonstrated with the comparison with the traditional algorithm. The results indicate the effectiveness of the new algorithm on the vibration signal of the bearing.

In this section, the processing signal is the acoustic signal. Its property is different from the vibration signal. So a new algorithm is needed. The development of the new algorithm is based on the understanding obtained from the vibration signal processing work.

In this work, the vibration sensor application is used as a reference system of the acoustic microphone application which can prove the system construction can work. As per discussed in chapter 3, due to the high quality of the vibration signal, especially compared to the sound intensity collected by the air coupled acoustic microphone, the data processing technique is less complicated than the data processing of the acoustic microphone application. So using the vibration sensor application as a reference system can help the developer understand the behaviour of the roller bearings.

In this section, the acoustic microphone application is going to be discussed. Acoustic microphone technique has many advantages, one of which is its capability to extract more comprehensive information from audio signal than vibration or acoustic emission sensor with proper audio signal analysis. The useful information in audio signal can retrieve the scenario rather than telling the anomalies in acoustic energy generation [198]. In this thesis, one of the most significant advantage of the acoustic microphone application compared to the vibration and acoustic emission sensor is that in certain circumstances, e.g. where physical access to the bearing is limited or difficult, air coupled acoustic condition monitoring systems can be advantageous in the characterisation of system health and in fault prediction.

The experiments are carried out in the anechoic chamber room (shown in Figure 4.4) which aims at reducing echo reflection and simulating the free field conditions. The data are collected using an air coupled acoustic microphone mounted beside the test rig, shown in Figure 4.5.

5.3.1 Test programme

As the vibration sensor application is used as a reference system of the acoustic microphone application, the test programmes were shared between these two applications. So the

experiments were carried out at from 250 RPM to 1000 RPM as well. The characteristic frequencies of the acoustic signal are the same as the characteristic frequencies of the vibration signal which is listed in Table 5.2.

5.3.2 Novel processing algorithm on the experimental acoustic signal

This section describes the processing algorithm of the experimental acoustic signal. Little literature is the application on the acoustic noise response method, most of the condition-based signals processing techniques are applied on vibration and acoustic emission signals. As per discussed in chapter 3, these processing techniques are divided into the basic, intermediate and advanced processing techniques. In the application on the vibration signal, the advanced processing techniques have been used and combined to extract the bearing faulty information. However, the contents of acoustic microphone signal are complicated since the signal strength is weak when it is recorded by the air coupled microphone. Also the issue of low signal-to-noise ratio (SNR) results in the difficulties in the acoustic microphone signal processing. The algorithm proposed here is capable to overcome these obstacles. It is the combination of the processing techniques in different levels in the different stages. The purpose is to extract the faulty information from the complicated contents of the signal.

The proposed algorithm is divided into three stages: acoustic noise filtering, non-stationary feature extraction and the diagnosis results analysis. Within the three stages, the procedure can be further divided into six steps. The flowchart of the proposed processing algorithm is shown in Figure 5.18. The following sections are describing the algorithm by stages.

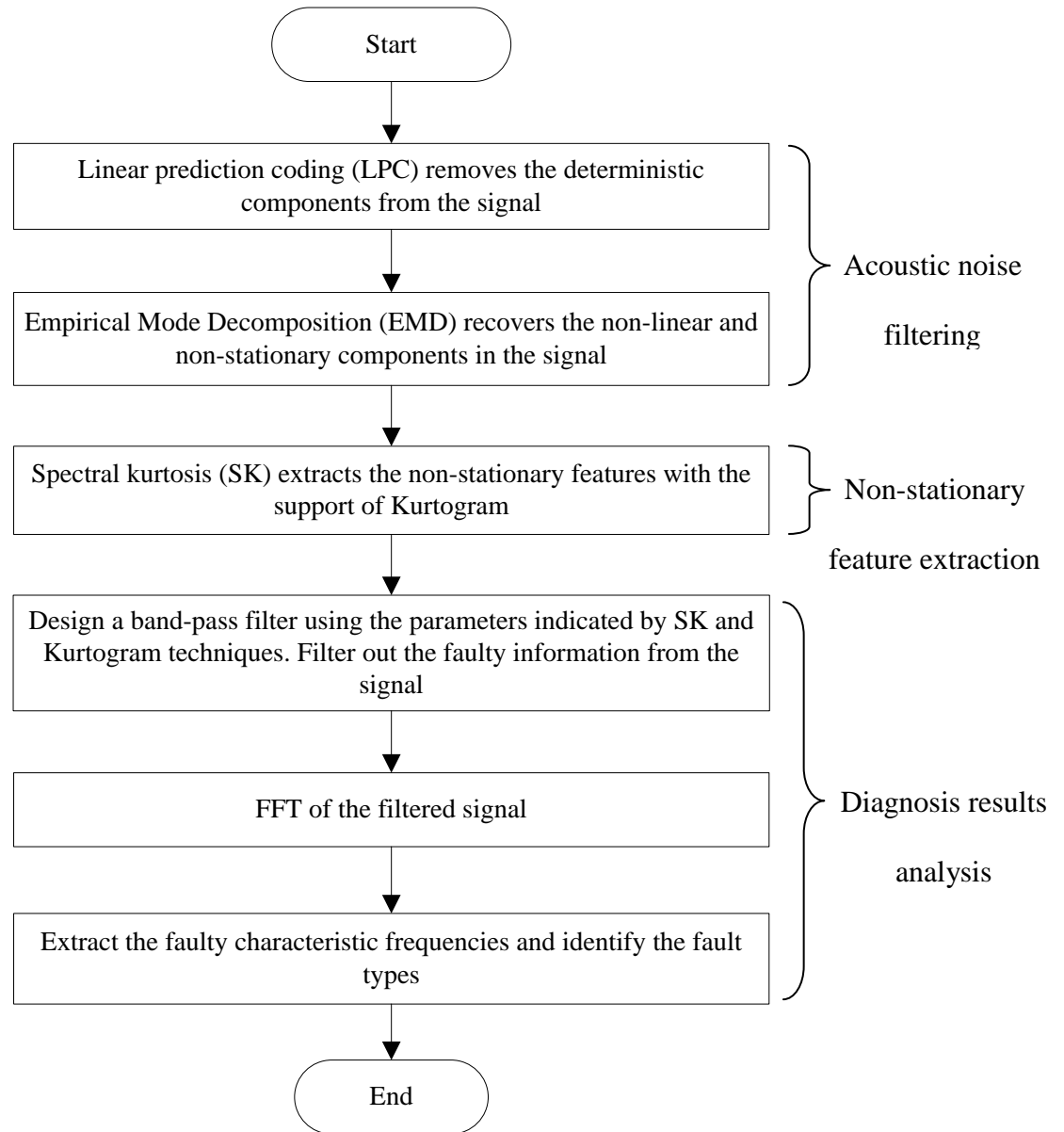


Figure 5.18 – Flowchart of the novel processing algorithm on the acoustic signal

5.3.2.1 Acoustic noise filtering: Integration of LPC & EMD

In this section, the objective is to filter the acoustic noise from the signal. As per discussed in chapter 3, Linear Prediction Coding (LPC) is effective on audio signal filtering. And based on its working principle, LPC can remove the deterministic components from the signal, the residual of which contains the non-linear bearing signal in interests. Empirical Mode Decomposition (EMD) can be well suited to recover the non-linear and non-stationary signals.

Also it can reduce the signal distortion, which makes up the limitation of the band pass filter [199].

So in the acoustic noise filtering stage the integrated filtering technique applying LPC followed with EMD is proposed.

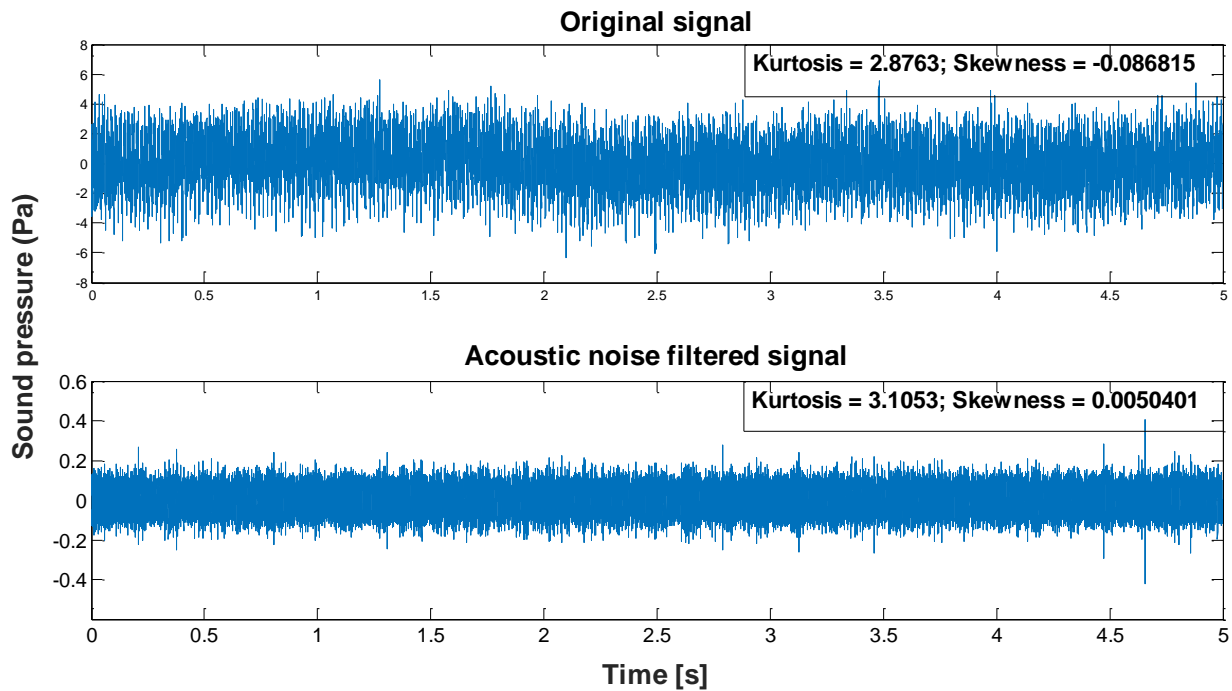


Figure 5.19 – Signal of the outer race damaged bearing spinning at 400 RPM (Top) original signal (Bottom) acoustic noise filtered signal

In Figure 5.19, the waveform on the top is the experimental signal of an outer race damaged bearing spinning at 400 RPM. The waveform is the processed signal without the DC offset. In the demonstration of the filtering procedure, this scenario is used as an example. As per introduced above, kurtosis is a measurement of the relative “peakness” of a signal relative to the Gaussian distribution, and skewness is a measure of the degree of asymmetry of a distribution. Theoretically, for the distribution of a healthy bearing, kurtosis value is 3 [49]. In the waveform, the kurtosis and skewness values are close to the theoretical values of a

healthy bearing, which means the faulty information is masked under the noise components in the signal.

After the acoustic noise filtering stage, the high energy “deterministic” acoustic noise has been filtered, and the representative IMF has been chosen inferred by EM calculation from the EMD process. The waveform at the bottom is the acoustic noise filtered signal. As the indication of the fault information, the kurtosis and skenewss value do not change much. So the faulty information is still masked under the noise. The average amplitude of the filtered signal has significantly decreased since the high energy acoustic noise is filtered out.

5.3.2.2 Non-stationary feature extraction: Application of Spectral Kurtosis (SK) and Kurtogram

The objective of this step is to extract the non-linear and non-stationary faulty feature of the bearing. The SK is proposed in this step due to its effectiveness in the extraction of the non-stationary features. The working principle of SK has been discussed in chapter 3. The following feature extraction demonstration corresponds to its working principle. And the demonstration procedure references the SK application on vibration signal of roller bearings in [160, 200].

In the spectral kurtosis working procedure, there are no rules for setting the duration of the analysis window. The strategy is to compute the Short-Time Fourier Transform (STFT)-based SK for different durations and uses the maximum value of SK to infer the most appropriate analysis window length.

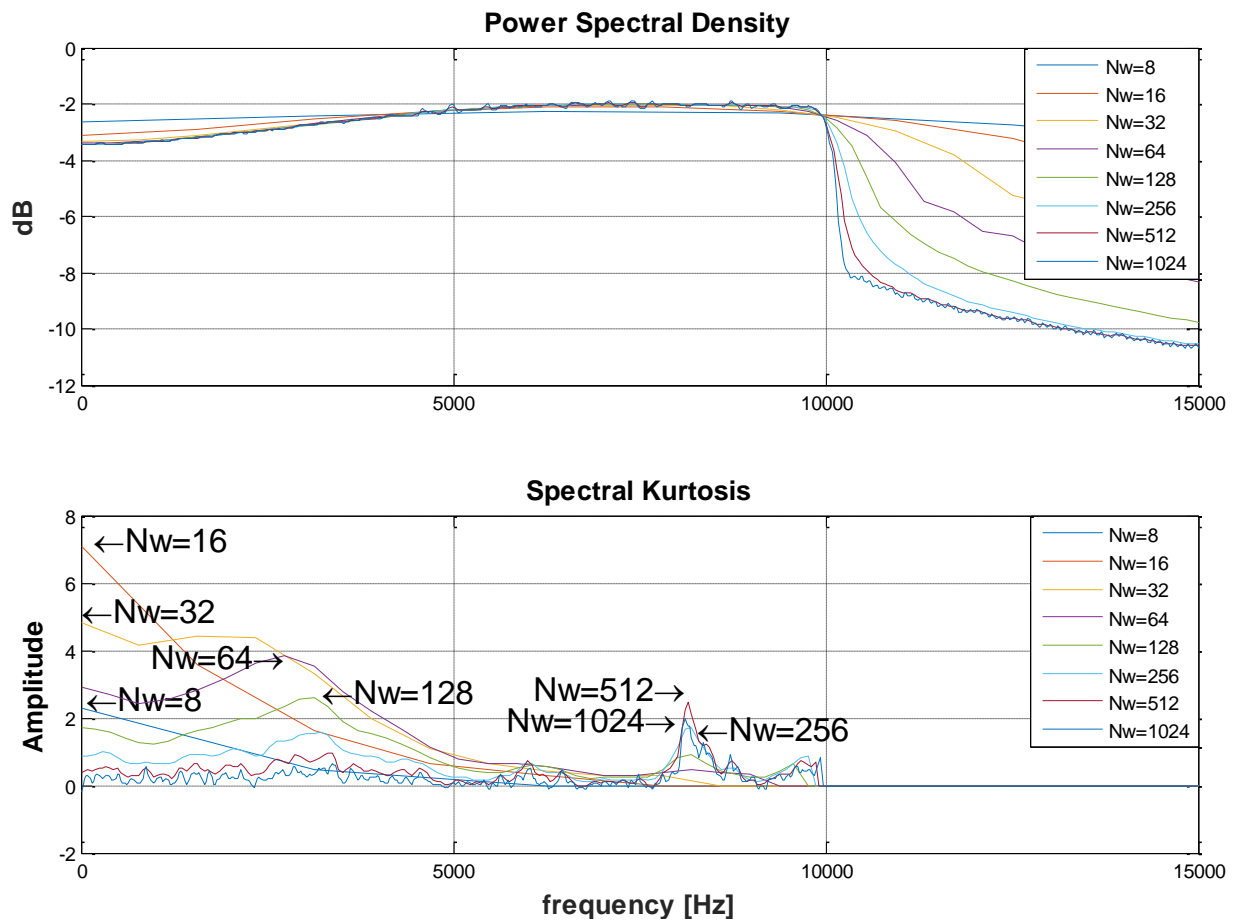


Figure 5.20 – (top) PSD and (bottom) SK computed in different frequency resolution ($N_w = 8, 16, 32, 64, 128, 256, 512, 1024$). The analysed signal is from an outer race damaged bearing @ 400RPM

Figure 5.20 shows the Power Spectral Density (PSD) (on the top) and SK (at the bottom) of the acoustic signal from the case of an outer race damaged bearing spinning at 400 RPM. Different waveforms in different colours correspond to window lengths $N_w = 8, 16, 32, 64, 128, 256, 512, 1024$ (the sampling frequency is 50 kHz, so the spectral resolutions are 6250, 3125, 1563, 781, 391, 195, 98 Hz). In all cases, the PSD does not indicate the differences with the window length changes. On the other side, the SK clearly reveals the presence of a transient signal in the frequency band from 0 Hz to around 4 kHz. The maximum SK values are reached at 0-1 kHz where the theoretical Ball Passing Frequency Outer Race (BPFO) frequency in Table 5.2 locates in.

From the figure of the SK waveforms, it can be seen that the SK value in the frequency band of interests increases from the window length $N_w = 8$ to $N_w = 16$, then the value decreases to nearly zero when the window length $N_w \geq 512$ which means the frequency bandwidth is over split by the analysis window. Therefore, an appropriate window length should be between 8 and 32, the corresponding spectral resolution is 1563-6250 Hz. It can be 14 and 3125 Hz as the optimal window length and the corresponding spectral resolution.

The strategy of setting the duration of the analysis window can be called as logarithmic grid estimation since all the estimated window lengths are the powers of two. Considering the settings strategy development of the analysis window's duration, the window length N_w and the central frequency f_c are the two key parameters of a narrow-band filter. And both of them can be indicated by the maximum SK value of the window length estimation. Once the optimal f_c and N_w are decided, the narrow-band filter can be designed to filter out the non-stationary features which are the faulty features of interest.

Kurtogram is the function to realise the goal. It is the map formed by the the Short-Time Fourier Transform (STFT)-based SK as a function of f_c and N_w [160]. So, the optimal f_c and N_w are found as those values jointly maximise the kurtogram. A typical kurtogram diagram is shown in Figure 5.21, in which the signal is from an outer race damaged bearing (spinning at 400 RPM). As stated above, the fundamental of kurtogram is to calculate the SK value corresponding to the different window lengths N_w . X axis is the frequency, Y axis is the window length represented in terms of the logarithm of two, and the colours in the graph reflects the SK values which can be read from the colour bar on the right.

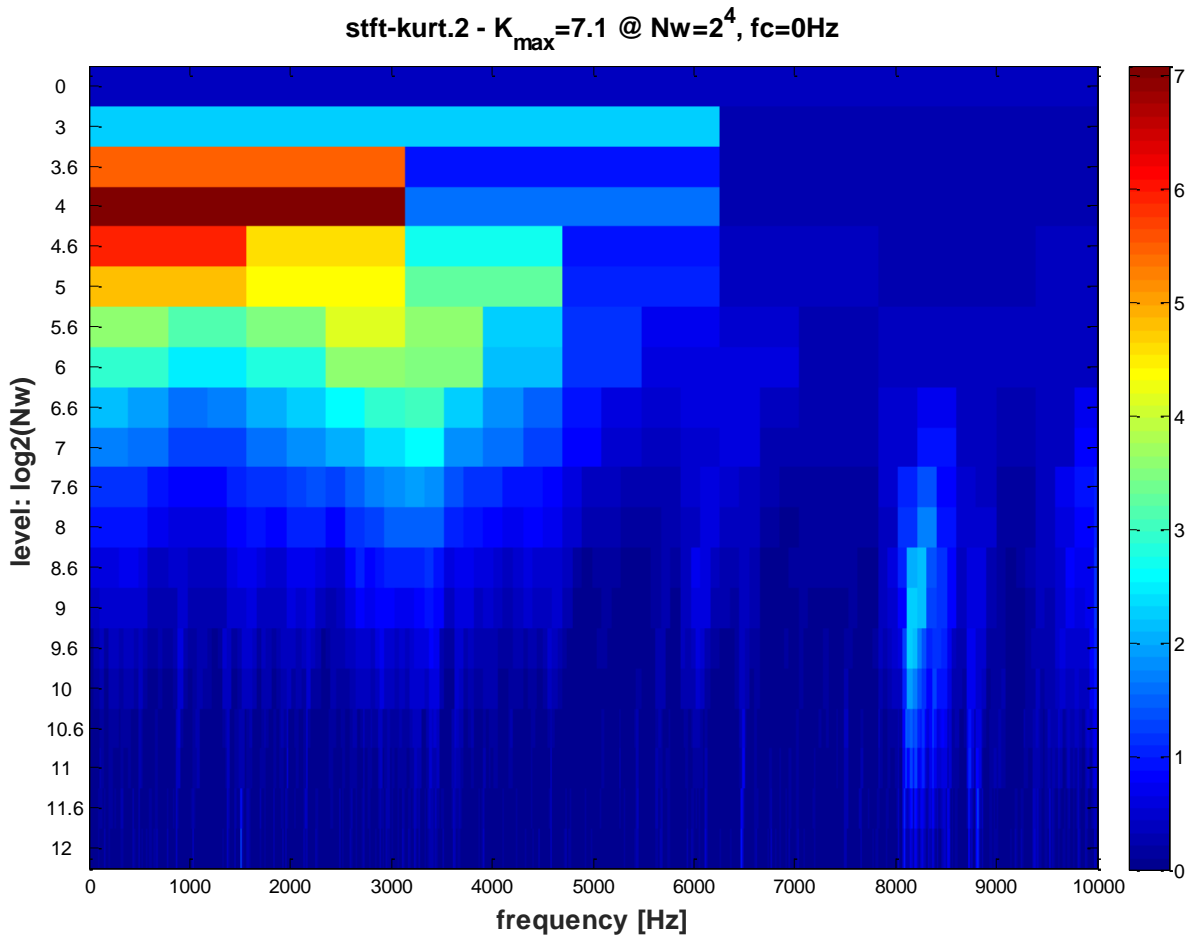


Figure 5.21 – Kurtogram of the signal from an outer race damaged bearing @ 400RPM

In the kurtogram diagram, the window lengths are shortening from bottom to the top. In correspondence, the spectral resolutions are reducing with the shortening of the window lengths. So in the diagram, the colour blocks keep becoming bigger from bottom to the top.

Comparing to the strategy of logarithmic grid estimation, kurtogram can reveal the pair of the central frequency and window length $\{f_c, N_w\}$ more clearly. In Figure 5.21, the presence of the maximum SK value locates at $\{f_c, N_w\} = \{0 \text{ Hz}, 2^4\}$. The corresponding envelop magnitude of the sub signal in $\{f_c, N_w\} = \{0 \text{ Hz}, 2^4\}$ is shown in Figure 5.22 with the referencing input acoustic signal.

Having discussed the feature extraction procedure, the next and final step is to diagnose the signals from the faulty bearings.

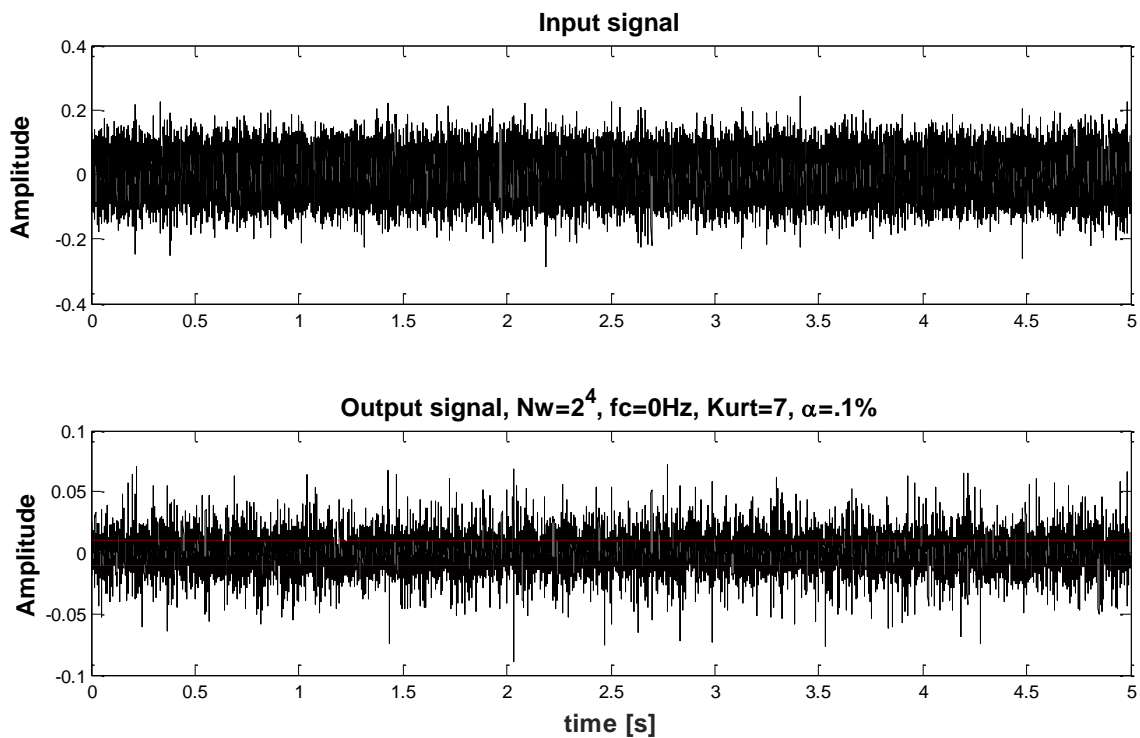


Figure 5.22 – (a) Input acoustic signal and (b) magnitude of the envelope $\{0 \text{ Hz}, 2^4\}$ which maximises the kurtogram, together with its 0.1% signification threshold

5.3.2.3 *Diagnostics with the SK*

The SK is valuable to detect the presence of incipient faults, and indicating the central frequency and the window length for the “detection filter” design. This is the main advantage of using the SK to design filters blindly without any prior information on the system.

Many “detection filters” exist in the literature. They all correspond to different criteria. But all of them can be blindly designed with the support of the SK. Among these filters, typical detection filters used in bearing signal (mostly applied to vibration signal) analysis are the Wiener filter, the matched filter, and the dB-spectrum difference filter [160]. The difference in dB-spectra is an empirical technique used in vibration monitoring. The Wiener filter is the optimal filter that well recovers the interesting signal from background noise. So it can recover the exact shape of the transient signal [160]. In this case, the experimental acoustic

signal processing, filtering the transient signal with the maximum signal-to-noise ratio is the most important. A “matched filter” is the solution in this circumstance. The fundamental of the “matched filter” $m(t)$ is to maximise the ratio of the power of fault signal $X(t) * m(t)$ to the power of additive noise $N(t) * m(t)$. [160]

To sum up, in order to realise the objective of designing a narrow-band filter to extract the faulty information from the signal, the “matched filter” is the solution. Acoustic data recorded from faulty bearings with minor damage on the outer race and on the roller (F1 and F2), spinning at speeds from 400 RPM to 1000RPM, are used verify the diagnosis results. The results of the lowest rotational speed of 400 RPM (6.67 Hz) and the highest speed of 1000RPM (i.e. 16.7 Hz) are presented. The former case illustrates the bearing diagnosis results when the acoustic signal generated from bearing spinning is weak and the latter shows the results when the acoustic noise is high. The spectrums of the signals filtered from the “matched filter” are shown in Figure 5.23 and Figure 5.24. The equivalent results from F0 healthy bearing are also presented for comparison purposes, in order to clearly indicate the abnormal behaviour of the faults.

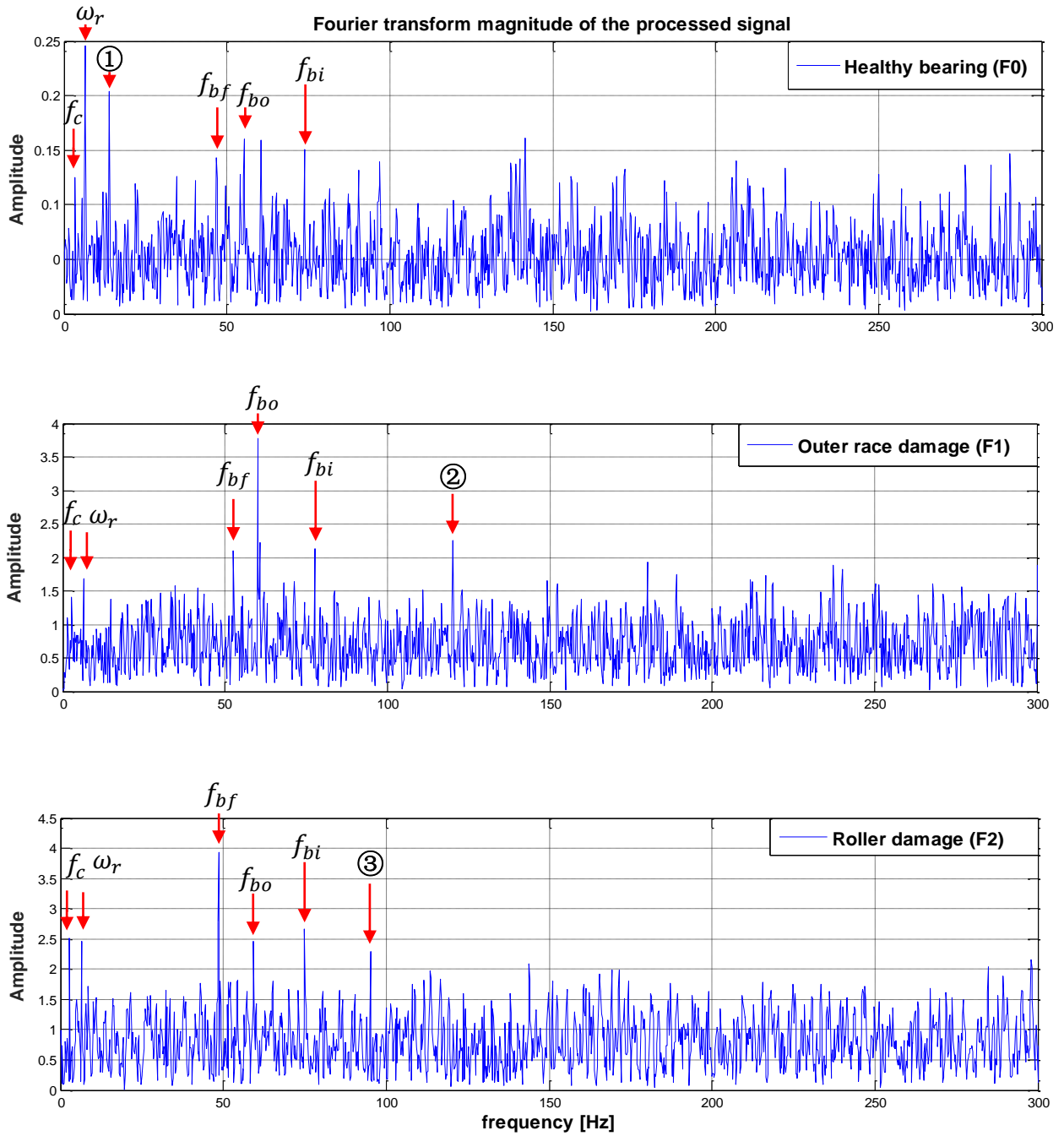


Figure 5.23- FFT envelope of healthy and faulty bearing spinning at 400 RPM (Top) healthy bearing (Middle) outer race damaged bearing (Bottom) roller damaged bearing 's processed acoustic data

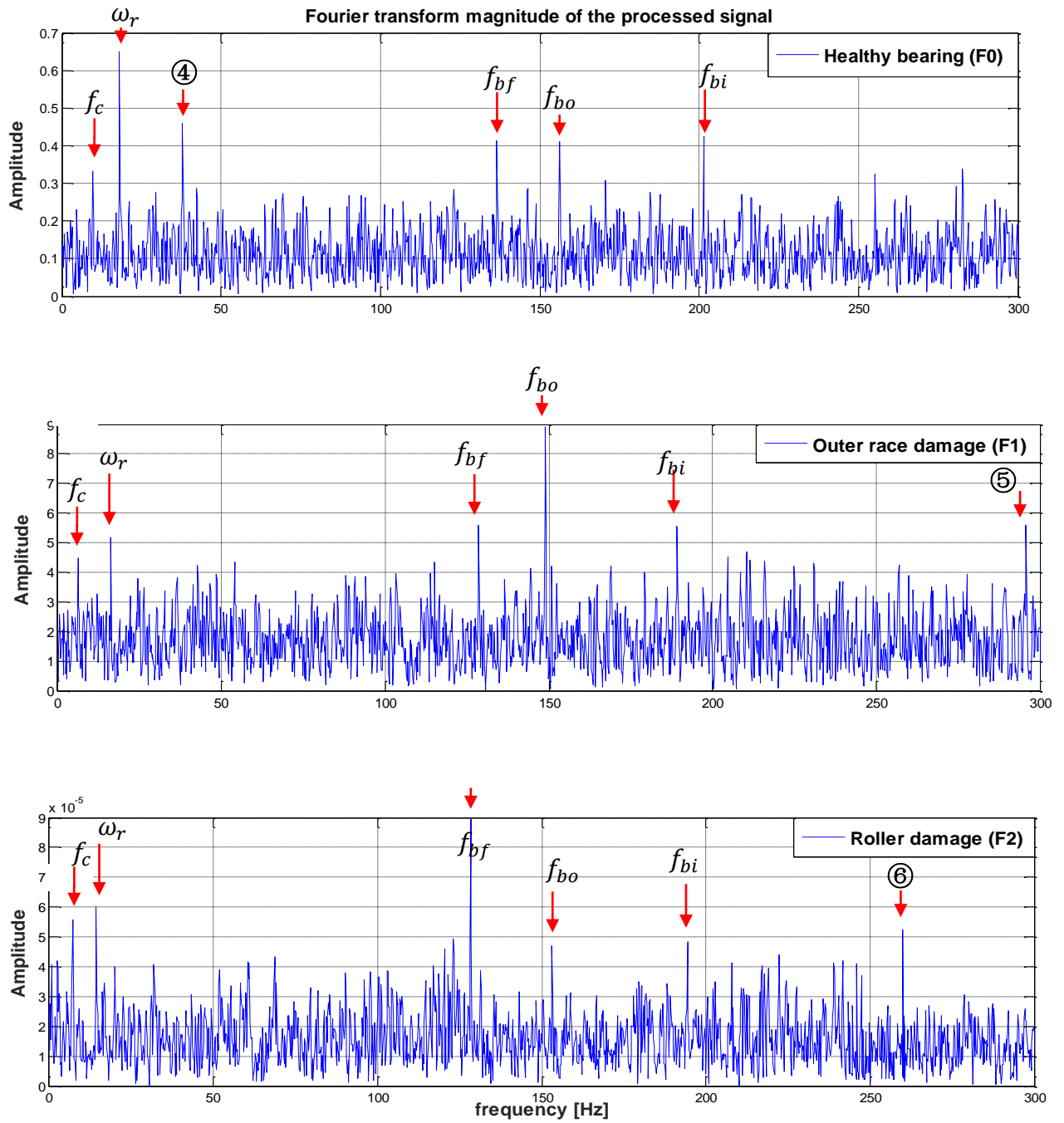


Figure 5.24- FFT envelope of healthy and faulty bearing spinning at 1000 RPM (Top) healthy bearing (Middle) outer race damaged bearing (Bottom) roller damaged bearing's processed acoustic data

The same as the result analysis in section 5.2.3.5, f_c , f_{bo} , f_{bi} and f_{bf} are pointed by the red arrows to the corresponding peaks in the spectrums.

The peaks numbered 2, 5 and 3, 6 are at the frequencies of the principle 1st harmonic of the respective fault frequencies (f_{bo} for the bearing with the damaged outer race, and f_{bs} for the bearing with the damaged roller). This demonstrates that the proposed processing approach can be used to identify not only the fundamental frequency, but also the first harmonic components of fault information in the frequency domain.

5.3.2.4 *Summary*

A novel signal processing technique has been applied to the acoustic data of the roller bearing spinning on the test rig. It can extract the introductory faults information and to generate frequency spectra which demonstrate the key frequencies associated with each different fault type. Tests have been carried out with particularly minor levels of the selected faults in order to demonstrate the technique's ability to detect early stage (minor) symptoms.

This novel signal processing technique was modified from the EMEME technique. Due to the low signal-to-noise ratio (SNR) of the acoustic signal, the acoustic noise filtering is important in the signal processing. Empirical Mode Decomposition (EMD) is still useful in decomposing the signal and selects the useful sub signal which contains the bearing faults information. But in the case of acoustic signal, EMD is not powerful enough to directly extract the bearing faults information. So EMD and Linear Prediction Coding (LPC) are used in the acoustic noise filtering stage. Spectral Kurtosis (SK) is a useful method being sensitive to the non-stationary features. These features are the signs of the bearing defects in the case. So the filter design indicated by the SK is powerful to accurately filter out the faulty information of the bearing. The fundamental of how the SK indicates the filter design has been discussed. And the results have been demonstrated with the outer race and roller defects. The next step is to extend the experiments from laboratory to the field tests.

5.4 Acoustic microphone application on the Class 117 train – field tests based

In this section, the acoustic microphone system application is extended to the field tests. The field tests were carried out at the Motorail Long Marston storage site. The site connects to the national railway network at Honeybourne via a section of line operated by Network Rail. The test train is a Class 117 train consisted of a single car DMU hauling two tea wagons as shown in Figure, and test speeds of approximately 50 km/h were achieved



Figure 5.25- Test train

The first consideration of the differences between the field tests and the laboratory experiments is the roller bearings move with the running train rather than spinning on the static testing rig. The problems led from the consideration include the decline in the signal quality and the Doppler Effect on the acoustic signal. To solve these problems is the primary task in the case because the processing algorithm developed in the laboratory experiments cannot be applied to the original field test signal to extract the faulty information of the bearings.

The author and his colleagues have proposed the solution of microphone array design to realize the signal quality enhancement; the lightgates speed measurement system and beamforming algorithm are applied to eliminate the Doppler Effect on the acoustic signal.

Correspondingly, the following three sections discuss the microphone array design, lightgates speed measurement system and the beamforming algorithm. The signal processing algorithm is demonstrated at last.

5.4.1 Microphone array design

In order to enhance the signal quality, a microphone array is used in the field test. In the laboratory experiments, the bearing is spinning on the static testing rig. The recording range was not an issue. But in the field tests, the enhancement of the signal acquisition is badly needed with the train speed increasing. The author is involved in the microphone array structure design. The developing process is published in [201]. During the development process, the testing involved two array mounting plates including a horizontal linear array and a 2D spiral array. The linear array shows a better reduction of the side lobes compared to the main lobe in a relatively lower frequency bandwidth [201]. So the horizontal linear array (shown in Figure 5.26) is used in the field tests.



Figure 5.26 – Horizontal linear array

Despite the microphone array design, the funnel with the acoustic foam inside (shown in Figure 5.27) was developed to cover the front of the array in order to reduce the noise level within the listening area of the microphone array. AKG C417 microphones [202] were used and data was gathered using a hardware unit consisting of two synchronised sound processing units, Focusrite OctoPre MkII [203], and a sound card interface, Streinberg UR824 [204], capable of outputting up to 24 channels of data over a single USB 2.0 lead.

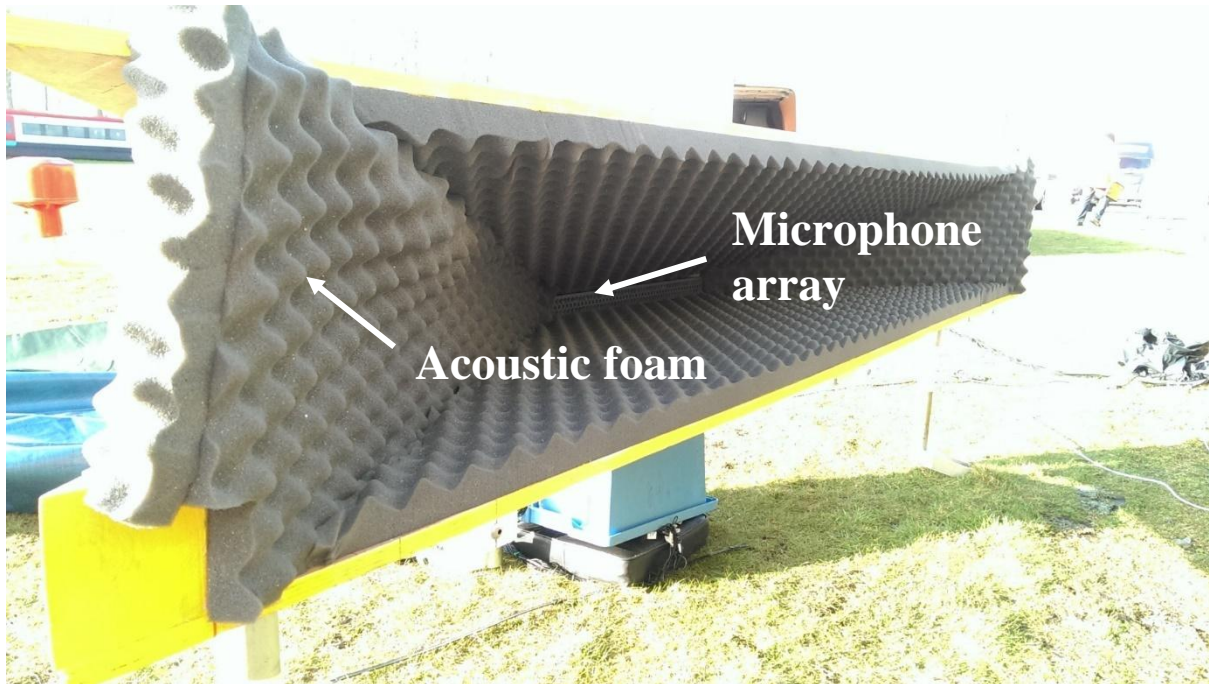


Figure 5.27 – Acoustic funnel

5.4.2 Lightgates speed measurement system

The lightgates speed measurement system was designed to feed the location information to the time-domain beamforming algorithm which works on the elimination of the Doppler Effect. It was designed to be an automatic triggering system that could avoid unnecessary data collection. Three sets of IR light gates were used [205] that could be triggered by passing trains (shown in Figure 5.28). In order to be able to perform the bearing diagnostic algorithms, the shaft speed must be known. The speed of the train could be determined by knowing the time and the distance. Also this system can indicate the exact position of the axle so the time-domain beamforming algorithm can focus on the correct point. The light gate signals are fed in to the data acquisition unit and synchronised with the audio signals for the finest accuracy.

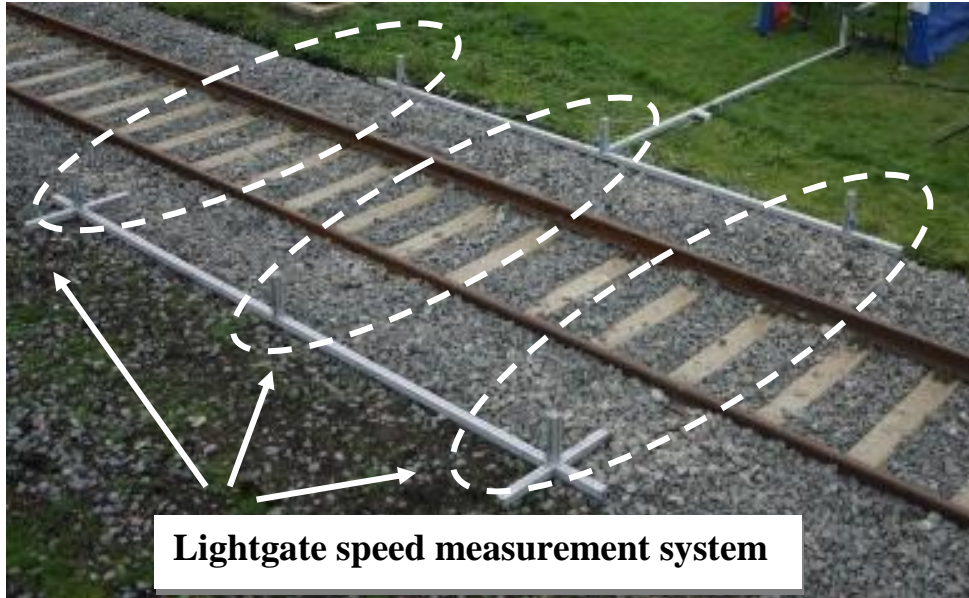


Figure 5.28- Lightgate speed measurement system

The two impulses in Figure 5.29 represent a single axle passing through the two pairs of lightgates. The average train speed between the two pairs of lightgates is calculated by using the fixed distance divided by the difference in the times that the wheel blocked the infrared signal, which was about 45 km/h in this test.

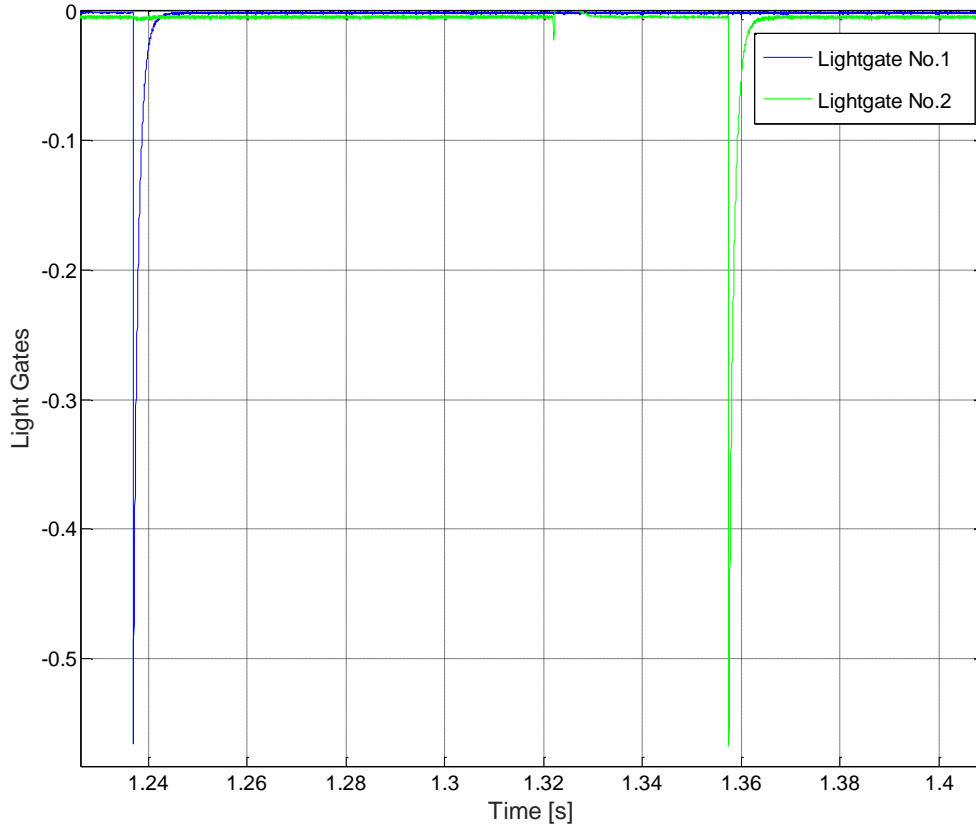


Figure 5.29- Lightgate signals for a single axle

In this case, the distance between the two pairs of lightgates is, $S = 1.5 \text{ meters}$ (shown in Figure 5.32). And the times that the wheel blocked the infrared signal of the two pairs of lightgates is, $t = 0.12 \text{ second}$ (shown in Figure 5.29). So the average train speed, V , between the two pairs of lightgates is:

$$V = \frac{S}{t} = \frac{1.5}{0.12} * 3.6 \text{ km/h} = 45 \text{ km/h} \quad (5-13)$$

5.4.3 Time-domain Beamforming algorithm

Beamforming is a signal processing technique used in conjunction with an array of sensors to provide a versatile form of spatial filtering [206]. In this application, the application of beamforming algorithm is to locate sound sources on fast-moving trains. The algorithm needs to be capable of solving the practical problems in this task: the algorithm needs to be able to eliminate the affect from the object movement, which is the frequency shifts caused by the

Doppler Effect; the accuracy of the algorithm should allow the system to achieve an “acoustic still image” from very short signal samples [207]. Based on the requirement analysis above, a time-domain beamforming algorithm proposed in [207] is chosen to apply in this work.

This beamforming algorithm is based on delay-and-sum beamforming assuming point monopoles and spherical wave propagation as described in [206]. The arrangement for the beamforming based on the array and the point of focus is shown in Figure 5.30.

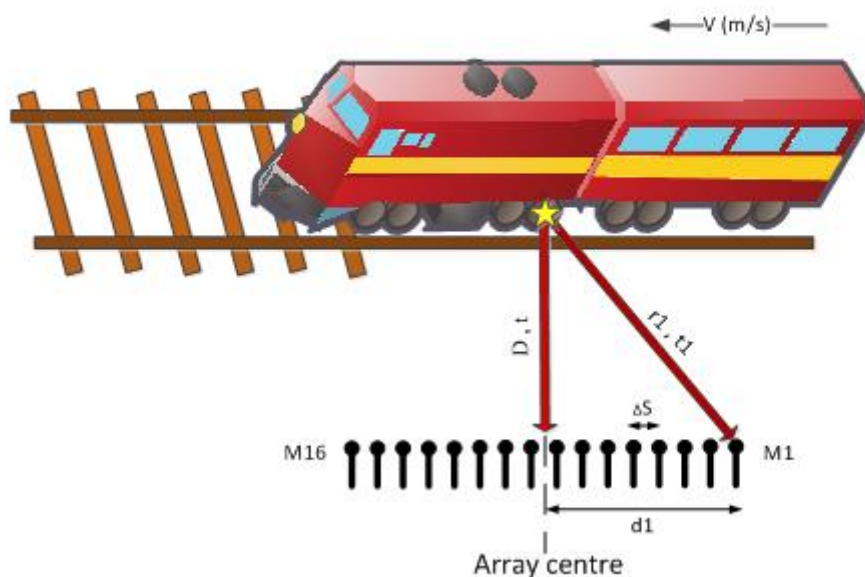


Figure 5.30- Beamforming arrangement

where:

V (m/s) is the train speed;

D (m) is the distance from the track to the centre of the array;

t (s) is the time that takes the sound emitted from the point of focus to travel to the centre of microphone;

ΔS (m) is the spacing between the microphones in the array;

r_m (m) is the distance from the microphone m to the point of focus;

t_m (s) is the time that takes the sound emitted from the point of focus to travel to the microphone m ;

t_0 (s) is the time that the axle breaks the light beam;

d_m (m) is the distance from the microphone to the centre of the array.

The distance from each microphone to the point of focus (r_m) is calculated by

$$r_m = \sqrt{D^2 + d_m^2} \quad (5-14)$$

The time of arrival (delay t_m) for each data point to arrive at microphones is calculated by

$$t_m = r_m/c \quad (5-15)$$

where c is the speed of sound.

The beamforming output signal, $p(t)$ is achieved by

$$p(t) = \frac{1}{M} \sum_{m=1}^M w_m \cdot p_m(t_0 + t_m) \quad (5-16)$$

Where m is the number of microphones, p_m is the recorded sound from microphone m , and w is a weighting coefficient based on the distance to the source:

$$w_m = \frac{r_m}{D} \quad (5-17)$$

The working flow of the algorithm applied to the field tests is shown in the flowchart in Figure 5.31.

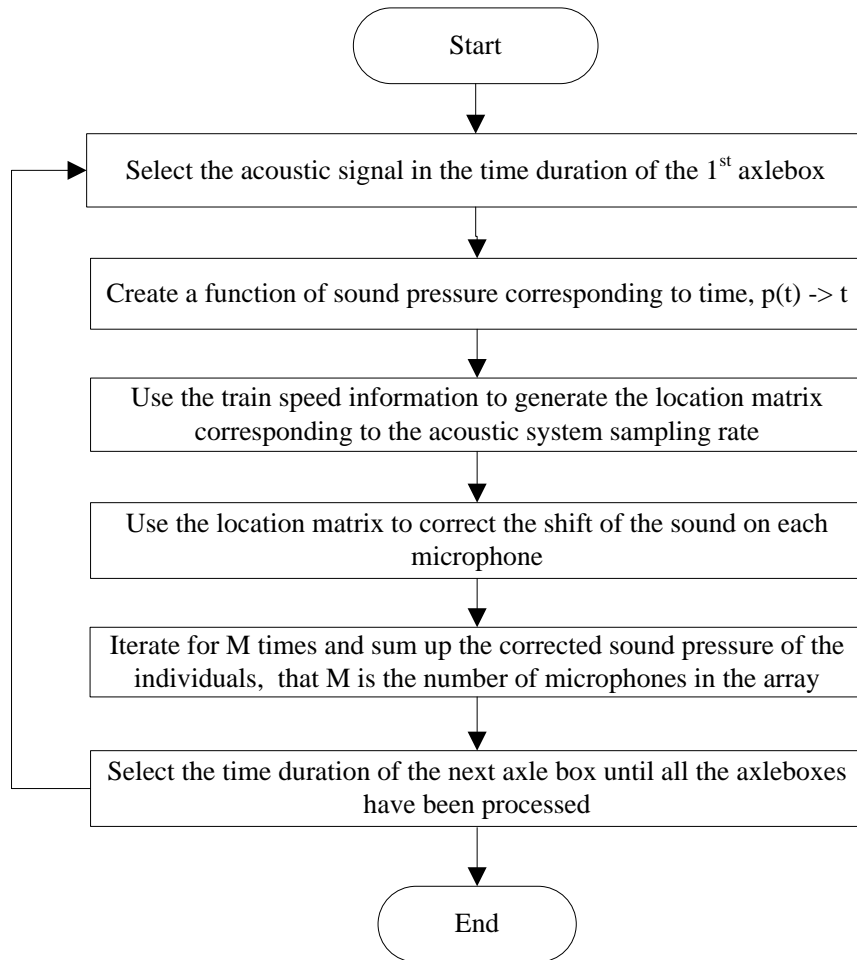


Figure 5.31- Flow chart of the time-domain beamforming algorithm working flow

5.4.4 Field test plan overview

A set of tests were carried out to assess the microphone array and the beamforming algorithm. These tests measured and investigated the effect of environmental noise, noise emitted by the wheel and rail and the Doppler Effect caused by the moving vehicle on the recorded signals for the final processing procedure.

The field test arrangement plan is shown in Figure 5.32. The microphone array was installed at the trackside. The lightgates speed measurement system was formed of three pairs of lightgates. The moving beam targets at the monitoring roller bearing within the acoustic acquisition area.

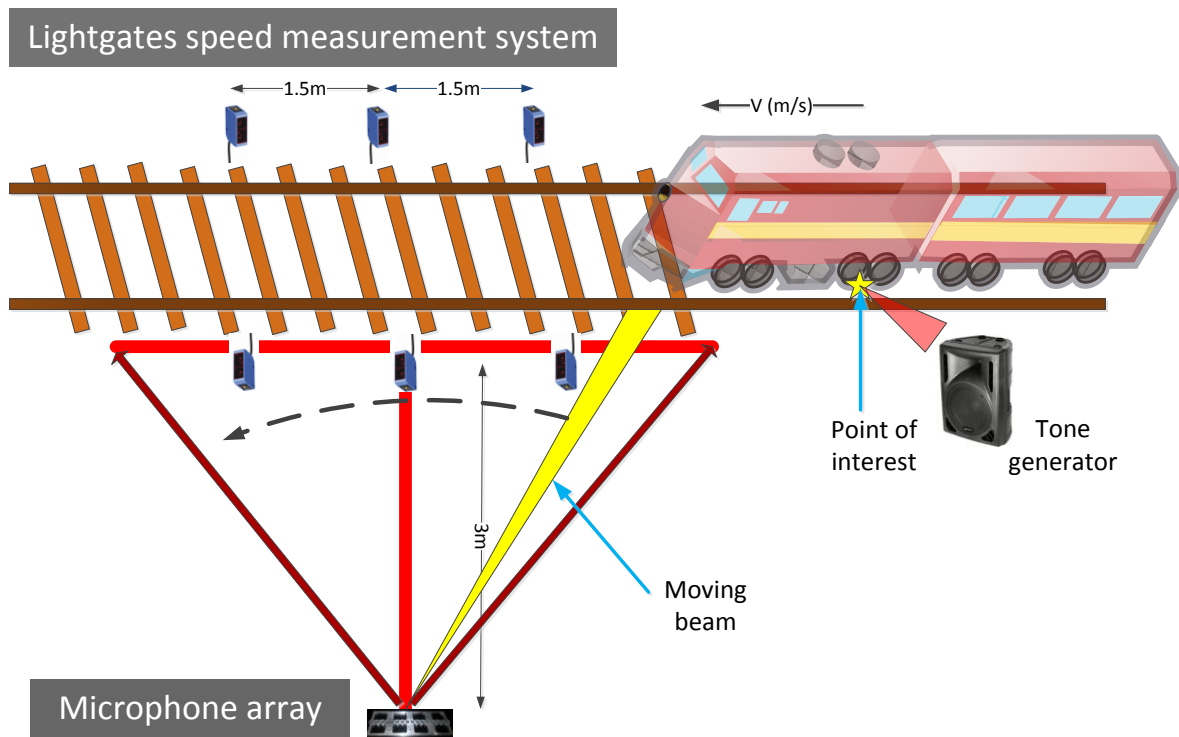


Figure 5.32 – Field test arrangement plan overview

There were a number of requirements for the test site. These included:

- Open, soft ground for less reflective surfaces in terms of acoustics
- Space for instrumentation to be installed vertically level with bearings and at a distance of up to 3 m from the track
- 200 m of straight track with designated 20 m test section capable of supporting fixed speeds of up to 50 kmh^{-1}
- Track to be continuously welded within 200 m test area, to reduce the possibility of impulsive noise from the track site

The final equipment arrangements are shown in Figure 5.21. The microphone array was positioned 3 meters away from the track and the light gates were 1.5 meter away from the one in the centre.

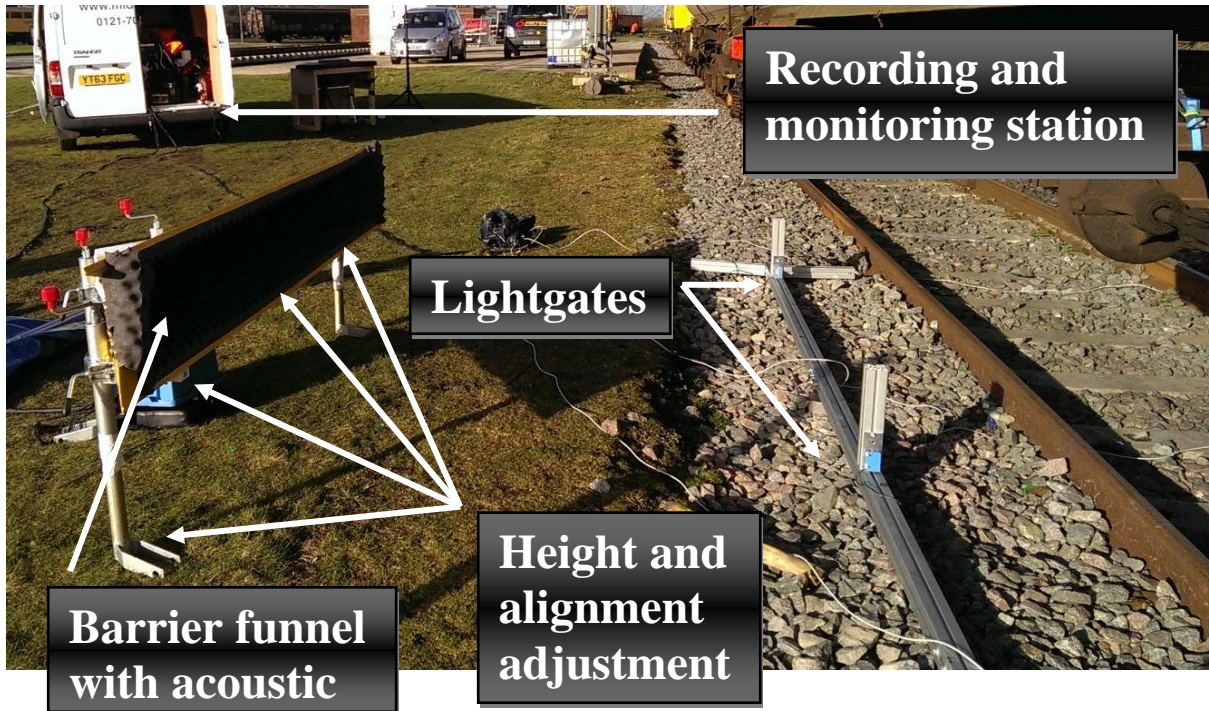


Figure 5.33 – Final set up at the test site

Having validated the microphone array design and beamforming algorithm, the aim of the task is to monitor the condition of the roller bearing. Considering the safety issue of operating train in the faulty condition, a tone generator (shown in Figure 5.32) was used to bring the acoustic signal from the ideal non-acoustic reflection environment to the real world.

The following signal processing algorithm demonstration sections are divided into two cases. The microphone array design and beamforming algorithm validation is the first case. And the condition monitoring of the roller damage fault tone is the second case.

5.4.5 Processing algorithm on the experimental acoustic signal

5.4.5.1 Case 1 – 8 kHz tone

In order to verify the directionality of the array within the test configuration, a standard tone generator was fitted to the test vehicle. The tone generator (shown in Figure 5.32) was configured to emit sine wave test tones at a number of frequencies between 4 kHz and 16 kHz.

5.4.5.1.1 Time-domain beamforming algorithm validation

Using an 8 kHz test tone as an example to demonstrate the signal acquisition of the microphone array and the effectiveness of the time-domain beamforming algorithm. The 2-D spectrogram of the 8 kHz experimental signal is shown in Figure 5.34. The spectrogram is cut off at 10 kHz which is the upper boundary of the non-distortion responding bandwidth of the microphones. A significant shift occurs at the frequency of 8 kHz and heavy noise around which indicates the Doppler Effect existence. There is a lot of background noise across the frequency spectrum, particularly at the low frequencies bandwidth. The noise at the low frequencies represent the environmental noise including the wind brought by the fast moving train, the air compression when the train passing into the acquisition area and etc.

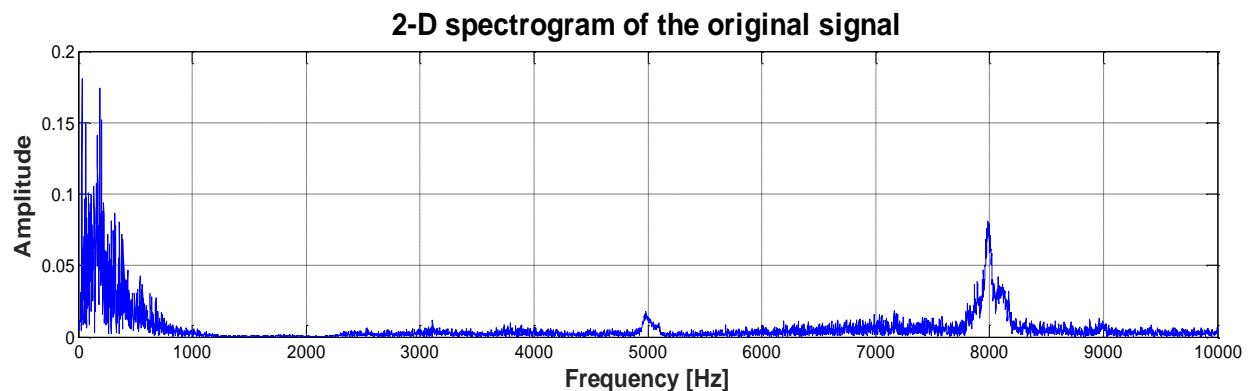


Figure 5.34 – 2-D spectrogram of the 8 kHz tone

Figure 5.35 shows the results from the beamforming algorithm on the 8 kHz tone. The reduction of the background noise in the low frequencies bandwidth is achieved by applying a high-pass filter, the lower cut off frequency is set as 700 Hz and the higher cut off frequency is 10 kHz, the upper boundary of the non-distortion responding bandwidth of the microphones. The compensation of the Doppler Effect can also be observed and the 8 kHz tone is clearly identifiable and reasonably consistent across the sampling interval.

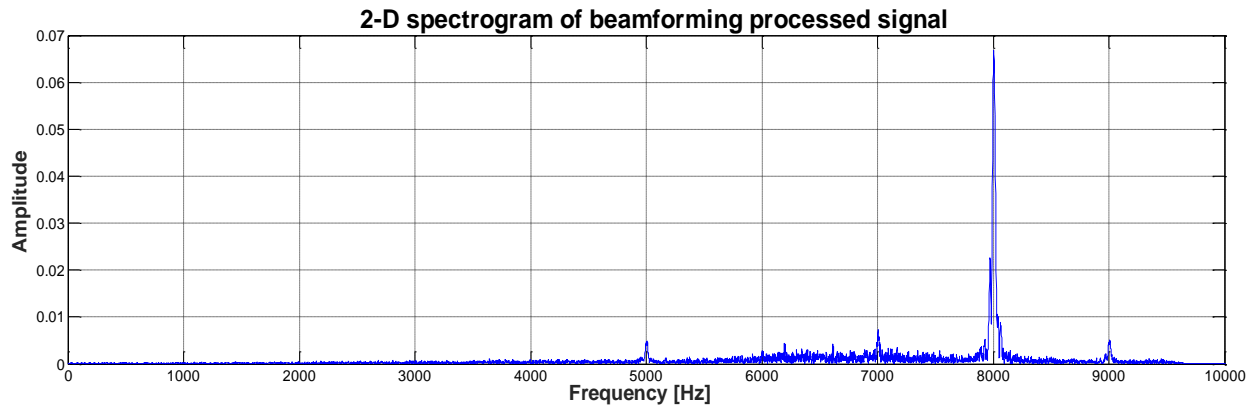


Figure 5.35 – 2-D spectrogram of the beamforming processed 8 kHz tone

5.4.5.2 Case 2 – Roller damage fault tone

As per discussed in the field test plan overview, considering the safety issue of operating train in the faulty condition, the tone generator was used to play the acoustic signal with the introductory bearing faults. The acoustic signal in the ideal non-reflection environment was brought to the real world.

From the processing algorithm perspective, the pre-processing of the signal includes the elimination of the Doppler Effect on the acoustic signal and the reduction of the environmental noise. The time-domain beamforming algorithm is used to eliminate the Doppler Effect on the signal, and the high-pass filter is applied to the signal to reduce the environmental noise. Having finished the pre-processing of signal, the following processing algorithm applied to this case is using the novel algorithm applied in 5.3.2. The results are demonstrated in the following sections correspondingly.

5.4.5.2.1 Signal pre-processing: beamforming and high-pass filtering

In this section, the results of the signal pre-processing are demonstrated. The waveforms in Figure 5.36 and Figure 5.37 are the original signal of the roller damage fault tone and the beamforming algorithm processed signal.

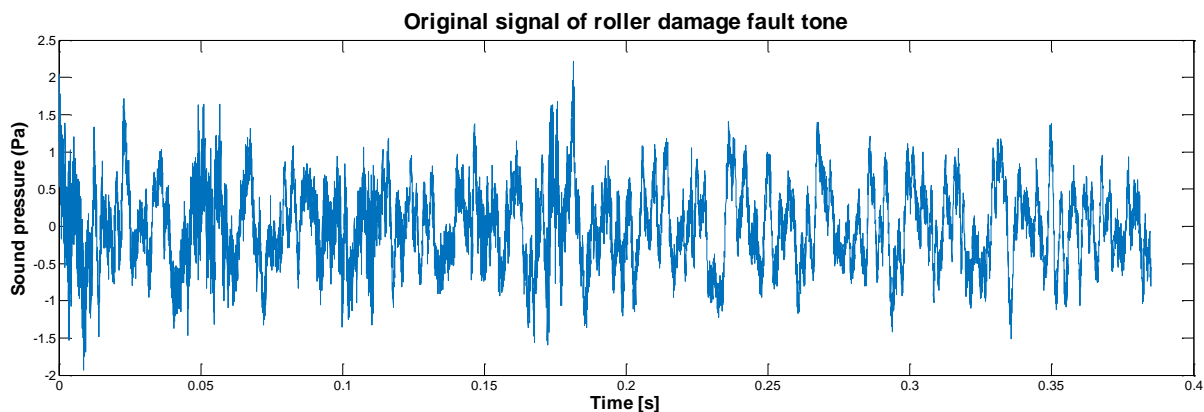


Figure 5.36 – Original signal of the roller damage fault tone

Having used the time-domain beamforming algorithm, the unwanted high frequency elements resulted from the Doppler Effect has been reduced, which is revealed by the signal becoming smooth.

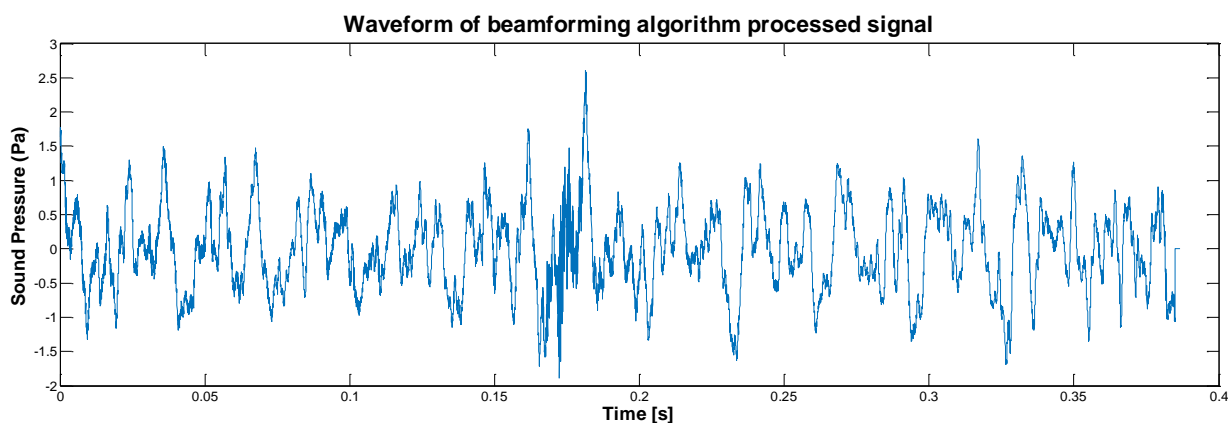


Figure 5.37 – Beamforming algorithm processed signal of the roller damage fault tone

The same strategy as the 8 kHz case, the reduction of the background noise in the low frequencies bandwidth is achieved by applying a high-pass filter, the lower cut off frequency is set as 700 Hz and the higher cut off frequency is 10 kHz, the upper boundary of the non-distortion responding bandwidth of the microphones. The filtering result is shown in

Figure 5.38 (Top). Comparing the result to the waveform in Figure 5.37, the low frequency component is filtered out which performs as a “carrier wave” of the useful bits of the signal.

The remains are the useful bits of the signal which contains the discontinuous signal generated from the roller bearing.

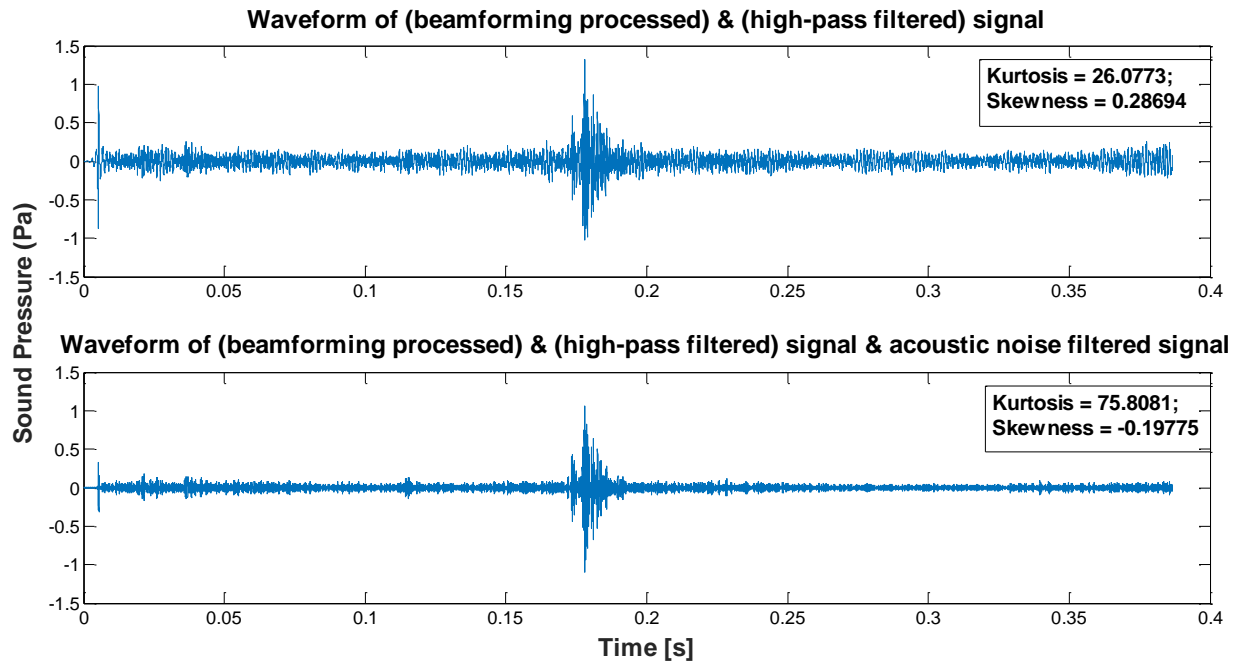


Figure 5.38 – The processed signal of roller damage fault tone (Top) beamforming processed and high-pass filtered signal (Bottom) beamforming processed, high-pass filtered and acoustic noise filtered signal

5.4.5.2.2 Signal post-processing: the processing algorithm developed from the laboratory experiments in Anechoic Chamber room

In this section, the processing algorithm developed from the laboratory experiments in Anechoic Chamber room is applied to the pre-processed field test signal. Following the fundamental of algorithm, it is divided into three stages: acoustic noise filtering, non-stationary feature extraction and diagnostics with the SK.

In the acoustic noise filtering stage, Linear Prediction Coding (LPC) and Empirical Mode Decomposition (EMD) are jointly used to filter the acoustic noise. As per discussed, LPC is effective on audio signal filtering. And based on its working principle, LPC can remove the

deterministic components from the signal, the residual of which contains the non-linear bearing signal in interests. EMD can be well suited to recover the non-linear and non-stationary signals. After the acoustic noise filtering stage, the high energy “deterministic” acoustic noise has been filtered, and the representative IMF has been chosen inferred by EM calculation from the EMD process. As there is no significant change on the filtered waveform, the figure is not shown here. But the average amplitude of the filtered signal has significantly decreased since the high energy acoustic noise is filtered out.

Comparing the two waveforms in Figure 5.38, there is no significant change on the average amplitude of the filtered signal. It is because the high-pass filter has filtered the deterministic components from the signal at the pre-processing stage. As the indicator of faulty information of the roller bearing, the kurtosis value increases after the acoustic noise filtering. So the next stage is to use Spectral Kurtosis (SK) and Kurtogram to extract the non-stationary feature and indicate the central frequency and the window length for the “detection filter” design. These are the stages of non-stationary feature extraction and diagnostics with the SK in section 5.3.2.2 and 5.3.2.3.

In Figure 5.39, the presence of the maximum SK value locates at $\{f_c, N_w\} = \{0 \text{ Hz}, 2^4\}$, where N_w is the window length and f_c is the central frequency. This pair of $\{f_c, N_w\}$ is the same as the pair for the scenario of the outer race damaged bearing spinning at 400 RPM in the laboratory. Since the tone is the acoustic signal from the laboratory, the same pair of window length and central frequency for the filter design is expected.

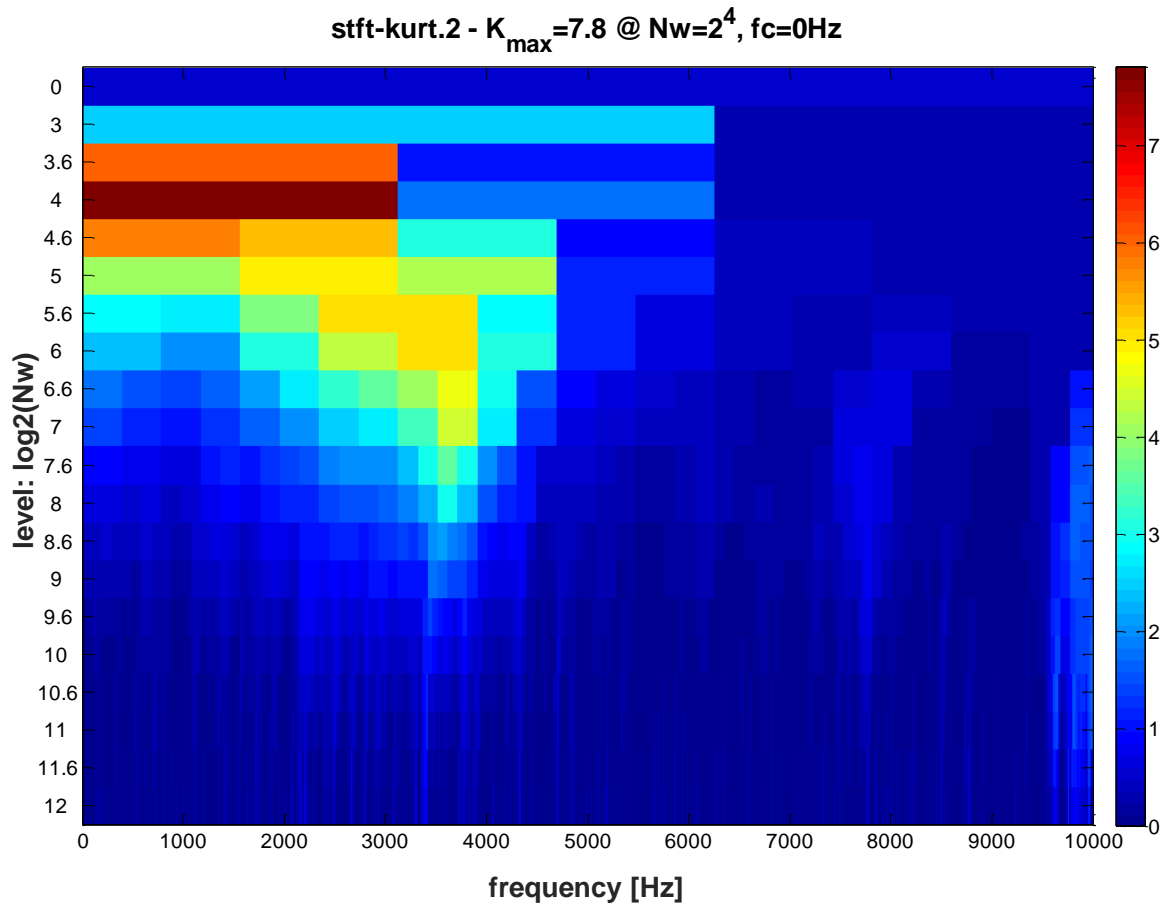


Figure 5.39 – Kurtogram of the processed signal of roller damage fault tone

Using the “matched filters” designed by the pair of $\{f_c, N_w\}$ indicated from the Kurtogram, the Fourier Transform envelope of the result is shown in Figure 5.40. The Ball Fault Frequency (f_{bf}) for the bearing with the damaged roller, as well as its 1st and 2nd harmonics are found in the spectrum. But the resolution of the spectrum is relatively low which reveals the energy loss in this low frequency bandwidth. The other fundamental frequencies, the Fundamental Train Frequency (f_c), the Ball Frequency of the Outer Race (f_{bo}), the Ball Frequency of the Inner Race (f_{bi}), and their harmonics are not remained in the Fourier transform envelope in the graph. It reveals the energy loss of the signal during the signal processing algorithm as well.

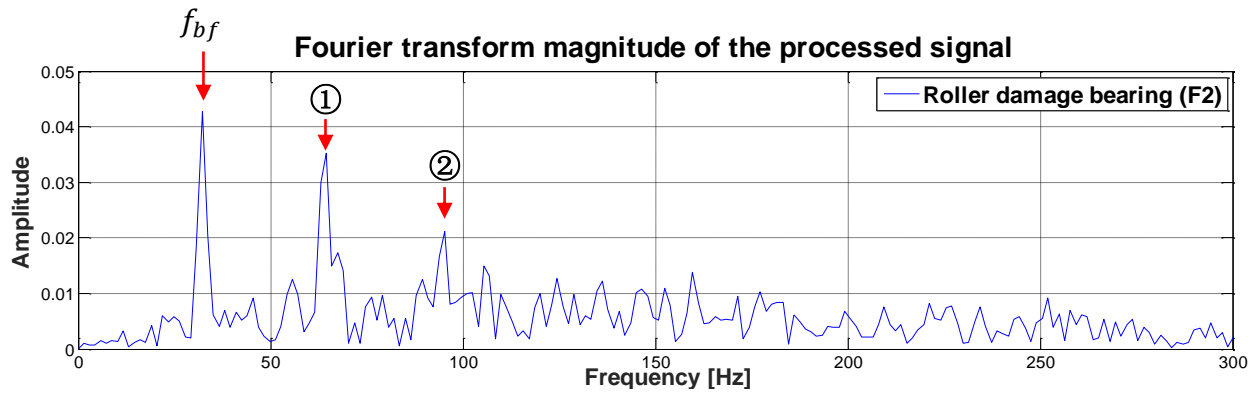


Figure 5.40- FFT envelope of roller damaged bearing's processed acoustic data

5.4.6 Summary

In this application, the acoustic inspection and monitoring system has been brought to the research testing site. The field tests requirements are different from the laboratory experiments and more critical. In the field tests, the single microphone system has been extended to the microphone array and been in order to collect higher signal energy. From the signal processing perspective, this system modification achieves the signal enhancement through the mechanical system design. Within the microphone array, the acoustic beams from each microphone require the processing technique to direct and integrate them. Also the processing technique is required to eliminate the Doppler Effect brought by the fast moving train. So the time-domain beamforming algorithm has been developed and applied to the field test data. A consistent 8 KHz tone was used to validate the effectiveness of the algorithm.

Comparing the processing algorithm in the field test to the algorithm applied in the laboratory, the field test signal is surrounded by higher volume of noise on site. The interested acoustic signal is buried in the environmental noise which can be seen from the original signal waveform. So having integrated the acoustic beams together, a high-pass filter is applied in the pre-processing stage to filter out the low-frequency noise especially the constant air flow between the microphone array and the moving vehicle. After this stage, the processing technique developed in the laboratory has been applied to the field tests acoustic signal. The

bearing introductory faults information in the tone can be extracted. In the pre-processing stage, the high-pass filter could potentially result in a certain amount of energy loss of the interested signal components. The processing technique can still generate frequency spectra which demonstrate the key frequencies associated with roller damage fault, but not the other fundamental frequencies associated to the healthy components of the bearing. To sum up, the low signal-to-noise ratio (SNR) issue is the challenge in the field tests signal processing technique development.

5.5 Summary

In this chapter, the investigation of acoustic sensing technology has been demonstrated. The acoustic sensing technology has been applied to three different scenarios: vibration signal of the introductory bearing faults in the laboratory, acoustic signal of the introductory bearing faults in the laboratory and acoustic signal of the introductory bearing faults at the research testing site.

The demonstration of the results follows the development procedure of the signal processing algorithms. The first two scenarios are the preparation of the third scenario of field tests signal. Two novel processing algorithms have been developed in the preparation work. One is the Empirical Mode Envelope with Minimum Entropy (EMEME) algorithm developed from the scenario of vibration signal of the introductory bearing faults in the laboratory. The other novel processing technique was developed from acoustic signal of the introductory bearing faults in the laboratory which is a three-step processing chain: acoustic noise filtering, non-stationary feature extraction and diagnostics with the Spectral Kurtosis (SK).

The processing technique of the third scenario of field tests signal has involved the mechanical system design and the algorithm development. The acoustic signal enhancement was achieved through extending the single microphone to a microphone array. In order to

integrate the acoustic beams together for the follow processing, the time-domain beamforming algorithm has been developed and applied. Then the processing technique developed from the laboratory has been inherited in this scenario. The results have proved the developed acoustic inspection and monitoring system can work properly. And during the investigation, the potential integrating point with the vision imaging system has emerged. The further improvement can be achieved at the stage of integrating the acoustic beams of the microphone array through enhancing the speed measurement of the vehicle. The discussion in details is in section 7.5.1. In the next chapter, the investigation of vision imaging technology is going to be demonstrated.

6 Vision imaging technology application

6.1 Overview

Vision imaging technology is one of the target integrating condition monitoring (CM) technologies in this thesis. This chapter is demonstrating the application of vision imaging technology. The work on vision imaging technology is presented in the order of hardware system development and video stream processing algorithm development. As noted in chapter 0, the hardware system in this application is a commercialised high-speed camera. The existing commercialised high-speed camera can fully meet the requirements of the vision imaging system in this work; it can also shorten the hardware system development procedure allowing the work to focus on signal processing technique development. Selecting the right high-speed camera is important which is going to be discussed in following sections.

In terms of video stream processing algorithm development, it is a processing chain which combines multiple computer vision processing techniques. Computer vision is the area involving the computational processing of the vision signal, such as images and dynamic video streams. Each technique is explained and the algorithm is demonstrated in the relevant cases in the following sections.

With the knowledge of hardware system development and video stream processing algorithm development, vision imaging technology was applied to the coupler and pantograph condition monitoring. These two case studies are demonstrated at the end of this chapter.

6.2 Hardware system overview

As noted in chapter 0, vision imaging technology monitors the condition of vehicle by “seeing”; therefore the system needs an image capturing device as well as a processing core. The hardware equipment requirements differ in the various applications. Considering high

speed trains are the inspecting object, the image capturing device should be able to capture fast motion events without blurring, so called high-speed camera. In the next section, the fundamental of high-speed camera is going to be discussed with the work requirements analysis.

6.2.1 High-speed camera fundamental

A high-speed camera is capable of capturing an event that happens too fast to be seen by a normal camera or the naked eye. For example, Britain Rail Class 395 travels at 230 km/h, British Rail Class 373/374, Eurostar e300/e320 travels at 300 km/h in the British section of the High Speed 1 Line. To choose a right high-speed camera, the following key parameters need to be carefully considered: frame rate, image resolution, exposure time (shutter speed), sensitivity, colour or monochrome, bit depth (dynamic range), camera physical size and on board memory, interface, and triggering.

6.2.1.1 Frame rate

The most obvious place to start for most applications is the frame rate. Three parameters need to be known in order to calculate the frame rate:

- i. Target size in metres [D]

This has a major impact on the required frame rate.

- ii. Object velocity in metres per second [V]

As the velocity of an object increases the image rate will also need to increase to break the movement down into smaller steps.

- iii. Number of steps we wish to break the movement down into (time resolution) [N]

A higher time resolution requires a higher frame rate.

So the equation to obtain frame rate is:

$$\text{Frame rate } [f] = (1/D)VN \quad (6-1)$$

6.2.1.2 Image resolution

Image resolution influences the features in image that can be extracted. A low resolution can result in an indistinct image. But it is not always appropriate to choose a high resolution because the scaling of frame rate and the resolution is approximately linear, such that double the frame rate halves the resolution. In addition, all high-speed cameras can only achieve maximum resolution at a particular frame rate. Hence, to decide the appropriate image resolution is actually the decision on pixel size, so called pixel calibration.

If the target size in metres [D] is known, as well as the percentage of target within image [r]; and the pixel resolution in the same direction [x] is known, and then the equation of pixel calibration is:

$$\text{Pixel calibration } [P_c] = \frac{D}{xr} \quad (6-2)$$

6.2.1.3 Exposure time

Exposure time is also referred to as shutter speed. Exposure time has an impact on how much motion blur there is on an image. A small amount of blur on an image can be acceptable but if there is a significant amount, the contrast between the object and the background can become less and features can become washed out.

Default exposure time [E] = 1/frame rate [f]. In order to ascertain the extent of blur, two parameters can be used: blur in distance in metres and blur in number of pixels. Blur in distance in metres is:

$$\text{Blur in distance } [M] = VE \quad (6-3)$$

Blur in number of pixels is:

$$\text{Blur in pixels } [B] = M / P_c \quad (6-4)$$

With the blur in pixels [B], complete blur removal is achievable by shortening the exposure time. In practical, the exposure time is relevant to the amount of light beam falling on the shutter sensor which decides the brightness of image. So it is unnecessary to achieve blur free image, but needs to balance the other factors which may affect on image quality.

6.2.1.4 *Sensitivity*

High-speed camera by default have short exposure time due to the high frame rate used. A short exposure limits the time that light has to fall on the sensor for each image. There are two ways to improve the brightness of the image: use additional light source to illuminate the subject, or alternative camera with increased light sensitivity in the case that additional lighting is unavailable, such like filming in a heat/light sensitive subject, and filming outside.

Sensitivity for film cameras is given as an ISO / ASA value. For digital systems there is no easy way to relate the sensitivity of a digital sensor to this standard, although all manufacturers attempt to do so. What can be done however is to provide the relative sensitivity of one digital system to another. The comparison result can help you to choose. But it is difficult to select a camera for an application based on data given for its sensitivity, the only certain way to select the right camera is to evaluate it under the user's own specific test conditions.

6.2.1.5 *Colour or Monochrome*

This decision is really quite an important one. Monochrome and colour systems share the same sensor; however to obtain colour information a colour mask is fitted to the sensor which has the effect of reducing the sensitivity by approximately 2-3x. For some applications it is clearly important to be able to distinguish colours but for the majority it is not strictly

necessary and the benefit of additional light sensitivity outweighs the ability to get colourful pictures.

6.2.1.6 Bit depth (dynamic range)

Bit depth defines the number of grey levels that can be distinguished on an image. An 8-bit sensor has a maximum of 255 grey levels and a 12-bit image has a maximum of 4096 grey levels. Normally, a dynamic range of 8-bit is sufficient. The additional range is useful when the features in interests are at a similar grey level which is difficult to analysis in the further processing.

6.2.1.7 Camera physical size

Physical size of the camera can be important if it is necessary to record within a confined space. Cameras that consist of an image processor with a remote camera head can be chosen should it be necessary.

6.2.1.8 Interface

There are a range of camera interfaces available:

- 1) PCI – The camera is supplied with a PCI card, which contains the control electronics for the camera and the image storage.
- 2) IEEE1394 ‘Firewire’ – This is the most common interface between camera and PC. Cameras with this interface are self contained units.
- 3) Ethernet – Standard Ethernet or Gigabit Ethernet options are available for some systems. This permits the camera to appear as a device on a network. The camera can be controlled over great distances and many people can also have access to the camera.

- 4) Optical – This interface provides a faster download time compared to Firewire but requires a PCI interface card to be fitted in a desktop computer or PCI expansion box. It permits a distance in excess of 50 metres between the camera and control PC

Among these interfaces, the option with fastest download speed and longest control distance between camera and PC is optical interface. The most economic option is PCI. The balancing option is Ethernet interface. It requires the least complicated installation, and provides reliable system communication and fast image download.

6.2.1.9 *Triggering*

- 1) Manual trigger

Manual trigger allows user to trigger the system while watching for the event occur. The pre setting time duration needs to include the additional time for reaction which is generally in the region of 0.5 seconds. A proper pre setting time duration is important to ensure capturing the start of event.

- 2) Automatic trigger

Automatic trigger allows capturing triggered automatically internally and externally. The external automatic trigger is called hardware trigger as well. The vision system is normally set as the slave system which is triggered by the electronic trigger signal from the external master system. The internal automatic trigger is called software trigger as well. Normally, the software provided by manufacturer includes the software trigger function. It allows users to set a threshold of brightness changes within image (or a certain area within image). If the current brightness change exceeds the threshold, the system will be triggered to start capturing. Both automatic triggers have time delay. Normally, the delay of software trigger is longer than hardware trigger. The exact duration of delay needs to validate in the experiments.

6.2.1.10 On board memory

Typical high speed events do not require long record durations as by their very nature they are over in a short space of time, for this reason the standard memory in most high-speed cameras is limited to period provided around 1 or 2 seconds at the maximum resolution / frame rate.

To calculate the required amount of memory, the following parameters are needed: horizontal resolution [x] pixels, vertical resolution [y] pixels, frame rate [f] fps, event duration [t] seconds, bit depth [b]. So the required memory is:

$$\text{memory [R] bytes} = ((xyb) / 8) ft \quad (6-5)$$

Divide this figure by 1024 to get the value in Kilobytes, divide again by 1024 to get the value in Megabytes, divide again by 1024 to get the value in Gigabytes.

6.2.2 High-speed camera selection

Based on the knowledge of high-speed camera above, the FASTCAM Mini UX100 shown in Figure 6.1 was chosen to build the hardware system of vision imaging application.



Figure 6.1- Image capture device (FASTCAM Mini UX100)

The manufacturer is Photron, a worldwide manufacturer of high speed digital imaging systems. This high-speed camera can provide 1,280 by 1,024 pixel resolution to 4,000 frames per second (fps) and reduced resolution operation up to 800,000 fps. Its electronic shutter is able to provide blur free imagery with a minimum shutter speed of 1 μ s with 12-bit pixel depth.

6.2.2.1 Key features of the selected high-speed camera

In this section, the key features corresponding to section 6.2.1 is presented in tables. The maximum frame rate that FASTCAM Mini UX100 can reach is 800,000 fps. But it cannot be reached with the maximum resolution. The frame rates and corresponding maximum resolution are listed in Table 6.1. The other key features of FASTCAM Mini UX100 are listed in Table 6.2.

Table 6.1- Table of frame rate and corresponding maximum resolution

FASTCAM Mini UX100							
	Frame rate up to[frame per second]						
	4,000	5,000	6,250	8,000	20,000	200,000	800,000
Maximum resolution [pixel \times pixel]	1280 \times 1024	1280 \times 1000	1280 \times 800	1280 \times 624	1280 \times 248	1280 \times 24	640 \times 8

Table 6.2- Table of key features

FASTCAM Mini UX100	
Shutter speed/exposure time	Minimised to 1 μ s
Sensitivity	High light sensitivity of 10,000 ISO
Colour or monochrome	Monochrome
Bit depth (dynamic range)	12 - bit
Camera physical size	120mm x 120mm x 90mm Camera Body, weighting 1.5Kg
Interfacing	Gigabit Ethernet Interface
On board memory	16GB

In the next section, the system settings of selected high-speed camera are going to be presented in an example case study. The example case study is field tests on the Network Rail High Speed 1 Line.

6.2.3 Example of high-speed camera settings - British Rail Class 395

British Rail Class 395 is travelling at approx. 230 km/h in the UK section of the High Speed 1 Line. Considering the high speed specialty in this case, exposure time is taken into the first consideration.

Parameters declaration:

- Image size in metres [D],
- Object velocity in metres per second [V],
- Number of steps we wish to break the movement down into (time resolution) [N],
- Pixel calibration [P_c],
- exposure time [E],
- frame rate [f],

- horizontal resolution [x] pixels,
- vertical resolution [y] pixels.

6.2.3.1 How to choose exposure time

In this example, $V = 63.89 \text{ m/s}$ (230 km/h), $x = 1280 \text{ pixels}$, $D = 3\text{m}$ (assumption).

Assume the blur tolerance is 1 pixel;

The pixel calibration $P_c = D/x = 3/1280 = 0.00234 \text{ m/pixel} = 2.34 \text{ mm/pixel}$.

Exposure one time generates one frame, which contains all pixels. So,

Exposure time = $P_c/V = 0.00234/63.89 = 3.66 * 10^{-5} \text{ s/pixel} = 36.6 \text{ us/pixel}$.

Default, $E = 1/f$; so $f = 1/E = 1/3.66 * 10^{-5} = 27322.4 \text{ fps}$ (frame per second).

The calculation results indicate that in the case of Class 395, if the blur tolerance is 1 pixel, the exposure time should be shorter than 36.6 us/pixel . If the camera saves the frames generated by every exposure, the frame rate is up to 27322.4 fps .

It is unnecessary to saves every frames, but need to make sure how many times you wish to see the object before it moves out of the field of view.

6.2.3.2 How to choose frame rate

In this example, $V = 63.89 \text{ m/s}$ (230 km/h), $D = 3\text{m}$ (assumption), so $N = ?$

Equation (6-1) can be transformed into $= fD/V$, then

If $f = 4,000 \text{ fps}$, $N = 187.8$, with the full resolution $1280 * 1024$ pixels.

If $f = 5,000fps$, $N = 243.8$, with the resolution up to $1280 * 1000$ pixels (camera functionality).

If $f = 6,250fps$, $N = 293.0$, with the resolution up to $1280 * 800$ pixels (camera functionality).

If $f = 800,000fps$, $N = 37564.5$, with the resolution up to $640 * 8$ pixels (camera functionality).

The times that bearing can be seen before it moves out from the image [N] can effect on the accuracy of the axle bearing tracking because the existing deviation. But the higher frame rate, the more strict requirements of the camera light sensitivity. Comparing the confliction of these problems, guarantee the image of a good quality is more important when the environment condition is poor.

6.2.3.3 How to choose resolution

In this example, with the assumption of $D = 3m$,

The pixel calibration $P_c = D/x$. Then,

$$\text{If } f = 4,000fps, P_c = 0.00075 \text{ m/pixel} = 0.75 \text{ mm/pixel}.$$

$$\text{If } f = 5,000fps, P_c = 0.00060 \text{ m/pixel} = 0.60 \text{ mm/pixel}.$$

$$\text{If } f = 6,250fps, P_c = 0.00048 \text{ m/pixel} = 0.48 \text{ mm/pixel}.$$

$$\text{If } f = 800,000fps, P_c = 0.00000375 \text{ m/pixel} = 0.00375 \text{ mm/pixel}.$$

Typically the scaling of frame rate and resolution is approximately linear: double the frame rate, halve the resolution.

In the example picture Figure 6.2, the bearing lid diameter is 23cm, so the choice of resolution should not lead to the features illegible or disappear.



Figure 6.2- Example axle bearing lid

6.2.4 Summary

Based on the hardware system requirements, FASTCAM Mini UX100 monochrome high speed camera was chosen. An example linking the camera settings to the real application was demonstrated. In the following applications, the hardware system is ready for use. In terms of the research on video stream processing algorithm development, the computer vision techniques are going to be discussed next.

6.3 Computer vision techniques overview

Computer vision is the area involving the computational processing of the vision signal, such as images and dynamic video streams. There are various computer vision techniques. The completed map of computer vision techniques can be found in [75]. In Figure 6.3 is a simplified map which contains the techniques having been used in this work.

The image resources in this work are 2-dimension monochromes. The processing procedure is generally divided into two steps: image processing and feature detection & matching. In the first step, the image processing techniques are applied to downgrade the image from the greyscale image into a binary image using an appropriate threshold. Then in the second step, the feature detection and matching techniques are applied to extract the key features that can represent the targeting objects in the image. These two steps are fundamental steps that most computer vision applications need.

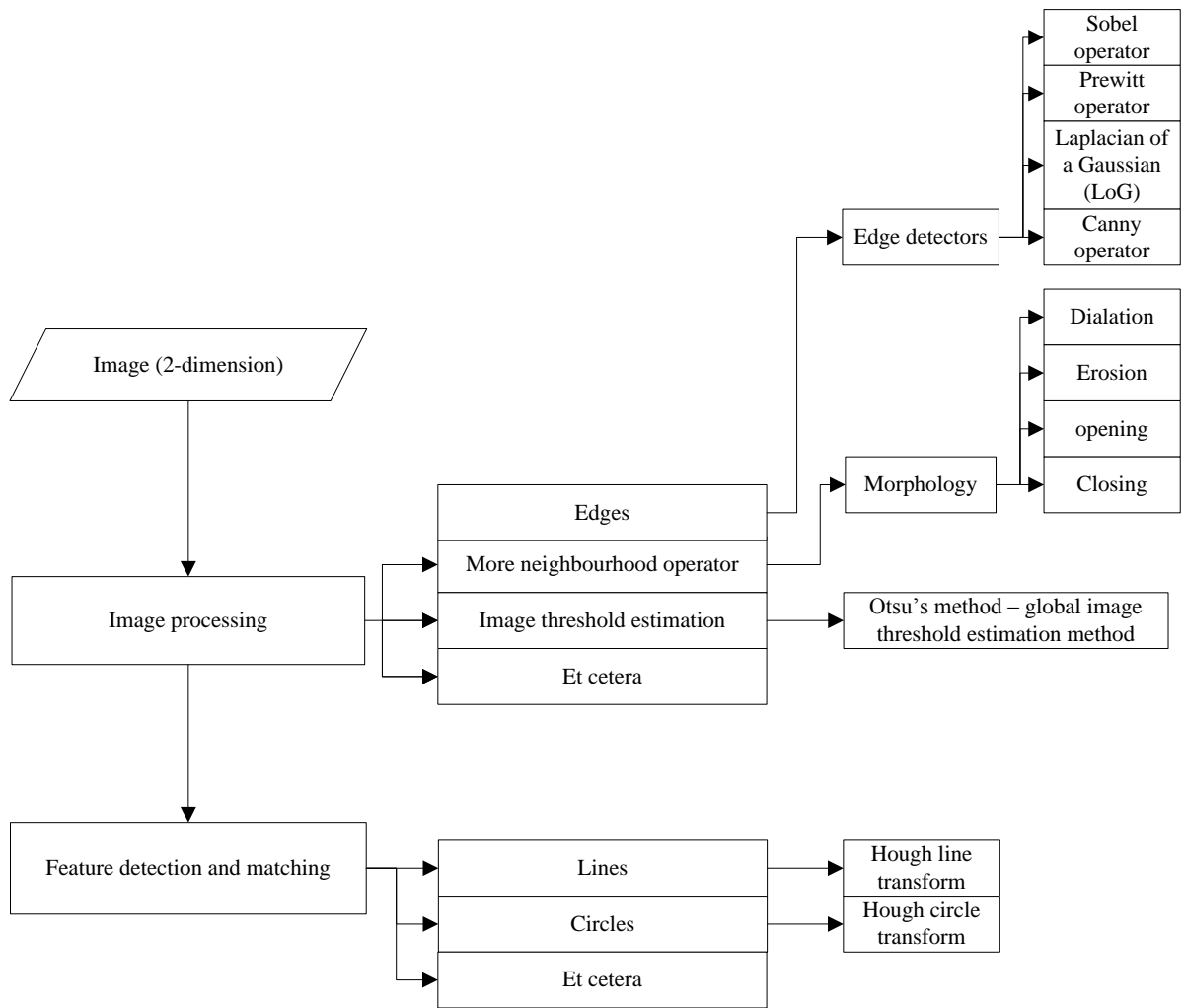


Figure 6.3- Map of the applied computer vision techniques

6.3.1 Edge detectors

Edge detection works by detecting discontinuities in brightness. The edge detection algorithms use different operators which are called edge detectors. Common operators include Sobel, Prewitt, Laplacian of a Gaussian (LoG), Canny operator and etc. Generally, the working strategy follows one of these two rules:

- a. Compare the 1st order derivatives of the brightness with a user defined threshold. If the value is bigger, the point is considered as an edge point.
- b. Find the zero crossing points of the 2nd order derivatives of the brightness. These points are the edge points.

6.3.1.1 Sobel and Prewitt operator

Sobel and Prewitt operator follows the first rule. They use two 3*3 kernels which contains the brightness information of the original image to calculate the 1st order derivatives. One kernel represents the horizontal changes, and the other represents the vertical. The kernals of Sobel and Prewitt operator are shown in Figure 6.5 and Figure 6.6.

Z ₁	Z ₂	Z ₃
Z ₄	Z ₅	Z ₆
Z ₇	Z ₈	Z ₉

Figure 6.4- A 3*3 block in the source image

-1	-2	-1
-1	-2	-1
1	2	1

-1	0	1
-2	0	2
-1	0	1

Figure 6.5- Two 3*3 kernels of Sobel operator (left) G_x – Horizontal kernel (right) G_y –

Vertical kernel

-1	-1	1
0	0	0
1	1	1

-1	0	1
-1	0	1
-1	0	1

Figure 6.6- Two 3*3 kernels of Prewitt operator (left) G_x – Horizontal kernel (right) G_y –

Vertical kernel

So the formulation of Sobel operator is:

$$\begin{aligned}
 g &= [G_x^2 + G_y^2]^{1/2} \\
 &= \{[(z_7 + 2z_8 + z_9) - (z_1 + 2z_2 + z_3)]^2 \\
 &\quad + [(z_3 + 2z_6 + z_9) - (z_1 + 2z_4 + z_7)]^2\}^{1/2}
 \end{aligned} \tag{6-6}$$

And the formulation of Prewitt operator is:

$$\begin{aligned}
 g &= [G_x^2 + G_y^2]^{1/2} \\
 &= \{[(z_7 + z_8 + z_9) - (z_1 + z_2 + z_3)]^2 \\
 &\quad + [(z_3 + z_6 + z_9) - (z_1 + z_4 + z_7)]^2\}^{1/2}
 \end{aligned} \tag{6-7}$$

If $g \geq T$, T is the user defined threshold, the point is considered as an edge point.

Low computational cost is one of the advantages of these two operators. These two operators suit the case without critical requirement of the details remaining.

Usually, the threshold is decided during the experiments because the image processing is so affected by the source image. Meanwhile, in this work, a global image threshold estimation method, Otsu's method, is used in the case of coupler condition monitoring. This method is suitable for the unsupervised decision procedure of the threshold.

6.3.1.2 LoG and Canny operator

LoG is a typical zero crossing detector. It calculates the image intensity gradient. When it starts increasing or decreasing, zero crossings occur at those places. Such points often occur at edges in the image.

The formulation of LoG is:

$$\nabla^2 h(r) = -\left[\frac{r^2 - \sigma^2}{\sigma^4}\right]e^{-\frac{r^2}{2\sigma^2}} \quad (6-8)$$

Where $r^2 = x^2 + y^2$, $f(x, y)$ is the point in an 2D image, σ is the standard deviation which is the width of Gaussian kernel.

Then follow the strategy below to obtain the edge points:

- 1) Applying LoG to the image.
- 2) Detection of zero-crossings in the image.
- 3) Threshold the zero-crossings to keep only those strong ones (large difference between the positive maximum and the negative minimum).
- 4) The last step is to suppress the weak zero-crossings most likely caused by noise.

Hence, it is not difficult to find LoG operator is easily affected by noise.

Regarding to Canny operator, it is one of the most strictly defined methods among the edge detection methods. The fundamental of Canny edge detection is more computational complex than the others:

- 1) Apply Gaussian filter to the image in order to smooth the image and remove the noise
- 2) Calculate the intensity gradients of the image.
- 3) Apply non-maximum suppression to get rid of spurious response to edge detection.
- 4) Apply double threshold to determine potential edge points.
- 5) The last step is the similar to LoG's strategy. Filter and delete the edges that are weak and not connected to strong edges.

Canny operator can provide good and reliable detection when the requirement of the details remaining is strict.

6.3.2 Morphology

Morphological image processing is a series of non-linear operations based on the shape or morphology features in the image. Morphology is especially suited to the processing of binary images because of its fundamental is the calculation on the relative ordering of pixel values rather than the numerical values in each pixel.

6.3.2.1 Dilation and erosion

Erosion and dilation are two basic operators in the morphological operations. The basic effect of erosion operator on a binary image is to erode away the boundaries of foreground pixels. Thus areas of foreground pixels shrink in size, and "holes" within those areas become larger.

Morphological operations probe an image with a small shape or template called a structuring element. To compute the erosion of a binary input image by this structuring element, each of the foreground pixels in the input image is considered in turn. For each input pixel the structuring element is superimposed on top of the input image so that the origin of the structuring element coincides with the input pixel coordinates. In summary, the strategy is:

- 1) If the input pixel is set to foreground and all its 8 neighbours are also set to foreground, then the pixel remains set to foreground.
- 2) If the input pixel is set to foreground, but at least one of its 8 neighbours is not, the pixel is set to background.
- 3) Input pixels set to background remain such.

The dilation is the other of the two basic operators in the morphological operations, the first one being erosion. The basic effect of dilation on binary images is to enlarge the areas of foreground pixels at their borders. The areas of foreground pixels thus grow in size, while the background "holes" within them shrink.

So its strategy is:

- 1) If the pixel is set to foreground, it remains such.
- 2) If the pixel is set to background, but at least one of its eight neighbours is set to foreground, the pixel is converted to foreground.
- 3) If the pixel is set to background and none of its eight neighbours is set to foreground, the pixel remains set to background.

6.3.2.2 *Opening and closing*

The opening is a composite operator, constructed from the two basic operators described above. Opening of set A by set B is achieved by first the eroding set A by B, then dilating the resulting set by B.

The closing, like opening, is also a composite operator. The closing of set A by set B is achieved by first dilating of set A by B, then eroding the resulting set by B.

6.3.3 Hough line/ circle transform

The Hough transform is particularly useful for computing a global description of a feature(s) given local measurements. The motivating idea behind the Hough transform for line detection is that each input measurement indicates its contribution to a globally consistent solution (*e.g.* the physical line which gives rise to that image point).

A line segment can be analytically described in a number of forms. However, a convenient equation for describing a set of lines uses parametric or normal notion:

$$x \cos \theta + y \sin \theta = r \quad (6-9)$$

Where r is the length of a normal from the origin to this line and θ is the orientation of r with respect to the X-axis. For any point on this line, r and θ are constant.

The Hough Line Transform (HLT) is a parameter space matrix whose rows and columns correspond to r and θ values respectively. The elements in the HLT represent accumulator cells. Initially, the value in each cell is zero. Then, for every non-background point in the image, r is calculated for every θ . r is rounded off to the nearest allowed row in HLT. That accumulator cell is incremented. At the end of this procedure, a value of Q in $HLT(i,c)$ means that Q points in the xy -plane lie on the line specified by $\theta(c)$ and $r(i)$. Peak values in the HLT represent potential lines in the input image.

The same procedure can be used to detect circles. The parametric equation is:

$$(x - a)^2 + (y - b)^2 = r^2 \quad (6-10)$$

where a and b are the coordinates of the center of the circle and r is the radius. In this case, the computational complexity of the algorithm begins to increase as we now have three coordinates in the parameter space and a 3-D accumulator. (In general, the computation and the size of the accumulator array increase polynomially with the number of parameters)

The fundamental of Hough Circle Transform (HCT) is divided into accumulator array computation, center estimation and radius estimation. In the HCT coordinate system, the circle elements are represented in the format of (a, b, r) that do not have to collect all the elements to retrieve a circle. So there is a fuzzy coefficient to indicate the how much percentage of a circle can be recognised as a whole circle. The setting of this coefficient is the balance between the accuracy and efficiency.

The details of how these computer vision techniques are combined to apply to the applications are demonstrated in the following two case studies.

6.4 Case study – Coupler condition monitoring application

In this section, the objective is to extract the coupler from the image and then apply the monitoring strategy to the coupler monitoring. The data were from the field tests at Long Marston using a Class 117 DMU and a mobile railway laboratory carriage shown in Figure 6.7. The coupler type is the buffer and chain coupler shown in Figure 6.10.



Figure 6.7- Test train

The computer vision techniques applied to the coupler extraction and tracking procedure is divided into the seven steps shown in the flow chart in Figure 6.8.

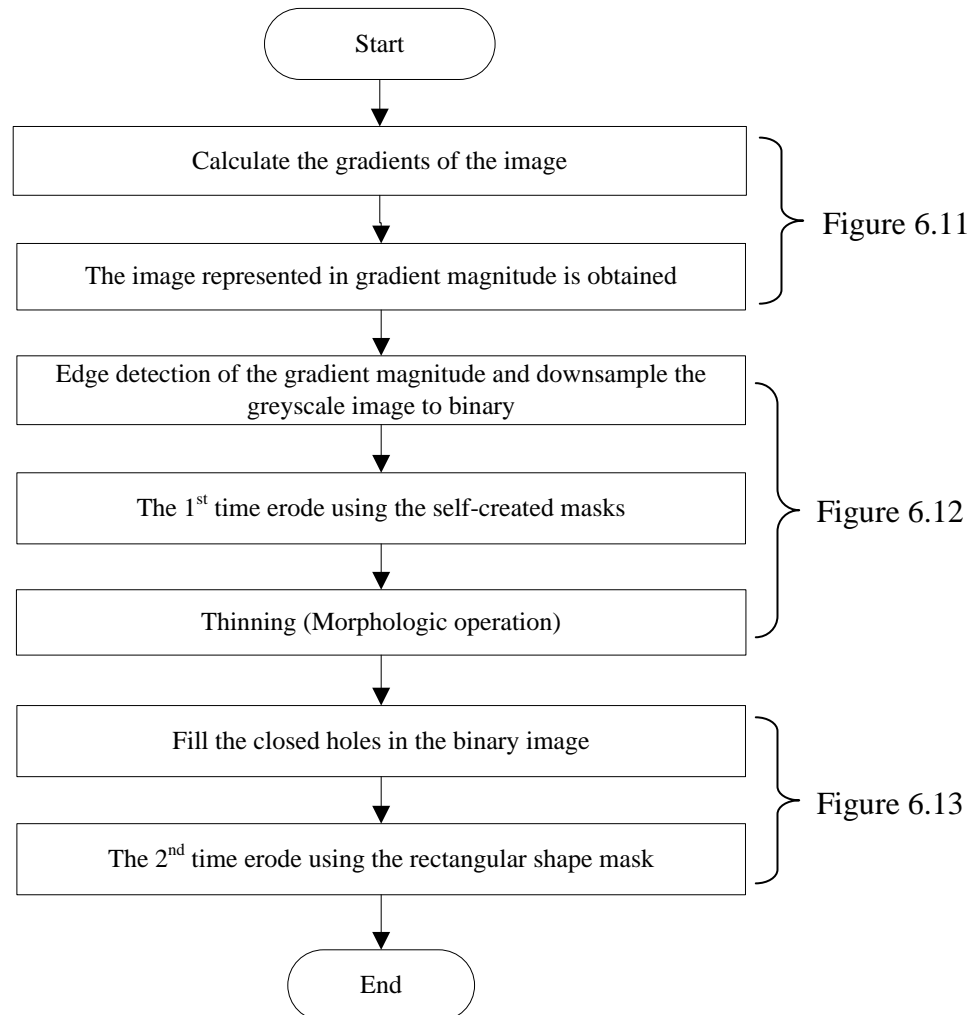


Figure 6.8- Flow chart of the coupler extraction and tracking procedure

In the first step, the image gradient is calculated by firstly computing directional gradients with respect to the x-axis and y-axis, and then the gradient magnitude and direction are computed from the orthogonal directional gradients. The Sobel operator is applied in this step. Then in the second step, the image represented in gradient magnitude is obtained, shown in Figure 6.11. The task of the third step is to apply the edge detection to the image in order to downgrade the greyscale image to binary. To find a proper threshold to downgrade, the global image threshold estimation method, Otsu's method is used. Otsu's method chooses the

threshold to minimize the intraclass variance of the black and white pixels. The working principle is introduced in Otsu's publication [208]. Then the morphologic operation is followed to erode and thinning the image to obtain sharper edges. The erode operator takes two pieces of data as inputs. One is the image needs to be eroded. The other one is a structuring mask (also known as a kernel), which determines the precise effect of the erosion on the input image. The structuring masks used in this step are eight self-created masks (shown in Figure 6.9) corresponding to the eight key structure elements of the none-filled rectangular shape which is the outline of the two coupler pad structure in Figure 6.11. The outcome image of this step is shown in Figure 6.12.

1	1	1	1	1	1	1	1	1	1	1	1	1	1	1
1	1	1	0	0	0	0	0	0	0	0	0	1	1	1
1	1	1	0	0	0	0	0	0	0	0	0	1	1	1

1	1	1	0	0	0	0	1	1	1
1	1	1	0	0	0	0	1	1	1
1	1	1	0	0	0	0	1	1	1

1	1	1	0	0	0	0	0	0	0	0	0	1	1	1
1	1	1	0	0	0	0	0	0	0	0	0	1	1	1
1	1	1	1	1	1	1	1	1	1	1	1	1	1	1

Figure 6.9- The eight self-created masks for the 1st erode operation



Figure 6.10- Original picture



Figure 6.11- The image represented in gradient magnitude



Figure 6.12- Edge detection, erode and thinning processed Image

In the sixth step, it performs a flood-fill operation in the closed holes on background pixels of the binary image. A hole is a set of background pixels that cannot be reached by filling in the background from the edges of the image. After the closed holes are filled, the 2nd erosion is to extract the full filled rectangular shape by applying a fixed size rectangular shape structuring mask. The extraction result is shown in Figure 6.13.

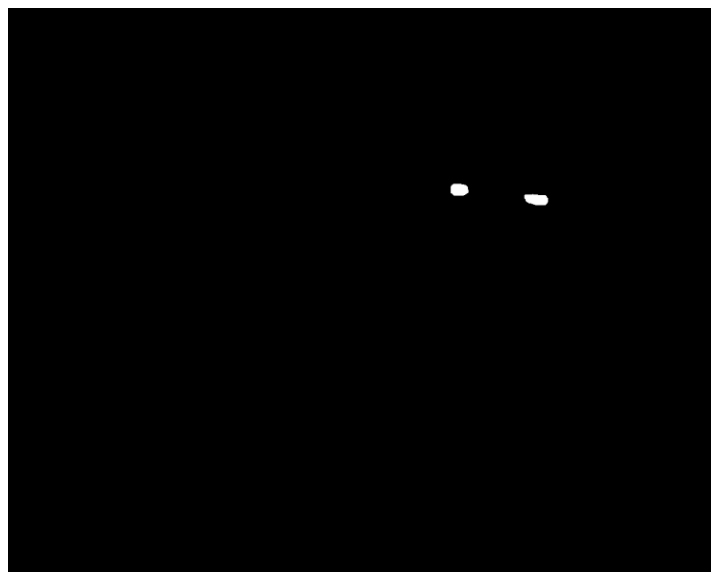


Figure 6.13- Closed holes filled and erode processed Image

After a series of operations, only the closed areas of two coupler pad structure are left in the image. But this satisfying extraction result does not represent the results of all the images. In some cases, some residuals are left in the image still. To increase the precision of the coupler extraction, a local optimisation strategy is applied: (The final coupler extraction result is shown in Figure 6.14)

Requirement 1 – Size of the closed region.

Requirement 2 – Distance between the two coupler pads in both x-axis and y-axis; in the case that one coupler pad in the screen, a fixed range of y-axis magnitude is applied to the closed region location.

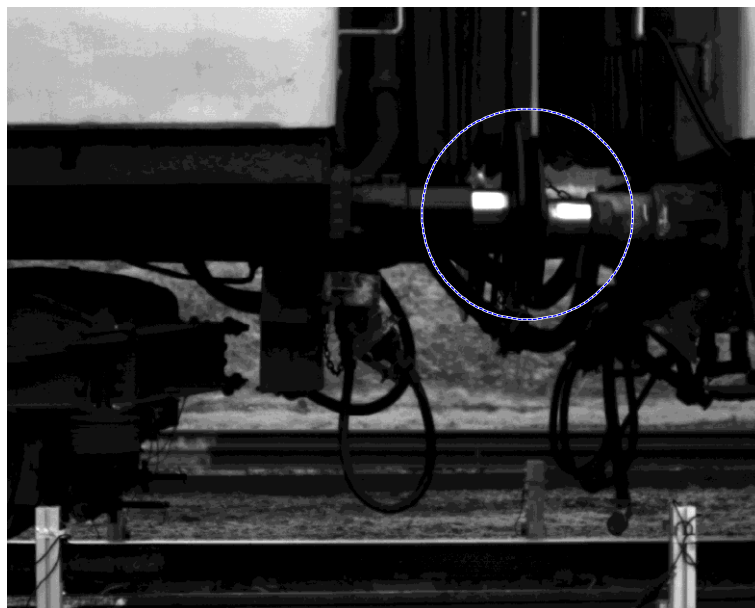


Figure 6.14- Coupler extraction result

With the coupler information within the captured image, the inspection and monitoring strategy can be allied to the coupler condition monitoring system. A pair of healthy buffer and chain coupler is supposed to be attached to each other. The coupler in the figure was working properly. When the coupler is detached, the two halves will separate from each other.

Neither the distance between the two coupler pads are out of range, nor only one half of the coupler is found in the image, the system could generate a faulty signal to the outer system.

6.5 Case study – Pantograph condition monitoring application

In this section, the objective is to extract the pantograph from the image so as to monitor its condition. The data were from the field tests at Network Rail High Speed 1 Line using an in-service train British Rail Class 395 (shown in Figure 6.15). The captured image of pantograph is shown in Figure 6.10.



Figure 6.15- British Rail Class 395 used in the ISMS tests at the High Speed 1 Line [209]



Figure 6.16- Original picture of pantograph

The computer vision techniques applied to the pantograph extraction and tracking procedure is divided into the seven steps shown in the flow chart in Figure 6.17.

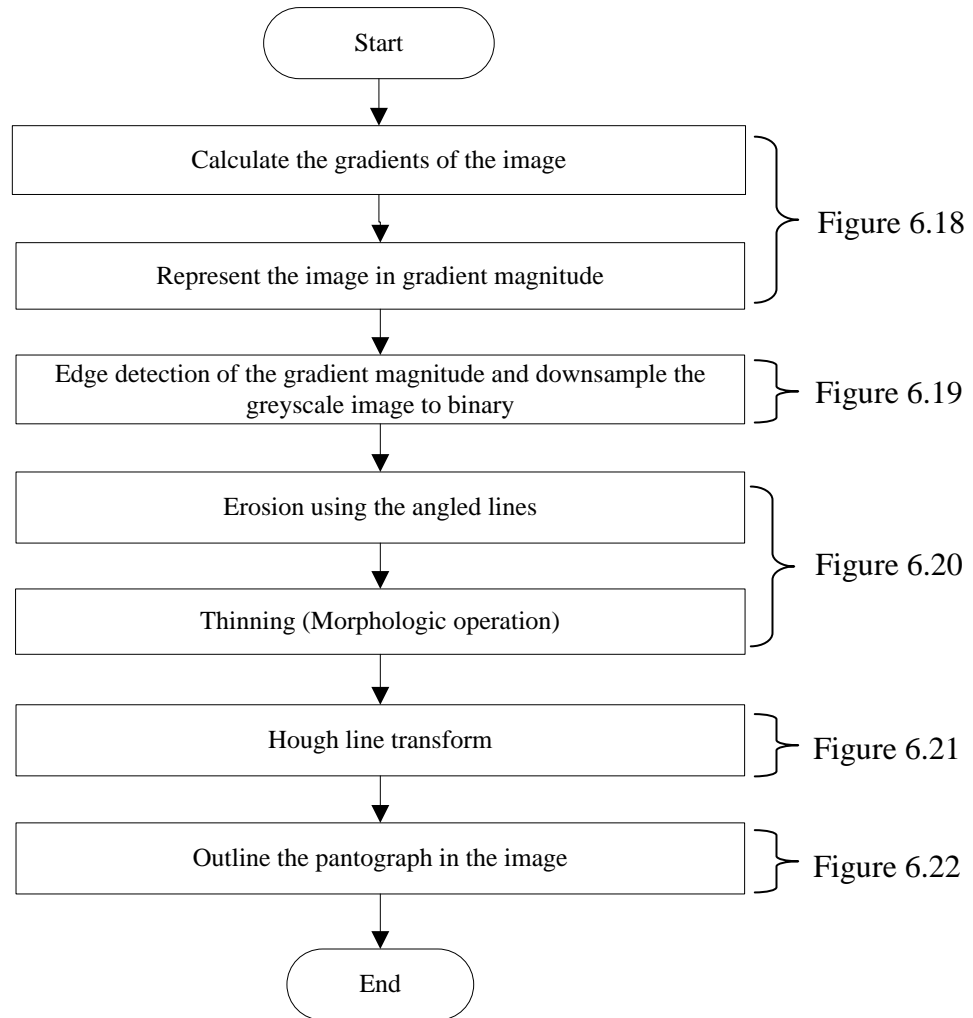


Figure 6.17- Flow chart of the pantograph extraction and tracking procedure

The first five steps are similar to the coupler extraction and tracking procedure. In the first step, the image gradient is calculated. The pantograph image represented in gradient magnitude is shown in Figure 6.18. In the third step the edge detection is applied using the Sobel operator. Otsu's method is used to find a proper threshold to downgrade the image to a binary image. The edge detection processed image is shown in Figure 6.19. The morphologic operations are followed to erode and thinning the image to obtain sharper edges. The erode and thinning processed image is shown in Figure 6.20. The structuring masks used in the erosion are the angled lines which matches the angled arms of the pantograph. The outcome image of this step is shown in Figure 6.20. In the sixth step, Hough line transform is applied to the morphological processed image, the line detection results are shown in Figure 6.21.

The two pantograph arms have been detected. The pantograph extraction result is shown in Figure 6.22.

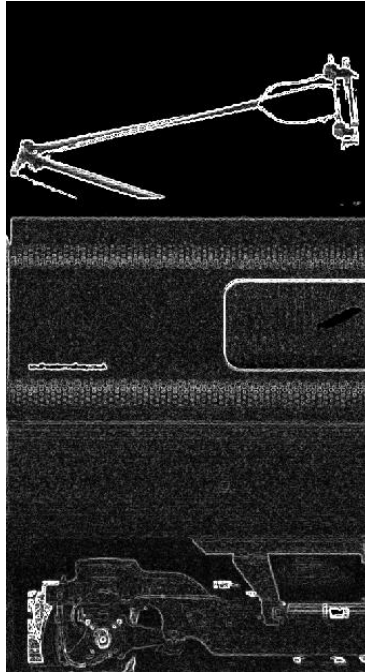


Figure 6.18- The pantograph image represented in gradient magnitude

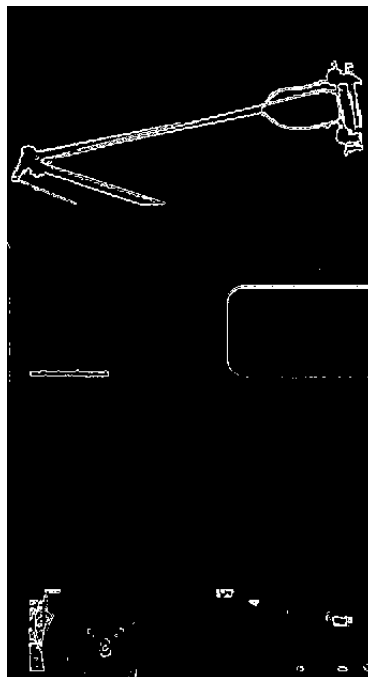


Figure 6.19- Edge detection processed Image

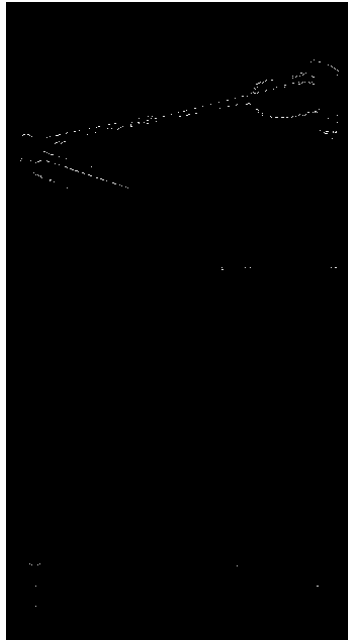


Figure 6.20- Erode and thinning processed Image

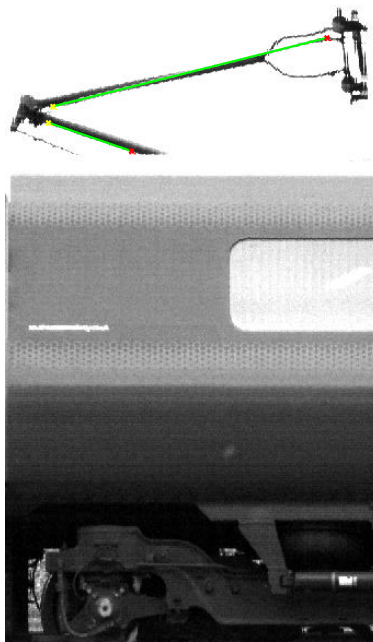


Figure 6.21- Hough line transform processed image

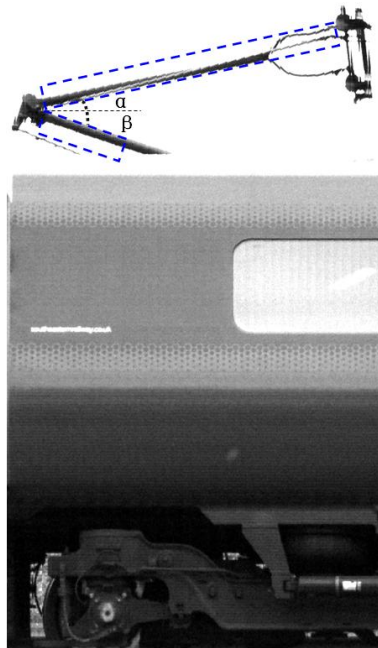


Figure 6.22- Pantograph extraction result

With the pantograph information within the captured image, the inspection and monitoring strategy can be allied to the pantograph condition monitoring system. The angles of the two arms between the horizontal line are the important parameters in the pantograph dynamic behaviour monitoring. These two angles are α and β in the graph. They should be within a range. Any anomalous behaviour of pantograph could be detected by the angle varies.

6.6 Summary

In this chapter, the vision imaging technology has been applied to two applications with two different data scenarios. The data in both scenarios are from the field tests. One is collected from the Rail Alliance test facility at Long Marston using a Class 117 DMU and a mobile railway laboratory carriage; and the other is collected from an in-service British Rail Class 395 at High Speed 1 Line.

The same as the development of acoustic inspection and monitoring system, the developing phase is divided into hardware system design and signal processing algorithm development.

The difference is that it is a commercialised high-speed camera used in the vision imaging system. So the understanding of camera fundamental is important because it decides the selection of device. This procedure has been demonstrated in section 6.2.

Computer vision is the terminology of the processing techniques involving the computational processing of the vision signal. The processing algorithm development started with the overview of computer vision techniques. As the side view of the vehicle could vary from the companies, especially the body painting, the processing algorithm of the vision imaging system is driven by the scenario. In the scenario of the Rail Alliance test facility at Long Marston, the processing algorithm aims at the coupler condition monitoring of the Class 117 DMU and a mobile railway laboratory carriage; while in the scenario of the High Speed 1 Line, the processing algorithm aims at the pantograph condition monitoring of the in-service British Class 395. In each scenario, the capability of the vision imaging inspection and monitoring system has been verified. In the next chapter, the acoustic sensing technology and vision imaging technology are going to be integrated. The needs of integration, integration plans and the experiment results are going to discuss and demonstrate in the next chapter.

7 Integration of the condition monitoring sensing technologies

Acoustic sensing and vision imaging are two technologies, previously demonstrated individually, which will now be integrated in order to test the hypothesis of increased value, and to explore different mechanisms for integration. Previous sections of this thesis have investigated these two technologies in isolation in order to first obtain a good understanding of their operation.

The hardware system and associated computer vision techniques have been discussed in the previous section on vision imaging technology. The so-designed system has been applied to generate metrics for coupler and pantograph condition monitoring applications which are the two case studies explored in chapter 6. The investigations into both the hardware system and computer vision techniques developed understanding thus allowing integration with acoustic sensing technology as demonstrated in this chapter.

Two novel processing algorithms have been developed and presented in the previous chapter relating to acoustic sensing technology. The first is the Empirical Mode Envelope with Minimum Entropy (EMEME) algorithm developed using vibration signals obtained by introducing bearing faults under controlled conditions in the laboratory. The other novel processing technique was developed using acoustic signals from the same bearing faults and laboratory conditions. This is a three-step processing chain: acoustic noise filtering, non-stationary feature extraction, and diagnostics using Spectral Kurtosis (SK). These two novel techniques can improve the performance of acoustic bearing condition monitoring through signal processing.

In this chapter, the integration of these two technologies will be discussed. The chapter starts with a discussion of the need for integration, followed by a discussion of integration approaches, and concludes with demonstration of the developed system and test results.

The field tests of the integrated system were carried out using an in-service British Rail Class 395 vehicle. The system was brought to the trackside of the Network Rail High Speed 1 Line. The Network Rail High Speed 1 Line is the first (and currently only) high speed line in the UK. A Class 395 can run at speed of up to 225 km/h. The test site was an open area by the trackside of the down line with a corresponding section on the up side. The location of the tests site is shown in Figure 4.8. Access to the trackside was authorised by Network Rail High Speed1 Line site office because of the significance of the research and value of a non-invasive measurement system.

7.1 Integration of monitoring systems

Wayside acoustic monitoring systems can inspect and monitor the health condition of axle bearings. If anomalies are detected, the system can report the suspicious carriage to the relative personnel, so that maintenance can be arranged at an appropriate time. Wayside vision imaging monitoring systems can monitor different mechanical components of a vehicle, e.g. identifying missing components or anomalous behaviour of mechanical systems such as pantographs. In the following sections, integration of these technologies will be explored on two levels: system level integration and signal level integration.

System level integration considers the two technologies and integrates them at a hardware system level. A carriage should to be paid serious attention if it is identified as suspicious by both of the two systems. Such direct integration can provide more information than each individual monitoring system, and so can increase the efficiency of maintenance organisation in order to save costs.

High-speed vision imaging inspection and monitoring systems have the potential to monitor the condition of pantographs, as well as the vehicle doors and windows from the side view of the vehicle. Acoustic inspection and monitoring systems have the potential to monitor the

anomalies in mechanical movements, especially related to contact between wheel and rail surfaces because they repeatedly generate high energy acoustic signals during train travel. From a wayside condition monitoring system perspective, system level integration has the potential to rival the GOTCHA system because the system does not cause the interference to the existing railway line. From a condition monitoring efficiency perspective, an integrated system can merge the inspection and monitoring results from both the acoustic and vision systems to provide information on wheel defect condition and pantograph condition, as well as door and window status.

Signal level integration is an integration plan that uses signal merging. Results are of particular interest if the independent technologies can be integrated in an intelligent fashion. This approach needs detailed knowledge of each technology in order to identify the point that one technology can support the other by overcoming its limitations.

As noted in chapter 5, the main difficulty associated with acoustic inspection and monitoring is low signal-to-noise ratio (SNR) which results in difficulty in the fault diagnosis. The two novel processing algorithms proposed in sections 5.2.3 and 5.3.2 are signal enhancement strategies based on improving processing techniques. In the field tests, a microphone array was used to collect acoustic signals. To interpret the acoustic signal, the location of a target for acoustic beamforming within the signal collection area is needed. The precision of location information is important because it determines the quality of the retrieved signal.

The current solution for positioning is to use a lightgate based speed measurement system. It can give the speed of the train, but at a low resolution making it incapable of monitoring variations in the speed of a train. Even in the case of constant speed train, a high resolution speed measurement could more precisely direct the acoustic beamforming in order to retrieve higher quality acoustic signals for the condition monitoring algorithms. Increasing the number of pairs of light gates is the most straight forward solution to increase the resolution,

but the installation and alignment of a lightgate system is complicated (discussed in section 7.5.1.2). And the light beams between the upside and downside light gates can easily lose connection. From this perspective, a high-speed imaging speed measurement system (ISMS) could be a useful alternative. ISMS is a precise real-time wayside speed measurement system. In the integrated system, it is combined with an acoustic inspection and monitoring system. The detailed speed information from ISMS can be fed into the acoustic inspection and monitoring system, improving the directionality of acoustic signal acquisition systems.

In ISMS, the pairs of light gates are replaced by the frames in a visual recording. The frame rate of the high-speed camera can reach up to 800,000 frames per second. Furthermore, the installation of ISMS is simple. In this way, the performance of the acoustic system can be improved by integration of the high-speed vision system.

Field tests of both system level integration and signal level integration system were carried out on the Network Rail High Speed 1 Line. There were no test vehicles but in-service vehicles were present. These were generally expected to be in healthy condition. With these blind tests, the working fundamentals of the integrated system can still be demonstrated using in-service high speed trains. The details of the field tests are discussed in the following section.

7.2 Field tests on the Network Rail High Speed 1 Line

The field tests carried out on the Network Rail High Speed 1 Line were at Nashenden. The entrance to the site is located off the Maidstone Rd, Chatham, Kent ME5 9QG, shown in Figure 4.8. The key dimensions and general layout of the site are shown in Figure 7.1.

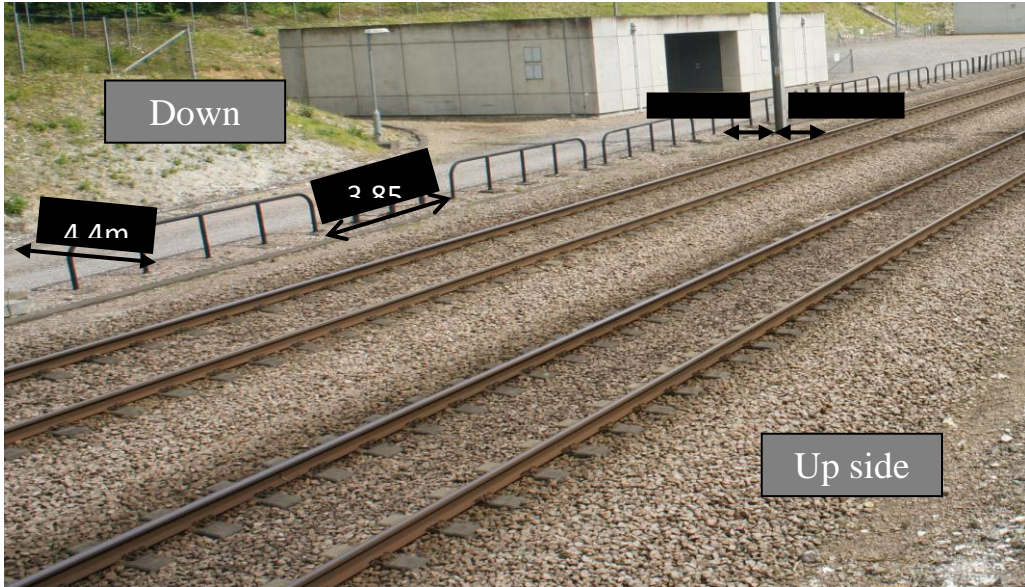


Figure 7.1- Site measurements

The majority of the equipment was installed on the down side. On the down side, the barriers are approximately 4.5 metres away from the track. The electrification mast in the figure is 2.25 metres from track which aligns with the boarder of the “Danger Zone” as defined by Network Rail. Entry into this area is prohibited during live running of trains. A wireless control and monitoring station was set up next to the building. The integrated monitoring system was installed between the electrification mast and the barrier in the indicated 3.85 metres, and the light gates were installed at the boarder of the Danger Zone.

7.2.1 Site requirements

The site was selected based on a number of parameters including acoustic conditions, line speed consistency, and availability of a power source. To obtain the Network Rail (HS) Danger Zone Entry Permit, Network Rail safety requirements state that every individual needs to pass a drug and alcohol test and an online HS1 safety knowledge test. Access to the site was arranged by NRHS1. A task supervisor and a rail safety leader were present at all times during the trial that site access was required.

7.2.2 Test equipment

7.2.2.1 *Acoustic hood*

The microphone array is made of sixteen high sensitivity microphones. Each microphone is installed in a spacing framework (shown in Figure 5.26) installed inside an acoustic hood which known as an Acoustic recording funnel (shown in Figure 5.27).

7.2.2.2 *High-speed camera*

The high-speed camera is Photron FASTCAM Mini UX100 (shown in Figure 6.1). To prevent the camera from being exposed to extreme weather, i.e. rain or snow, a protection hood was made to cover the camera body.

7.2.2.3 *Light gates*

As part of the standard acoustic system deployment, there are three light gate transmitters installed on the up side. The light gates are battery powered. The battery is stored in a plastic weatherproof enclosure. Each light gate is mounted on a stand and is weighted down by concrete blocks as shown in Figure 7.2. All concrete blocks are secured with ties. The light gates are installed approximately 2.75 metres away from the track, at the boarder of the Danger Zone.



Figure 7.2- Lightgate stand

7.2.3 Field test plan

The field test plan for the integrated system is shown in Figure 7.3. As part of the standard acoustic system deployment, a lightgate speed measurement system is installed on the two sides of track. The integrated system is installed on down side, between the electrification mast and the barrier (shown in Figure 7.1), approximately 3 metres away from the track. It consists of the acoustic hood and the high-speed camera. For reasons of safety, NRHS1 required a substantial support frame for the integrated system during the field tests on the High Speed 1 Line.

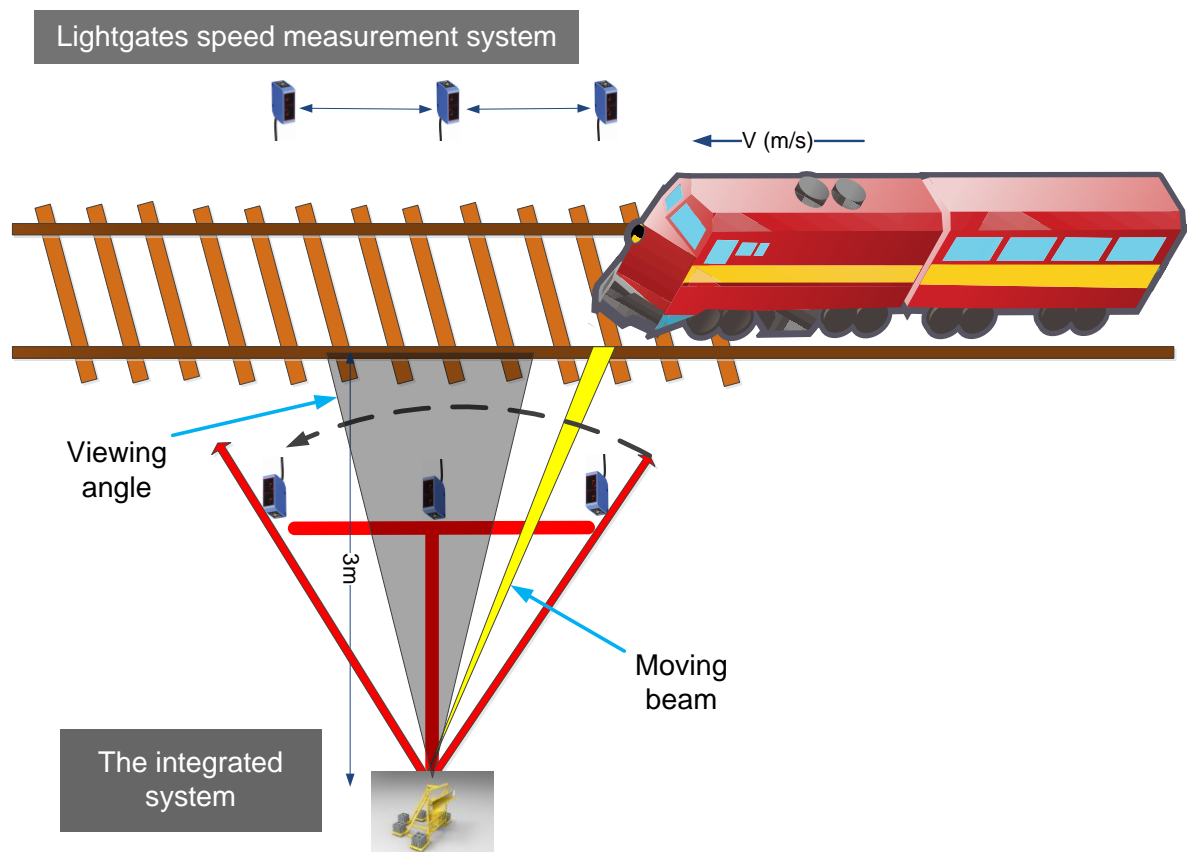


Figure 7.3- Field test plan for the integrated system

7.3 System and signal level integrated system on the High Speed 1 Line

The frame for the integrated system is shown in Figure 7.4. The painted steel frame (grey BS480000A05) was designed and built by Thompson Engineering Design (TED) to hold the acoustic hood and to mount the high-speed camera. There are five concrete blocks stands for weight, and the control equipment is mounted underneath the acoustic hood. The frame is installed on the down side, approximately 3 metres away from the rail. The high-speed camera is installed at one of two mounting points aligned with the centre of the frame.

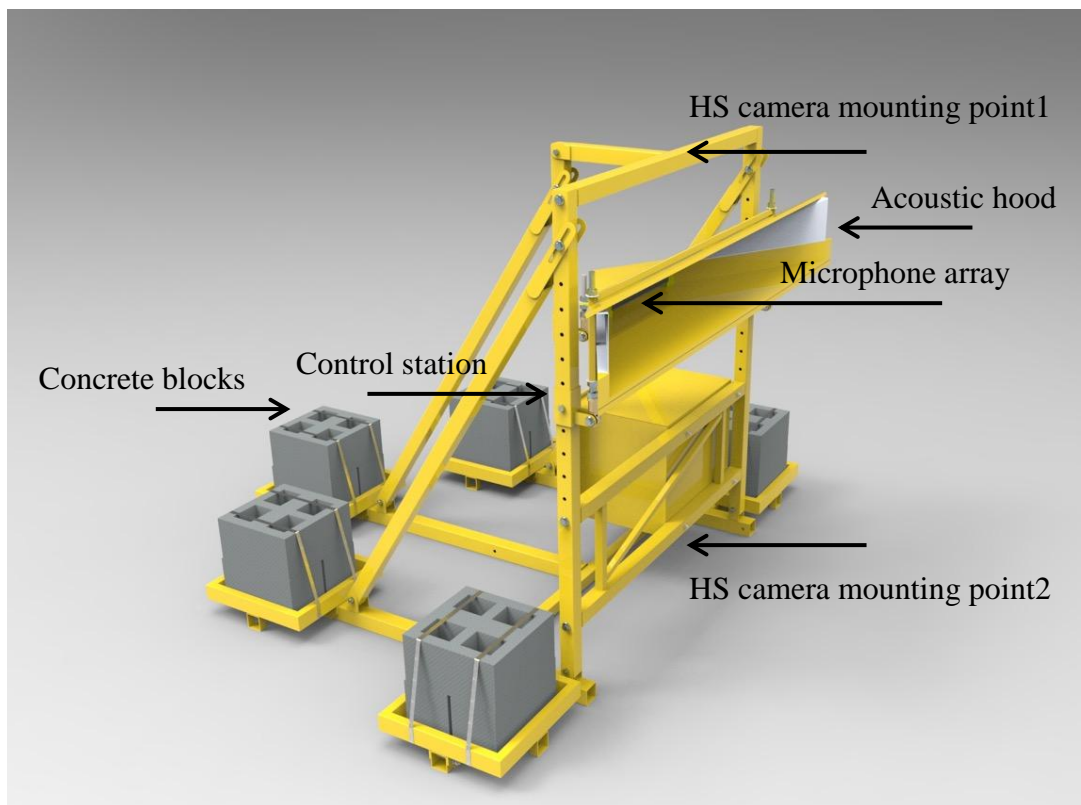


Figure 7.4- Integrated system frame

The two high-speed camera mounting points correspond to the two levels of integration: system level integration and signal level integration. Mounting point 1 is located on top of the frame and is used for system level integration. Installing the high-speed camera there allows the camera to record a side view of the vehicle as well as the overhead line. Mounting point 2, located at the bottom of the frame, is used for signal level integration. The camera captures

clear images of the bogie and wheel profile. The profiles can be used to track vehicle movement and measure the train speed. In this way the acoustic and vision systems can be integrated at a signal level.

These two approaches to integration are going to be discussed in the following sections along with system performance and results.

7.4 System level integration

System level integration allows the acoustic system and vision system to collect data independently. The results from each system can then be integrated to provide more comprehensive vehicle information. For instance, if the acoustic system reports potential hazards on carriage No.1, 2 and 3, while the high-speed vision system has identified anomalies on carriage No.3, 4 and 5, then carriage No.3 should be may have underlying issues and should be considered more closely. Such direct integration of the two systems can provide more information than each individual monitoring system. This can increase the efficiency of maintenance arrangements and save costs. The system level integration system is shown in Figure 7.5.

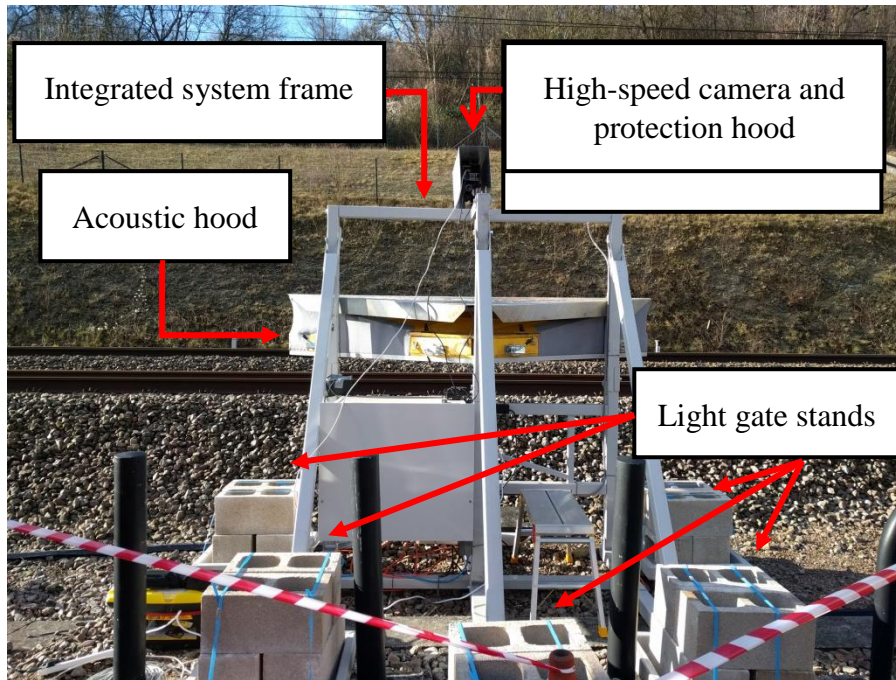


Figure 7.5- System level integration system

7.4.1 High-speed vision inspection and monitoring system – Pantograph and vehicle side view inspection and monitoring

High-speed vision inspection and monitoring system work on the recorded vehicle side view images to achieve condition monitoring of the important components, such as pantograph and train doors, windows etc. With the extracted metrics relating to the pantograph and train doors & windows, condition-based maintenance of these components is achievable. One of the vehicle side view images is shown in Figure 7.6.

7.4.1.1 System settings

The settings of high-speed camera were discussed in section 6.2.3 with the knowledge of high-speed camera fundamental. To decide the actual settings, the requirements from integration need to be taken into consideration as well.

As one element of the integrated condition monitoring (CM) system, high-speed vision system needs to balance the requirements from the integration while deciding the system

settings. For example, in terms of the distance between integrated system frame and the vehicle, high-speed vision CM system prefer a long distance in order to record wide angle images which contain much information to analysis; while acoustic CM system prefer a short distance in order to record high energy acoustic signal from the vehicle. Furthermore, environment factors need to be taken into consideration of the system settings of high-speed CM system. For example, balance between shutter speed and the brightness of image; balance between frame rates and recording duration and etc. Considering all the factors discussed above, settings of high-speed camera in the vision inspection and monitoring system are decided and listed in Table 7.1.

Table 7.1- High-speed camera settings in system level integration

Camera model	Frame rate (frames per second)	Resolution	Shutter speed/Exposure time (us)
Photron FASTCAM Mini UX100	4,000	1280×1024	31.25

Linking to the discussion in section 6.2.3, the exposure time was set 31.25 us which allows high-speed camera capturing the image with the blur of less than 1 pixel. As the pixel calibration is approximately 2.34 mm, the blur of capturing is less than 2.34 mm. Correspondingly, the frame rate can reach up to 32,000 *fps*. But it is not necessary because the corresponding maximum resolution is 1,280 by 24 pixels (shown in Table 6.1) which narrows the view height of vehicle side view. Also the huge amount of frame in each frame costs long time to save which could result in missing recording the pass train. Considering the frame rate and corresponding maximum resolution, as well as the saving time duration and capacity of on board memory, the frame rate was set 4,000 *fps* with full resolution of 1,280 by 1,024 pixels.

As noted that there is a conflict between acoustic and vision CM system on the requirements of distance between integrated system frame and vehicle. To meet the requirements of two systems, the author has proposed stitching the vehicle side view images to obtain a wide angle picture. At the meantime, the acoustic hood assembled on integrated system frame stays the distance that it plans to be.

7.4.1.2 *Image stitching*

The working fundamental of image stitching is based on stitching a strip that is extracted from the centre of each image, as shown in Figure 7.6. Choosing the appropriate width of strip is important in order to achieve a smooth stitching of the image. Four parameters are needed to decide the width of the central strip: frame rate (f_r), image width in horizontal (L), image horizontal resolution (R_H) and train speed (V).

Based on the theory that the ratio of the central strip width and the image horizontal resolution should be the same as the ratio of the horizontal movement of the train and the image horizontal width, the width of the central strip (W_s) in pixel is:

$$W_s = \frac{S * R_H}{L} \quad (7-1)$$

where S is the horizontal movement of the train between each frame in metres.

The reciprocal of the frame rate, $\frac{1}{f_r}$, is the time duration between two adjacent frames. So S is obtained by:

$$S = \frac{V}{f_r} \quad (7-2)$$

In this case, the train speed (V) is a rough range rather than an accurate value. One reason for this is that the width of the central strip (W_s) in pixels needs to be an integer which is

approximated from the calculated value of W_S . Another reason is that the overlap between the adjacent images can help narrow down the range until the correct central strip width is found.

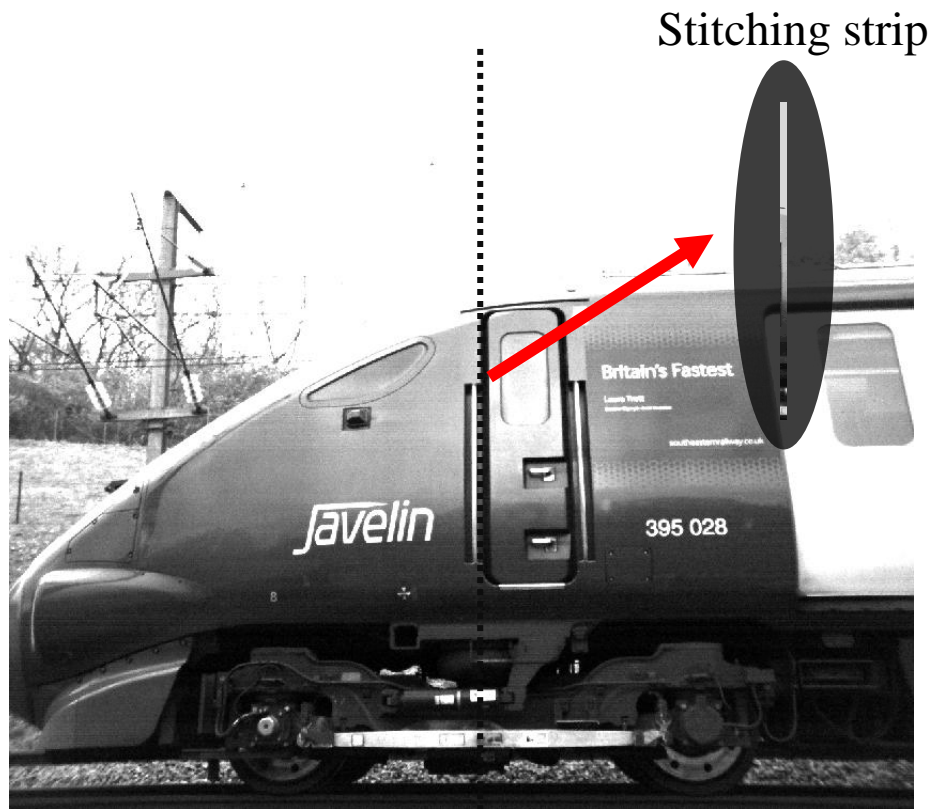


Figure 7.6- Original image with the stitching strip from the high-speed vision system

The stitched image is shown in Figure 7.7. The length of the stitched image can vary based on the requirements of the further processing. The stitched image in Figure 7.7 is the locomotive and one carriage. This includes the pantograph and train door & window and so computer vision techniques can be applied in order to achieve metrics for condition monitoring of these vehicle components.



Figure 7.7- Stitched image

7.4.1.3 Pantograph and train door & window inspection and monitoring

The computer vision techniques applied to the stitched image are divided into the five steps shown in the flow chart in Figure 7.8.

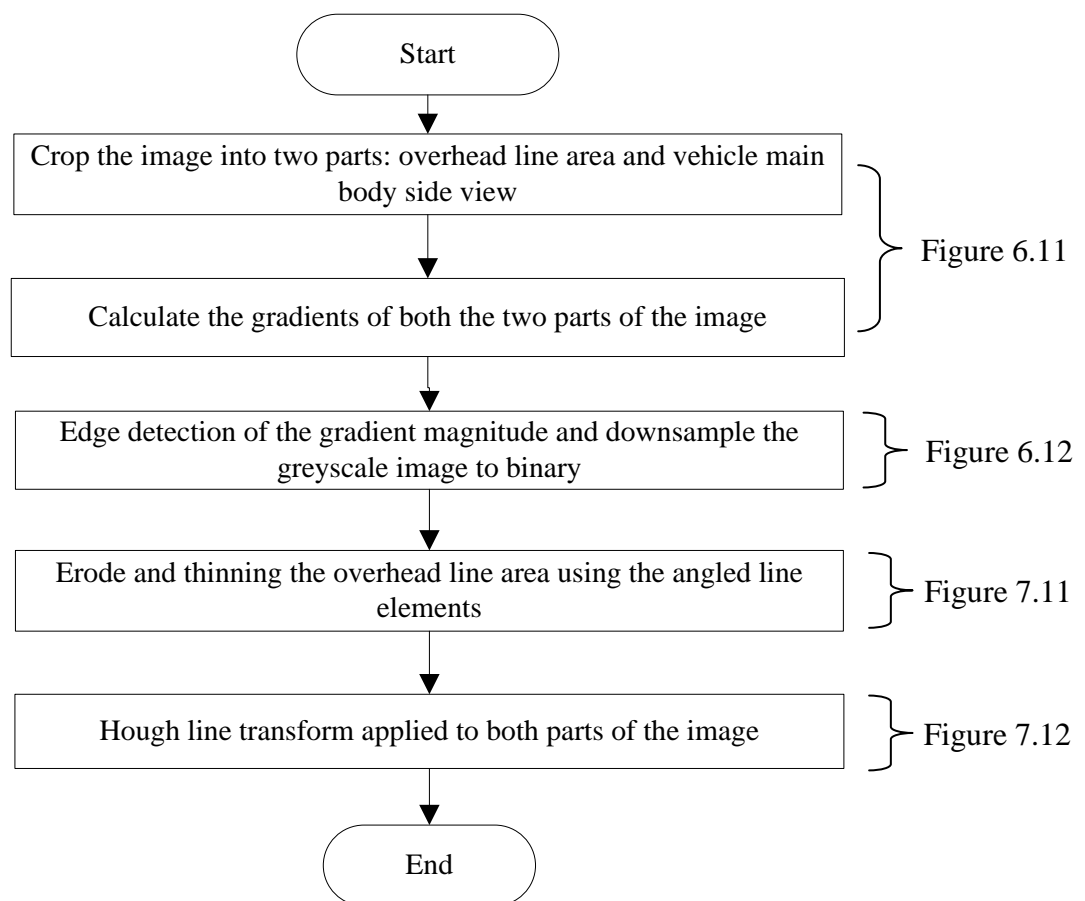


Figure 7.8- Flow chart of the and vehicle side view extraction and tracking procedure

In the first step, the image is cropped to extract only the overhead line area and vehicle main body side view. This is because the cloud in the area above the vehicle has a negative effect

on global image threshold estimation as used for the door & window extraction. In the second step, image gradient is calculated in both parts of the image by firstly computing directional gradients with respect to the x-axis and y-axis, and then computing the gradient magnitude and direction from the orthogonal directional gradients. The Sobel operator (discussed in section 6.3.1) is applied in this step. At this point the image represented in gradient magnitude is obtained, shown in Figure 7.9. In the third step, edge detection is applied to the image in order to downsample the greyscale image to binary. To find an appropriate threshold the global image threshold estimation method, Otsu's method, is used. Otsu's method chooses the threshold to minimize the intraclass variance of the black and white pixels. The edge detection results are shown in Figure 7.10.



Figure 7.9- The image represented in gradient magnitude: (Top) Overhead line area, (Bottom) vehicle main body side view



Figure 7.10- Edge detection processed image: (Top) Overhead line area, (Bottom) vehicle main body side view

In the fourth step, morphologic operations (discussed in section 6.3.2) are applied to the overhead line area of the image to erode and thin the image to obtain sharper edges. The edges in the vehicle main body area are sharp and clear enough for further processing. The erode operator takes two pieces of data as inputs. One is the image to be eroded. The other is a structuring mask (also known as a kernel). The structuring masks used in this step are angled line elements representing the outline of the two arms of the pantograph in Figure 6.12. The outcome of this step is shown in Figure 7.11.



Figure 7.11- Erode (Top) and thinning (Bottom) processing applied to the overhead line area of the image

In the fifth step, the Hough Line transform (discussed in section 6.3.3) is applied to both parts of the image. The important line shape edges are all found in the image, as shown in Figure 7.12. The highlighted extraction result is shown in Figure 7.13.



Figure 7.12- Hough Line transform processed image: (Top) Overhead line area, (Bottom) vehicle main body side view

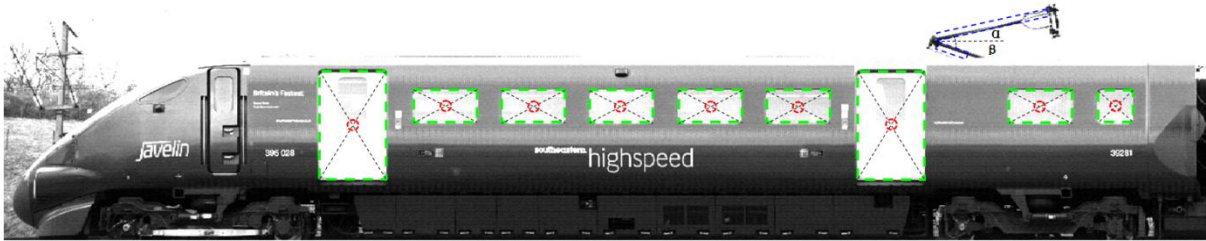


Figure 7.13- Pantograph and vehicle side view inspection result

As noted in section 7.1, there was no expectation to detect any faults on the in-service high speed train. But with this automatic tracking information, the pantograph and train door & window statuses can be monitored when the train passes by. In the case of the pantograph monitoring application, the angles of the two arms between the horizontal line, α and β in the figure, should be within a set range if the pantograph is operating correctly [43]. Anomalous behaviour of the pantograph could be detected if these angles were seen to vary.

7.4.2 Acoustic inspection and monitoring system – Wheelflat detection

Although the acoustic signal processing algorithms (discussed in chapter 5) were applied to the acoustic signal from the High Speed 1 Line field tests, there was no expectation to find any faults on the in-service high speed trains. However, a nearby GOTCHA system reported a wheel flat detection during the trial dates. GOTCHA is a modular wayside monitoring platform to measure the quality of various aspects of trains. The most common module used is the one for Wheel Defect Detection which monitors the quality of the wheels. A GOTCHA system comparable to the type used on the High Speed 1 Line is shown in Figure 6.8. In the following sections, a processing algorithm for acoustic signals to identify wheelflat defects will be demonstrated.



Figure 7.14- GOTCHA system on High-speed 1 line [44]

7.4.2.1 *Acoustic recording system configuration*

The acoustic recording system is triggered by the first light gate. The system has been designed with a 5 second circular buffer to be able to store the audio signals occurring prior to the arrival of the vehicle. The system can also record for 5 seconds after the last gate is triggered. Thus the total recording is 10 seconds plus the time takes for a vehicle to pass the area covered by the light gates.

7.4.2.2 *Signal pre-processing: beamforming and high-pass filtering*

A beamforming algorithm is used to target the key audio sources and to eliminate the Doppler Effect from the moving train. In addition to the air flow from the high speed train, the acoustic signal is buried in an extremely high level of environmental noise. A high-pass filter is applied to output of the beamforming algorithm for each axlebox. The lower cut off frequency was set to 700 Hz (experimental threshold) and the higher cut off frequency to 10 kHz, the upper boundary of the non-distorted response based on the bandwidth of the microphones. An example output signal for the original acoustic beam and the high-pass filtered acoustic beam are shown in Figure 7.15. The filtering result is shown in red, while the original acoustic beam is plotted in blue. Comparing these two waveforms, the high-energy,

low frequency, components have been removed from the original (blue) signal waveform. The remaining signal contains the faulty information relating to the wheel sets.

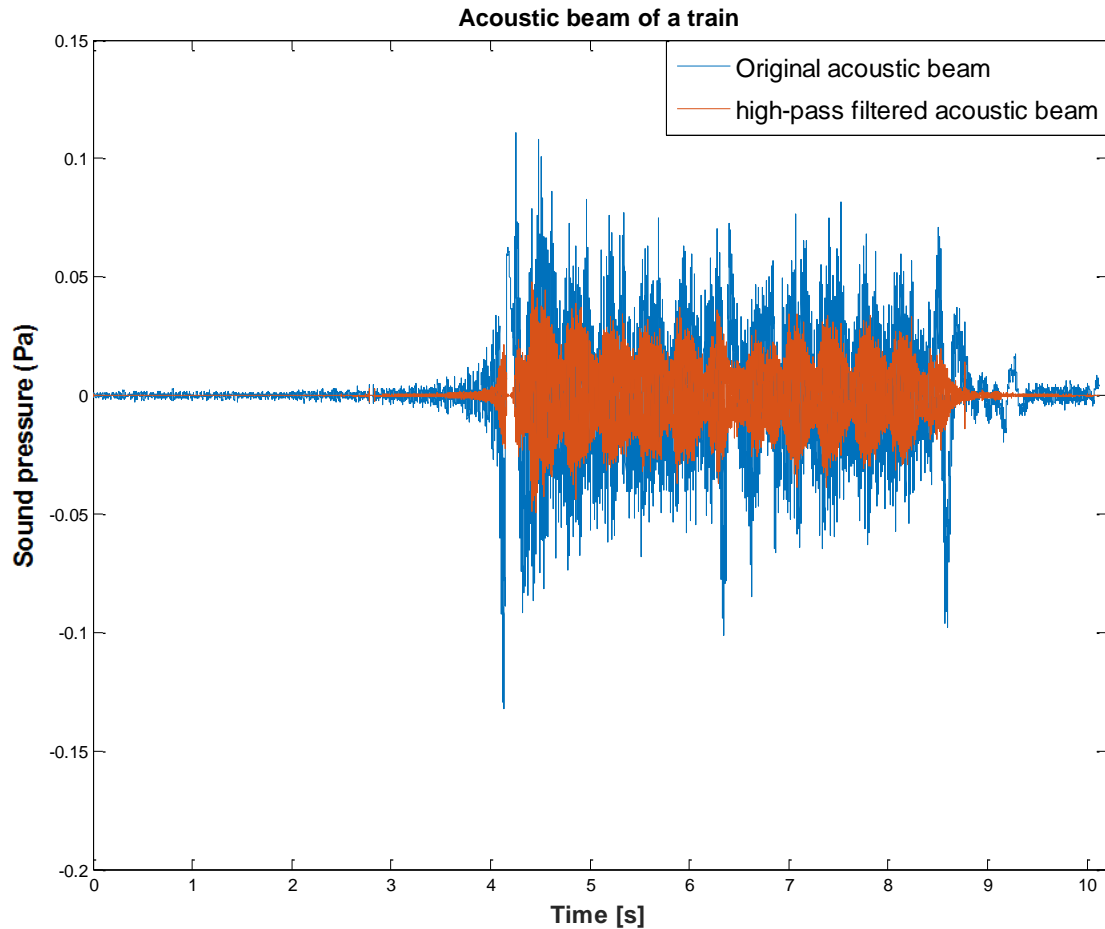


Figure 7.15- Acoustic signal of a high speed train: (Blue) the original signal, (Red) the pre-processed signal

7.4.2.3 Signal post-processing: Acoustic noise filtering

Acoustic noise filtering (ANF) is achieved using the integration of Linear Prediction Coding (LPC) and Empirical Mode Decomposition (EMD) (discussed in section 5.3.2.1). An example of the filtered acoustic signal from an axlebox is shown in Figure 7.16.

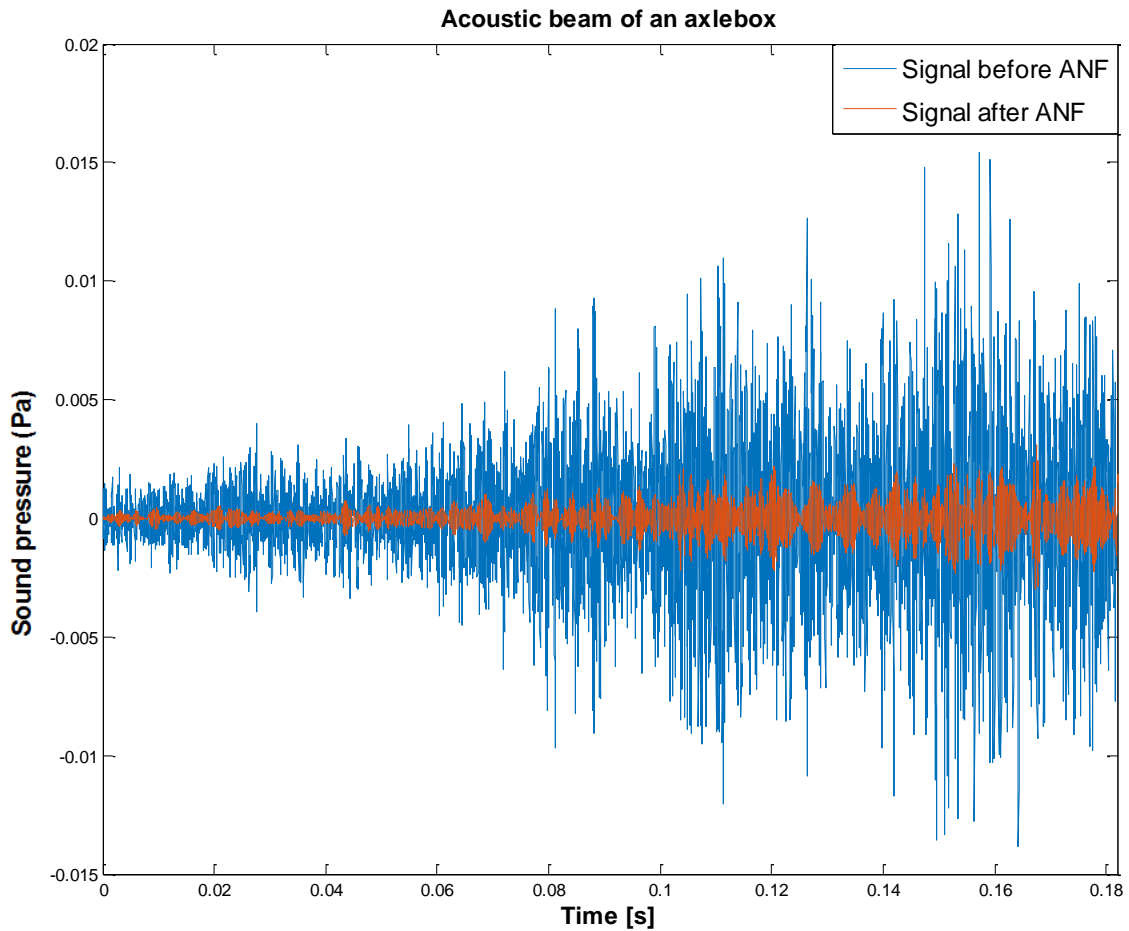


Figure 7.16- Acoustic signal from an axlebox: (Blue) the signal before ANF processing, (Red) the signal after ANF processing

The next step is to extract the feature of the wheelflat from the signal. As this is not roller bearing feature extraction, the spectral kurtosis and kurtogram techniques discussed previously are not appropriate in this case. The RMS value is calculated and plotted in order to use the energy of the signal to reveal the condition of the in-service wheel sets.

7.4.2.4 *Wheel flat inspection*

Figure 7.17 shows the RMS values of ten sets of data (ten trains). The points on the x-axis correspond to the numbered axlebearings on each train, while the y-axis is the amplitude of the sound pressure. The graph shows that the RMS values of the axlebearing signals on the ten trains are approximately at the same level, which indicates that similar levels of energy of

the acoustic signal are generated by the axlebearings as expected. This pattern indicates a relatively healthy condition of the wheel sets, as expected because these mechanical components are on in-service vehicles.

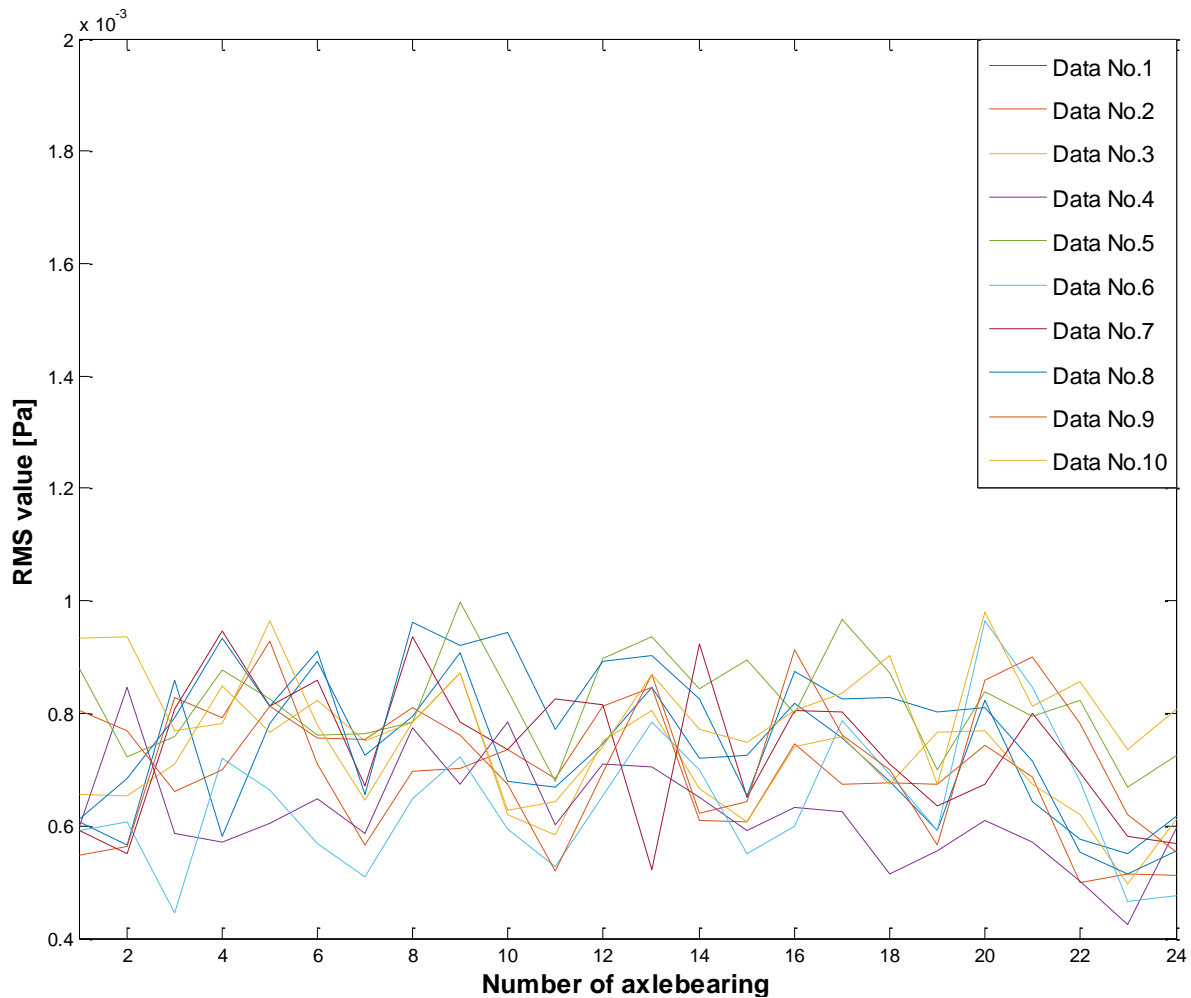


Figure 7.17- RMS values of ten sets of data (ten trains)

The same processing was applied to the train with the wheelflat. The RMS value was compared with the ten data sets shown in Figure 7.17 (as shown in Figure 7.18). A significant peak can be seen in the figure (black with marks). The significant peak corresponds to the No.12 bogie which is the same as the report from the GOTCHA system.

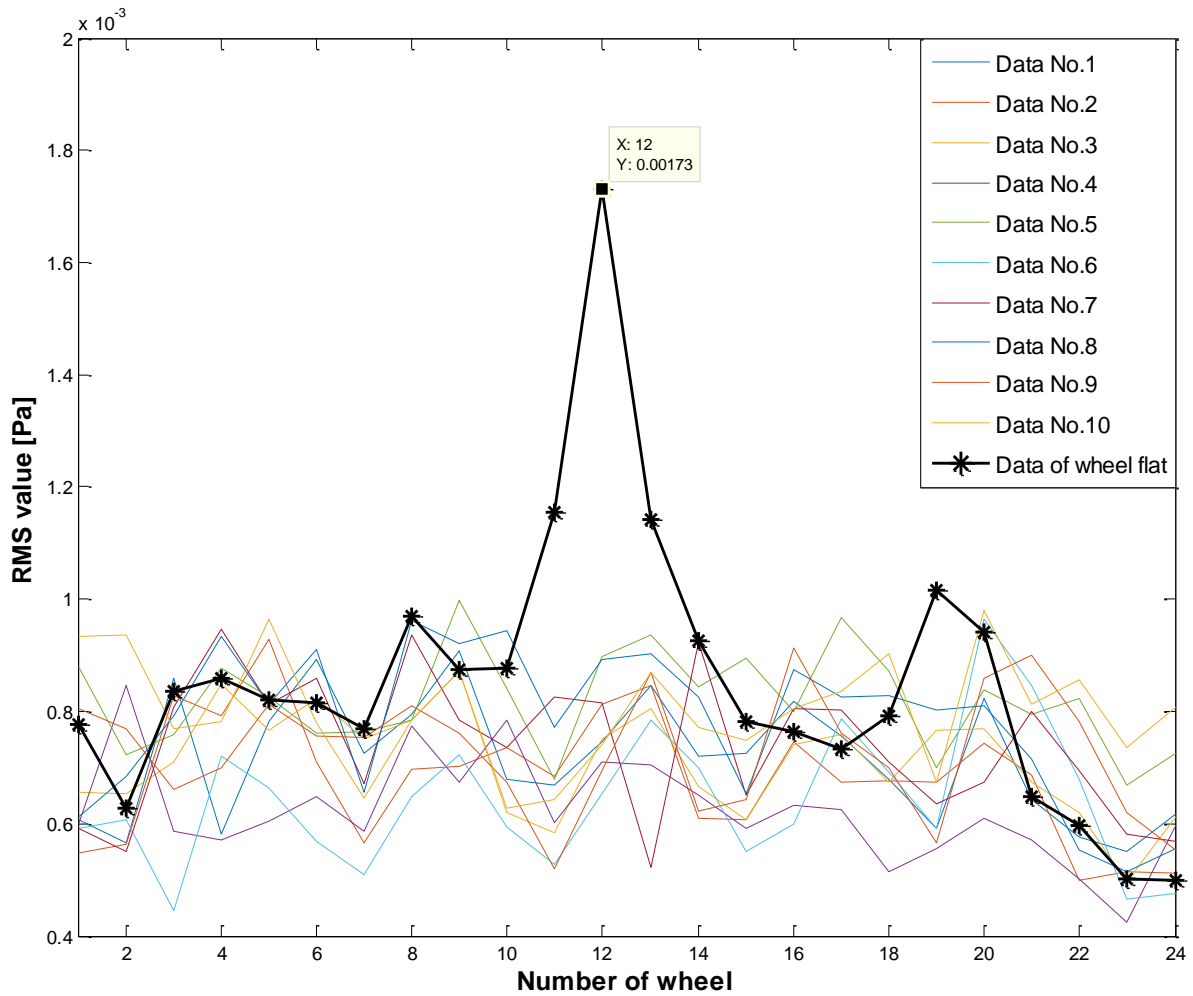


Figure 7.18- RMS values of data set with wheelflat versus ten sets of data (ten trains) in healthy condition

7.4.3 Summary

This section has demonstrated system level integration of acoustic condition monitoring (CM) and high-speed vision CM systems. An integration system frame has been built allowing tests to be carried out at on the Network Rail High Speed 1 Line. The integrated system can provide more information on the vehicle condition, and its installation does not interfere with the existing railway infrastructure. The high-speed vision imaging CM system is capable of inspecting and monitoring pantographs, as well as train door & window statuses; while the acoustic CM system is capable of inspecting bearings and wheelflats from the trackside.

From a wayside condition monitoring system perspective, the system level integrated system is preferable to the Wheel Defect Detection module in the GOTCHA system because it does not physically interact with the existing railway line. From a condition monitoring efficiency perspective, the integrated system can merge the inspection and monitoring results from both acoustic and vision systems focusing on wheel defect condition, pantograph condition and train door & window statuses. The achievements of the system level integration drive the integration into the next stage, signal level integration.

7.5 Signal level integration

The motivation for signal level integration is driven by the limitations of independent condition monitoring technologies. Even combining technologies on a system level, the technologies are not improved. Signal level integration aims to improve the performance of acoustic CM systems through integrating vision CM technologies. It is therefore necessary to understand the limitations of the acoustic CM system and the capabilities of the vision CM system.

7.5.1 Limitations of acoustic sensing technologies

The working fundamental of acoustic bearing CM systems is recording and analysing the acoustic signal generated from the rolling axle bearings on moving trains. The precise location of where the signal comes from within the signal collection area is important. One reason is that the signal to noise ratio of the fault signal is low; but also because of the Doppler Effect caused by the movement of the train.

As discussed in section 5.4.3, a time-domain beamforming algorithm is used to solve the problems of locating target bearings and eliminating the Doppler Effect. The algorithm requires train speed information. The performance of the algorithm relies on the accuracy of the train speed.

7.5.1.1 Limitation of vehicle speed measurement

Knowing the train speed is a key component in locating the target bearings. If the speed of the train is known, time synchronisation between the acoustic system and the train position becomes achievable.

The current solution uses lightgates to provide a speed measurement system. It can give the speed of the train but only at a low resolution. Increasing the number of pairs of light gates increases the resolution. Vision based systems are one approach to further increasing the resolution. It is possible to measure the real-time speed of a moving train using a high-speed camera. The frame rate of the high-speed camera used in this work is up to 800,000 frames per second.

7.5.1.2 Complexity of system installation

The installation and alignment of the lightgate based speed measurement system is complicated. Ideally it requires entry to the Network Rail (HS) Danger Zone, or if not still requires simultaneous access to both sides of the railway. It is also unreliable as light beams between the up side and down side light gates can easily lose connection. A high-speed camera based solution can be simply installed at the trackside. The train speed can be obtained through applying a proper imaging processing algorithm using the computer vision processing techniques to recorded side view images of the vehicle.

Hence, a high-speed imaging speed measurement system (ISMS) could be a useful alternative to lightgates. The pairs of light gates would be replaced by the frames in the recording and the installation of an ISMS is simple and does not require access to the track. In this way, the performance of the acoustic CM technology could be improved with the integration of a high-speed vision based CM technology.

7.5.2 Improved speed measurement through ISMS – Rail Alliance Long Marston storage site

The imaging system developed for this application identifies and tracks key components of the vehicle. From this, alignment and speed information can be passed to the acoustic microphone array processing to allow it to target and track the axle bearings. The Imaging Speed Monitoring System (ISMS) presented in this thesis makes use of a high speed camera to measure the real time train speed in order to solve the microphone array alignment problem. Feature extraction and object tracking technologies similar to those used in the independent CM techniques have been applied to the data from the ISMS camera to generate vehicle speed profiles and to allow alignment with key components such as the axle bearings.

7.5.2.1 Field Test Using a High-Speed Camera

Field tests to verify the performance of The Imaging Speed Monitoring System (ISMS) were carried out at the Rail Alliance test facility at Long Marston with the support of Motorail Logistics. The test facility consists of a 5 km loop of rail; tests were carried out using a Class 117 DMU and a mobile railway laboratory carriage as shown in Figure 6.7. Tests were carried out at a variety of speeds ranging from 8 km/h (simulating shunting) to 50 km/h. The ISMS and lightgate systems were used in parallel to allow a direct comparison of performance. A general overview of the test system is shown in Figure 7.19.

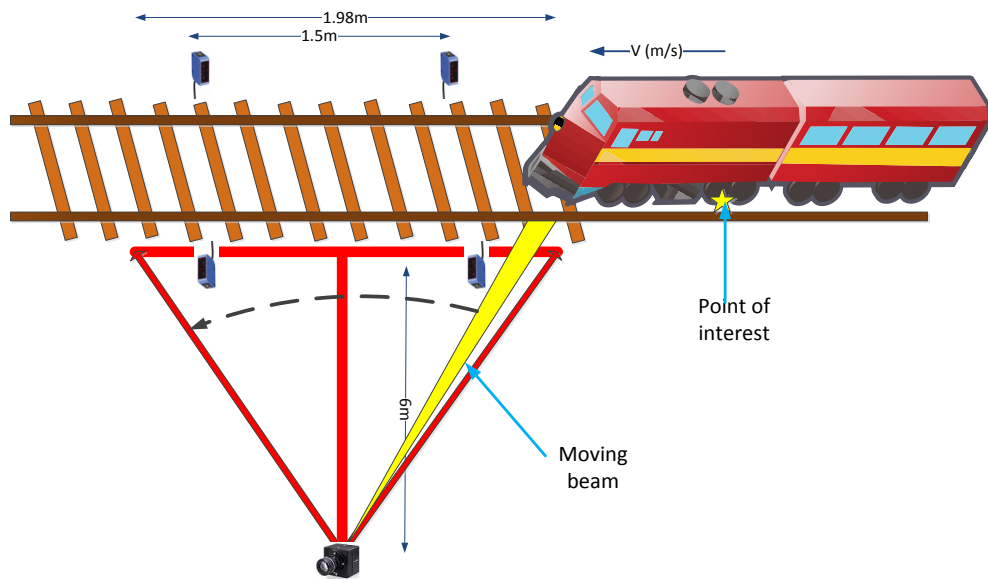


Figure 7.19- Field test plan overview

7.5.2.2 Results and Analysis

An example image captured by the ISMS high-speed camera is shown in Figure 7.20. It is a monochrome image, containing two poles (1.5 m apart) with the lightgates mounted on them. The image shows that the bearing lid has significantly different features from the components around it. In this case, the exposed nature and clarity of the target object means that pre-processing of the image is not necessarily needed, and feature detection for the bearing lid can be applied directly. The feature detection technology used is the Hough circle transform [210]. The fundamental of Hough line / circle transform has been described in section 6.3.3.

Using this technology, the detected bearing lid is shown to be highlighted in Figure 7.20 by the dashed curves.



Figure 7.20- Example image captured by the high speed camera

Having obtained the bearing location information from the image, the real time speed of the train can be calculated by comparing the pixel change of the bearing lid center in consecutive frames. At the same time, the lightgates system is used to measure the train speed as a reference for comparison.

The two impulses in Figure 7.21 represent a single axle passing through the two pairs of lightgates. The average train speed between the two pairs of lightgates is calculated using the fixed distance divided by the difference in the times that the wheel blocked the infrared signal. The speed recorded was approximately 48 km/h in this test.

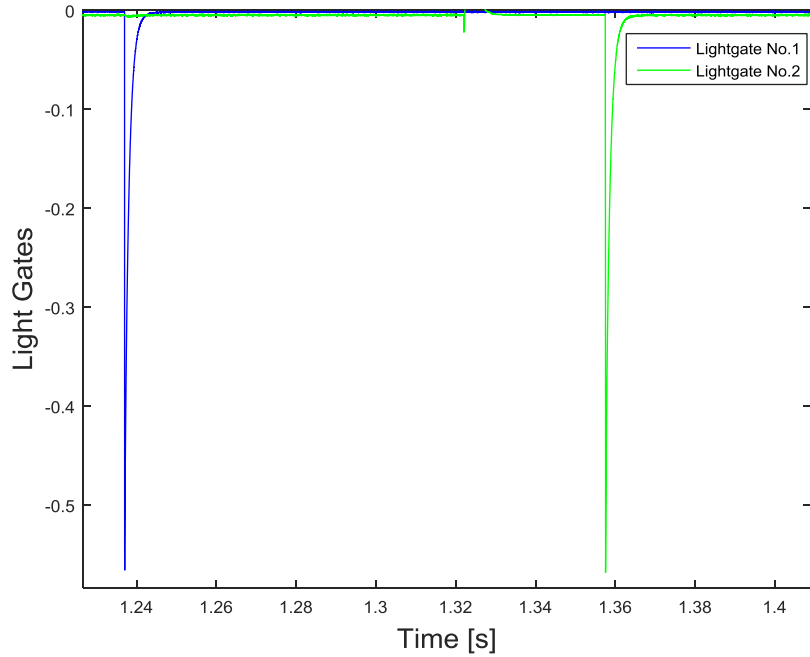


Figure 7.21- Lightgate signals for a single axle

To demonstrate the enhancement of the ISMS over the lightgate reference system, a comparison was made by plotting the speed/time curves of the ISMS and the lightgate systems, this is shown in the Figure 7.22. The speeds were calculated from the four axles of the railway laboratory carriage and are shown together in a single figure. On the graph, the first two triggers correspond to the two axles of the first bogie, while the second two are caused by the axles of the second bogie. Both systems indicate that the train was accelerating when it passed through the inspection area. However, while the ISMS can produce a measurement of acceleration from only one axle passing, the lightgate system requires at least 2 axles to pass before any acceleration can be identified. This is because the ISMS captures multiple frames for each axle, giving multiple speed measurements, whereas the lightgate system captures only 2 impulses, producing a single speed measurement.

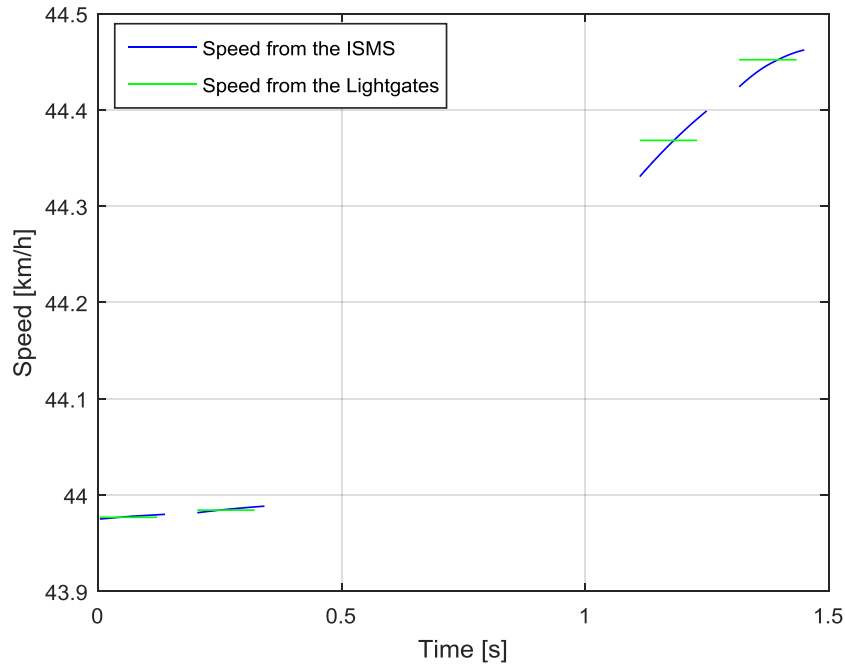


Figure 7.22- Speed/time curves from the ISMS and the lightgate systems

7.5.3 Enhanced ISMS applied to partially seen wheel profile scenario – The Class 323

The Long Marston tests shown that the Imaging Speed Monitoring System (ISMS) is capable of monitoring the speed of a train and that it can give an accurate speed measurement to support the acoustic system by locating where an acoustic signal comes from. In this system, the speed measurement is realised by tracking the wheel from the trackside. Ideally, the wheel profile can be clearly seen from the trackside and so the computer vision technologies do not need to be particularly complex. But in the real world, the situation is often that the wheel profile can only be partially seen. In this case study, a processing algorithm is developed to identify axlebearing positions in this more challenging scenario.

Modern (passenger) trains, have components on and around the axle bearing which complicate and restrict the view of the wheel profile, as shown in Figure 7.24(a). The development of a processing chain to automatically identify partially occluded wheels has been carried out using video of a Class 323 vehicle. The wheel tracking procedure is generally divided into three stages, shown in Figure 7.24, Figure 7.25 and Figure 7.26:

Stage 1 - Extracting the bogie section in the image;

Stage 2 - Filtering operation applied to the bogie section to enhance the wheel profile;

Stage 3 - Wheel detection.

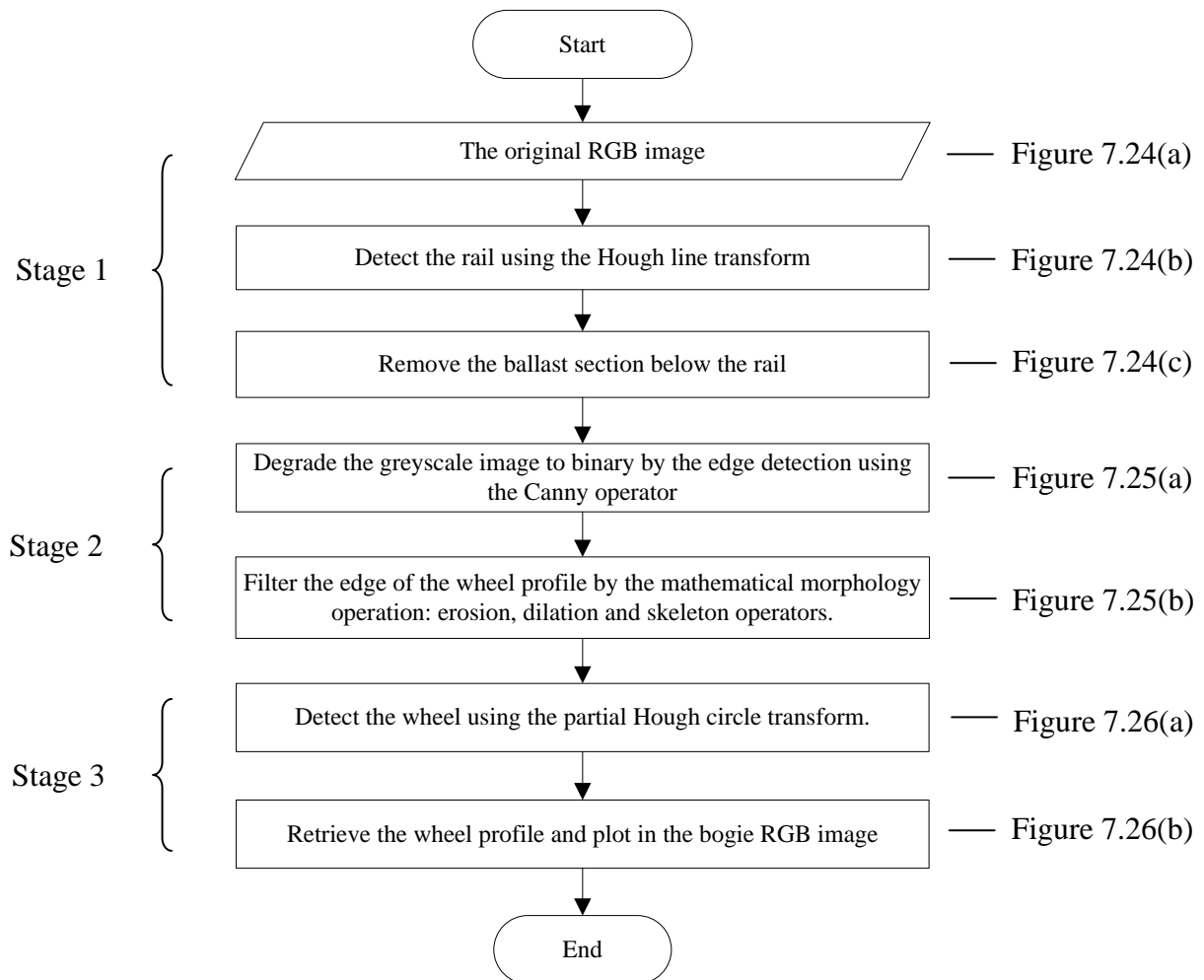


Figure 7.23- Flow chart of the wheel tracking procedure

A flow chart showing the working principles of the processing chain is shown in Figure 7.23.

In Stage 1, the original RGB image is converted into greyscale; then the rail is detected using a Hough line transform and the ballast section below the rail is removed from the image in order to reduce the image size and processing complexity.

In Stage 2, the important edges are identified in the image, using a Canny operator (discussed in section 6.3.1). This operator was selected because of its reduced susceptibility to noise in

the image [211, 212]; The Canny operator is then followed by a series of mathematical morphology operations (discussed in section 6.3.2): erosion, dilation and skeletonisation. This series of morphological operations aims to construct an unbroken and clear line representation of the wheel. The result of this process is shown in Figure 7.25(b). In the figure, the bearing lid is surrounded by the other components found around the wheelset, which makes it difficult to identify and extract it.

In Stage 3, the parts of wheel that can be seen are used in the detection of the entire wheel. In this case, the bottom part of the wheel, shown in Figure 7.26(a), is used to estimate the position of the whole wheel (Figure 7.26(b)). The algorithm used is the partial Hough circle transform. This is similar to the standard Hough circle transform (discussed in section 6.3.3), and uses a parameter threshold to specify the size of a circular sector that can be extrapolated to identify a complete circle. The parameter threshold is an experimental threshold. It needs to be adjusted when the algorithm is applied in other scenarios.

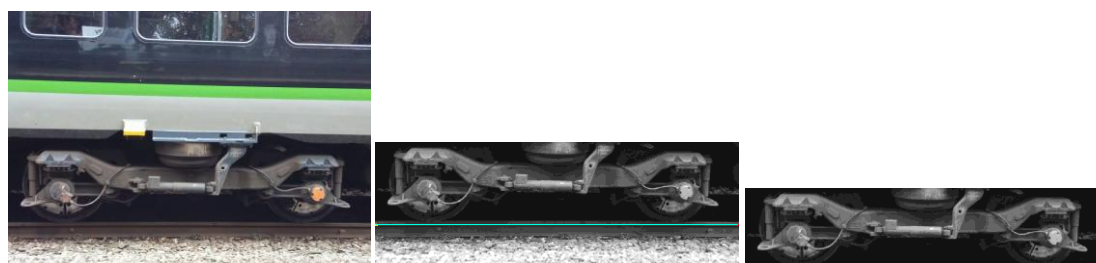


Figure 7.24- Stage 1, (a): the original RGB image; (b): the rail detection; (c): removal of the ballast section from the image



Figure 7.25- Stage 2, (a): edge detection; (b): mathematical morphology operations



Figure 7.26- Stage 3, (a): circle detection; (b): wheel profile retrieval

In the case of the Class 323 example above, the ISMS system has been improved to be able to extract and track the partially hidden wheel profile. It is achieved by the application of a series of computer vision techniques similar to those used in the stand alone vision based CM technologies described in chapter 6. The algorithm required in this case is more complicated than the techniques applied to the images in the recordings from the Rail Alliance facility at the Long Marston storage site. With the enhanced algorithm, the ISMS is then suitable for application to the High Speed 1 Line.

7.5.4 Improved speed measurement through ISMS – High Speed 1 Line

7.5.4.1 Signal level integration– High Speed 1 Line

The general arrangement of the instrumentation for the High Speed 1 Line tests is shown in Figure 7.3. The lightgate based speed measurement system was used as a reference system to compare with the output of the ISMS system. The light gates were installed on the two sides of the track, approximately 2.75 metres away from the rails, at the boarder of the Danger Zone. The integrated system was installed on the down side, approximately 3 metres away from the track. It consists of the acoustic hood and the high-speed camera mounted in a frame structure. As noted, in the system level integration discussion, the high-speed camera was mounted on the lower mounting, mounting point 2 in Figure 7.4.

During the tests at the High Speed 1 Line, in order to compare the systems, the synchronisation between the ISMS and lightgate based speed measurement system became a key issue. During the field tests at the Rail Alliance Long Marston Storage site the trigger signal of the ISMS could be manually generated when the researcher saw the train

approaching. This was not possible with the high speed tests as the system required unattended operation, and the positional accuracy was being evaluated as well as the speed detection mechanism. The synchronisation was achieved using the time stamp on both systems. The triggering plan between the two speed measurement systems is discussed in section 7.5.4.3.

7.5.4.2 *Lightgates speed measurement system configuration*

Installation of the lightgates based speed measurement system requires both height and alignment adjustment. In terms of height adjustment, the ideal would be to make only the bottom of the wheel trigger the light gates as this corresponds to the narrowest position and is in line with the bearing. This means that the height of the light gate wants to be as close as it can be to the rail surface. If the gate is too low this could lead to a potential risk that light gates are miss triggered by the track.

The LED indicators at back of each lightgate receiver can be used to ensure that a clear link is made to each lightgate transmitter on the up side of the track. When the whole system is set up, the first train and the axle counting algorithm can be used to assess the position of the light gates. A photograph from the trial site indicating a lightgate installation is shown in Figure 7.27.



Figure 7.27- The lightgate based speed measurement system at the High Speed 1Line

7.5.4.3 *Triggering between the high-speed camera and the light gates*

The high-speed vision system is triggered by itself. The recording software developed by the camera manufacturer provides an image trigger method. This method allows users to set a brightness threshold that triggers the camera to start recording. The user can also apply this triggering method in a certain area in the image which is helpful in this case as the train entry position is known. The other settings for the high-speed camera are the same as those found in the high-speed vision CM system settings in section 7.4.1.1.

An example graph showing the lightgates signal and the camera triggering signal waveform is shown in Figure 7.28. The red waveform is the signal from the first lightgate. The two pairs of red impulses indicate that two axles (wheels) have passed through. The blue impulse is generated by the high speed camera when it is triggered. In the user's manual for the camera, it states that the delay of the image trigger method is always around 130ms which is proved

right in the graph by the gap between the first red impulse and the blue impulse on the time line. To ensure the whole length of the train can be captured and recorded, a 0.5 second buffer is set to start recording prior to the “arrival” of the vehicle.

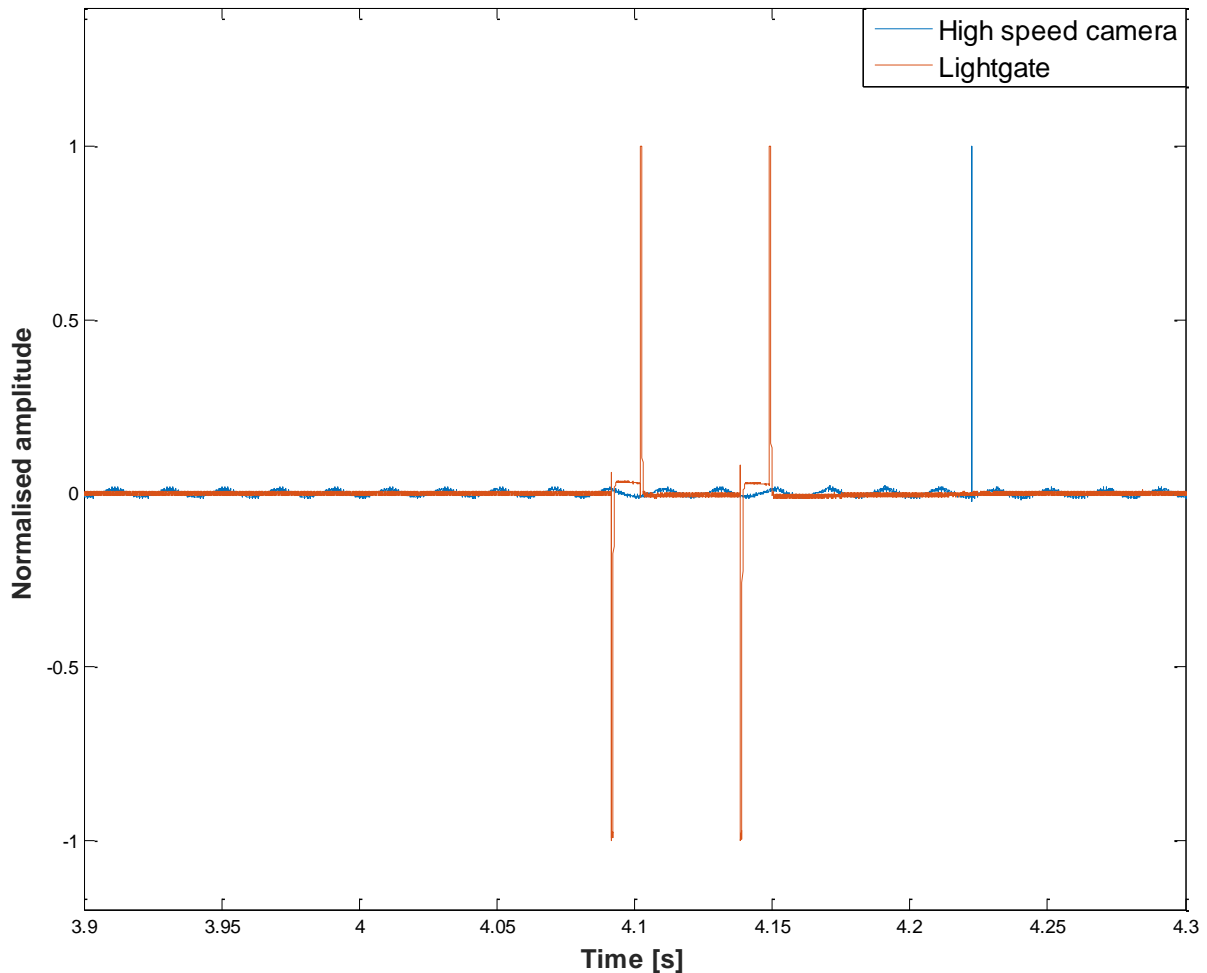


Figure 7.28- The waveform of lightgate and high speed camera signals

7.5.4.4 Results and Analysis

During the High Speed 1 Line tests, the Imaging Speed Monitoring System (ISMS) was applied to a British Rail Class 395, shown in Figure 6.15. An example image of the wheel profile is shown in Figure 7.29. Comparing Figure 7.29 with Figure 7.20, the edge of the wheel profile of the British Rail Class 395 is not as sharp as the axlebox’s edge in the image of the Class 117. Furthermore, the wheel profile is partially hidden so the enhanced ISMS processing strategy proposed in section 7.5.3 is needed in this case.

The morphological thinning operation is applied in the pre-processing stage, in order to sharpen the edge of the wheel profile. Then the partial Hough circle transform is applied to extract the wheel profile.

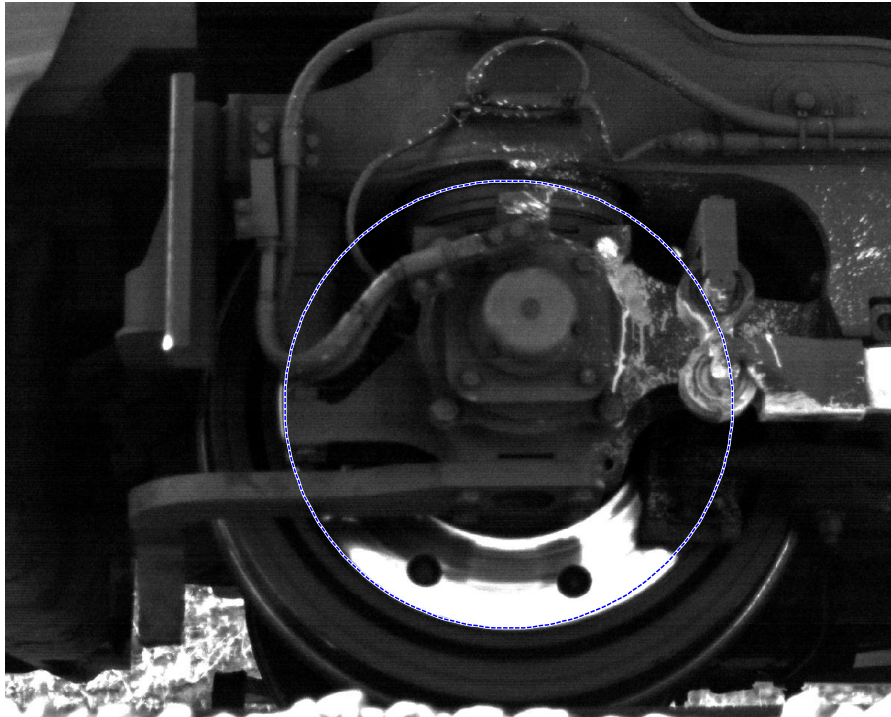


Figure 7.29- Example image of extracted wheel profile

During the field tests, three pairs of lightgates were installed. Figure 7.30 and Figure 7.31 show the signals from lightgate pair No.1 and No.3 generated during the passage of a British Rail Class 395 train. The blue impulse is the high-speed camera triggering signal. Each British Rail Class 395 train has 12 bogies. Each bogie has 2 sets of wheels. So there are 24 wheelsets on each British Rail Class 395 train. “B1” stands for bogie No.1 (the leading bogie) which has 2 sets of wheels representing in the two pairs of impulses in the figures. “B2” is bogie No. 2 which is located at the back of the first carriage, “B3” is located at the front of the second carriage and so on.

The field test general arrangement including three lightgates is shown in Figure 7.3. The train moves from the right to the left in the figure, triggering the light gates in order of No.1, No.2 and No.3. So in Figure 7.30, the high-speed camera triggering signal (blue impulse) arrived after the first wheelset bogie passed lightgate No.1. Also, the blue impulse arrived during the first bogie passing lightgate No.3 (shown in Figure 7.31).

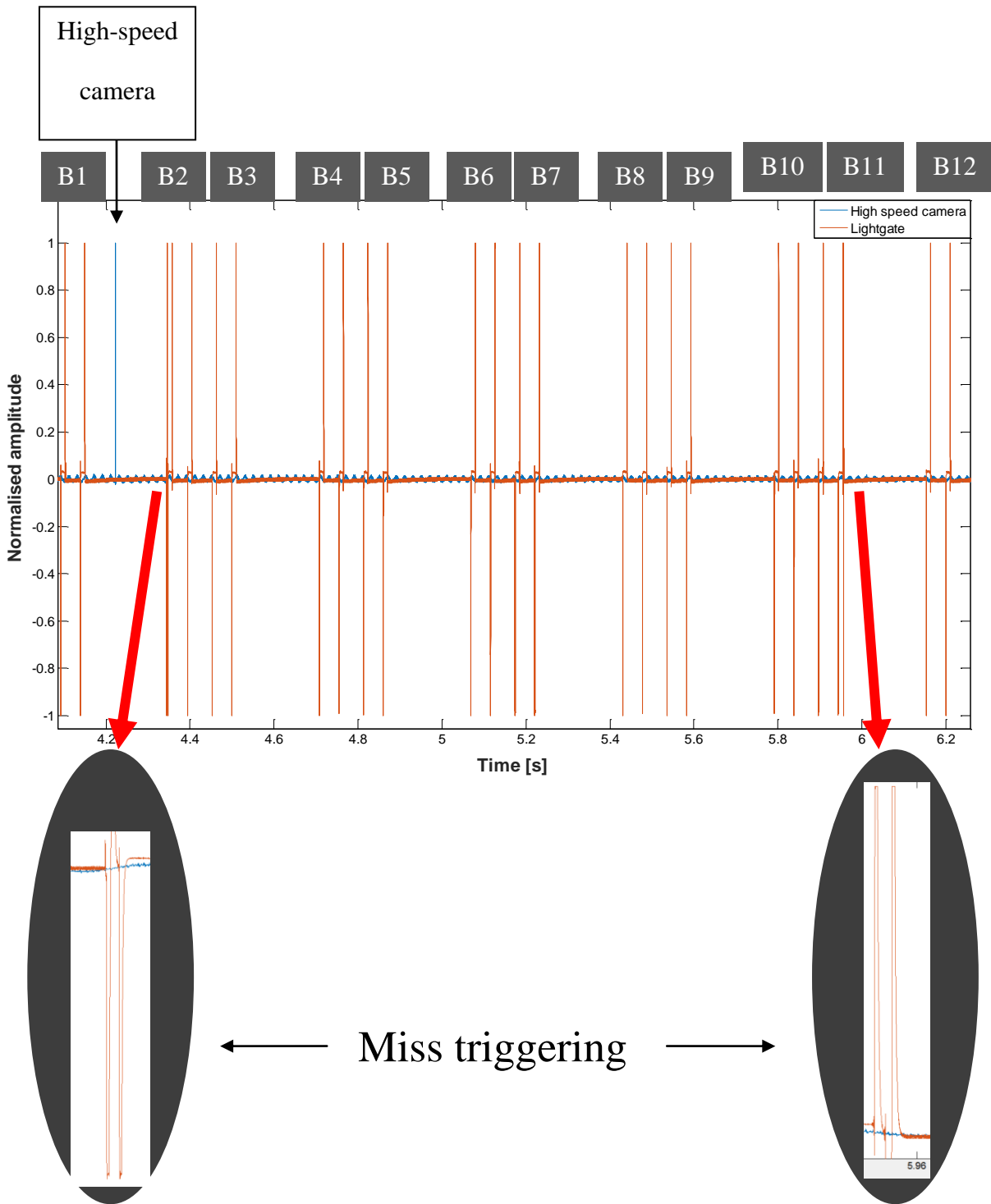


Figure 7.30- The light gate No.1 signal of a British Rail Class 395 train

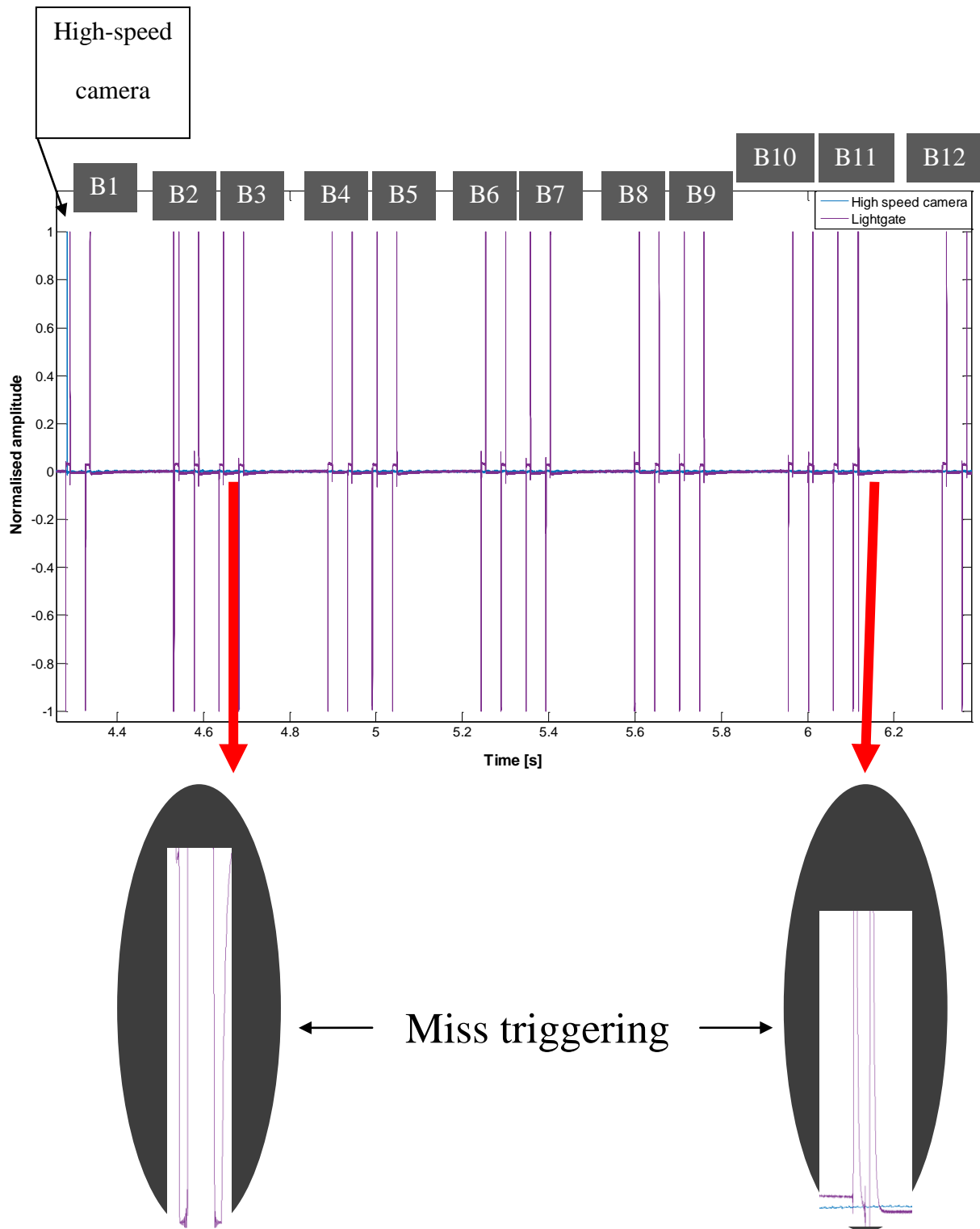


Figure 7.31- The light gate No.3 signal of a British Rail Class 395 train

All twelve bogies can be seen in the figures, but there are also several miss triggering impulses generated by the lightgate based speed measurement system. These are shown in the zoomed windows. This was likely caused by miss alignment between the light gates on the up side and down side.

An example image showing an extracted wheel profile from the Imaging Speed Monitoring System (ISMS) is shown in Figure 7.29. It is a wheel set on British Rail Class 395 train. Having extracted the wheel set location information in the image, the train speed can be calculated between each two adjacent frames. Similar to the results from the Rail Alliance Long Marston tests shown in Figure 7.22, the speed/time graph demonstrating the comparison between the ISMS and lightgate based speed measurement system is shown in Figure 7.32.

As noted, a British Rail Class 395 train has 12 bogies. Each bogie has 2 sets of wheels. So there are 24 wheelsets on each British Rail Class 395 train. The 24 horizontal red lines are the average speed from the lightgate speed measurement system. The three pairs of light gates measure the train speed when each wheelset passes through consecutive pairs of gates. The three pairs of light gates could provide up to two average speed of vehicle. But due to the noted miss triggering issue, there was few comprehensive data sets in the lightgate speed measurement system. A section of the horizontal red line shown in Figure 7.32 is obtained from the average speed between lightgate No.1 and No.2, No.2 and No.3 or No.1 and No.3. Hence, the lightgate speed measurement system monitors speed once when a wheel set passes through.

The blue dash lines are speed measurements from the ISMS. Considering the field test plan of the integrated system shown in Figure 7.3, the ISMS monitors the train speed when it passes through the viewing angle of system. The frame rate of the high-speed camera is set to 4,000

frames per second (discussed in section 7.4.1.1). So the ISMS calculates the train speed 4,000 times per second when train is passes through the field of view.

Both systems indicate that the train was decelerating when it passed through the inspection area. Taking the lightgate based speed measurement system as a reference, the ISMS has been shown to provide values for vehicle speed as designed. Additionally, with the ISMS solution, the installation complexity is significantly reduced, and it is not necessary to access both sides of the line.

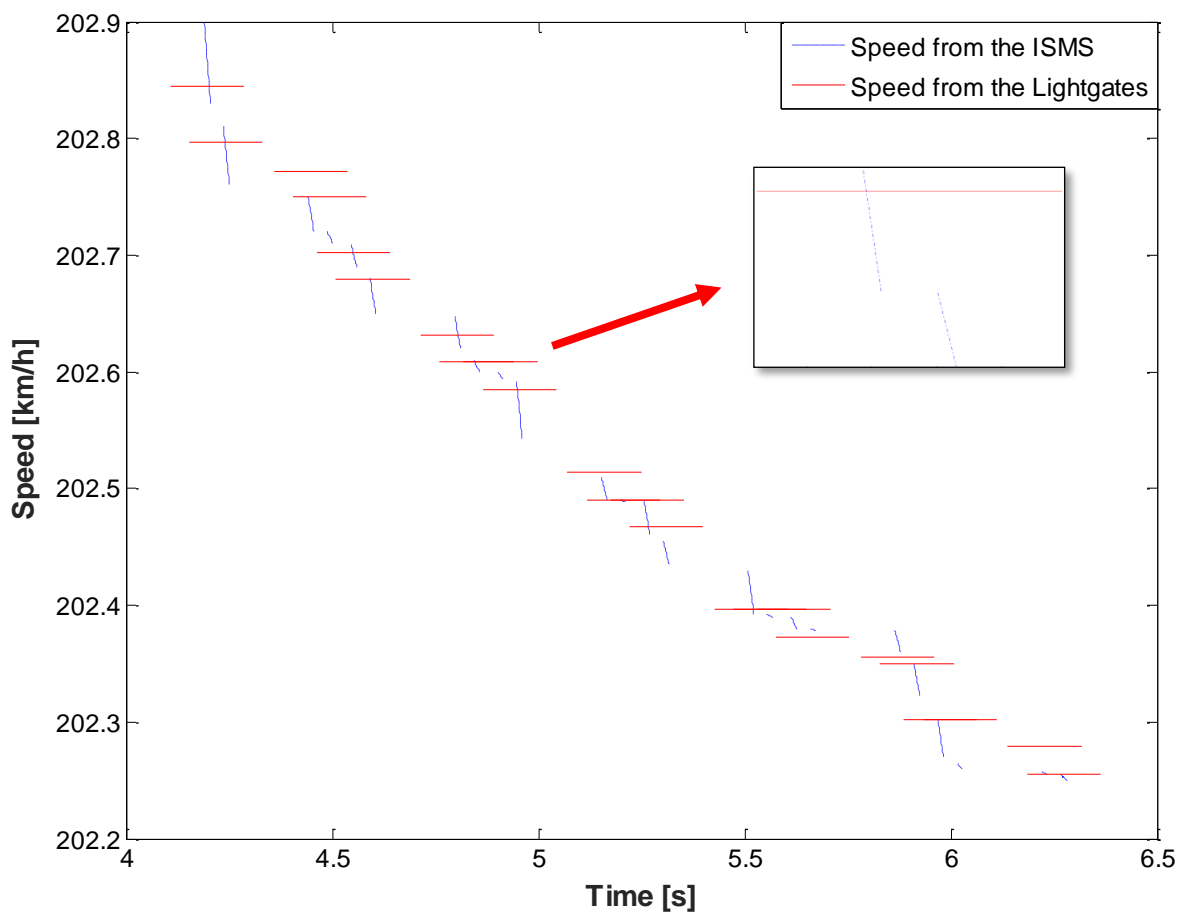


Figure 7.32- Speed/time curves from the ISMS and the lightgate speed measurement systems

7.5.5 Summary

Signal level integration is driven by the limitations of acoustic sensing technology. As discussed in section 7.5.1 two of the biggest limitations are the accuracy of the vehicle speed

measurement and the complexity of the installation of the system. The integration of vision imaging technologies has been shown to overcome these limitations. The Imaging Speed Measurement System (ISMS) is a vehicle speed measurement system using vision imaging technology. The ISMS is installed at the trackside and does not interfere with existing railway lines. The high-speed camera used in the ISMS can replace a lightgate based speed measurement system and hugely increase the resolution of the speed measurement.

As noted, the field tests undertaken on the Network Rail High Speed 1 Line involved no testing vehicles but used in-service vehicles in healthy condition. The signal processing algorithms (developed in chapter 5) have been applied to the acoustic signals recorded at the High Speed 1 Line, but as expected no indication of bearing faults was seen. Despite the lack of bearing faults, improvements through signal level integration were demonstrated through improvements to the speed measurement support to the acoustic CM system which is now provided by the Imaging Speed Measurement System (ISMS).

In order to validate the ISMS, three scenarios have been used in the order of increasing difficulty: field tests at the Rail Alliance Long Marston storage site for basic tracking, field tests on the Class 323 for more difficult recognition, and field tests at the High-speed 1 Line for high speed performance. Images in the first scenario are clear and bright, and the wheel profile can be fully seen. In the second scenario, the wheel profile can only partially be seen. In the third scenario, the images are less clear and less bright due to the shutter speed being set fast enough to capture the high-speed train only allowing a limited amount of light to come through the lens. The results in all three scenarios have proved that the ISMS can work as designed. The comparison results between the ISMS and lightgate speed measurement systems have proved the idea of signal level integration between acoustic sensing and vision imaging technologies to solve the limitations of the acoustic inspection and monitoring system.

From a wayside condition monitoring system perspective, the signal level integrated system can be considered to be advantageous compared to the TADSTM [74] and RailBAMTM [73] systems because it does not interfere with existing railway lines but only requires installation at the trackside to inspect and monitor axle bearings.

7.6 Conclusions

In this chapter, the integration of acoustic sensing technology and vision imaging technology has been demonstrated. Both system level and signal level integrations have been proved through tests carried out on the Network Rail High Speed 1 Line. Additionally, the integrated system frame used to combine the technologies in the two integration methods has been developed.

Both integration plans have the potential to improve the existing commercialised condition monitoring (CM) systems. The system level integrated system has the potential to rival the Wheel Defect Detection module in the GOTCHA system (discussed in section 7.4.2), and the signal level integrated system has the potential to improve on the TADSTM [74] and RailBAMTM [73] wayside bearing inspection and monitoring systems.

In terms of the approaches of the two integration plans, system level integration aims to provide more information on the condition of a vehicle through integration of otherwise independent systems; while signal level integration aims to overcome the limitations of the acoustic sensing technology through support from the vision imaging technology.

As noted in chapter 4, following the methodology in this thesis, the integrated systems were developed from laboratory-based experiments to a series of proof-of-concept field tests. From the vision based CM system, and with the extracted metrics relating to the pantograph and train doors & windows, condition-based maintenance of these components is achievable. From the acoustic system, and with the wheel flat anomalies in the acoustic signals

identifiable, condition based maintenance of these components is also achievable. Combining the two systems, with the higher resolution train speed information from the Imaging Speed Measurement System (ISMS) being presented to the acoustic system, a non-invasive wayside acoustic bearing CM system is achievable.

8 Conclusion and future work

This thesis has demonstrated the author's contribution to research in the field of railway condition monitoring. Specifically, the work focuses on the incremental development and integration of multiple CM technologies. The work in this thesis supports the author's hypothesis that it is possible to develop intelligent solutions for the integration of existing technologies in order to achieve improvements in railway vehicle condition monitoring. This has been demonstrated through the integration of acoustic sensing and vision imaging CM technologies.

8.1 Contribution to knowledge

The investigation and development of the two chosen technologies in isolation (chapter 5 and 6) allowed the development of the final integrated solutions. Two novel algorithms have been developed during the investigation into acoustic sensing technologies. One of these two algorithms is the subject of a published paper [190], and a publication relating to the second is currently in development. During the investigation of vision imaging technologies, the author has presented extracted metrics relating to several vehicle components which demonstrates the potential of the technology for use in coupler and pantograph condition monitoring. The thesis has described two integration solutions: system level integration and signal level integration. Both system and signal level integration solutions have demonstrated the potential to rival existing commercial condition monitoring systems. System level integration has the potential to rival the Wheel Defect Detection module in the GOTCHA system (discussed in section 7.4.2) because of its capability of detecting wheel flats without requiring physical interactions with the existing railway line. Signal level integration has demonstrated the potential to make some improvement on the TADSTM [74] and RailBAMTM [73] wayside bearing inspection and monitoring systems. This is partly because the system

does not require physical interactions with existing railway line, but also because of the vehicle speeds which the system is capable of supporting. The system taking advantage of signal level integration has been demonstrated on the first (and currently only) high speed line in the UK, Network Rail's High Speed 1 Line. An imaging speed measurement system (ISMS) was developed using vision imaging technology visual processing algorithms. This is a vehicle speed measurement system which can then support acoustic sensing technology through direct integration of the speed signal. A paper describing the ISMS and demonstrating this signal level integration with the acoustic system has been published by the author [213].

The hypothesis of this thesis is that it is possible to achieving enhancements in condition monitoring systems for use with railway vehicles through the integration of independent condition monitoring technologies.

The hypothesis was considered in the context of four questions as described in the introduction of the thesis (chapter 0). These four questions related to the identification of specific vehicle components to be inspected, the selection of corresponding CM technologies, investigation into the possibility of improving the CM technologies in isolation, and the development of intelligent integration solutions in order to improve overall CM system performance. The first two of these questions were considered through review of the literature and existing railway condition monitoring systems. The latter two questions were addressed through practical development and testing work.

The investigation into acoustic sensing CM technologies was decomposed into hardware system design and signal processing algorithm development. In terms of the hardware system design, work was divided into three phases: laboratory experiments, field tests at a research testing site, and field tests at Network Rail's High Speed 1 Line. This staged approach is described in chapter 4. An axle bearing test rig was built to carry out experiments using both

vibration (accelerometer) and acoustic (microphone) sensors. The microphone was selected for use in the field tests because the other two acoustic sensors (vibration and acoustic emission) need access to the track area for installation of the sensors.

The experiments were carried out in an anechoic chamber to reduce the effect of reflected noise. This allowed efforts to be focused on detecting and characterising the noise from the bearings. The test facility and use of the environmental chamber is described in chapter 4.

Following the lab work, the main challenges in roller bearing inspection and monitoring using acoustic sensing technology are noise filtering and signal enhancement. The geometric characteristic frequencies of roller bearings are a well-known and effective indicator that can be used for fault diagnosis once a clear signal has been obtained. During the study, two novel processing algorithms were developed to enhance noise filtering and signal clarity. One was applied to the vibration signals (accelerometer) and the other was applied to the acoustic signals obtained from the microphone. The author has published a paper on the first of these [190], and has one in preparation on the second.

The signal to noise issue becomes even more significant when the acoustic CM system is applied to the real railway. To enhance the signal quality, improvements were made to both the mechanical system design and the processing algorithms applied. The acoustic signal acquisition system design was extended from a single microphone to a microphone array. This was done in order to combine the acoustic signals from each microphone together to allow targeted recording. A time-domain beamforming algorithm was developed and applied to the signals obtained during the field tests. With processing algorithm developed in the laboratory tests, an acoustic inspection and monitoring system suitable for use on the railway was developed and tested. One limitation of the developed acoustic inspection and monitoring system is that it uses a lightgate based speed measurement to identify the position of the axleboxes. This system is not particularly accurate and doesn't work well if the vehicle

speed is not constant. This weakness is overcome through the signal level integration with the vision system

The investigation into the use of vision imaging technologies for railway CM was carried out differently from the acoustic sensing technology development because the associated technologies are further evolved and commercial equipment is more readily available. The key tasks were to ensure that the images captured were bright and clear enough to be passed to processing algorithms. A series of algorithms were then used to identify and extract the vehicle components from vehicle side view images. The hardware used in the vision imaging technology investigation is a commercialised high-speed camera. This was selected specifically for the study and so required a thorough understanding of vision system fundamentals. A discussion of this can be found in chapter 6.

The computer vision techniques used in this work were applied in three stages: sampling & adjusting, image processing to or enhance the components of interest, and feature detection and matching. While the processing chain for the acoustic bearing work was developed based on bearing quality, in the visual inspection case the required elements are more driven by the scenario. The two scenarios that the vision imaging technologies have been applied to are the British Rail Class 117 DMU with a mobile railway laboratory carriage at a closed test track research facility, and the British Rail Class 395 on Network Rail's High Speed 1 Line. The inspection targets were the coupler and the pantograph systems respectively. In each scenario, the capability of the visual imaging inspection system to extract metrics for condition monitoring has been verified. Details of this can be found in (chapter 6).

The novel use of vision imaging technology in this thesis was achieved through accurate measurement of vehicle speed for high speed trains.. This led to the development of the Imaging Speed Measurement System (ISMS) as part of a signal level integration with acoustic systems as described in chapter 7.

An analysis of the weaknesses of the individual condition monitoring technologies was used to establish the integration solutions to be developed. This is described in section 7.1. Integration was considered on two levels: the system level and the signal level.

System level integration considers the two technologies and integrates their outputs. Such integration can provide more information than each individual monitoring system, and so can increase the efficiency of maintenance organisation in order to save costs. In this case, high-speed vision imaging inspection and monitoring systems have the potential to monitor the condition of pantographs, as well as the vehicle doors and windows from the side view of the vehicle. Acoustic inspection and monitoring systems have the potential to monitor the anomalies in mechanical movements, such as those related to contact between wheel and rail surfaces. From a wayside condition monitoring system perspective, system level integration has the potential to rival the GOTCHA system because the developed system does not require any physical interaction with the existing railway line. From a condition monitoring efficiency perspective, an integrated system can merge the inspection and monitoring results from both the acoustic and vision systems to provide information on wheel defect condition and pantograph condition, as well as door and window status, into a single dataset. This would be more easily used by the maintainer and could improve maintenance efficiency.

Signal level integration is an integration plan that combines signals directly within the CM systems. This approach needs detailed knowledge of each technology which makes the investigation of the two CM technologies in isolation particularly useful. The main difficulty associated with acoustic inspection and monitoring is low signal-to-noise ratio (SNR) which results in difficulty in the fault diagnosis. In the field tests, a microphone array and beamforming algorithm was used to collect acoustic signals. To interpret the acoustic signal, the location of a target for acoustic beamforming within the signal collection area is needed.

The precision of location information is important because it determines the quality of the retrieved signal.

The previous solution for positioning was a lightgate based speed measurement system. This could give the speed of the train, but at a low resolution making it incapable of monitoring variations in the speed of a train. Furthermore, during the field tests on the Network Rail High Speed 1 Line, its installation was shown to be complicated and difficult to achieve. This is described in detail in section 7.5.1.2.

A precise, real-time, wayside speed measurement system would be a useful alternative and significantly improve performance of the acoustic CM system. The system developed within this study and based on computer vision techniques similar to those used for independent visual inspection is the High-speed Imaging Speed Measurement System (ISMS). A paper describing the signal level integration of the ISMS with the acoustic monitoring system has been published by the author [213].

8.2 Conclusion

In conclusion, the aim of this thesis was to investigate the potential for improvements in wayside railway condition monitoring systems. This thesis has demonstrated the implementation and further development of two individual wayside condition monitoring technologies. The developments in signal processing have led to the publication of a journal paper, with another in development. Increased improvement has also been shown through the integration of two condition monitoring technologies in two different ways. System level integration has been shown to provide more information than each of the individual monitoring systems, and so could be used to increase the efficiency of maintenance organisation in order to save costs. Signal level integration has been demonstrated to be capable of replacing lightgate based speed measurement systems using the imaging speed

measurement system (ISMS). This has been developed within this study using computer vision techniques similar to those used in the original visual inspection system. This integration solution increases the resolution of the speed and position detection system used by the acoustic sensing technology. This signal level integration has also generated a journal paper.

8.3 Future work

The development of integrated systems is a multi-discipline exercise. It has involved elements of mechanical design, electronics, and signal processing. The author believes that there are many further improvements available through the development and integration of acoustic and vision imaging technologies. Alternatively, with the knowledge gained from how to integrate acoustic sensing and vision imaging technologies, the author can see a promising future for wider condition monitoring technology integration.

APPENDIX A

PUBLISHED JOURNAL PAPERS

- A.1** Z. Zhang, M. Entezami, E. Stewart and C. Roberts, “Enhanced fault diagnosis of roller bearing elements using a combination of empirical mode decomposition and minimum entropy deconvolution,” *Proceedings of the Institution of Mechanical Engineers, Part C: Journal of Mechanical Engineering Science*, vol. 231, 4: pp. 655-671. , First Published December 23, 2015; Issue published: February 1, 2017.
DOI: <https://doi.org/10.1177/0954406215623575>
- A.2** Z. Zhang, M. Entezami, E. Stewart, G. Yeo, G. Xu, M. Rusu and C. Roberts, “Improvement of Axle Bearing Monitoring Systems Through the Use of High Speed Imaging for Directing Acoustic Beamforming,” *Condition Monitor*, no. 353, pp. 5-9, 2016.

[Not available in the digital version of this thesis]

References

- [1] I. 13372, “Condition monitoring and diagnostics of machines,” *Vocabulary*, 2012.
- [2] T. Andersen, “Analysis of past derailments: Information from data bases, investigation reports and surveys,” DNV presentation on the results of the D-RAIL FP7 Project,, 2011.
- [3] J. H. Lewis, “Structural crashworthiness – possibilities and practicalities,” *J Rail and Rapid Transit*, vol. 216, pp. 117-121, 2002.
- [4] R. A. Smith, “Crashworthiness of Trains: Principles and Progress,” in *Crashworthiness and Occupant Protection in Transportation Systems*, Vols. AMD-Vol. 210, ASME,, 1995, pp. 79-88.
- [5] HM Railway Inspectorate, “Railway Accident at Rickerscote: A Report of the Investigation into the Derailment of a Freight Train and the Subsequent Collision with a Travelling Post Office Train on 8 March 1996,” Health & Safety Executive, 1996.
- [6] WIKIPEDIA, “Eschede train disaster,” WIKIPEDIA, 23 March 2016. [Online]. Available: https://en.wikipedia.org/wiki/Eschede_train_disaster.
- [7] R. A. I. U. Ireland, “Investigation Report: Bearing failure on a train at Connolly Station,” in *RAIU*, Ireland, 2011.
- [8] D. Barke and W. K. Chiu, “Structural Health Monitoring in the Railway Industry: A Review,” *Structural Health Monitoring*, p. 23, April 2005.

- [9] P. Mayorkinos, Z. Huang, A. Arash, V. Patrick, D. Nigel, S. Rajesh, K. Yannis and K. Spyridon, "Advanced wayside condition monitoring of rolling stock wheelsets," in *11th European Conference on Non-Destructive Testing (ECNDT 2014)*, Prague, Czech Republic, 2014.
- [10] "Online condition monitoring of rolling stock wheels and axle bearings," *Proceedings of the Institution of Mechanical Engineers, Part F: Journal of Rail and Rapid Transit*, p. 10.1177/0954409714559758, 2014.
- [11] D. H. Shreve, *Integrated condition monitoring technologies*, IRD Balancing LLC 4740, 2003.
- [12] T. i. I. Board, "National Rail Trends," OFFICE OF RAIL AND ROAD, 31 October 2015. [Online]. Available: <https://dataportal.orr.gov.uk/displayreport/report/html/21c19868-5153-4d1c-8157-c1606b0ebe50>.
- [13] P. Li and R. Goodall, "Model-based condition monitoring for railway vehicle systems," in *Proceedings of the UKACC international conference on control*, Bath, UK, 2004.
- [14] S. Yella, M. Dougherty and N. K. Gupta, "Condition monitoring of wooden railway sleepers," *Transportation Research Part C*, vol. 17, pp. 38-55, 2009.
- [15] A. Herring, *Mode of detecting defects in railroad*, 1877.
- [16] D. Bray, "Historical review of technology development in NDE," in *the 15th WCNDT*, Roma, 2000.
- [17] M. Papaelias, C. Robert and C. L. Davis, "A review on non-destructive evaluation of rails: State-of-the-art and future development," *Proceedings of the Institution of*

- Mechanical Engineers, Part F: Journal of Rail and Rapid Transit*, vol. 222, no. 4, pp. 367-384, May 2008.
- [18] P. Steets and Y. Tse, "Conrail's integrated automated wayside inspection," in *Proceedings of the IEEE/ASME Joint Railroad Conference*, Piscataway, NJ, USA, 1998.
- [19] D. Stone, S. Kalay and A. Tajaddini, "Statistical behaviour of wheel impact load detectors to various wheel defects," in *Tenth International Wheelset Congress*, Sydney, Australia, 1992.
- [20] S. Kalay and A. S. D. Tajaddini, "Detecting wheel tread surface anomalies," in *In: Rail Transportation - 1992 American Society of Mechanical Engineers (ASME), Rail Transportation Division (RTD)*, New York, 1992.
- [21] S. Lechowics and C. Hunt, "Monitoring and Managing Wheel Condition and Loading". *Teknis Electronics and National Rail*.
- [22] Mermec, "Wheel Parameters," Mermec, [Online]. Available: <http://www.mermecgroup.com/inspect/train-monitoring/87/wheel-parameters.php>.
- [23] ImageMap, "WheelSpec Wheel and Bogie Condition Monitor," in *Columbia SC, USA*, 2003.
- [24] Technogamma, in *Doc.: 112 UK-R1*, BADOERE DI MORGANO(TV) Italy.
- [25] M. Ward, "Development of a semi automatic/automatic rolling stock wheel ultrasonic testing facility," in *In: Mechanical Engineering Transactions - Institution of Engineering*, Australia, 1990.

- [26] H. Widmayer, "10 years of experience with our high speed wheelset diagnosis for high-speed trains," in *In: Thirteenth International Wheelset Conference* , Rome, 2001.
- [27] H. Widmayer, "Wheelset diagnosis for high-speed traffic," in *In: National Conference Publication - Institute of Engineers* , Barton, Australia, 1992.
- [28] D. Hackenberger and C. Lonsdale, "Initial feasibility study to develop a wayside cracked railroad wheel detector," in *In: Proceedings of the IEEE/ASME Joint Railroad Conference*, Philadelphia, PA, USA, 1992.
- [29] J. Mian and H. Naumann, "In rail comprehensive wheel set inspection for the 21st Century," in *In: International heavy Haul Association STS-Conference*, 1999.
- [30] D. Stock and D. (. Barke, "Hot Box Detector Use at QR," Rockingham, Queensland, 2003.
- [31] R. Lagnebäck, Lagnebäck, Robert. Evaluation of wayside condition monitoring technologies for condition-based maintenance of railway vehicles, Luleå: Luleå University of Technology, 2007.
- [32] S. Haigh and D. (. Barke, "Trakblaze Train Weighing Systems," Melbourne, Australia, 2003.
- [33] R. Beebe, machine Condition Monitoring: How to predict Maintenance Requirements for Rotating and Stationary Plant, 2nd Edition ed., Victoria, Australia: MCM Consultants, Pty. Ltd., 1995.
- [34] P. Bartle, "Locomotive bearing condition update 2. Report No: Monash/RT/2003/100," in *Institute of Railway technology, Monash Unversity*, Melbourne, Australia, 2003.

- [35] H. Choe, Y. Wan and A. Chan, "Neural pattern identification of railroad wheel-bearing faults from audible acoustic signals: comparison of FFT, CWT, and DWT features," in *In: Proceedings of SPIE - The International Society for Optical Engineering 1997*, Bellingham, WA, USA: Society of Photo-Optical Instrumentation Engineers, 1997.
- [36] K. Kilian and D. (. Barke, "LynxRail," in *ATex Automatic train Examiner*, 2003.
- [37] T. IQ, "FleetONE," Track IQ, [Online]. Available: <http://www.trackiq.com.au/fleet-one.html>.
- [38] A. pink, "Buffers and chain coupler: Characteristics," America pink, [Online]. Available: <http://america.pink/images/7/8/1/1/5/5/en/2-buffers-and-chain-coupler.jpg>.
- [39] ENFORM, "Tractor-Trailer Uncoupling Results in Accident," The Safety Association for Canada's Upstream Oil and Gas Industry, Canada, 2014.
- [40] The steel rails advocate Future tralls on ralls, "Pantograph," The steel rails advocate Future tralls on ralls, [Online]. Available: [http://thesteelrailsadvocate.com/Photos/STREETCAR%20TECHINICAL%20PHOTOS/The%20\(asymmetrical\)%20%27Z%27-shaped%20pantograph%20800px.jpg](http://thesteelrailsadvocate.com/Photos/STREETCAR%20TECHINICAL%20PHOTOS/The%20(asymmetrical)%20%27Z%27-shaped%20pantograph%20800px.jpg).
- [41] S. Ostlund, A. Gustafsson, L. Buhrkall and M. Skoglund, "Condition monitoring of pantograph contact strip," in *Railway Condition Monitoring, 2008 4th IET International Conference on*, 2008.
- [42] R. A. I. Branch, "Accident involving a pantograph and the overhead line near Littleport," GOV.UK, Cambridgeshire, 2012.
- [43] İ. Aydın, E. Karaköse, M. Karaköse, M. T. Gençoğlu and E. Akın, "A new computer vision approach for active pantograph control," in *Innovations in Intelligent Systems*

and Applications (INISTA), 2013 IEEE International Symposium on, 2013.

- [44] Gotha, "Gotcha description," [Online]. Available: <http://www.gotchamonitoringsystems.com/Gotcha.php>.
- [45] Silberwolf, "Cutaway view of a tapered roller bearing," Wikipedia, 27 1 2016. [Online]. Available: https://en.wikipedia.org/wiki/Tapered_roller_bearing#/media/File:Tapered-roller-bearing_din720_120.png. [Accessed 27 1 2016].
- [46] S. Ganeriwala, "Review of Techniques for Bearings & Gearbox Diagnostics," in *IMAC Conference*, Richmond, 2010.
- [47] B. P. Blog, "Do I Have a Bad Wheel Bearing?," [Online]. Available: <https://gobdp.com/wp-content/uploads/2014/09/pitted-bearing-www-therabricator-com.jpg>.
- [48] T. Sundström, "Condition Monitoring Redefined The Low RPM Challenge," [Online]. Available: <http://www.maintworld.com/Applications/Condition-Monitoring-Redefined-The-Low-RPM-Challenge>.
- [49] N. Tandon and A. Choudhury, "A review of vibration and acoustic measurement methods for the detection of defects in rolling element bearings," *Tribology International*, no. 32, pp. 469-480, October 1999.
- [50] F. Wardle and S. Poon, "Rolling bearing noise - cause and cure," *Chartered Mech Engr*, pp. 36-40, July/August 1983.
- [51] N. Lynagh, H. Rahnejat, M. Ebrahimi and R. Aini, "Bearing induced vibration in precision high speed routing spindles," *International Journal of Machine Tools &*

Manufacture, no. 40, pp. 561-577, 2000.

- [52] S. Vafaei and H. Rahnejat, "Indicated repeatable runout with wavelet decomposition (IRR-WD) for effective determination of bearing-induced vibration," *Journal of Sound and Vibration*, no. 260, pp. 67-82, 2003.
- [53] S. Vafaei, H. Rahnejat and R. Aini, "Vibration monitoring of high speed spindles using spectral analysis techniques," *International Journal of Machine Tools & Manufacture*, no. 42, pp. 1223-1234, 2002.
- [54] A. Farshidianfar, A. R. Abbasi and S. Abbasion, "Dynamic Modelling of Chaotic Response of Bearing Systems due to Surface Defects," in *16th Annual (International) Conference on Mechanical Engineering-ISME2008*, Shahid Bahonar University of Kerman, Iran, May 14th-16th, 2008.
- [55] J. Antoni and R. B. Randall, "The spectral kurtosis: application to the vibratory surveillance and diagnostics of rotating machines," in *Mechanical Systems and Signal Processing* 23, 2009.
- [56] V. Rai and A. Morhanty, "Bearing fault diagnosis using FFT of intrinsic mode functions in Hilbert-Huang transform," *Mechanical Systems and Signal Processing*, no. 21, pp. 2607-2615, 2007.
- [57] A. Johnston and A. Stronach, "Bearing fault detection in a hostile environment," in *In: Proceedings of International Conference on Condition Monitoring*, Brighton, UK, May, 1986.
- [58] M. S. Darlow, R. H. Badgley and G. W. Hogg, "Application of high frequency resonance techniques for bearings diagnostics in helicopter gearboxes," in *US Army Air*

Mobility Research and Development Laboratory, 1974.

- [59] F. Elasha, M. Greaves, D. Mba and A. Addali, "Application of Acoustic Emission in Diagnostic of Bearing Faults within a Helicopter gearbox," in *The Fourth International Conference on Through-life Engineering Services*, Cranfield, UK, 2015.
- [60] B. E. V. Hecke, "Development of Novel Acoustic Emission Based Methodology and Tools for Bearing Fault Diagnostics," University of Illinois at Chicago, Chicago, 2015.
- [61] J. L. F. Chacon, "Fault Detection in Rotating Machinery Using Acoustic Emission," Brunel University London, London, 2015.
- [62] S. Sun, "Experimental investigation on double impulses phenomenon of outer race spalled rolling element bearings based on acoustic emission signals," in *2015 IEEE International Conference on Information and Automation*, Lijing, 2015.
- [63] L. Han, C. Li and H. Liu, "Feature Extraction Method of Rolling Bearing Fault Signal Based on EEMD and Cloud Model Characteristic Entropy," *Entropy*, vol. 17, no. 10, pp. 6683-6697, 2015.
- [64] J. Kim, M. Kang, I.-K. Jeong, H. Jun, J.-M. Kim and B.-K. Choi, "Real-time and energy-efficient bearing fault diagnosis using discriminative wavelet-based fault features on a multi-core system," in *2015 IEEE Conference on Prognostics and Health Management (PHM)*, Austin, TX, 2015.
- [65] N. Tandon and B. Nakra, "Defect detection in rolling element bearings by acoustic emission method," *J Acoust Emission*, vol. 1, no. 9, pp. 25-28, 1990.
- [66] N. Tandon, "Adaptive noise cancellation of acoustic noise in ball bearing".

- [67] S. Bagnoli, R. Capitani and P. Citti, "Comparison of accelerometer and acoustic emission signals as diagnostic tools in assessing bearing," in *Proceedings of 2nd International Conference on Condition Monitoring*, 1988.
- [68] M. Tavakoli, "Bearing fault detection in the acoustic emission frequency range," in *Proceedings of the 11th National Conference on Noise Control Engineering*, Tarrytown, NY, 1991.
- [69] A. Smulders and C. Loob, "Machine condition monitoring using multi-parameter measurement," in *Proceedings of Condition Monitoring and Diagnostic Engineering Management Conference*, New Delhi, 1994.
- [70] M. Entezami, E. Stewart, S. Kent, P. Weston, L. Saade and C. Roberts, "Experimental comparison of acoustic and vibration-based analysis techniques for condition monitoring of roller bearings," in *The Eleventh International Conference on Condition Monitoring and Machinery Failure Prevention Technologies (CM2014/ MFPT2014)*, Manchester, UK, 2014.
- [71] J. Stack, R. Harley and T. Habetler, "An Amplitude Modulation Detector for Fault Diagnosis in Rolling Element Bearings," *IEEE TRANSACTIONS ON INDUSTRIAL ELECTRONICS*, vol. 51, no. 5, pp. 1097-1102, 2004.
- [72] W. Baker, P. Westine and F. Dodge, *Similarity Methods in Engineering Dynamics: Theory and Practice of Scale Modelling*, Revised Edition ed., Elsevier Science Publishers, 1991.
- [73] C. Southern, D. Rennison and U. Kopke, "RailBAM® - An advanced bearing acoustic monitor: Initial operational performance results," in *CORE-Conference On Railway*

Engineering, Darwin, Australia, 2004.

- [74] R. Donnelly, M. Lynch and M. Darby, "The use of automation and technology in improving maintenance practices in heavy haul railroad," in *Proceedings 8th International heavy haul conference IHHA*, Rio De Janeiro, Brazil, 2005.
- [75] R. Szeliski, "Introduction," in *Computer Vision - Algorithm and Applications*, Springer-Verlag London, 2010, pp. 1-23.
- [76] S.-C. Oh, S.-H. Park and C.-M. Lee, "Railway Platform Monitoring System Using Stereo Vision Algorithm For Passenger's Safety," in *Telecommunications Energy Conference, 2009. INTELEC 2009. 31st International*, Incheon , 2009.
- [77] T. Chow and S.-Y. Cho, "Industrial neural vision system for underground railway station platform surveillance," *Advanced Engineering Informatics*, vol. 16, pp. 73-83, 2002.
- [78] E. Prassler, J. Scholz and A. Elfes, "Tracking People in a Railway Station during Rush-Hour," in *Computer Vision Systems*, Berlin Heidelberg, Springer Berlin Heidelberg, 1999, pp. 162-179.
- [79] S. Oh, S. Park and C. Lee, "A Platform Surveillance Monitoring System using Image Processing for Passenger Safety in Railway Station," in *International Conference on Control, Automation and Systems*, Seoul, Korea, 2007.
- [80] S. Oh, C. Lee, H. Lee, D. Lee and Y. Park, "Vision Based Platform Monitoring System for Railway Station Safety," in *Telecommunications, 2007. ITST '07. 7th International Conference on ITS*, Sophia Antipolis, 2007.

- [81] S. Oh, C. Lee and H. Lee, "Vision Based Monitoring System for Passenger's Safety in Railway Platform," in *International Conference on ICEE*, 2008.
- [82] S.-C. Oh, G.-D. Kim, W.-T. Jeong and Y.-T. Park, "Vision-based Object Detection for Passenger's Safety in Railway Platform," in *International Conference on Control, Automation and Systems 2008*, Seoul, Korea, 2008.
- [83] M. Singh, S. Singh, J. Jaiswal and J. Hempshall, "Autonomous Rail Track Inspection using Vision Based System," in *CIHSPS 2006 – IEEE International Conference on Computational Intelligence for Homeland Security and Personal Safety*, Alexandria, VA, USA, 2006.
- [84] E. Resendiz, L. F. Molina, J. M. Hart, J. R. Edwards, S. V. Sawadisavi, N. Ahuja and C. P. L. Barkan, "Development of a machine vision system for inspection of railway track components," in *12th WCTR*, Lisbon, Portugal, 2010.
- [85] S. Zheng, X. Chai, X. An and L. Li, "Railway Track Gauge Inspection Method Based on Computer Vision," in *Proceedings of 2012 IEEE International Conference on Mechatronics and Automation*, Chengdu, China, 2012.
- [86] h. Zhang, J. Yang, W. Tao and H. Zhao, "Vision method of inspecting missing fastening components in high-speed railway," *Applied optics*, vol. 50, no. 20, pp. 3658-3665, 2011.
- [87] I. Aydin, "A new approach based on firefly algorithm for vision-based railway overhead inspection system," *Measurement*, vol. 74, pp. 43-55, 2015.
- [88] R. Marmo, L. Lombardi and N. Gagliardi, "Railway Sign Detection and Classification," in *2006 IEEE Intelligent Transportation Systems Conference*, Toronto,

Canada, 2006.

- [89] M. Technologies, "Brake Wear Measurement," MRX Technologies, 2015. [Online]. Available: <http://www.mrxtech.com.au/brake-monitoring.html>.
- [90] J. Blair and D. (. Barke, "MRX Technologies - Wayside Detection Systems," Perth.
- [91] K. Kilian, V. Mazur and M. Kilian, "Automated rolling stock maintenance," in *In: Oghanna, W. and Bock, B. (eds), Seventh International Heavy haul Conference 2001* , International Heavy Haul Association: Brisbane Australia, 2001.
- [92] J. Hart, E. Resendiz, B. Freid, S. Sawadisavi, C. Barkan and N. Ahuja, "Machine vision using multi-spectral imagin f for undercarriage inspection of railroad equipment," in *Proceedings of the 8th World Congress on Railway Research*, Seoul, Korea, 2008.
- [93] J. Vazquez and M. Mazo, "Detection of moving objects in raliway using vision," in *2004 IEEE Intelligent Vehicle Symposium*, Parma, Italy, 2004.
- [94] W. Q. Wang, F. Ismail and M. F. Golnaraghi, "Assessment of gear damage monitoring techniques using vibration measurements," *Mechanical Systems and Signal Processing*, vol. 15, no. 5, pp. 905-922, 2001.
- [95] M. Wang, A. Vandermaar and K. Srivastava, "Review of condition assessment of power transformers in service," *Electrical Insulation Magazine, IEEE*, vol. 18, no. 6, pp. 12-25, 2002.
- [96] A. El-Shafei and N. Rieger, "Automated diagnostics of rotating machinery," in *ASME Turbo Expo 2003, collocated with the 2003 International Joint Power Generation*

Conference, Atlanta, 2003.

- [97] T. K. Saha, "Review of modern diagnostic techniques for assessing insulation condition in aged transformers," *IEEE Transactions on Dielectrics and Electrical Insulation*, vol. 10, no. 5, pp. 903-917, 2003.
- [98] R. M. Tallam, S. B. Lee, G. C. Stone, G. B. Kliman, J. Yoo, T. G. Habetler and R. G. Harley, "A survey of methods for detection of stator-related faults in induction machines," *IEEE Transactions on Industry Applications*, vol. 43, no. 4, pp. 920-933, 2007.
- [99] G. Sabnavis, R. G. Kirk, M. Kasarda and D. Quinn, "Cracked shaft detection and diagnostics: a literature review," *The Shock and Vibration Digest*, vol. 36, no. 4, p. 287, 2004.
- [100] R. B. Randall and J. Antoni, "Rolling element bearing diagnostics-a tutorial," *Mechanical Systems and Signal Processing*, vol. 25, no. 2, pp. 485-520, 2011.
- [101] A. K. Jardine, D. Lin and D. Banjevic, "A review on machinery diagnostics and prognostics implementing condition-based maintenance," *Mechanical Systems and Signal Processing*, no. 20, pp. 1483-1510, 2006.
- [102] G. K. Chaturvedi and D. W. Thomas, "Bearing Fault Detection Using Adaptive Noise Cancelling," *Journal of Mechanical Design*, vol. 104, no. 2, pp. 280-289, 1982.
- [103] C. C. Tan, "An Adaptive Noise Cancellation Approach for Condition Monitoring of Gear Box Bearings," in *International Tribology Conference 1987*, Melbourne, 1987.
- [104] J. Antoni and R. B. Randall, "Optimisation of SANC for separating gear and bearing

- signals,” in *Proceedings of the Comadem Conference*, Manchester, 2001.
- [105] R. B. Randall, *Vibration-based Condition Monitoring: Industrial, Aerospace and Automotive*, Hoboken, United States: John Wiley & Sons, 2011.
- [106] M. John, “Linear Prediction: A Tutorial Review,” *Proceedings of the IEEE*, vol. 63, no. 4, 1975.
- [107] W. Wang, J. Chen, X. Wu and Z. Wu, “The application of some non-linear methods in rotating machinery fault diagnosis,” *Mechanical Systems and Signal Processing*, vol. 15, p. 697–705, 2001.
- [108] W. Wang and R. Lin, “The application of pseudo-phase portrait in machine condition monitoring,” *Journal of Sound and Vibration*, vol. 259, pp. 1-16, 2003.
- [109] T. Koizumi, N. Tsujiuchi and Y. Matsumura, “Diagnosis with the correlation integral in time domain,” *Mechanical Systems and Signal*, vol. 14, p. 1003–1010, 2000.
- [110] W. Wang, Z. Wu and J. Chen, “Fault identification in rotating machinery using the correlation dimension and bispectra,” *Nonlinear Dynamics*, vol. 25, pp. 383-393, 2001.
- [111] Q. Zhuge and Y. Lu, “Signature analysis for reciprocating machinery with adaptive signal-processing,” *Proceedings of the Institution of Mechanical Engineers Part C—Journal of Mechanical Engineering Science*, vol. 205, pp. 305-310, 1991.
- [112] N. Baydar, Q. Chen, A. Ball and U. Kruger, “Detection of incipient tooth defect in helical gears using multivariate statistics,” *Mechanical Systems and Signal Processing*, vol. 15, pp. 303-321, 2001.
- [113] Y. He, X. Zhang and M. Friswell, “Defect diagnosis for rolling element bearing using

- acoustic emission,” *Journal of Vibration and Acoustics*, vol. 6, no. 131, p. 061012, 2009.
- [114] R. B. Randall, N. Sawalhi and M. Coats, “A comparison of methods for separation of deterministic and random signals,” *International Journal of Condition Monitoring*, vol. 1, no. 1, pp. 11-19, 2011.
- [115] C.-C. Wang and G.-P. Too, “Rotating machine fault detection based on HOS and artificial neural networks,” *Journal of Intelligent Manufacturing*, vol. 13, pp. 283-293, 2002.
- [116] “Bispectral and trispectral features for machine condition diagnosis,” *IEE Proceedings—Vision, Image and Signal Processing*, vol. 146, pp. 229-234, 1999.
- [117] L. Qu and D. Shi, “Holospectrum during the past decade: Review & prospect,” *Zhendong Ceshi Yu Zhenduan/Journal of Vibration, Measurement & Diagnosis*, vol. 18, pp. 235-242, 1998.
- [118] J. Antoni, “The spectral kurtosis: a useful tool for characterising non-stationary signals,” *Mechanical Systems and Signal Processing*, vol. 20, no. 2, pp. 282-307, February 2006.
- [119] G. F. Bin, J. J. Gao, X. J. Li and B. S. Dhillon, “Early fault diagnosis of rotating machinery based on wavelet packets—Empirical mode decomposition feature extraction and neural network,” *Mechanical Systems and Signal Processing*, vol. 27, pp. 696-711, February 2012.
- [120] P. Bonato, R. Ceravolo, A. De Stefano and M. Knaflits, “Bilinear time–frequency transformations in the analysis of damaged structures,” *Mechanical Systems and Signal*

Processing, vol. 11, pp. 509-527, 1997.

- [121] S. U. Lee, D. Robb and C. Besant, "The directional Choi-Williams distribution for the analysis of rotor-vibration signals," *Mechanical Systems and Signal Processing*, vol. 15, no. 4, pp. 789-811, 2001.
- [122] R. Young, *Wavelets Theory and Its Applications*, Boston: Kluwer Academic Publishers, 1993.
- [123] Z. H, J. Z, Q. M and Y. N, "Wavelet transform in tandem with autoregressive technique for monitoring and diagnosis of machinery," in *Proceedings of Condition Monitoring and Diagnostic Engineering Management Conference*, New Delhi, 1994.
- [124] N. Tandon and A. Choudhury, "A review of vibration and acoustic measurement methods for the detection of defects in rolling element bearings," *Tribology International*, no. 32, pp. 469-480, 1999.
- [125] J. Lin, "Feature extraction based on Morlet wavelet and its application for mechanical fault diagnosis," *Journal of Sound and Vibration*, vol. 234, no. 1, pp. 135-148, 2000.
- [126] H. Guo, H. Odegard, J. E. Burrus and C. S. Wells, "Noise reduction using an undecimated discrete wavelet transform," *IEEE transactions on Signal Processing Letters*, pp. 10-12, 1996.
- [127] W. Su, F. Wang, H. Zhu, Z. Zhang and Z. Guo, "Rolling element bearing faults diagnosis based on optimal Morlet wavelet filter and autocorrelation enhancement," *Mechanical Systems and Signal Processing*, vol. 24, pp. 1458-1472, 2010.
- [128] Q. Du and S. Yang, "Application of the EMD method in the vibration analysis of ball

- bearings,” *Mechanical Systems and Signal Processing*, no. 21, pp. 2634-2644, 2007.
- [129] F. Elasha, D. Mba and C. Ruiz-Carcel, “Effectiveness of Adaptive Filter Algorithms and Spectral Kurtosis in Bearing Faults Detection in a Gearbox,” in *Vibration Engineering and Technology of Machinery*, Springer International Publishing, 2014, pp. 219-229.
- [130] N. Huang, Z. Shen, S. Long, M. Wu, H. Shih, Q. Zheng, N. Yen, C. Tung and H. Liu, “The empirical mode decomposition and the Hilbert spectrum for nonlinear and non-stationary time series analysis,” in *Proceedings of the Royal Society of London, Series A 454*, 1998.
- [131] D. Pandya, S. Upadhyay and S. Harsha, “Fault diagnosis of rolling element bearing with intrinsic mode function of acoustic emission data using APF-KNN,” *Expert System with Applications*, no. 40, pp. 4137-4145, 2013.
- [132] R. Dwywr, “Detection of non-Gaussian signals by frequency domain kurtosis estimation,” in *International Conference on Acoustic, Speech, and Signal Processing*, Boston, 1983.
- [133] S.-F. Lei and e. al., “The applicaiton of frequency and time domain kurtosis to the assessment of hazrdous noise exposures,” *Journal of the Acoustical Society of America*, vol. 3, no. 96, pp. 1435-1444, 1994.
- [134] J. Zarei, “Induction motors bearing fault detection using pattern recognition techniques,” *Expert Systems with Applications*, no. 39, pp. 68-73, 2012.
- [135] D. Kateris, D. Moshou, X.-E. Pantazi, I. Gravalos, N. Sawalhi and S. Loutridis, “A machine learing approach for the condition monitoring of rotaing machinery,” *Journal*

of Mechanical Science and Technology, vol. 1, no. 28, pp. 61-71, 2014.

- [136] B. Li, M. Chow, Y. Tipsuwan and J. Hung, "Neural-network-based motor rolling bearing fault diagnosis," *IEEE Transactions on Industrial Electronics*, no. 47, pp. 1060-1069, 2000.
- [137] N.-T. Nguyen, H.-H. Lee and J.-M. Kwon, "Optimal feature selection using genetic algorithm for mechanical fault detection of induction motor," *Journal of Mechanical Science and Technology*, no. 22, pp. 490-496, 2008.
- [138] B. Samanta and K. Al-Balushi, "Artificial neural network based fault diagnostics of rolling element bearings using time-domain features," *Mechanical Systems and Signal Processing*, vol. 2, no. 17, pp. 317-328, 2003.
- [139] A. Widodo, E. Y. Kim, J.-D. Son, B.-S. Yang, A. C. Tan, D.-S. Gu, B.-K. Choi and J. Mathew, "Fault diagnosis of low speed bearing based on relevance vector machine and support vector machine," *Expert Systems with Applications*, vol. 36, no. 3, pp. 7252-7261, 2009.
- [140] B.-S. yang, T. Han and W.-W. Hwang, "Fault diagnosis of rotating machinery based on multi-class support vector machines," *Journal of Mechanical Science and Technology*, vol. 19, no. 3, pp. 846-859, 2005.
- [141] S. Yuan and F. Chu, "Fault diagnosis based on support vector machines with parameter optimization by artificial immunization algorithm," *Mechanical Systems and Signal Processing*, vol. 21, no. 3, pp. 1318-1330, 2007.
- [142] S. Yuan and F. Chu, "Fault diagnostics based on particle swarm optimisation and support vector machines," *Mechanical Systems and Signal Processing*, vol. 21, no. 4,

p. 1787–1798, 2007.

- [143] B. Samanta and C. Nataraj, “Use of particle swarm optimization for machinery fault detection,” *Engineering Applications of Artificial Intelligence*, vol. 22, no. 2, pp. 308–316, 2009.
- [144] V. Sugumaran and K. Ramachandran, “Effect of number of features on classification of roller bearing faults using SVM and PSVM,” *Expert Systems with Applications*, vol. 38, no. 4, p. 4088–4096, 2011.
- [145] W. Lu, W. Jiang, H. Wu and J. Hou, “A fault diagnosis scheme of rolling element bearing based on near-field acoustic holography and gray level co-occurrence matrix,” *Journal of Sound and Vibration*, vol. 331, no. 15, p. 3663–3674, 2012.
- [146] Y. Yuan, P. Zhao and Q. Zhou, “Research of speaker recognition based on combination of LPCC and MFCC,” in *2010 IEEE International Conference on Intelligent Computing and Intelligent Systems (ICIS)*, Xiamen, 2010.
- [147] T. S. Wijoyo, “Speech recognition using linear predictive coding and artificial neural network for controlling movement of mobile robot,” in *Proceedings of International Conference on Information and Electronics Engineering (ICIEE 2011)*, 2001.
- [148] M. R. Schroeder, “Linear predictive coding of speech: Review and current directions,” *Communications Magazine, IEEE*, vol. 23, no. 8, pp. 54–61, 1985.
- [149] S. Jothilakshmi, “Automatic system to detect the type of voice pathology,” *Applied Soft Computing*, vol. 21, pp. 244–249, 2014.
- [150] Wikipedia, “Frequency domain,” Wikipedia, 15 August 2015. [Online]. Available:

- https://en.wikipedia.org/wiki/Frequency_domain. [Accessed 15 August 2015].
- [151] T. Rossing, “Vibrational Modes of Instruments,” in *Springer Handbook of Acoustics*, Springer Science & Business Media, 2007, p. 549.
- [152] B. & K. S. & V. M. A/S., “Envelope Analysis - Type 7773,” Brüel & Kjær Sound & Vibration Measurement A/S., [Online]. Available: <http://www.bksv.com/Products/analysis-software/signal-analysis/envelope-analysis/envelope-analysis-7773>.
- [153] ppgb, “Intro 3. Spectral analysis,” ppgb, 5 September 2007. [Online]. Available: http://www.fon.hum.uva.nl/praat/manual/Intro_3__Spectral_analysis.html. [Accessed 5 September 2007].
- [154] M. S. Darlow, R. H. Badgley and G. W. Hogg, “Application of High-Frequency Resonance Techniques for Bearing Diagnostics in Helicopter Gearboxes,” Mechanical Technology Inc Latham N Y, Technical Report, US Army Air Mobility Research and Development Laboratory, 1974.
- [155] MathWorks, “Envelope Detection - MATLAB & Simulink Examples,” [Online]. Available: <http://www.mathworks.co.uk/help/dsp/examples/envelope-detection.html>. [Accessed 14 April 2014].
- [156] A. Brandt, “Central Moments,” in *Noise and Vibration Analysis: Signal Analysis and Experimental Procedures*, John Wiley & Sons, 2011.
- [157] C. Spatz, “Theoretical Distributions Including the Normal Distribution,” in *Basic Statistics: Tales of Distributions*, Cengage Learning, 2010, pp. 130-133.

- [158] G. M. D. Athayde and R. G. Flores, "Incorporating skewness and kurtosis in portfolio optimization," in *Advances in Portfolio Construction and Implementation*, Elsevier, 2003, pp. 243-257.
- [159] N. Sawalhi and R. B. Randall, "The application of spectral kurtosis to bearing diagnostics," in *Acoustics*, Gold Coast, Australia, 2004.
- [160] J. Antoni and R. Randall, "The spectral kurtosis: application to the vibratory surveillance and diagnostics of rotating machines," *Mechanical Systems and Signal Processing*, vol. 6, no. 18, pp. 1285-1314, 2004.
- [161] R. Wiggins, "Minimum entropy deconvolution," *Geoplotation*, no. 16, pp. 21-35, 1978.
- [162] G. Gonzalez, R. Badra, R. Medina and J. Regidor, "Period estimation using minimum entropy deconvolution (MED)," in *Signal Proceeding 41*, 1995.
- [163] M. Boumadhi and J. Lacoume, "Blind identification using the kurtosis: results of field data processing," *IEEE Transactions of Signal Processing*, Vols. 0-7803-2431-5, no. 95, pp. 1960-1983, 1995.
- [164] J. Lee and A. Nandi, "Extraction of impacting signals using blind deconvolution," *Journal of Sound and Vibration*, vol. 232, no. 5, pp. 945-962, 1999.
- [165] A. Nandi, D. Mampel and B. Roscher, "Blind deconvolution of ultrasonic signals in non-destructive testing application," *IEEE Transactions of Signal Processing*, vol. 5, no. 45, 1997.
- [166] H. Endo and R. Randall, "Enhancement of autoregressive model based gear tooth fault detection technique by the use of minimum entropy deconvolution filter," in

Mechanical Systems and Signal Processing 21, 2007.

- [167] S. Loutridis, "Damage detection in gear systems using empirical model decomposition," *Engineering Structures*, no. 26, pp. 1833-1841, 2004.
- [168] R. Ricci, P. Borghesani, S. Chatterton and P. Pennacchi, "The combination of empirical mode decomposition and minimum entropy deconvolution for roller bearing diagnostics in non-stationary operation," in *Proceedings of the ASME 2012 International Design Engineering Technical Conferences & Computers and Information in Engineering Conference*, Chicago, Illinois, USA, 2012.
- [169] S. Chatterton, R. Ricci and P. Pennacchi, "Signal Processing Diagnostic Tool for Rolling Element Bearings Using EMD and MED," in *Advances in Condition Monitoring of Machinery in Non-Stationary Operations*, Springer, 2014, pp. 379-388.
- [170] Z. Zhang, M. Entezami, E. Stewart and C. Roberts, "Enhanced fault diagnosis of roller bearing elements using a combination of empirical mode decomposition and minimum entropy deconvolution," *Proceedings of the Institution of Mechanical Engineers, Part C: Journal of Mechanical Engineering Science*, vol. 0, no. 0, p. 0954406215623575, 2015.
- [171] W. Yang and P. Tavner, "Empirical mode decomposition, and adaptive approach for interpreting shaft vibration signals of large rotating machinery," *Journal of Sound and Vibration*, no. 321, pp. 1144-1170, 2009.
- [172] R. Ricci and P. Pennacchi, "Diagnostics of gear faults based on EMD and automatic selection of intrinsic mode functions," in *Mechanical Systems and Signal Processing*, 2011.

- [173] P. Pennacchi, R. Ricci, S. Chatterton and P. Borghesani, "Effectiveness of MED for Fault Diagnosis in Roller Bearings," *Vibration Problems ICOVP*, pp. 637-642, (ISBN: 9789400720688) 2011.
- [174] D. Forsyth and J. Ponce, *Computer Vision: A Modern Approach*, New Jersey: Pearson, 2003, pp. 165, 200-202.
- [175] R. Szeliski, "Feature detection and matching," in *Computer Vision - Algorithms and Applications*, Springer-Verlag London, 2010, pp. 181-226.
- [176] R. Dahyot, P. Charbonnier and F. Heitz, "Unsupervised statistical detection of changing objects in camera-in-motion video," in *ICIP - 2001 International Conference on Image Processing*, Thessaloniki, Grecia, 2001.
- [177] D. Jang, G. Young and H. Choi, "Model-based tracking of moving object," *Pattern recognition*, vol. 30, no. 6, pp. 999-1008, 1997.
- [178] V. Zeljkovic and M. Popovic, "Detection of moving objects in video signal under fast changes of scene illumination," in *5th International Conference on Telecommunications in Modern satellite, Cable and broadcasting Services*, TELSIKS 2001, Yugoslavia, 2001.
- [179] G. Foster and N. Namazi, "Detection of non-uniform motion in image sequences using a reduced order likelihood ratio test," in *Proceedings of the 2000 international conference on image processing (ICIP 2000)*, Vancouver, BC, Canada, 2000.
- [180] Q. Gao, A. Parlow and M. Tan, "Object motion detection based on perceptual edge tracking," in *Digital and Computational Video, 2001. Proceedings. Second International Workshop on*, Tampa, Florida, 2001.

- [181] W. Baker, P. Westine and F. Dodge, *Similarity Methods in Engineering Dynamics: Theory and Practice of Scale Modelling*, Elsevier Science Publishers, 1991.
- [182] J. WU, "The complete-similitude scale models for predicting the vibration characteristics of elastically restrained flat plates subjected to Dynamic Loads," *Journal of Sound and Vibration*, p. 286, 2003.
- [183] J.-J. Wu, "Prediction of lateral vibration characteristics of a full-size rotor-bearing system by using those of its scale models," *Finite Elements in Analysis and Design*, vol. 43, no. 10, pp. 803-816, 2007.
- [184] SKF, "Tapered roller bearings," SKF, [Online]. Available: <http://www.skf.com/group/products/bearings-units-housings/roller-bearings/tapered-roller-bearings/index.html>.
- [185] Z. Zhang, M. Entezami, E. Stewart, G. Yeo, G. Xu, M. Rusu and C. Roberts, "Improvement of Axle Bearing Monitoring Systems Through the Use of High Speed Imaging for Directing Acoustic Beamforming," in *CM2015/MFPT2015 CONFERENCE*, Oxford, 2015.
- [186] C. Sunnersjo, "Rolling bearing vibrations - geometrical imperfections and wear," *J Sound Vibr*, vol. 4, no. 98, pp. 455-474, 1985.
- [187] L. Meyer, F. Ahlgren and B. Weichbrodt, "An analytic model for ball bearing vibrations to predict vibration response to distruted defects," *Trans ASME, J Mech Design*, vol. 3, no. 8, pp. 195-207, 1980.
- [188] A. Choudhury and N. Tandon, "A theoretical model to predict vibration response of rolling bearings to distributed defects under radial load," *Tran ASME, J Vibr Acoust*,

vol. 1, no. 120, pp. 214-220, 1998.

- [189] M. Washo, "A quick method of determining root causes and corrective actions of failed ball bearings," *Lubric Eng*, vol. 3, no. 52, pp. 206-213, 1996.
- [190] Z. Zhang, M. Entezami, E. Stewart and C. Roberts, "Enhanced fault diagnosis of roller bearing elements using a combination of empirical mode decomposition and minimum entropy deconvolution," *Proceedings of the Institution of Mechanical Engineers, Part C: Journal of Mechanical Engineering Science*, vol. 0, no. 0, pp. 1-17, 2015.
- [191] J. Cheng, D. Yu, J. Tang and Y. Yang, "Application of frequency family separation method based upon EMD and local Hilbert energy spectrum method to gear fault diagnosis," *Mechanism and Machine Theory*, vol. 6, no. 43, pp. 712-723, 2008.
- [192] Y. Yu and J. Cheng, "A roller bearing fault diagnosis method based on EMD energy entropy and ANN," *Journal of sound and vibration*, vol. 1, no. 294, pp. 269-277, 2006.
- [193] D. Yu, J. Cheng and Y. Yang, "Application of EMD method and Hilbert spectrum to the fault diagnosis of roller bearings," *Mechanical Systems and Signal Processing*, no. 19, pp. 259-270, 2005.
- [194] A. Parey and R. B. Pachori, "Modified Empirical Mode Decomposition Process for Improved Fault Diagnosis," in *The 8th IFToMM International Conference on Rotor Dynamics*, Seoul, Korea, 2010.
- [195] J. Dron, F. Bollaers and I. Rasolofondraibe, "Improvement of the sensitivity of the scalar indicators (crest factor, kurtosis) using a de-noising method by spectral subtraction: application to the detection of defects in ball bearing," *Journal of sound and vibration*, vol. 270, no. 1-2, pp. 61-73, 2004.

- [196] The MathWorks, Inc., “Generate white Gaussian noise,” [Online]. Available: <http://uk.mathworks.com/help/comm/ref/wgn.html>. [Accessed 2 December 2014].
- [197] Radicon, “Radicon,” [Online]. Available: http://www.radicon.com/_docs/salagears%20eng.pdf. [Accessed 12 02 2015].
- [198] A. Ahmaida, D. Zhen, F. Gu and A. Ball, gear wear process monitoring using acoustic signals, Beijing: 21st International Congress on Sound and Vibration, 2014.
- [199] D. Pandya, S. Upadhyay and S. Harsha, “Fault diagnosis of rolling element bearing with intrinsic mode function of acoustic emission data using APF-KNN,” *Expert Systems with Applications*, no. 40, pp. 4137-4145, 2013.
- [200] J. Antoni, “Fast computation of the kurtogram for the detection of transient faults,” *Mechanical Systems and Signal Processing*, no. 21, pp. 108-124, 2007.
- [201] M. Entezami, E. Stewart, J. Tutchter, W. Driscoll, R. Ellis, G. Yeo, Z. Zhang, C. Roberts, T. Kono and S. Bayram, “Acoustic Analysis Techniques for Condition Monitoring of Roller Bearings,” in *6th IET Conference on Railway Condition Monitoring (RCM 2014)*, Birmingham, UK, 2014.
- [202] AKG Acoustics GmbH, “C417 | Lavalier Microphone,” AKG, [Online]. Available: <http://www.ake.com/C417-931.html?pid=969>. [Accessed January 2014].
- [203] Focusrite Audio Engineering Ltd., “Octopre MkII | Focusrite,” Focusrite, [Online]. Available: <http://uk.focusrite.com/mic-pres/octopre-mkii>. [Accessed January 2014].
- [204] Steinberg Media Technologies GmbH , “UR824,” Steinberg, [Online]. Available: http://www.steinberg.net/en/products/audio_interfaces/ur_serie/modelle/ur824.html.

[Accessed January 2014].

- [205] SICK Sensor Intelligence, "SICK AG," [Online]. Available: <https://www.mysick.com/saqqara/im0045019.pdf>. [Accessed January 2014].
- [206] B. D. Van Veen and K. M. Buckley, "Beamforming: A Versatile Approach to Spatial Filtering," *IEEE ASSP MAGAZINE*, vol. 5, no. 2, pp. 4-24, APRIL, 1988.
- [207] G. Zechel, A. Zeinbig and M. Beitelschmidt, "Time-domain beamforming on moving objects with known trajectories," in *Beamforming Conference*, Berlin, 2010.
- [208] N. Otsu, "A threshold selection method from gray-level histograms," *IEEE Transactions on Systems, Man, and Cybernetics*, vol. 9, no. 1, pp. 62-66, 1979.
- [209] wikimedia, "Class 395 "Javelin" operated by Southeastern at Ebbsfleet International. These trains are used on Southeastern's high speed services.," [Online]. Available: https://upload.wikimedia.org/wikipedia/commons/c/ca/Unit_395008_at_Ebbsfleet_International.JPG.
- [210] D. Ballard, "Generalizing the Hough transform to detect arbitrary shapes," *Pattern recognition*, vol. 2, no. 13, pp. 111-122, 1981.
- [211] G. Shrivakshan and C. Chandrasekar, "A Comparison of various Edge Detection Techniques used in Image Processing," *International Journal of Computer Science Issues*, vol. 9, no. 5, pp. 269-276, 2012.
- [212] P. Dhankhar and N. Sahu, "A Review and Research of Edge Detetion Techniques for Image Segmentation," *International Journal of Computer Science and Mobile Computing*, vol. 2, no. 7, p. 86092, 2013.

- [213] Z. Zhang, M. Entezami, E. Stewart, G. Yeo, G. Xu, M. Rusu and C. Roberts, "Improvement of Axle Bearing Monitoring Systems Through the Use of High Speed Imaging for Directing Acoustic Beamforming," *Condition Monitor*, no. 353, pp. 5-9, 2016.
- [214] C. Scheffer and P. Girdhar, "Machinery fault diagnosis using vibration analysis," in *Practical machinery vibration analysis & predictive maintenance*, Amsterdam, Elsevier, 2004, pp. 110-115.
- [215] W. K. C. D. Barke, "Structural Health Monitoring in the Railway Industry: A Review," *Structural Health Monitoring*, p. 23, April 2005.
- [216] C. B. N. Ahuja, "Machine Vision for Railroad Equipment Undercarriage Inspection Using Multi-Spectral Imaging," in *Transportation Research Board High-Speed Rail IDEA Program Final Report*, 2007.
- [217] J. M. Hart, N. Ahuja, C. P. Barkan and D. D. Davis, "A Machine Vision System for Monitoring - Railcar Health: Preliminary Results," *TIMELY TECHNOLOGY TRANSFER*, pp. 1-4, JUNE 2004.
- [218] C. Sunnersjo, "Varying compliance vibrations of rolling bearings," *J Sound Vibr*, vol. 3, no. 58, pp. 363-373, 1978.
- [219] V. Bansal, B. Gupta, A. Prakash and V. Eshwar, "Quality inspection of rolling element bearing using acoustic emission technique," *J Acoust Emission*, vol. 2, no. 1990, pp. 142-146, 1990.
- [220] R. Ricci, P. Borghesani, S. Chatterton and P. Pennacchi, "The combination of empirical mode decomposition and minimum entropy deconvolution for roller bearing

- disgnostics in non-stationary operation,” in *Proceedings of the ASME 2012 International Design Engineering Technical Conferences & Computers and information in Engineering Conference*, Chicago, Illinois, USA, 2012.
- [221] H. Endo and R. Randal, “Enhancement of autoregressive model based gear tooth fault detection technique by the use of minimum entropy deconvolution filter,” in *Mechanical System and Signal Processing 21*, 2007.
- [222] A. Morhain and D. Mba, “Bearing defect diagnosis and acoustic emission,” *Journal of Engineering Tribology Part I: Mechanical Engineering*, vol. 4, no. 217, pp. 257-272, 2003.
- [223] M. Abdullah and D. Al-Ghamd & Mba, “A comparative experimental study on the use of acoustic emission and vibration analysis for bearing defect identification and estimation of defect size,” in *Mechanical Systems and Signal Proceeding. 20*, 2006.
- [224] Y. He, X. Zhang and M. I. Friswell, “Defect diagnosis for rolling element bearings using acoustic emission,” *Journal of Vibration and Acoustics*, no. 131.061012-1, 2009.
- [225] Wikipedia, “Rolling-element bearing,” 10 January 2001. [Online]. Available: http://en.wikipedia.org/wiki/Rolling_element_bearing. [Accessed 14 December 2012].
- [226] y. W. A. K. C. Howard C. Choe, “Neural pattern identification of railroad wheel-bearing faults from audible acoustic signal: Comparision of FFT, CWT, and DWT features,” *SPIE*, vol. 3078, no. 0277-766X, p. 17, 1 January 1997.
- [227] S. Grassie, “Allowable impact loading and wheel irregularities,” in *In: Eighth International Rail Track Conference*, Sydney, 1990.

- [228] C. (. Sothern, "Effect of impact loads on bearings," in *In: System RCPWD*, 2002.
- [229] A. tajaddini, "testing the effects of wheel impact loads on bridges," *Railway Track and Structures*, pp. 17-20, 92(3) 1996.
- [230] D. Stone, C. Lonsdale and S. Kalay, "Effect of wheel impact loading on shattered rims," in *In: 13th international Wheelset Conference*, Rome, 2001.
- [231] S. Kalay and M. Hargrove, "Examining the economics of high-impact wheel loads," *Railway Track and Structures*, pp. 29-33, 90(3) 1994.
- [232] P. Mutton and E. Alvarez, "Failure modes in aluminothermic rail welds under high axle load conditions," in *In: International Conference on Failure Analysis (IFCA)*, Melbourne, 2002.
- [233] N. Frank, "New rail could solve rolling contact fatigue," *International Railway Journal*, pp. 49-50, 43(5) 2003.
- [234] K. Matoba, "Detection and warning systems form first line of defense," in *Railway Track and Structures*, 2000.
- [235] W. Jiang, W. Lu, H. Wu and J. Hou, "A fault diagnosis scheme of rolling element bearing based on near-field acoustic holography and gray level cooccurrence matrix," *Journal of Sound and Vibration*, no. 331, pp. 3663-3674, 2012.
- [236] P. Mitra, C. A. Murthy and S. K. Pal, "Density-based multiscale data condensation," *IEEE Transactions on Pattern Analysis and Machine Intelligence*, vol. 6, no. 24, pp. 734-747, 2002.
- [237] R. Szeliski, "Feature detection and matching," in *Computer Vision - Algorithms and*

Applications, Springer-Verlag London, 2010.

- [238] P. V. Hough, "Method and means for recognizing complex patterns". U.S. Patent 3,069,654, 1962.
- [239] R. Fisher, S. Perkins, A. Walker and E. Wolfart, "IMAGE PROCESSING LEARNING RESOURCES," Hypermedia Image Processing Reference (HIPR2), 2003. [Online]. Available: <http://homepages.inf.ed.ac.uk/rbf/HIPR2/morops.htm>.
- [240] L. Lam, S.-W. Lee and C. Y. Suan, "Thinning Methodologies-A Comprehensive Survey," *IEEE Transactions on Pattern Analysis and Machine Intelligence*, vol. 14, no. 9, pp. 879, bottom of first column through top of second column, 1992.